Fermi National Accelerator Laboratory

THEORETICAL EXPECTATIONS AT COLLIDER ENERGIES*

E. Eichten

Fermi National Accelerator Laboratory†

P. O. Box 500, Batavia, IL 60510

May 30, 1986

Abstract

This series of seven lectures is intended to provide an introduction to the physics of hadron-hadron colliders from the $S\bar{p}pS$ to the SSC. Applications in perturbative QCD $(SU(3))$ and electroweak theory $(SU(2) \otimes U(1))$ are reviewed. The theoretical motivations for expecting new physics at (or below) the TeV energy scale are presented. The basic theoretical ideas and their experimental implications are discussed for each of three possible types of new physics: (1) New strong interactions (e.g. Technicolor), (2) Composite models for quarks and/or leptons, and (3) Supersymmetry (SUSY).

I.   INTRODUCTION TO COLLIDER PHYSICS

These lectures are intended to provide a introduction to the physics of hadron-hadron colliders present and planned. During the last twenty years, great theoretical advances have taken place. The situation in elementary particle physics has been transformed from the state (twenty years ago) of a wealth of experimental results for which there was no satisfactory theory to the situation today in which essentially all experimental results fit comfortably into the framework of the **Standard Model**. The current generation of hadron-hadron colliders will allow detailed tests of the gauge theory of the strong interactions, QCD; while the hadron-hadron colliders which are being planned now will be powerful enough to probe the full dynamics of the electroweak interactions of the Weinberg-Salam model. The experiments performed at these colliders will confront this standard model and may show it inadequate for as we will discuss it is very likely incomplete.

After a brief review of the status of the standard model and experimental facilities present and planned, this introductory lecture will deal with the basics. The connection between hadron-hadron collisions and the elementary subprocesses will be reviewed, along with a discussion of the parton distribution functions which play a central role in this connection.

The second lecture will concentrate on QCD phenomenology. The basic two to two parton subprocess will be reviewed and applications to jet physics discussed. The two to three processes and their relation (in leading logarithmic approximation) to the two to two processes is demonstrated. Finally the production of the top quark is discussed.

The third lecture will concentrate on the other half of the standard model gauge theory, the electroweak interactions. The Weinberg-Salam model is reviewed. The main focus of this lecture is the fermions and gauge bosons of the electroweak model; the scalar sector is left to lecture four. The production and decay properties of single $W^\pm$'s and Z^0's are considered at present and future collider energies. Electroweak gauge boson pair production is also considered, with emphasis on what can be learned about the structure of the gauge interactions from measurement of pair production. Finally minimal extensions of the standard model are considered. In particular, the possibilities of a fourth generation of quarks and leptons and a W'

or Z' are considered.

The fourth lecture will be devoted to the scalar sector of the electroweak theory. The limits on the Higgs mass (or self coupling) and fermion masses (Yukawa couplings) imposed by the condition of perturbative unitarity are presented. The prospects for discovery of the standard Higgs are discussed. Finally 't Hooft's naturalness condition is used to argue the unnaturalness (at the TeV energy scale) of the Weinberg-Salam model with elementary scalars. The possibilities for building a natural theory are discussed in the remaining three lectures.

In the fifth lecture the possibility of a new strong interaction at the one TeV scale will be examined. The basics of Technicolor, Extended Technicolor, and mass generation for technipions are reviewed. The phenomenological implications of both a minimal model and the more elaborate (and somewhat more realistic) Farhi-Susskind model are discussed.

The sixth lecture is devoted to the possibility that quarks and/or leptons are composite. Since no realistic models of compositeness have been proposed, the emphasis will be on the general theoretical requirements of a composite model, e.g. 't Hooft 's constraint, and the model independent experimental signatures of compositeness.

In the last lecture the idea of a supersymmetric extension of the standard model is investigated. The basic idea of N=1 global supersymmetry and the present experimental constraints on the superpartners of known particles are reviewed. The production rates and detection prospects for superpartners in hadron-hadron collisions are presented.

There are many very good references to the various aspects of collider physics I will be discussing in these lectures and I will attempt to give some sources for each of the lectures as I discuss the material. It is however appropriate to mention one source before I begin, since I have drawn heavily on it and will refer frequently to it. This reference is "Supercollider Physics" by Eichten, Hinchliffe, Lane, and Quigg[1], hereafter denoted EHLQ. It contains a compendium of the physics opportunities for the next generation of hadron-hadron colliders, the so-called Super Colliders.

A. Status of the Standard Model

The present theory of elementary particles and their interactions, the **Standard Model**, is a great success:

- The fundamental constituents of matter have been identified as leptons and quarks.

- A gauge theory encompassing the weak and electromagnetic interactions has been developed.

- Quark confinement has been explained by an asymptotically free gauge theory of colored quarks and gluons, QCD.

No known experimental results are inconsistent with the present theory. In fact, the basics of the standard model are in a number of recent textbooks[2].

1. The Fundamental Constituents

The elementary leptons and quarks are arranged into families, or generations.

For the leptons:

$$\begin{pmatrix} \nu_e \\ e \end{pmatrix}_L \qquad \begin{pmatrix} \nu_\mu \\ \mu \end{pmatrix}_L \qquad \begin{pmatrix} \nu_\tau \\ \tau \end{pmatrix}_L$$
$$e_R \qquad\qquad \mu_R \qquad\qquad \tau_R$$

and for the quarks:

$$\begin{pmatrix} u \\ d \end{pmatrix}_L \qquad \begin{pmatrix} c \\ s \end{pmatrix}_L \qquad \begin{pmatrix} t \\ b \end{pmatrix}_L$$
$$u_R \;,\; d_R \qquad c_R \;,\; s_R \qquad t_R \;,\; b_R$$

All the left-handed fermions appear in $SU(2)_L$ weak doublets and the right-handed fermions are singlets. The vertical columns form the elements of a single generation of quarks and leptons. This pattern is repeated three times, i.e. there are

three known generations. The only missing constituent is the top quark, for which preliminary evidence has been reported by the UA1 Collaboration[3] at CERN.

The fundamental constituents have very simple basic properties:

- Pointlike and structureless down to the smallest distance scales we have probed ($\approx 10^{-16}$ cm)

- Spin 1/2

- Universal electroweak interactions

- Each quark comes in three colors

2. The Gauge Principle

The gauge principle has become the central building block of all dynamical models of elementary particles. As is well known, the gauge principle promotes a global symmetry of the Lagrangian, such as a phase invariance or invariance under a set of non-Abelian gauge charges, to a dynamics determined by the associated local (space-time dependent) symmetry. If, for example, the Lagrangian for a set of free Fermion fields

$$\mathcal{L} = i\overline{\psi}(x)\gamma^\mu \partial_\mu \psi(x) \tag{1.1}$$

is invariant under a set of global charges Q_a coupling with strength g

$$\psi_\alpha(x) \rightarrow e^{ig\alpha_a Q_a}\psi(x) \ , \tag{1.2}$$

then to preserve the symmetry under local gauge variations, $\alpha_a(x)$,

$$\psi_\alpha(x) \rightarrow e^{ig\alpha_a(x)Q_a}\psi(x) \tag{1.3}$$

massless gauge fields $A_a^\mu(x)$ transforming according to

$$gQ_a A_{a\alpha}^\mu(x) \rightarrow e^{ig\alpha_a(x)Q_a}[gQ_a A_a^\mu(x) - i\partial^\mu]e^{-ig\alpha_a(x)Q_a} \tag{1.4}$$

must be introduced and the Lagrangian must be modified to include an interaction between the fermions and these gauge bosons as well as kinetic terms for the gauge

bosons. The form of these interactions is dictated by the requirement of local gauge invariance. The Lagrangian becomes:

$$\mathcal{L} = i\overline{\psi}(x)\gamma^\mu \mathcal{D}_\mu \psi(x) + \frac{1}{4T_2 g^2} Tr([\mathcal{D}_\mu, \mathcal{D}_\nu]^2) \tag{1.5}$$

where $Tr(Q^a Q^b) = T_2 \delta^{ab}$ and $\mathcal{D}_\mu^A$ is the gauge covariant derivative

$$\mathcal{D}_\mu^A \equiv \partial_\mu + ig Q_a A_{a\mu}(x) \; . \tag{1.6}$$

The Lagrangian (Eq. 1.5) describes a set of massless non-Abelian gauge bosons interacting with massless fermions but the physical spectrum may realize the gauge symmetry in one of three different phases[4]:

- Confinement Phase - all physical states are singlets under the non-Abelian charges. This is the realization in the case of the color $SU(3)$ gauge interactions which describe the strong interactions.

- Higgs Phase - the symmetry is spontaneously broken. Only a subgroup of the original symmetry is manifest in the physical spectrum, while the other symmetries are "hidden". In this case the gauge bosons associated with the broken symmetries acquire a mass. The $SU(2)_L \otimes U(1)$ electroweak interactions exhibit this behaviour.

- Coulomb Phase - This is the simplest realization. The symmetry is manifest and the gauge bosons are massless physical degrees of freedom. Quantum Electrodynamics exhibits this phase.

Therefore, all three phases of a gauge theory are found in nature.

In addition to the fermions and the gauge interactions in the standard model, fundamental scalars are introduced which interact with the electroweak gauge bosons via gauge interactions and with the fermions by Yukawa interactions. The scalar self interactions (Higgs potential) are introduced to produce spontaneous symmetry breaking at the electroweak scale. There is as yet no direct experimental evidence for the scalar sector of the standard model. A detailed discussion of these scalars and their interactions is postponed until the third and fourth lectures.

The covariant derivative coupling of matter fields (fermions or scalars) with the carrier of the color interactions, the gluon field G, is given by:

$$\mathcal{D}_\mu^G = \partial_\mu + ig_s Q_s^a G_{a\mu}(x) \tag{1.7}$$

where Q_s^a is the color charge matrix of the matter field, while the covariant derivative coupling of matter fields to carrier of the $SU(2)_L$ electroweak interactions the W gauge triplet is given by:

$$\mathcal{D}_\mu^W = \partial_\mu + ig_2 Q_W^a W_{a\mu}(x) \tag{1.8}$$

where Q_W^a is the $SU(2)_L$ charge matrix of the matter field. The matter fields interact with the carrier of the $U(1)$ gauge interaction B by an Abelian gauge interaction (as in QED) with coupling strength g_1.

One can write the standard model including both the strong and electroweak interactions in a compact form using these covariant derivatives:

$$
\begin{aligned}
\mathcal{L} = {} & \sum_{j=1,2,3} i\overline{\psi}_{q_j}\gamma^\mu \mathcal{D}_\mu^G \psi_{q_j} + \frac{1}{2g_s^2}Tr([\mathcal{D}_\mu^G,\mathcal{D}_\nu^G]^2) + \sum_{j=1,2,3} i\overline{\psi}_{l_j}\gamma^\mu \partial_\mu \psi_{l_j} \\
& + \sum_{j=1,2,3}\sum_{f=q,l} i\overline{\psi}_{f_j}\gamma^\mu \frac{(1-\gamma_5)}{2} ig_2 Q_W^a W_\mu \psi_{f_j} + \frac{1}{2g_2^2}Tr([\mathcal{D}_\mu^W,\mathcal{D}_\nu^W]^2) \\
& + \sum_{j=1,2,3}\sum_{f=q,l} i\overline{\psi}_{f_j}\gamma^\mu [ig_1(\frac{1-\gamma_5}{2}\frac{Y_L^{f_j}}{2} + \frac{1+\gamma_5}{2}\frac{Y_R^{f_j}}{2})B_\mu]\psi_{f_j} \\
& -\frac{1}{4}(\partial_\mu B_\nu - \partial_\nu B_\mu)^2 \\
& +|\mathcal{D}_\mu^W + i\frac{g_1}{2}B_\mu)\phi|^2 - [-\mu^2|\phi|^2 + \lambda(|\phi|^2)^2] \\
& -[\sum_{i=1,2,3} \overline{\psi}_{L\ e_i}\Gamma_{e_i}\psi_{R\ e_i}\phi + h.c. \\
& + \sum_{i,j=1,2,3} \overline{\psi}_{L\ q_i}\Gamma_{ij}^{up}(\frac{1+\gamma_5}{2})\psi_{R\ q_j}\tilde{\phi} + h.c. \\
& + \sum_{i,j=1,2,3} \overline{\psi}_{L\ q_i}\Gamma_{ij}^{down}(\frac{1+\gamma_5}{2})\psi_{R\ q_j}\phi + h.c.]
\end{aligned}
\tag{1.9}
$$

with the notation

$$\psi_{q_i} \Rightarrow \begin{pmatrix} u_i \\ d_i \end{pmatrix}_L \quad \text{and} \quad \begin{pmatrix} u_i \\ d_i \end{pmatrix}_R \tag{1.10}$$

and

$$\psi_{l_i} \Rightarrow \begin{pmatrix} \nu_i \\ e_i \end{pmatrix}_L \quad \text{and} \quad e_{iR} \tag{1.11}$$

for the fermion fields, and

$$\phi = \begin{pmatrix} \phi_+ \\ \phi_0 \end{pmatrix}$$

$$\bar{\phi} = \begin{pmatrix} \phi_0^\dagger \\ \phi_- \end{pmatrix} \tag{1.12}$$

for the scalar fields. The indices i,j denote the generation. A possible CP violating strong interaction term (the so-called θ term) as well as gravitation interactions have not been included.

3.   Unanswered Questions

In spite of the great success of the standard model, there are still many open questions. A partial list would include:

- What determines the pattern of quark and lepton masses and the mixing angles of the Kobayashi-Maskawa (K-M) matrix[5]?

- Why do the quark - lepton generations repeat? How many generations are there?

- Why are there so many arbitrary parameters? In the standard model the arbitrary parameters are:

  3   coupling parameters α_s, α_{EM}, and $\sin\theta_w = g_1/\sqrt{g_1^2 + g_W^2}$

  6   quark masses

  3   generalized Cabibbo angles

  1   CP-violating phase in K-M matrix

  2   parameters of the Higgs potential

  3   charged lepton masses

  1   QCD vacuum phase angle

A total of 19 arbitrary parameters. This number is not generally less in Grand Unified Models (GUTS) such as SU(5).

• Is the spontaneous symmetry breaking of the electroweak interactions due to the instability of the Higgs potential with elementary scalars as in the Weinberg-Salam model or does it have a dynamical origin? If the scalars are elementary what determines the mass of the Higgs scalar and is there more than one doublet of scalars?

• Why are all the interactions we know of built on the gauge principle?

• What is the origin of CP-violation?

• How is gravity included in a unified way?

• Are the quarks and leptons of the standard model elementary or composite? The known fundamental fields in the standard model are:

18 quarks $3 \times (u \quad d \quad c \quad s \quad t \quad b)$

6 leptons $(\nu_e \quad e \quad \nu_\mu \quad \mu \quad \nu_\tau \quad \tau)$

1 photon

3 intermediate bosons $(W^+ \quad Z^0 \quad W^-)$

8 colored gluons

1 Higgs scalar   (not yet observed)

1 graviton   (not yet observed)

A total of 38 "elementary particles" - compare Air, Fire, Earth, and Water (A FEW). Is there a more economical substructure?

There are many theoretical speculations on these questions, but we are not likely to advance without new experimental observations.

B.   Experimental Facilities

Further progress in understanding elementary particles and their interactions will depend on the study of phenomena at higher energies/shorter distances. The experimental high energy facilities which exist or will exist by 1990 are listed below:

Date	Reaction	Location	Accelerator	Energy (CM)
Now	$\bar{p}p$ collisions	CERN	$S\bar{p}pS$	630 GeV
1986	$\bar{p}p$ collisions	Fermilab	TEV I	1,800 GeV
1987	e^+e^- collisions	Stanford	SLC	100 GeV
1989	e^+e^- collisions	CERN	LEP	100 GeV (phase 1) $\approx$ 200 GeV (phase 2)
1990	$e^{\pm}p$ collisions	DESY	HERA	314 GeV

Even though the center of mass energies of the hadron machines shown above are considerably higher than those of the lepton machines, the center of mass energies for the elementary constituent subprocesses are comparable. This is because the energy of a hadron is shared among its constituents, so that energy carried by a given quark or gluon is typically only a small fraction of the total energy.

The conclusion drawn from a careful study of the physics potential of the facilities above is that elementary processes with center of mass energies up to a few hundred GeV will be thoroughly explored by these machines[6,7,8]

However, a center of mass energy of 1 TeV is an important watershed in particle physics. For example:

- Unitarity limits on the standard model become relevant at about 1 TeV as will be shown in lecture 4.

- If electroweak symmetry breaking is dynamical, the Higgs scalars would be fermion-antifermion composite particles. As will be discussed in lecture 5, this internal structure, if it exists, should be observable at the one TeV scale.

- Low energy supersymmetry, which relates bosons and fermions, requires new particles whose masses are very likely below one TeV/c^2.

Therefore general arguments as well as specific speculations indicate that new phenomena should be observed at the energy scale of 1 TeV or below. Exploration of this energy scale is therefore the minimum requirement of the next generation of accelerators.

The two types of machines which are capable of this exploration are:

- A e^+e^- collider with a beam energy of 1-3 TeV. or

- A hadron collider (pp or $\bar{p}p$) with a beam energy of 10-20 TeV, thus producing numerous elementary constituent collisions with center of mass energy of a few TeV.

At present there is under serious consideration in the United States a proposal[9] to build by 1994 a the Superconducting Super Collider (SSC). This SSC would be a pp collider operating at a center of mass energy of 40 TeV with a collision rate for the protons (luminosity) of $10^{33}cm^{-2}sec^{-1}$. With present magnet technology($\approx$ 5 Tesla magnets) this accelerator would be about 20 miles in diameter. A smaller version of the SSC, the Large Hadron Collider[10] (LHC), could be built in the existing LEP tunnel. Field strengths of 6-10 Tesla would give center of mass energies of 10-18 TeV. The luminosity would depend on the choice of a pp or $\bar{p}p$ option for the beams.

The present hadron-hadron colliders in conjunction with the future SSC provide a formidable array of experimental resources for advancing our knowledge. Let me now begin the detailed discussion of the physics potential of these machines.

C.   Preliminaries

In order to understand the strong interactions within QCD, we must be able to interpret the hadron collisions in terms of quarks and gluons[11]. The quarks carry flavor, have spin 1/2, and are in the fundamental (triplet) representation of SU(3) color, whereas the only internal quantum number of the gluons, which are spin one bosons, is color and the gluons are in the adjoint (octet) representation of the SU(3) color gauge group. Color is confined, which means that all physical states are singlets of color SU(3). Therefore, unlike lepton physics in which the elementary particles can be studied directly, in strong interactions the physical particles at our disposal are the hadrons, which are bound states of the elementary quarks and gluons.

The basic property of QCD at short distance (high energy) is asymptotic freedom; i.e. the coupling strength of QCD becomes weak at short distance[12]. This property of QCD allows us to calculate in perturbation theory at high energy. The final states associated with high energy interactions are quarks and gluons in perturbation theory but must be hadrons in reality since color is confined. However
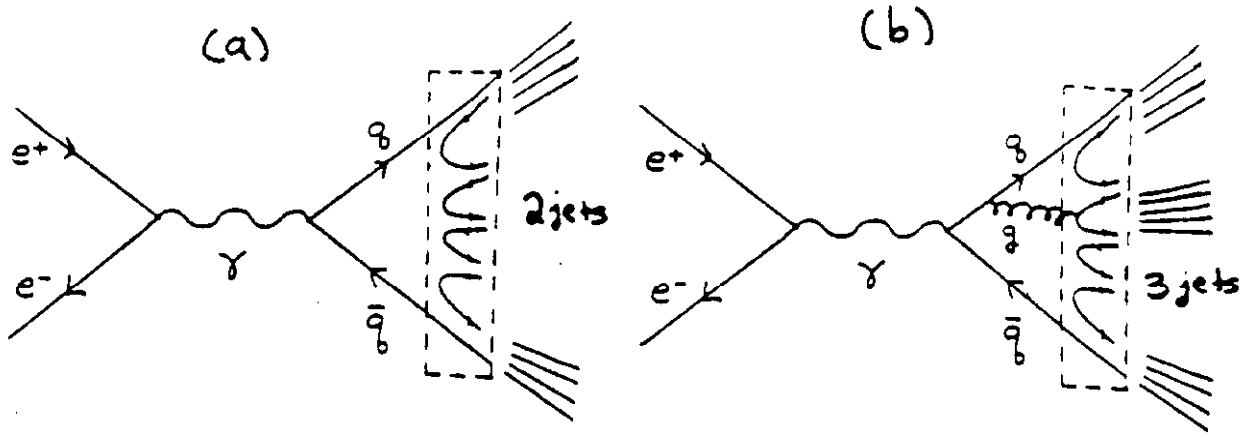
Figure 1: e^+e^- annihilation into (a) quark-antiquark pair and (b) quark-antiquark pair plus a gluon. Our ignorance of the hadronization process is contained within the dashed box

not all memory of the underlying quark and gluon final state is lost, as the hadrons appear in a striking way - as jets - at high energy. For our purposes a jet is simply a well collimated isolated spray of hadrons (we leave the precise criteria for a jet to the experimentalists). By observing these hadronic jets the underlying quark and gluon interactions can be inferred. For example, in e^+e^- scattering into hadronic final states, the lowest order Q.C.D. process is shown in Figure 1.

The $q\bar{q}$ final state of QCD perturbation theory is not the physical final state. On a distance scale of the confinement scale ($\approx \Lambda_{QCD}$), the strong interactions will produce sufficient gluons and quark-antiquark pairs to locally neutralize the color and produce the color singlet hadrons, the physical final states of the process. This hadronization process, is nonperturbative and presently uncalculable. It can only be modeled phenomenologically[13]. However, at high energies much of the information about the perturbative QCD interactions at short distance is remembered by the jets.[14] Crudely speaking the jets can be mapped one to one onto the quarks and gluons of the short distance (perturbative) process.
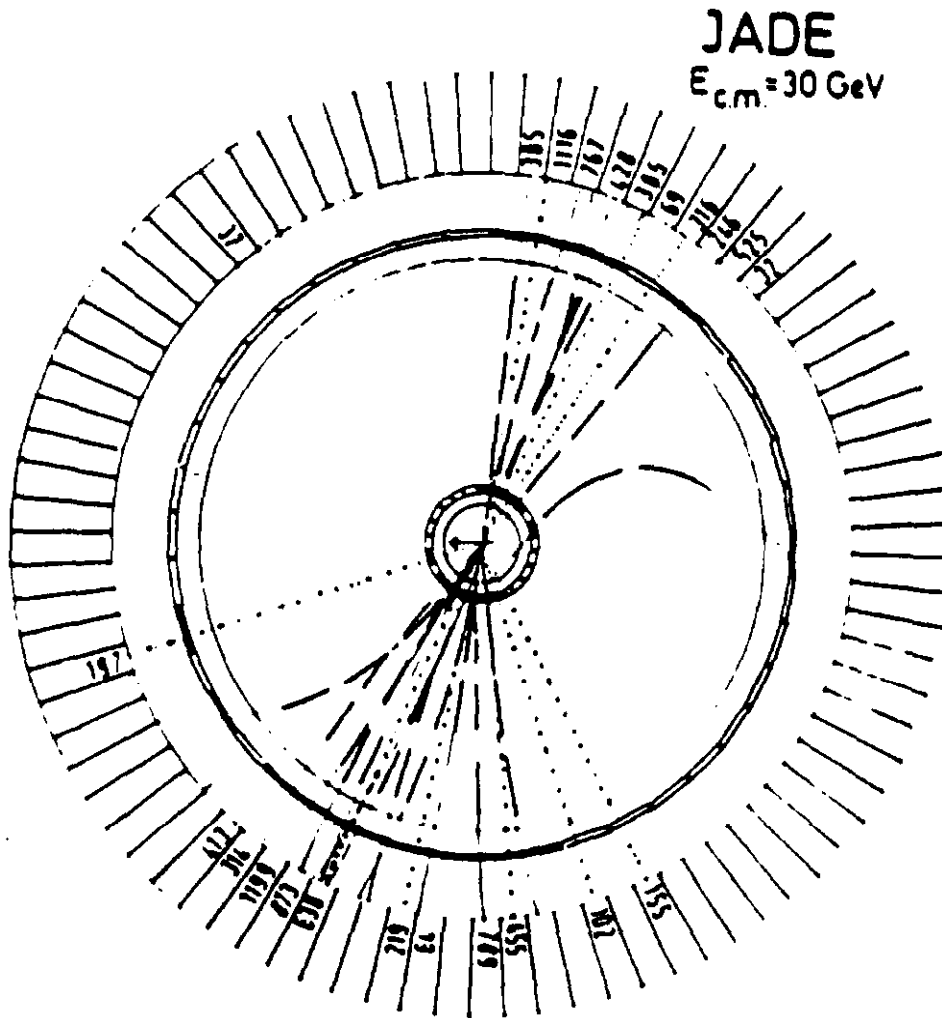
Figure 2: A two jet event in the JADE central detector[15]. The view is along the beam direction. Charged and neutral particles are denoted by solid and dotted lines respectively. The energy deposited into lead glass shower counters are given in MeV.

Figure 2 shows a e^+e^- event at $\sqrt{s} \approx 30$ GeV as seen in the JADE detector at PETRA[15]. This is a typical two jet event associated with the production of a quark-antiquark pair at high energy. The two hadronic jets are clearly visible in the event. The kinematic structure of two jet events retain knowledge of the production kinematics associated with the elementary process. For the production of two spin 1/2 fermions from the virtual photon the angular distribution is

$$\frac{d\sigma}{d\cos\theta} \sim 1 + \cos^2\theta \qquad (1.13)$$

where θ is the angle of the quark to the beam direction. To high accuracy[16], measured two jet events have this angular behaviour (characteristic of the production of two pointlike spin 1/2 fermions).

Sometimes in addition to a quark-antiquark a gluon is produced at short distance in e^+e^- collisions. The frequency of these events is dependent of the strength of the strong coupling α_s. These events should result in a three jet final state. Such three jet events are observed in e^+e^- collisions. An example is shown in Figure 3.

Unfortunately, PEP and PETRA energies are not sufficiently high to extract from the ratio of three to two jet events the value of the strong coupling without relying on the explicit modeling of the hadronization process[18]. Also no experimental procedure has yet been found which on a event by event basis can distinguish a jet associated with a light quark from one associated with a gluon. However all the qualitative features of these events agree well with expectations from QCD.[19]

For hadron-hadron collisions one would expect that it is much more difficult to expose the quark and gluon (partons) interactions, since the initial physical states (the hadrons) have a complicated structure in terms of the fundamental constituents- the quarks and gluons. It is true in fact, for many kinematic regions, that hadron-hadron collisions can not be calculated using perturbative QCD. One simple example is the pp (or $\bar{p}p$) total cross section. This cross section grows as rapidly as the unitarity bound allows. For a detailed discussion of this "soft" interaction physics in hadron-hadron collisions see the excellent review of Block and Cahn[20]. However, the situation is not as bad for processes which involve a "hard" parton interaction. A hard parton interaction is one in which all the invariants (energy scales) of the process are large and thus QCD perturbation theory should apply. We will restrict our attention to these hard processes for the remainder of
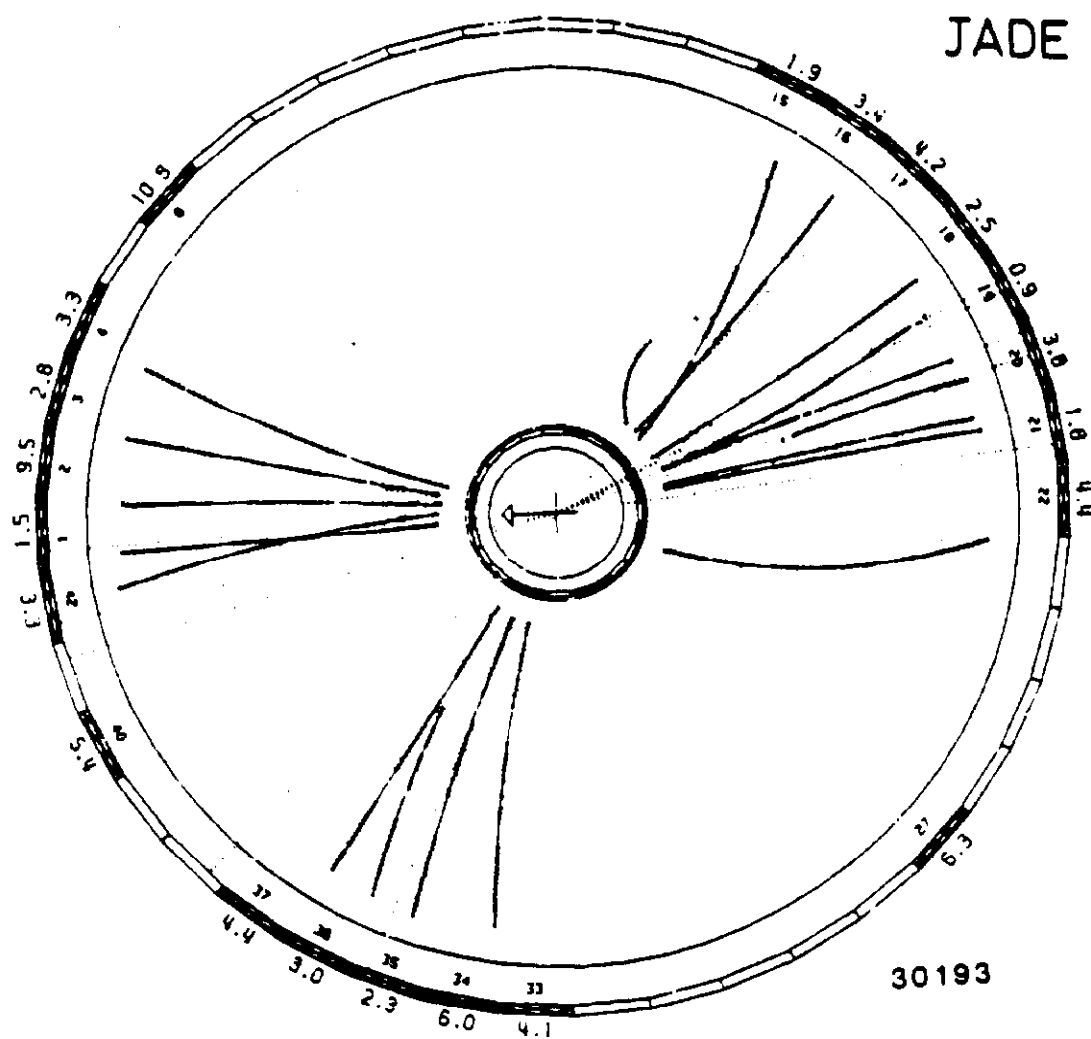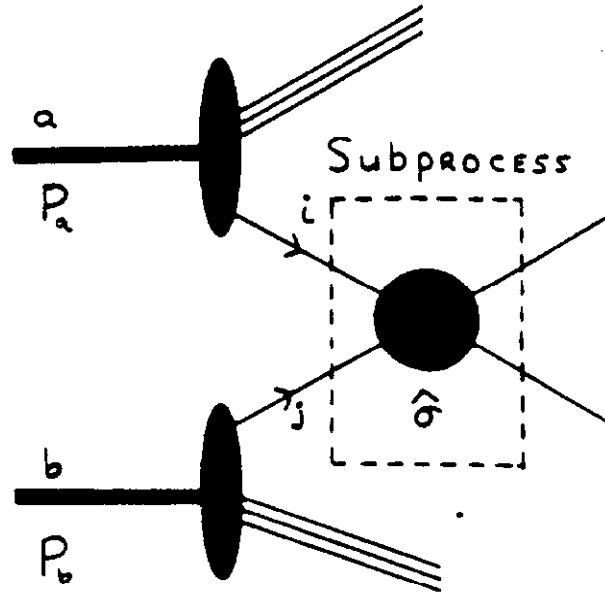
Figure 3: A three jet event in the JADE central detector[17].

Figure 4: Hadron-hadron collision showing two to two parton subprocess.

these lectures.

D. Parton Distributions

An example of a hadron-hadron collision process which involves a high energy sub-process is shown in Figure 4. The incident hadrons are composed of quarks and gluons and two of these partons, i and j, are assumed to interact at high energy. In such a case the final state will be recognizable as containing jets. However, to quantitatively understand the underlying parton interactions, it is necessary to separate out the effects of the physical hadrons. The inclusive cross-section for scattering of hadron a and hadron b to hadron c and anything X may be written as

$$d\sigma(a + b \rightarrow c + X) = \sum_{ij} \frac{1}{1 + \delta_{ij}} \int dx_a dx_b [f_i^{(a)}(x_a, \hat{Q}^2) f_j^{(b)}(x_b, \hat{Q}^2)$$

$$+ (i \leftrightarrow j)] d\hat{\sigma}(i + j \rightarrow c + X) \tag{1.14}$$

where $f_i^{(a)}(x_a, Q^2)$ is the probability that hadron a contains a parton i which carries a fraction x_a of the hadron's momentum. The cross-section for the subprocess $\hat{\sigma}$ involves only the elementary constituents. The kinematic variables are:

- $s = (P_a + P_b)^2$ - The square of the total energy of the initial hadrons in their CM frame.

- $\hat{s} = (x_a P_a + x_b P_b)^2$ -The square of the total energy of the partons in the subprocess CM frame.

$$\hat{s} = x_a x_b s \equiv \tau s \quad \text{for } (P_a^2, P_b^2 \ll s) . \tag{1.15}$$

The parameter τ is used extensively in describing the physics of these collisions.

- $\hat{Q}^2$ - an invariant of the subprocess which characterizes the physical scales(e.g. $\hat{s}, \hat{t}$, or $\hat{u}$). The exact invariant depends on the process.

For SSC energies, we will be interested in Q^2 in the range :

$$(10 GeV)^2 \ll Q^2 \ll (10 TeV)^2 \tag{1.16}$$

Below 10 GeV we probably cannot analyze the subprocesses perturbatively; while above 10 TeV (even at SSC energies) the number of partons is insufficient to produce observable rates for known subprocesses. The typical x's are $\approx \sqrt{Q^2/s}$ so for $\sqrt{s} = 40$ TeV we must consider:

$$10^{-4} \le x \le 1 . \tag{1.17}$$

Clear experimental evidence for jets in the hadronic final state had to wait for the UA1 and UA2 experiments at the CERN $S\bar{p}pS$ collider. Figure 5 shows a UA2 two jet event at $\sqrt{s} = 630$ GeV in the form of a "LEGO" plot[21]. This plot presents the energy deposition in the detector as a function of the solid angle measured from the interaction point. The horizontal axes are: ϕ, the azimuthal angle about the beam direction; and θ, the angle measured from the beam direction.The two jet structure of this event is obvious. Most of the events observed by UA1 or UA2 with total $E_T > 50$ GeV have this two jet energy deposition structure. The particular event shown in Fig. 5 is special in one way. This event has the highest transverse energy observed by UA2 in the 1984 run. The total observed transverse energy was 267 GeV in a $\bar{p}p$ collision with a total energy of 630 GeV. The remaining energy in this event, can be accounted for by soft hadrons which did not deposit enough energy into a cell of the detector to pass a minimum energy cut or by hadrons which

Transverse energy deposition
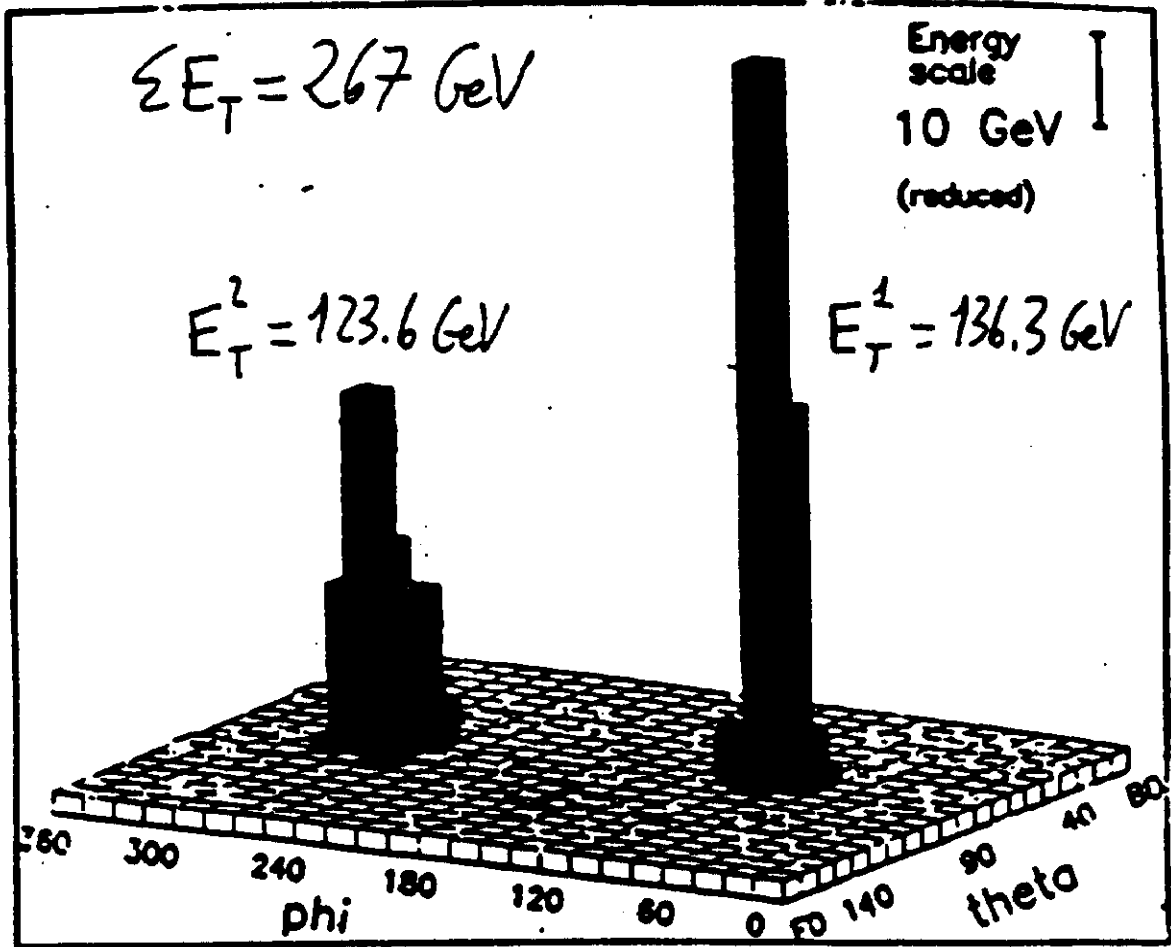
Figure 5: A LEGO plot of the event with the highest total transverse energy observed by UA2 in the 1984 run[21]. The height of each cell is proportional to the total energy deposition.

scattered into the far forward or far backward direction where the detector has poor efficiency. Clearly it is possible for the fundamental subprocess to have a significant fraction of the total available energy.

In order to quantitatively understand the quark/gluon subprocesses it is necessary to calculate the parton distribution functions $f_i^{(a)}(x_a, Q^2)$. The Q^2 dependence is due to QCD corrections to the Born approximation for the subprocess. If the distribution function is known at some Q_0^2 which is high enough that QCD perturbation theory is valid, then the distribution function can be calculated in the leading logarithmic approximation (to all orders of perturbation theory) for values of $Q^2 > Q_0^2$ by use of the Altarelli-Parisi equations[22] (which are based on the renormalization group). This evolution gives the well-known Q^2 dependent scale violation of the parton distribution functions. Therefore the high Q^2 behaviour of these parton distribution functions is completely determined by measuring them at some sufficiently high Q_0^2 so that they are determined at all higher Q^2 within perturbative QCD.

The first step is to determine the parton distributions at some reference Q_0^2. In principle one should also be able to calculate these distributions in QCD, but this nonperturbative calculation is presently beyond our ability.

There are constraints on initial distribution functions which arise from valence quark counting for the proton (i.e. two up quarks and one down quark):

$$\int_0^1 dx[u(x, Q^2) - \overline{u}(x, Q^2)] = 2 \qquad (1.18)$$

$$\int_0^1 dx[d(x, Q^2) - \overline{d}(x, Q^2)] = 1 . \qquad (1.19)$$

Moreover flavor conservation of the strong interactions implies:

$$s(x, Q^2) = \overline{s}(x, Q^2)$$
$$c(x, Q^2) = \overline{c}(x, Q^2) \qquad (1.20)$$

etc.

Finally, from momentum conservation:

$$\int_0^1 dx\, x \quad [\quad g(x, Q^2) + u(x, Q^2) + \overline{u}(x, Q^2) + d(x, Q^2) + \overline{d}(x, Q^2) + 2s(x, Q^2)$$

$$+2c(x,Q^2) + 2b(x,Q^2) + 2t(x,Q^2) + \ldots] = 1 . \tag{1.21}$$

Analysis of deep inelastic neutrino scattering data from the CDHS experiment[23] at CERN gives two sets of initial distributions corresponding to different values of the QCD scale parameter, Λ_{QCD}. The first set corresponds to $\Lambda_{QCD} = 200$ MeV for which the gluon distribution at the reference Q_0^2 is soft, i.e. it has a paucity of gluons at large x. The second set has $\Lambda_{QCD} = 290$ MeV and hard gluons, i.e. relatively more gluons at large x. Explicitly the CDHS analysis gives the following input parametrizations:

$$xu_v(x,Q_0^2) = 1.78x^{0.5}(1 - x^{1.51})^{3.5}$$

$$xd_v(x,Q_0^2) = 0.67x^{0.4}(1 - x^{1.51})^{4.5} \tag{1.22}$$

and for **Set 1** with $\Lambda_{QCD} = 200$ MeV (the "soft gluons" distribution)

$$x\overline{u}(x,Q_0^2) = x\overline{d}(x,Q_0^2) = 0.182(1 - x)^{8.54}$$

$$x\overline{s}(x,Q_0^2) = 0.081(1 - x)^{8.54}$$

$$xG(x,Q_0^2) = (2.62 + 9.17x)(1 - x)^{5.90} \tag{1.23}$$

while for **Set 2** with $\Lambda_{QCD} = 290$ MeV (the "hard gluons" distribution)

$$x\overline{u}(x,Q_0^2) = x\overline{d}(x,Q_0^2) = 0.185(1 - x)^{7.12}$$

$$x\overline{s}(x,Q_0^2) = 0.0795(1 - x)^{7.17}$$

$$xG(x,Q_0^2) = (1.75 + 15.575x)(1 - x)^{6.03} . \tag{1.24}$$

For both distributions

$$xc(x,Q_0^2) = xb(x,Q_0^2) = xt(x,Q_0^2) = 0 . \tag{1.25}$$

The CDHS fit to their measured structure functions F_2 and xF_3 is shown in Figure 6. The relation between these measured structure functions and the parton distribution functions is:

$$2xF_1 = x[(u + d + s + c + \ldots) + (\overline{u} + \overline{d} + \overline{s} + \overline{c} + \ldots)] \tag{1.26}$$
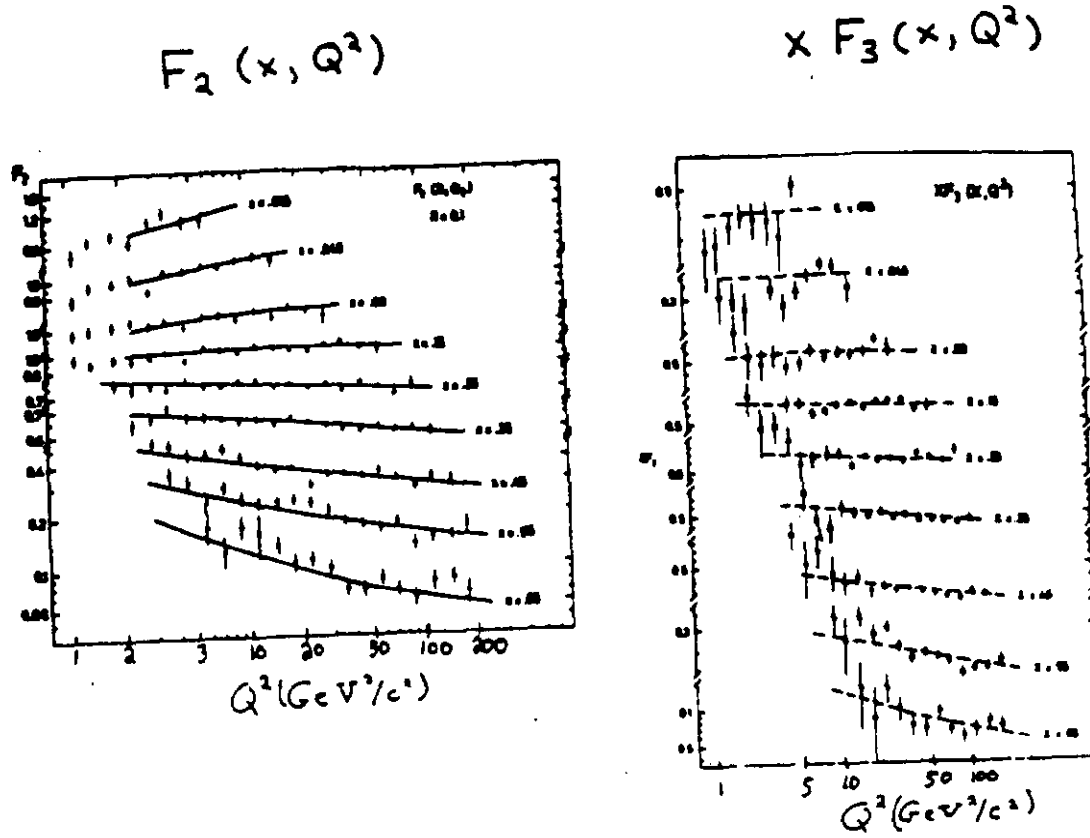
$$F_2 (x, Q^2)$$

$$x \, F_3 (x, Q^2)$$

Figure 6: The structure functions F_2 and xF_3 versus Q^2 for different bins of x from CDHS[33]. The solid lines are the result of their fit **Set 1** to the data.

$$F_2 = 2xF_1 \frac{(1 + R(x, Q^2))}{1 + 4M_p^2 x^2 / Q^2} \tag{1.27}$$

$$xF_3 = x[u - \bar{u} + d - \bar{d}] \tag{1.28}$$

where $R(x, Q^2)$ is the ratio of longitudinal to transverse cross section in deep-inelastic leptoproduction. R is predicted by QCD to go to zero at high Q^2 like $1/Q^2$, the data is not in disagreement with this behaviour however the measurements are not conclusive[24]. Different choices for R consistent with the data will affect the resulting distribution. The distribution Set 1 above uses $R = .1$ while Set 2 assumes the behaviour of R expected in QCD.

The up and down quark valence distributions can be separated using charged-current cross sections for hydrogen and deuterium targets. The parameterization use here is discussed by Eisele[25]. Once the valence distributions are known, the sea distribution may be determined from measurements of the structure function F_2 on isoscalar targets. It is also necessary to know the flavor dependence of the sea distribution. For this purpose, the strange quark distribution can be determined directly from antineutrino induced dimuon production[25]. Dileptons events arise mainly from production off the antistrange quarks in the proton hence the rate of opposite sign dilepton events gives information about the the ratio of strange to antiup quark distributions, assuming that both have the same x dependence. Also note that limits on same sign dimuon events put limits on the charm quark content of the proton[25].

Figure 7 shows a comparison of Set 2 of the distributions defined above with the results of the CHARM Collaboration[26]. We see that there is good agreement with the results presented here except for the antiquark distributions. Also a second independent experiment measuring the structure functions CCFRR[27] finds that $F_2(x, Q_0^2)$ is more strongly peaked at small x than the CDHS results. This again suggests a larger sea distribution. Recently, the disagreement has been resolved, CDHS has made a new analysis[28] which disagrees with their old results and is in agreement with the CCFRR results. Thus the sea distributions used here are too small at Q_0^2. In general the effects of this error will be small since the Q^2 evolution washes out much of the dependence on the initial distribution, as we will see in the case of the gluon distributions shortly.
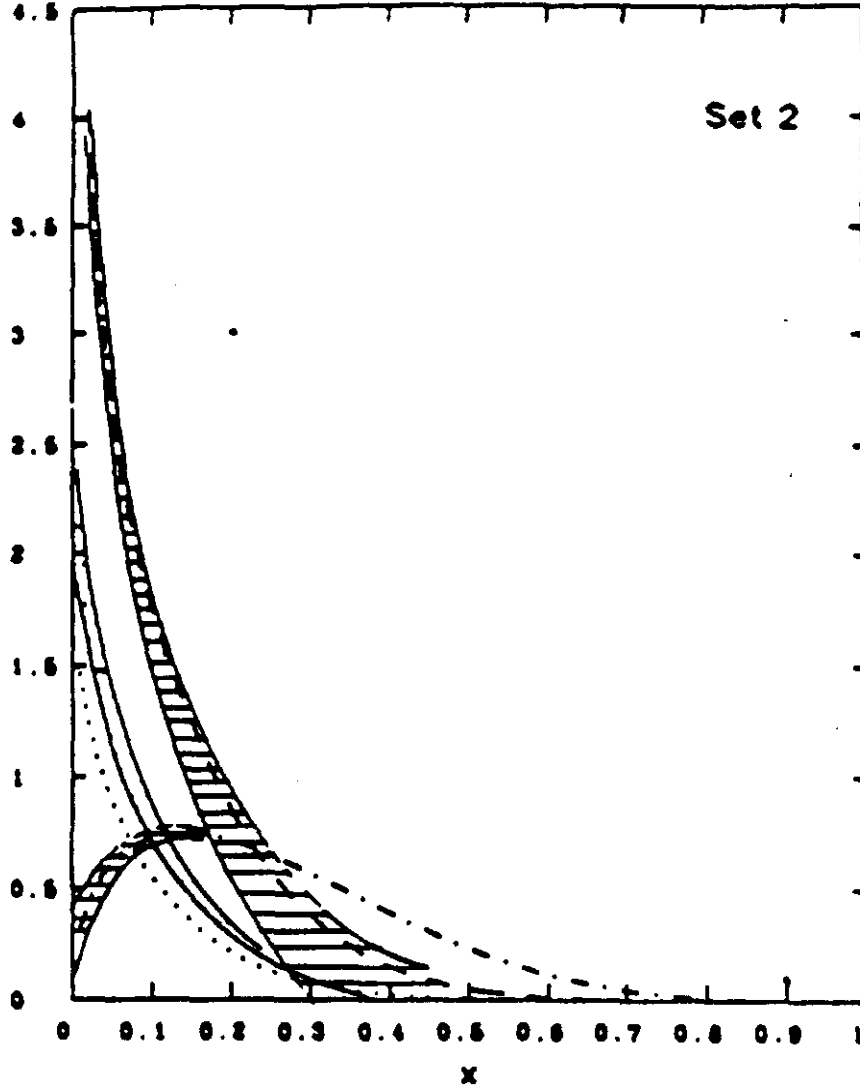
Figure 7: Comparison of the gluon distribution $xG(x, Q^2)$ (dashed line), valence quark distribution $x[u_v(x, Q^2) + d_v(x, Q^2)]$ (dot-dashed line), and the sea distribution $2x[u_s(x, Q^2) + d_s(x, Q^2) + s_s(x, Q^2) + c_s(x, Q^2)]$ (dotted line) of Set 2 with the determination (shaded bands) of the CHARM Collaboration[26].

After the determination of these distribution functions has been carried out, it is necessary to extend them to higher values of Q^2 by means of renormalization group methods of Altarelli and Parisi. Although a detailed description of this procedure is beyond the scope of this lecture (see A. Mueller lectures[29] for a more extensive treatment), I will describe the basic idea of this evolution.

Let $q_v(x, Q^2)$ be the valence quark distribution for the proton ($u_v = u - \bar{u}$). If the quark is probed by a virtual photon of momentum Q^2 then this photon will be sensitive to fluctuations on the distance scale $\sqrt{1/Q^2}$. For example, if the quark has a fraction y of the proton's momentum, then it may virtually form a gluon and a quark which has a fraction $x < y$ of the initial proton momentum. Let $z = x/y < 1$. The probability of observing the quark with fraction z of the initial momentum of the parent quark is given by

$$\frac{\alpha(Q^2)}{\pi} P_{q_v \to q_v}(z) d\ln(Q^2) \tag{1.29}$$

in which the coupling strength α has been written explicitly. The splitting function $P(z)$ is calculable in QCD perturbation theory. Finally the renormalization group analysis of Altarelli and Parisi shows that

$$\frac{dq_v(x, Q^2)}{d\ln(Q^2)} = \frac{\alpha(Q^2)}{\pi} \int_x^1 \frac{dy}{y} q_v(y, Q^2) P_{q_v \to q_v}(z) \tag{1.30}$$

where the integral over z ($0 < z < 1$) has been replaced by integration over y ($x < y < 1$). This equation then determines the distribution functions for the valence quarks. Since the valence quark lines continues throughout the process, the evolution of the valence quark distributions is determined by the valence quarks alone while the distribution of non-valence quarks and gluons is determined by all of the various distribution functions.

The equation for the evolution in QCD of the valence quark distribution, $v(x, Q^2) = x u_v(x, Q^2)$ or $x d_v(x, Q^2)$, is

$$\frac{dv(x, Q^2)}{d\ln(Q^2)} = \frac{2\alpha_s(Q^2)}{3\pi} \int_x^1 dz \frac{(1 + z^2)v(y, Q^2) - 2v(x, Q^2)}{1 - z}$$
$$+ \frac{\alpha_s(Q^2)}{\pi}[1 + \frac{4\ln(1 - x)}{3}]v(x, Q^2) \tag{1.31}$$

where $y = x/z$. The result of numerical integration of these lowest order Altarelli-Parisi equations using the initial distributions of Set 2 (Eq. 1.24) is shown in Figure 8 for valence up quarks. As Q^2 increases from 10 to 10^6 the valence momentum distribution functions decrease at large x while increasing modestly at small x. This shift is caused by the fact that higher x quarks scatter into lower x quarks.

For the gluon distribution, $g(x, Q^2) \equiv xG(x, Q^2)$, the evolution is more complicated:

$$\frac{dg(x, Q^2)}{d\ln(Q^2)} = \frac{\alpha_s(Q^2)}{\pi} \int_x^1 dz \Big[\frac{3[zg(y, Q^2) - g(x, Q^2)]}{1 - z} + \frac{3(1 - z)(1 + z^2)}{z} g(y, Q^2)$$

$$+ \frac{2}{3} \frac{1 + (1 - z)^2}{z} \sum_{\text{flavors } q} [yq_v(y, Q^2) + 2yq_s(y, Q^2)] \Big]$$

$$+ \frac{\alpha_s(Q^2)}{\pi} [\frac{11}{4} - \frac{N_f}{6} + 3\ln(1 - x)] g(x, Q^2) \qquad (1.32)$$

where N_f is the number of quark flavors. The evolution of the gluon distribution is feed by the valence (q_v) and sea (q_s) quark distributions as will as the gluon distribution (G) itself.

Figure 9 shows the evolution for the gluon distribution. The gluon distribution is peaked at small x due to the high probability of emission of soft gluons from quarks(and other gluons).

The evolved gluon distribution functions at large Q^2 and small x (where they are peaked) are fairly insensitive to drastic modifications of their initial form at Q_0^2. This is because the gluon distributions are determined through the Altarelli-Parisi Equation (1.32) by the initial valence quark distributions at larger x. For instance, Figure 10 shows the result of modifying the initial gluon distribution of Set 1 (Eq. 1.23) for $x < .01$, values of x at which there is no existing data. The variations were:

$$xG(x, Q_0^2) = \{ \begin{matrix} 0.444x^{-.5} - 1.866 & (a) \\ 25.56x^{.5} & (b) \end{matrix} \quad \text{for } x < .01 . \qquad (1.33)$$

These modifications match continuously at x=0.01 to Set 1 and are constrained to change the gluon momentum integral by no more than 10 percent. Fig 10 shows that a variation by a factor of 160 at $x = 10^{-4}$ for Q_0^2 yields only a factor of 2 difference at the same x for $Q^2 = 2000$ GeV^2 This insensitivity at high Q^2 to the initial distribution is reassuring, for it implies that the gluon distribution at small x
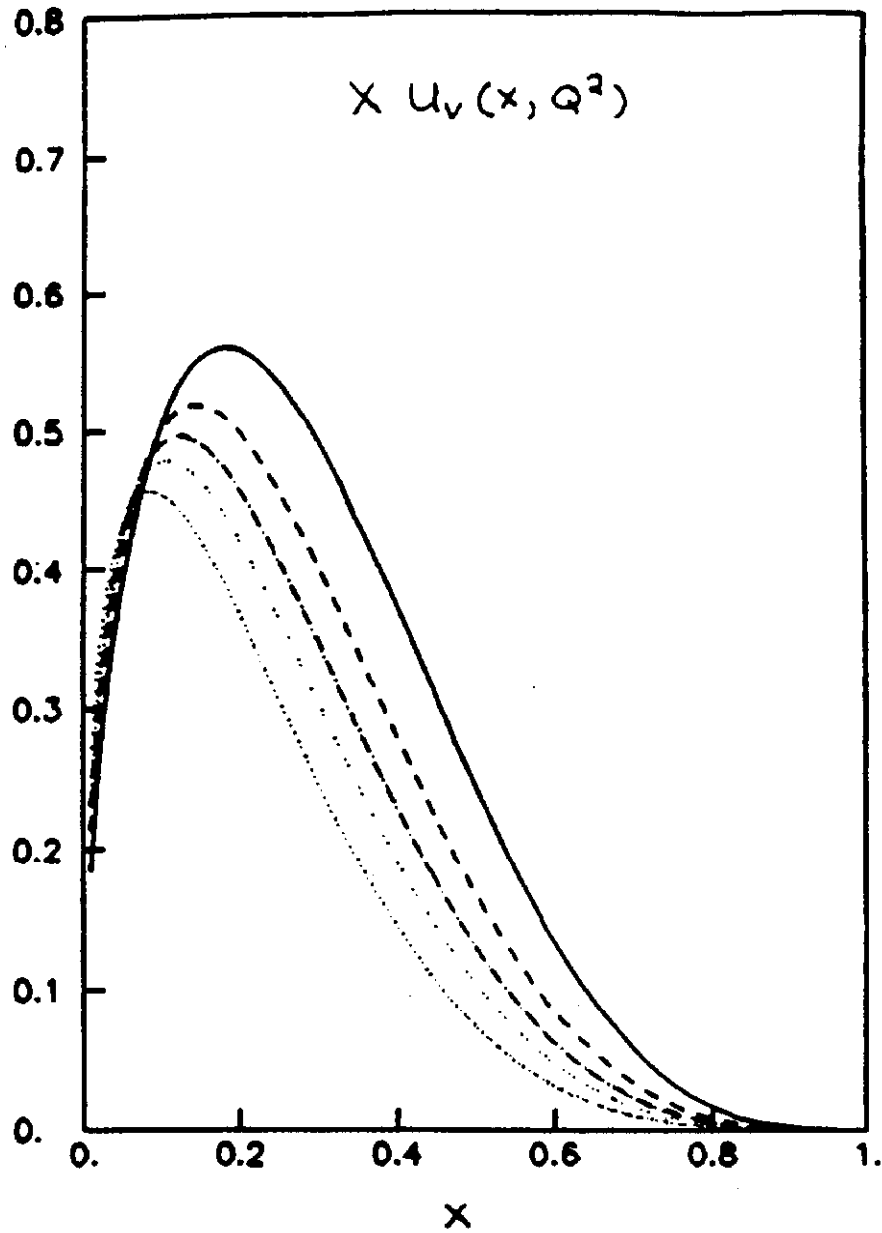
Figure 8: The valence up quark distribution of the proton, $xu_v(x, Q^2)$, as a function of x for various Q^2. The solid, dashed, dot-dashed, sparse dot, and dense dot lines correspond to $Q^2 = 10,\ 10^2,\ 10^3,\ 10^4$, and 10^6 $(GeV)^2$ respectively.
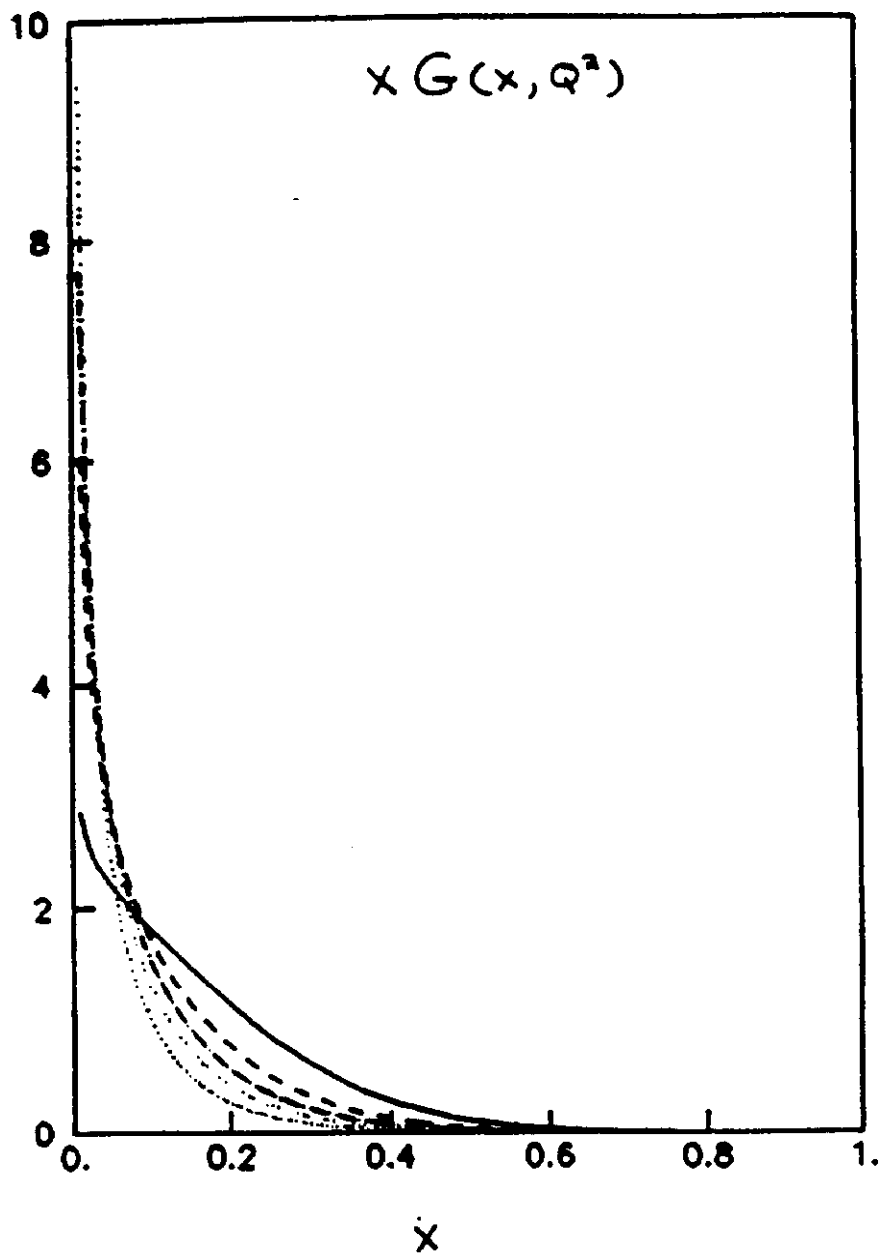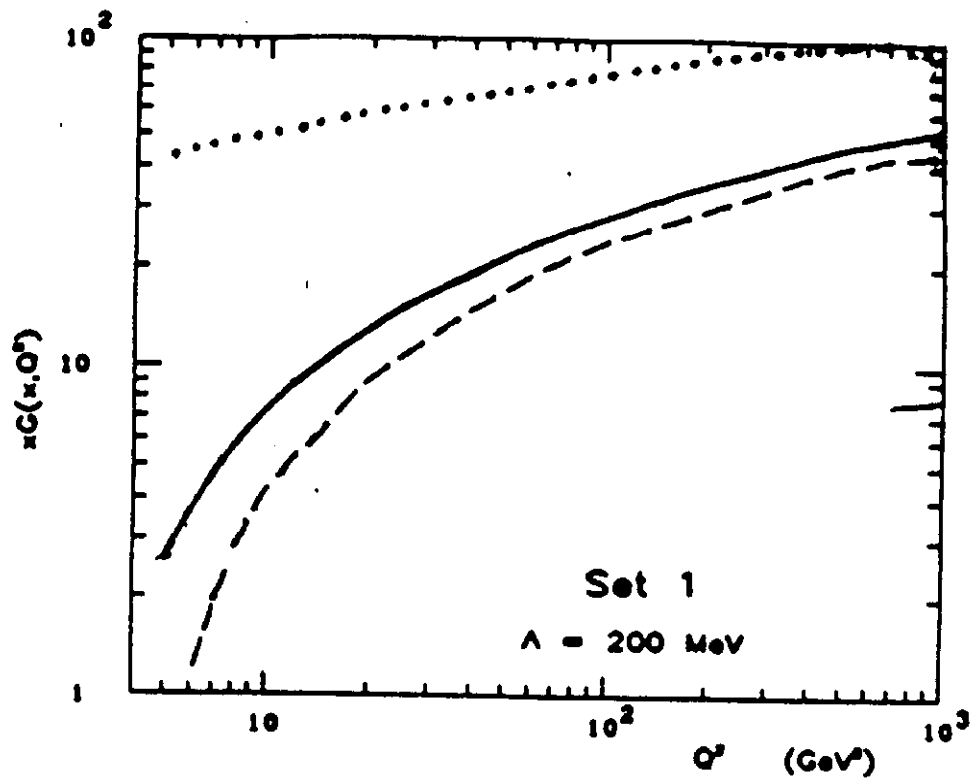
Figure 9: The gluon distribution of the proton, $xG(x, Q^2)$, as a function of x for various Q^2. The solid, dashed, dot-dashed, sparse dot, and dense dot lines correspond to $Q^2 = 10$, 10^2, 10^3, 10^4, and 10^6 $(GeV)^2$ respectively.

Figure 10: The Q^2 evolution of the gluon distribution $xG(x, Q^2)$ given in Set 1 (solid line) as compared to the two variations given in Eq. 1.33 for $x = 10^{-4}$. Distribution (a) is represented by a dotted line and distribution (b) is represented by a dashed line.

and large Q^2 is much better determined that our knowledge of the small x behaviour at Q_0^2 would lead one to expect.

The light sea quarks, $l(x,Q^2) = xu_s(x,Q^2)$ or $xd_s(x,Q^2)$ or $xs_s(x,Q^2)$, evolve according to:

$$\frac{dl(x,Q^2)}{d\ln(Q^2)} = \frac{2\alpha_s(Q^2)}{3\pi}\int_x^1 dz[\frac{(1+z^2)l(y,Q^2)-2l(x,Q^2)}{1-z} + \frac{3}{8}[z^2+(1-z)^2]g(y,Q^2)]$$

$$+\frac{\alpha_s(Q^2)}{\pi}[1+\frac{4}{3}\ln(1-x)]l(x,Q^2) \tag{1.34}$$

The results of numerical evolution for the up antiquark distribution $(xu_s(x,Q^2))$ is shown in Figure 11. The total up quark distribution function is given by $xu_v(x,Q^2)+xu_s(x,Q^2)$.

The initial distribution at $Q^2 = Q_0^2$ was consistent with zero for the heavy quarks and antiquarks (xc_s, xb_s, xt_s). But the probability of finding a charm, bottom, or even top quark in the proton can become significant when the proton is probed at high Q^2. The evolution for heavy quarks is also dictated by the Altarelli-Parisi Equation but some method must be employed to treat the kinematic effects of the nonnegligible masses of the quarks and the associated production thresholds in perturbation theory. The method used was proposed by Gluck, Hoffman, and Reya[30]. For more details see EHLQ. The evolution equation in lowest order QCD for the heavy quark distribution, $h(x,Q^2) = xc_s(x,q^2)$ or $xb_s(x,Q^2)$ or $xt_s(x,Q^2)$, in lowest order QCD is:

$$\frac{dh(x,Q^2)}{d\ln(Q^2)} = \frac{2\alpha_s(Q^2)}{3\pi}\int_x^1 dz[\frac{(1+z^2)h(y,Q^2)-2h(y,Q^2)}{1-z}$$

$$+\frac{3}{4\beta}[\frac{1}{2}-z(1-z)+\frac{m_q^2}{Q^2}\frac{(3-4z)z}{1-z}-\frac{16m_q^4z^2}{Q^4}]g(y,Q^2)$$

$$-\frac{3m_q^2}{2Q^2}[z(1-3z)+\frac{4m_q^4z^2}{Q^2}]\ln(\frac{1+\beta}{1-\beta})g(y,Q^2)]\theta(\beta^2)$$

$$+\frac{\alpha_s(Q^2)}{\pi}[1+\ln(1-x)]h(x,Q^2) \tag{1.35}$$

where the velocity of the heavy quark is:

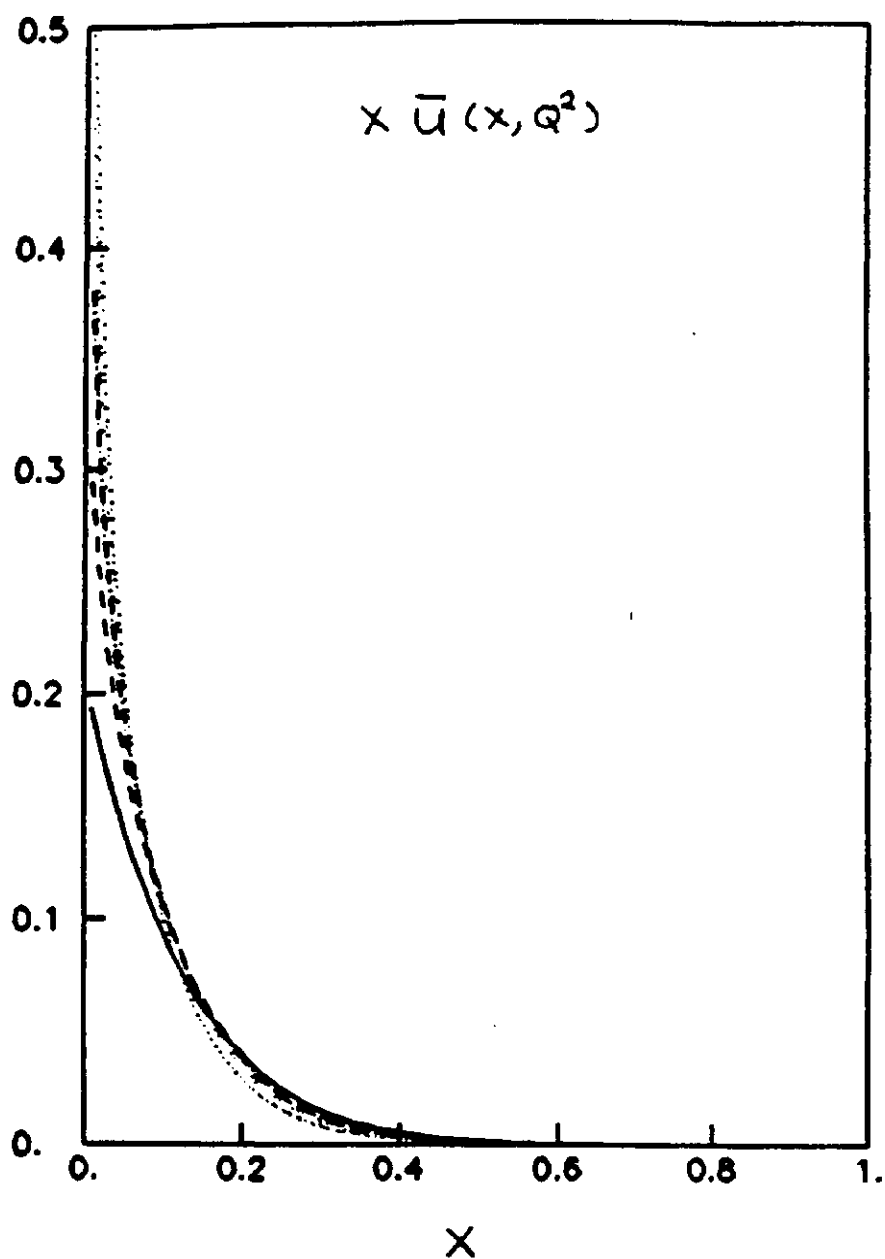$$\beta = [1-\frac{4m_q^2z}{Q^2(1-z)}]^{\frac{1}{2}}, \tag{1.36}$$

Figure 11: The up antiquark distribution of the proton, $xu_s(x, Q^2)$, as a function of x for various Q^2. The solid, dashed, dot-dashed, sparse dot, and dense dot lines correspond to $Q^2 = 10$, 10^2, 10^3, 10^4, and 10^6 $(GeV)^2$ respectively.

the strong coupling includes the heavy quark contribution

$$1/\alpha_s(Q^2) = \frac{25}{12\pi}\ln(\frac{Q^2}{\Lambda^2}) - \frac{1}{6\pi}\sum_{i=b,t}\theta(Q^2 - 16m_q^2)\ln(\frac{Q^2}{16m_q^2}) , \qquad (1.37)$$

and $m_c = 1.8 \text{ GeV}/c^2$, $m_b = 5.2 \text{ GeV}/c^2$, and $m_t = 30 \text{ GeV}/c^2$. The resulting distribution function for the bottom quark is shown in Figure 12.

As Q^2 increases the various quark distributions approach the asymptotic forms dictated by QCD. At infinite Q^2 the masses of the various quarks becomes unimportant and valence quark effects will be swamped by the virtual quark pair (i.e. the sea) ; hence there should be an $SU(6)$ flavor symmetry in this limit. Furthermore, QCD predicts[31] (at infinite Q^2) the the momentum fraction carried by any of these quark flavors to be 3/68 while that the momentum fraction carried by gluons should be 8/17. This approach to the asymptotic values is shown in Figure 13.

The effective parton-parton luminosity is:

$$\tau\frac{d\mathcal{L}_{ij}}{d\tau} \equiv \frac{\tau}{1 + \delta_{ij}} \int_\tau^1 \frac{dx}{x}[f_i^{(P)}(x,\hat{s})f_j^{(P)}(\frac{\tau}{x},\hat{s}) + (i \leftrightarrow j)] \qquad (1.38)$$

This effective luminosity is the number of parton i - parton j collisions per unit τ with subprocess energy $\hat{s} = \tau s$. For a elementary cross section

$$\hat{\sigma}(\hat{s}) = \frac{\kappa}{\hat{s}} \qquad (1.39)$$

with coupling strength κ, the total number of events/sec, N, is:

$$N(\text{events/sec}) = \mathcal{L}_{\text{hadrons}}(\tau\frac{d\mathcal{L}}{d\tau})_{\text{partons}}\hat{\sigma}(\hat{s}) \qquad (1.40)$$

where $\mathcal{L}_{\text{hadron}}$ is the hadron-hadron luminosity (measured in $cm^{-2} sec^{-1}$). Thus the combination

$$\frac{\tau}{\hat{s}}\frac{d\mathcal{L}}{d\tau} \qquad (1.41)$$

contains all the kinematic and parton distribution dependence of the rate. Hence this quantity can be used to make quick estimates of rates for various processes knowing only the coupling strength κ of the subprocess. This expression (Eq. 1.41) is shown for gg, $u\bar{u}$, $b\bar{b}$, and $t\bar{t}$ initial parton pairs in Figures 14-16 for the energies of the $S\bar{p}pS$ and Tevatron colliders. The corresponding figures for SSC energies are given in EHLQ (Figures 32-56).
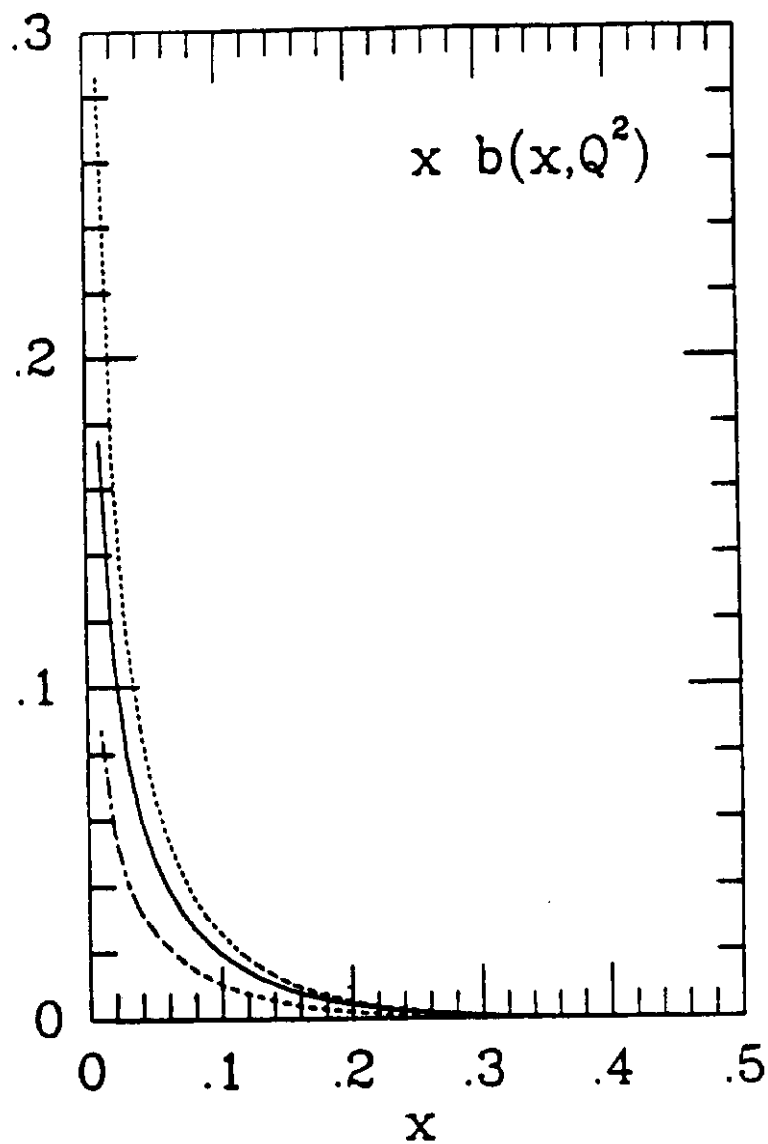
Figure 12: The bottom quark distribution, $xb(x, Q^2)$, as a function of x for various Q^2. The dot-dashed, solid, and dotted lines correspond to $Q^2 = 10^3$, 10^4, and 10^6 $(GeV)^2$ respectively.
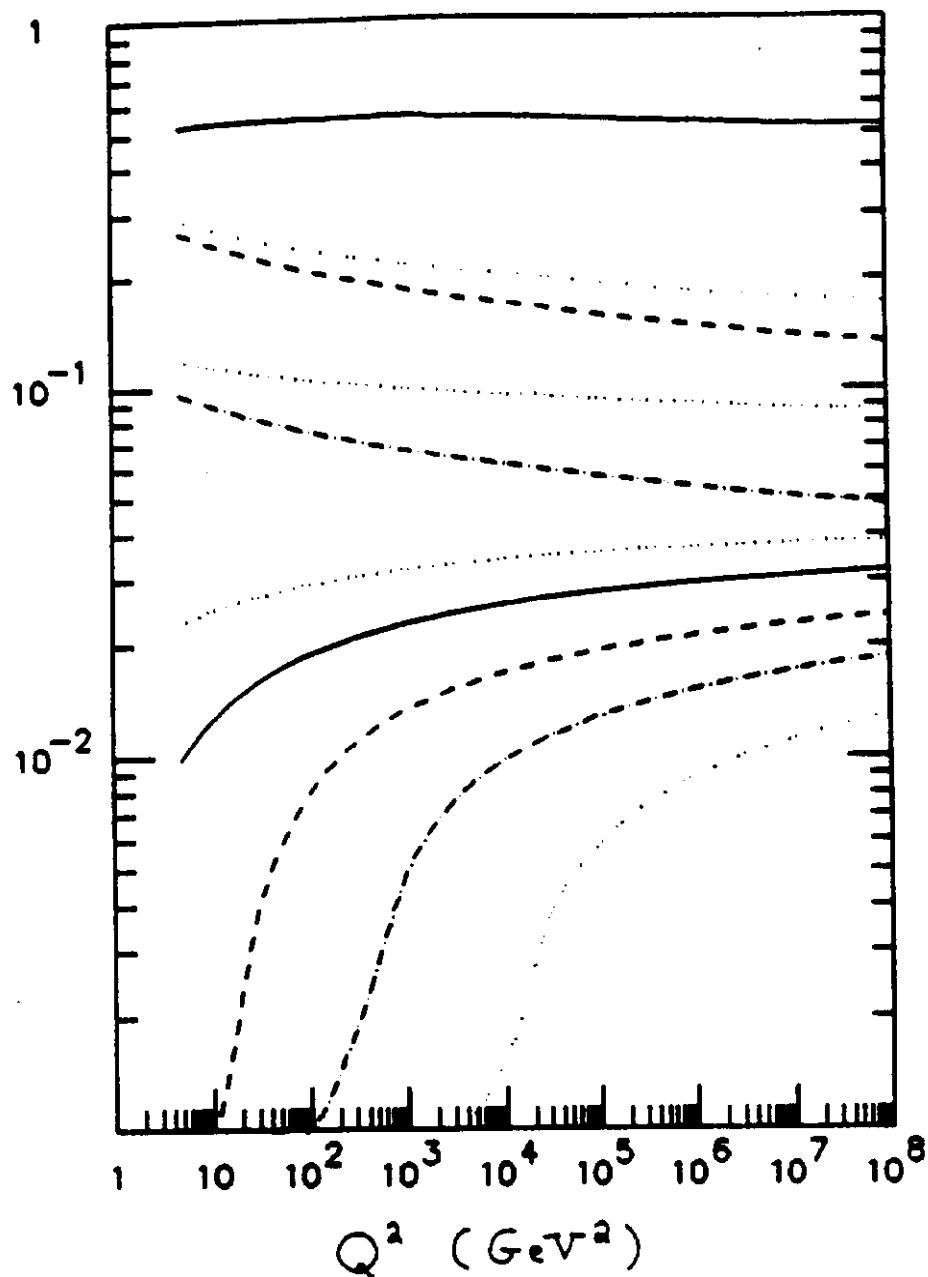
Figure 13: The fraction of the total momentum carried by each of the partons in the proton as a function of Q^2. From largest to smallest momentum fraction these partons are: gluon, up quark, up (valence only), down quark, down (valence only), antiup (or antidown) quark, strange quark, charm quark, bottom quark, and top quark.
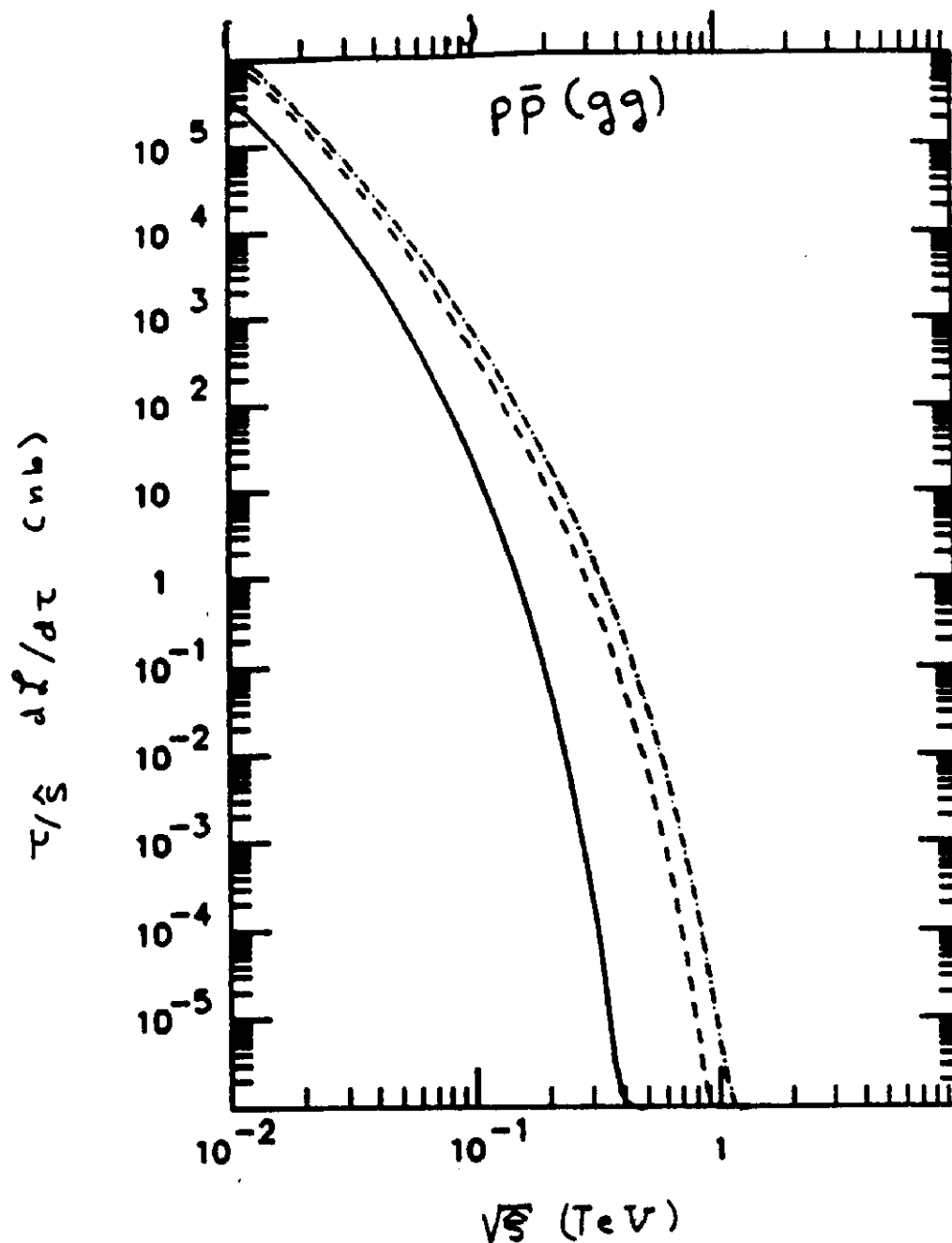
Figure 14: Quantity $(\tau/\hat{s})d\mathcal{L}/d\tau$ (in nb) for gg interactions in proton-antiproton collisions at energies: 630 GeV (solid line), 1.6 TeV (dashed line), and 2.0 TeV (dot-dashed line). $\sqrt{\hat{s}}$ is the subprocess energy (in TeV).

Figure 15: Quantity $(\tau/\hat{s})d\mathcal{L}/d\tau$ (in nb) for $u\bar{u}$ interactions in proton-antiproton collisions at energies: 630 GeV (solid line), 1.6 TeV (dashed line), and 2.0 TeV (dot-dashed line). $\sqrt{\hat{s}}$ is the subprocess energy (in TeV).
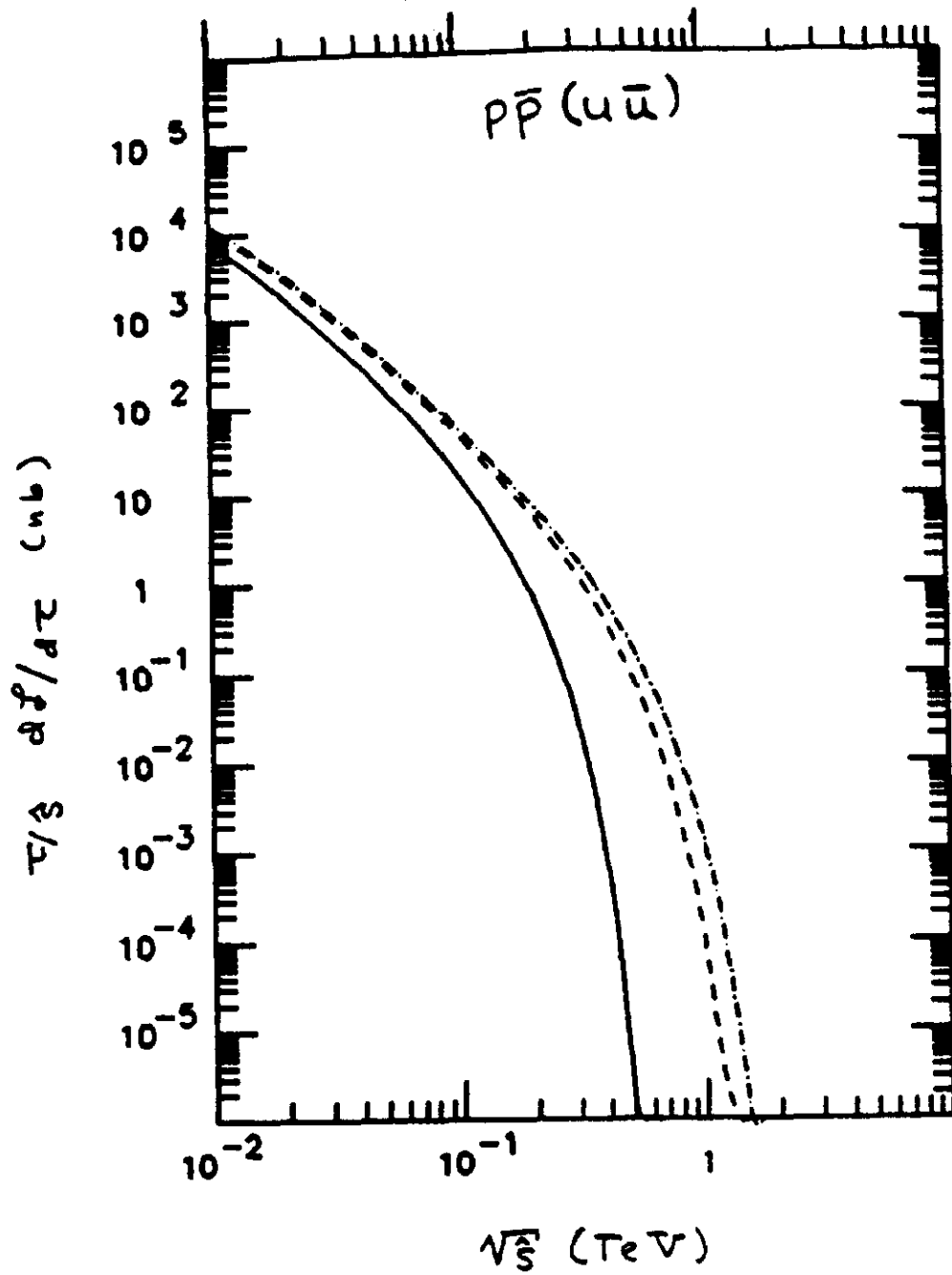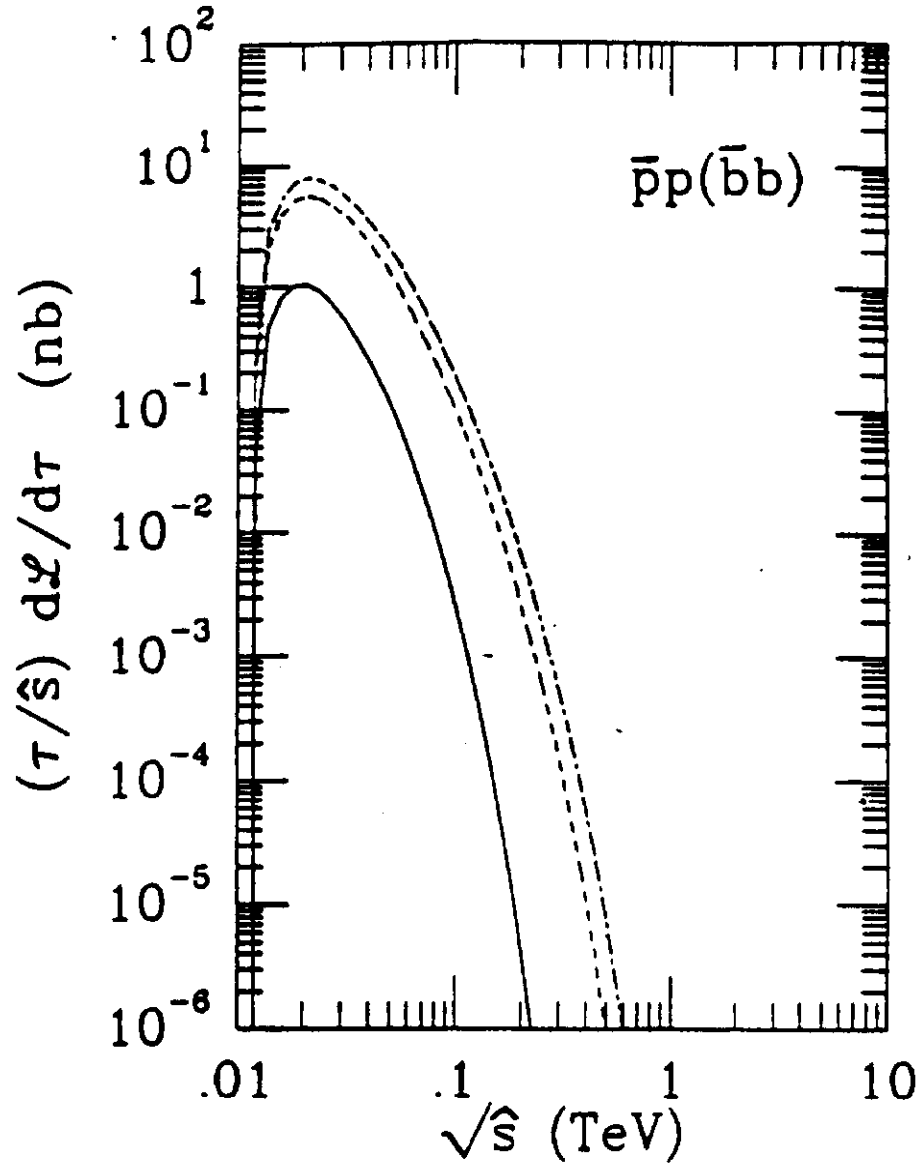
Figure 16: Quantity $(\tau/\hat{s})d\mathcal{L}/d\tau$ (in nb) for $b\bar{b}$ interactions in proton-antiproton collisions at energies: 630 GeV (solid line), 1.6 TeV (dashed line), and 2.0 TeV (dot-dashed line). $\sqrt{\hat{s}}$ is the subprocess energy (in TeV).

Finally, it is possible at high enough Q^2, to have substantial distributions for any elementary particles which couple to either quarks or gluons: For example, the luminosities for top quark-antiquark interactions is shown in Figure 17. An even more exotic example is the luminosity for electroweak vector boson pairs.[32] The quantity $(r/\hat{s})d\mathcal{L}/dr$ is shown for transverse and longitudinal $W^{\pm}$ and Z^0 bosons at $\sqrt{\hat{s}} = 40$ TeV in Figures 18(a) and 18(b) respectively. This property, that hadron collisions at high energies contain a broad spectrum of fundamental constituents as initial states in elementary subprocesses, is one of the most attractive features of using a hadron collider for the exploration of possible new physics at the TeV scale.

To summarize, the extraction of the elementary subprocesses from hadron-hadron collisions require knowledge of the parton distributions of the proton. By combining experimental data at low Q^2 and the evolution equations determined by perturbation theory in QCD we can obtain these distributions to sufficient accuracy at high energies to translate from the elementary subprocesses to estimates of experimental rates in hadron collisions. The evidence for this conclusion is:

- Cross sections obtained using different parametrizations (Set 1 and Set 2 of Eqs. 1.22-1.25) generally differ by less than 20 percent at SSC energies[1].

- The evolved gluon distribution $G(x, Q^2)$ is very insensitive to drastic modifications of the small x $(x < 10^{-2})$ behaviour at $Q_0^2 = (5\ GeV)^2$ where it is unknown experimental[1].

- Corrections to the lowest order Altarelli-Parisi evolution equations for $f_i(x, Q^2)$ due to $\ln(x)$ terms at small x and $\ln(1-x)$ terms at large x do not give important contributions to the distributions functions in the range of x and Q^2 relevant to new physics at either the present colliders or the SSC[33].
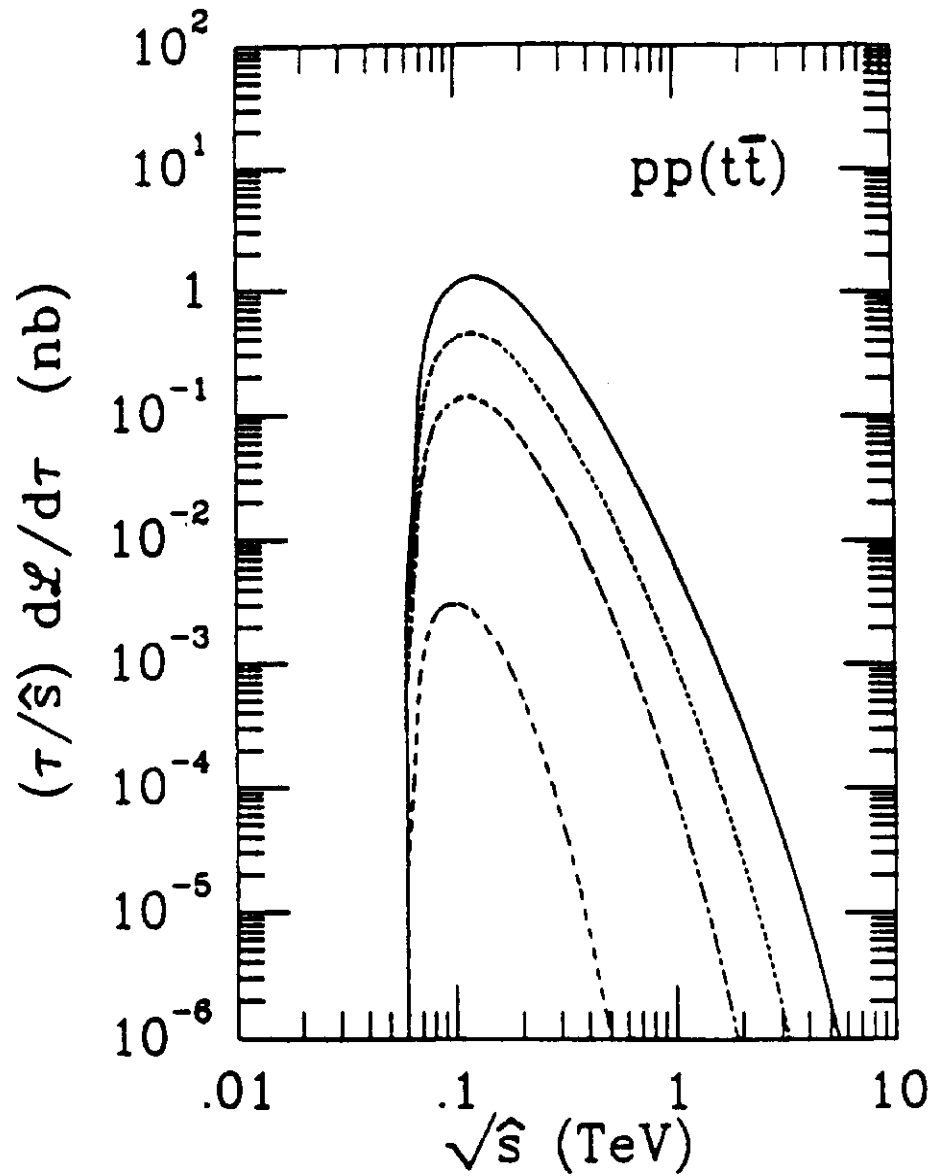
Figure 17: Quantity $(\tau/\hat{s})d\mathcal{L}/d\tau$ (in nb) for $t\bar{t}$ interactions in proton-proton collisions at energies: 2 TeV (dashed line), 10 TeV (dot-dashed line), 20 TeV (dotted line), and 40 TeV (solid line). $\sqrt{\hat{s}}$ is the subprocess energy (in TeV).
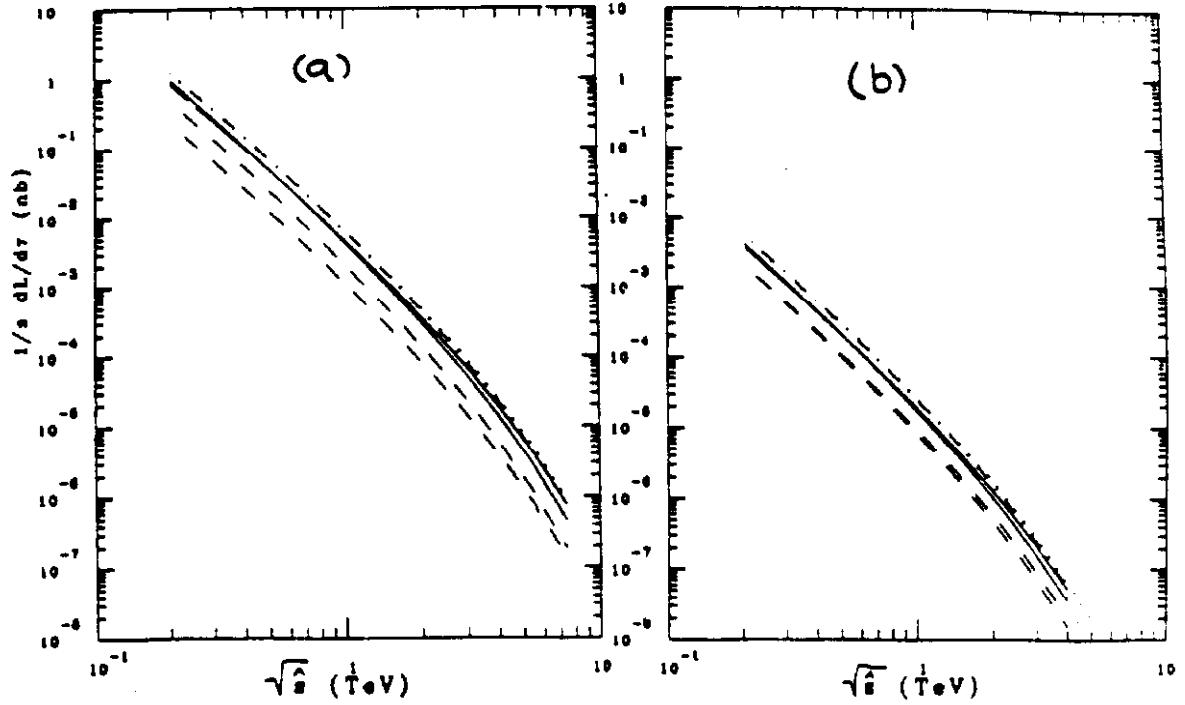
Figure 18: Quantity $(\tau/\hat{s})d\mathcal{L}/d\tau$ (in nb) for intermediate vector bosons interactions as a function of $\sqrt{\hat{s}}$ (in TeV) for proton-proton collisions at $\sqrt{s} = 40$ TeV. Transverse and longitudinal intermediate vector bosons are shown in Figures (a) and (b) respectively. In each figure, W^+W^-, W^+W^+, W^-Z^0, W^-W^-, and Z^0Z^0 pairs are denoted by dot-dashed, upper solid, lower solid, upper dashed, and lower dashed lines respectively. Figure from Ref. 32.

II. THE STRONG INTERACTIONS

This lecture is devoted to understanding the jet physics in hadron-hadron collisions in terms of the underlying QCD processes.

A. Two Jet Physics

Consider, first, the two to two parton scattering subprocess as shown in Figure 19.
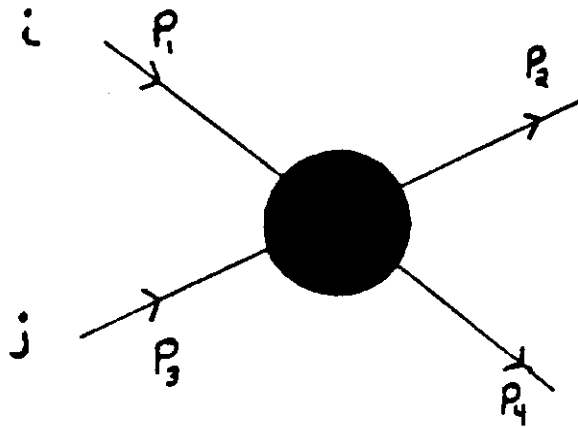

Figure 19: Two to two scattering process.

The invariants are:

$$\hat{s} = (p_1 + p_3)^2$$
$$\hat{t} = (p_1 - p_2)^2$$
$$\hat{u} = (p_1 - p_4)^2 \tag{2.1}$$

When $\hat{s}$ and $\hat{t}$ are both large the physical final state will consist of two jets. Two variables that will be very useful in describing the jet kinematics are:

- $y \equiv \frac{1}{2}\ln(\frac{E+p_{||}}{E-p_{||}})$, the jet rapidity. The relation between jet rapidity and angle of the jet relative to the beam direction is shown in Figure 20.
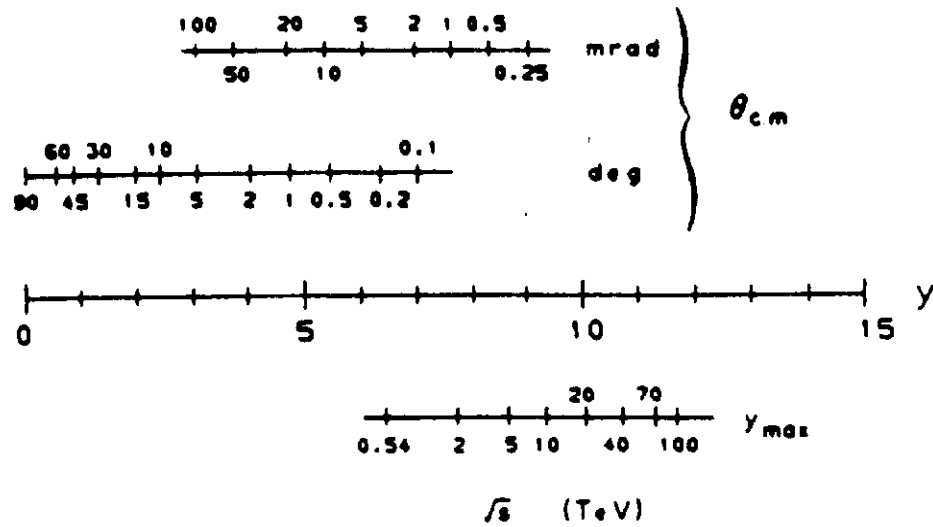
Figure 20: Correspondence of angles to the CM rapidity scale. Also shown is the maximum rapidity, $y_{max} = \ln(\sqrt{s}/M_{proton})$ accessible for light secondaries.

- $p_\perp$, the magnitude of the momentum of a jet perpendicular to the beam direction.

The differential cross section for incident hadrons a and b to produce a two jet final state with rapidities y_1 and y_2 and with given $p_\perp$ is

$$
\begin{aligned}
\frac{d^3\sigma}{dy_1 dy_2 dp_\perp} \;=\; & \frac{2\pi r \alpha_s^2}{\hat{s}^2} p_\perp \sum_{ij} \frac{1}{(1+\delta_{ij})} [f_i^{(a)}(x_a, Q^2) f_j^{(b)}(x_b, Q^2) |A_{ij}(\hat{s}, \hat{t}, \hat{u})|^2 \\
& +\; f_j^{(a)}(x_a, Q^2) f_i^{(b)}(x_b, Q^2) |A_{ij}(\hat{s}, \hat{u}, \hat{t})|^2]
\end{aligned}
\tag{2.2}
$$

where $f_i^{(a)}$ is the probability distribution function for the ith parton in the hadron a as discussed in the previous lecture. The sum is over all initial state quarks and/or gluons which can contribute and the cross section is summed over all final states which are not distinguishable experimentally. A crossed term must be included because parton 1 may have come from either hadron a or hadron b; and a symmetry factor is included to avoid overcounting in the case of identical partons in the initial state. Also, because the scale (Q^2) dependence of the distribution functions, it is necessary to know the appropriate value of Q^2 for the given subprocess. To give a complete determination of this quantity requires analysis beyond the Born approximation. A partial estimate of the one loop corrections has been done[34] which suggests $Q^2 = p_\perp^2/4$.

The final ingredient needed to determine the differential cross section is the Born approximation for the elementary subprocesses. The differential cross section for two to two parton scattering can be expressed as:

$$
\frac{d\hat{\sigma}}{d\hat{t}} = \frac{\pi \alpha_s^2}{\hat{s}^2} |A|^2
\tag{2.3}
$$

and the invariant matrix element squared, $|A|^2$, are listed in Table 1 for all the two to two processes[35]. All partons have been assumed to be massless.

In the subprocess CM frame the relationship between the scattering angle θ and $\hat{t}$ or $\hat{u}$ is

$$
\hat{t} = -\frac{\hat{s}}{2}(1 - \cos\theta)
$$

$$
\hat{u} = -\frac{\hat{s}}{2}(1 + \cos\theta)
\tag{2.4}
$$

Table 1: Two to two parton subprocesses. $|A|^2$ is the invariant matrix element squared. The color and spin indices are averaged (summed) over initial (final) states. All partons are assumed massless. The scattering angle in the center of mass frame is denoted θ.

Process	$|A|^2$	$\theta = \pi/2$
$q\,q' \to q\,q'$	$\dfrac{4}{9}\,\dfrac{\hat{s}^2 + \hat{u}^2}{\hat{t}^2}$	2.22
$q\,q \to q\,q$	$\dfrac{4}{9}\left(\dfrac{\hat{s}^2 + \hat{u}^2}{\hat{t}^2} + \dfrac{\hat{s}^2 + \hat{t}^2}{\hat{u}^2}\right) - \dfrac{8}{27}\,\dfrac{\hat{s}^2}{\hat{u}\hat{t}}$	3.26
$q\,\bar{q} \to q'\,\overline{q'}$	$\dfrac{4}{9}\,\dfrac{\hat{t}^2 + \hat{u}^2}{\hat{s}^2}$	0.22
$q\,\bar{q} \to q\,\bar{q}$	$\dfrac{4}{9}\left(\dfrac{\hat{s}^2 + \hat{u}^2}{\hat{t}^2} + \dfrac{\hat{t}^2 + \hat{u}^2}{\hat{s}^2}\right) - \dfrac{8}{27}\,\dfrac{\hat{u}^2}{\hat{s}\hat{t}}$	2.59
$q\,\bar{q} \to g\,g$	$\dfrac{32}{27}\,\dfrac{\hat{t}^2 + \hat{u}^2}{\hat{t}\hat{u}} - \dfrac{8}{3}\,\dfrac{\hat{t}^2 + \hat{u}^2}{\hat{s}^2}$	1.04
$g\,g \to q\,\bar{q}$	$\dfrac{1}{6}\,\dfrac{\hat{t}^2 + \hat{u}^2}{\hat{t}\hat{u}} - \dfrac{3}{8}\,\dfrac{\hat{t}^2 + \hat{u}^2}{\hat{s}^2}$	0.15
$g\,q \to g\,q$	$-\dfrac{4}{9}\,\dfrac{\hat{s}^2 + \hat{u}^2}{\hat{s}\hat{u}} + \dfrac{\hat{u}^2 + \hat{s}^2}{\hat{t}^2}$	6.11
$g\,g \to g\,g$	$\dfrac{9}{2}\left(3 - \dfrac{\hat{t}\hat{u}}{\hat{s}^2} - \dfrac{\hat{s}\hat{u}}{\hat{t}^2} - \dfrac{\hat{s}\hat{t}}{\hat{u}^2}\right)$	30.4

The third column in Table 1 gives the value of $|A|^2$ at 90^0 in the CM frame. Two features of these cross sections will be particularly important. First, by far the largest cross-section is for the process $gg \rightarrow gg$. Second, reactions in which initial parton type is preserved are considerably larger than those in which the final partons are different from the initial partons.

Using the structure functions of Set 2 determined in the last lecture and the sub-process cross section of Eq. 2.3, the single jet inclusive cross section at $\sqrt{s} = 540$ GeV is obtained from Eq. 2.1 simply by integrating over y_2. The single jet production rate can then be compared to the data from UA1[36,37] and UA2[38,39]. As shown in Figure 21, one obtains good agreement for $\Lambda = 290$ MeV and $Q^2 = p_\perp^2/4$ at rapidity $y = 0$ ($90°$ in hadron-hadron CM frame). Note that at low $p_\perp$ gluon-gluon scattering is dominant whereas at higher $p_\perp$ quark-gluon scattering dominates, and at the highest $p_\perp$ quark-quark scattering gives the leading contribution. Presently it is not possible to distinguish a light quark from a gluon jet experimentally; theoretical knowledge of which type of jet should be dominate at a given $p_\perp$ will be very helpful in finding their distinct experimental signature.

In the running at $\sqrt{s} = 540$ GeV there was a total integrated luminosity of about $100 nb^{-1}$. (One nanobarn (nb) is $10^{-33} cm^2$.) Thus if the minimum signal for jet study is 10 events/10GeV $p_\perp$ bin then the highest observable jet $p_\perp$ is about 100 GeV where the cross section becomes 10^{-2} nb.

In Figure 22 the data from UA2[40] is shown for both $\sqrt{s} = 540$ GeV and $\sqrt{s} = 630$ GeV along with our theoretical expectations.

Given the total running at $\sqrt{s} = 630$ GeV corresponds to an integrated luminosity of $\approx 400 nb^{-1}$, the maximum observable jet $p_\perp$ is ≈ 125 GeV/c.

If we extrapolate to SSC energies $\sqrt{s} = 40$ TeV, jets with very high $p_\perp$ will be observable. From EHLQ Fig.78, it is found that jets with $p_\perp \approx 4$ TeV/c are produced at the rate of 10 events per 10 GeV/c bin with an integrated luminosity 10^{40} cm^{-2}, about a year of running at the planned luminosity 10^{33} cm^{-2} sec^{-1}. The dominate two jet final states at various total transverse energy of the two jets $E_T \approx 2p_\perp$ is shown as a function of $\sqrt{s}$ for pp collisions in Figure 23. Also displayed are the values of E_T at which there be one jet event per bin of .01 $p_\perp$ for integrated luminosities of 10^{38} and 10^{40} cm^{-2} sec^{-1}. Notice that at $\sqrt{s} = 40$ TeV the quark-quark final states never dominates below these limiting E_T's even for integrated
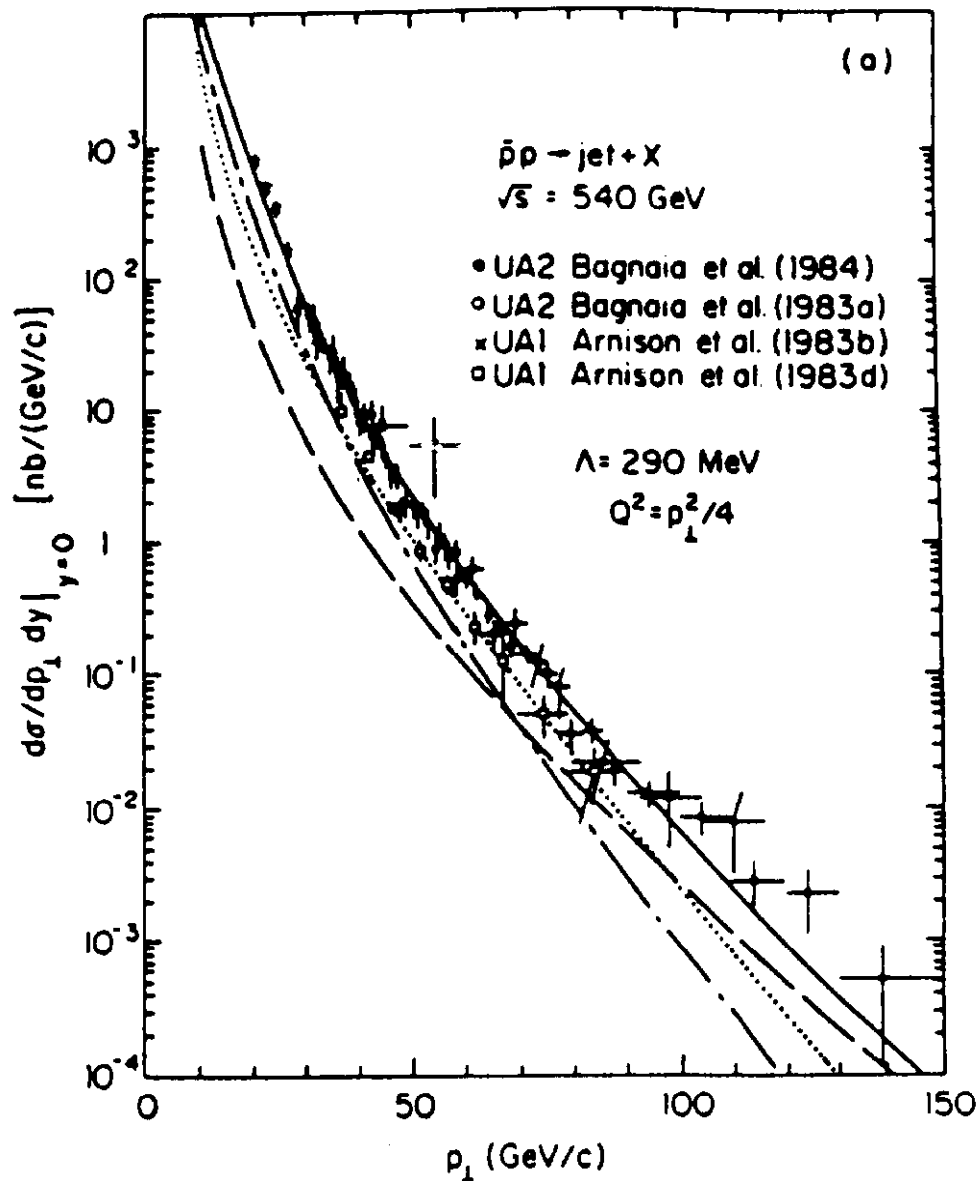
Figure 21: Differential cross section for jet production at $y = 0$ (90° CM frame) in $\bar{p}p$ collisions at 540 GeV according to the parton distributions of Set 2. The data are from Arnison et. al. (1983a is Ref. 36, 1983d is Ref. 37) and Bagnaia et.al. (1983b is Ref. 38, 1984 is Ref. 39) .
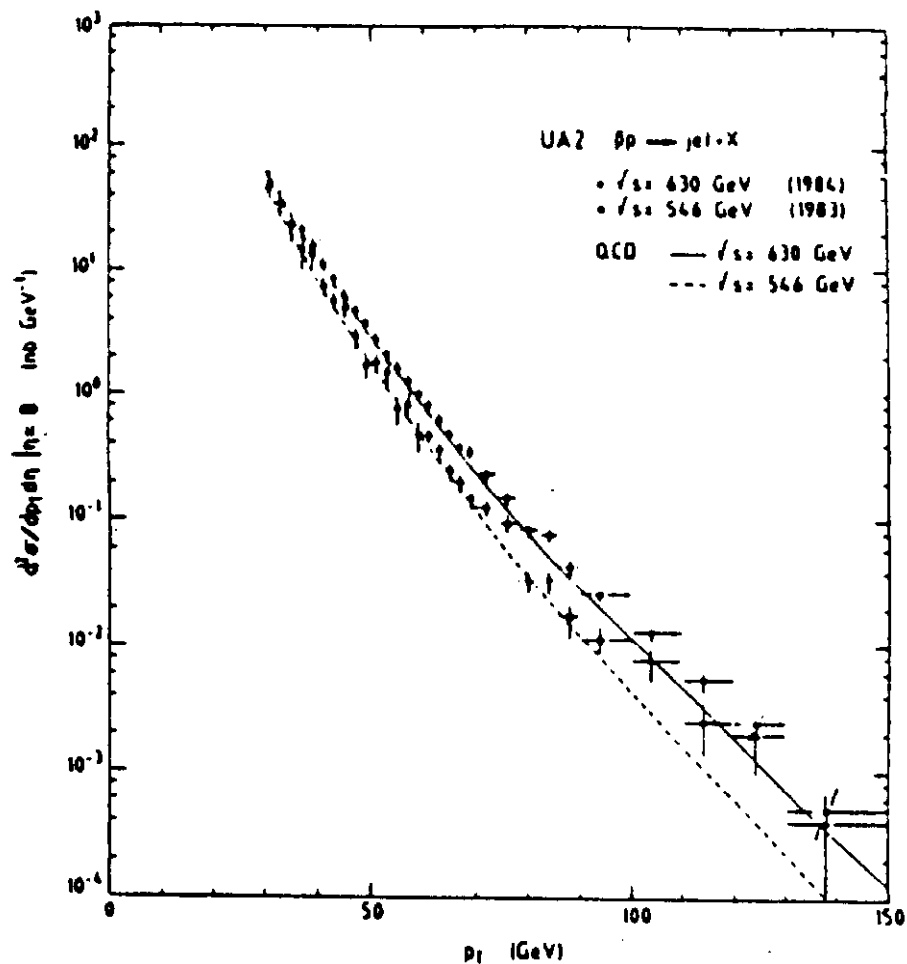
Figure 22: Inclusive jet production cross section (from UA2) at $y = 0$ as a function of the jet transverse momentum $p_\perp$. The data points for two collision energies 540 GeV (open circles) and 640 GeV (full circles) are compared to QCD predictions of Set 2 (solid lines). The additional systematic uncertainty ± 45 % in the data.[40]

luminosity of 10^{40}.

One can investigate the angular distributions for various processes as a function of the subprocess CM scattering angle. The scattering processes for lowest order QCD given in Table 1 exhibit a forward and backward peak which is due to the exchange of a vector particle and is familiar from QED. In fact defining a variable

$$\chi = \frac{(1 + \cos\theta)}{(1 - \cos\theta)} \tag{2.5}$$

a differential cross section behaving like

$$\frac{d\sigma}{d\cos\theta} \sim \frac{1}{(1 - \cos\theta)^2} \tag{2.6}$$

becomes

$$\frac{d\sigma}{d\chi} \sim \text{constant} . \tag{2.7}$$

Therefore to a good approximation the behaviour of $d\sigma/d\chi$ in lowest order perturbation theory is a constant. The expected angular distribution agrees well with the UA1 data[41] as shown in Figure 24.

B. Multijet Events

Multijet events are also observed. Most of these events are composed of three jets, an example from the UA1 data[41] is shown in Figure 25. There are also some four jet events; one example of a four jet event from the UA2 data[42] is shown in Figure 26. In this event the four jets emerge at equal angles in a plane perpendicular to the beam direction. Four jet events will not be considered further here, since the theoretical calculations for the two to four parton QCD processes are still in progress[43].

The three jet events arise from the two to three parton scattering subprocess as shown in Figure 27. One invariant is:

$$\hat{s} = (p_4 + p_5)^2 \tag{2.8}$$

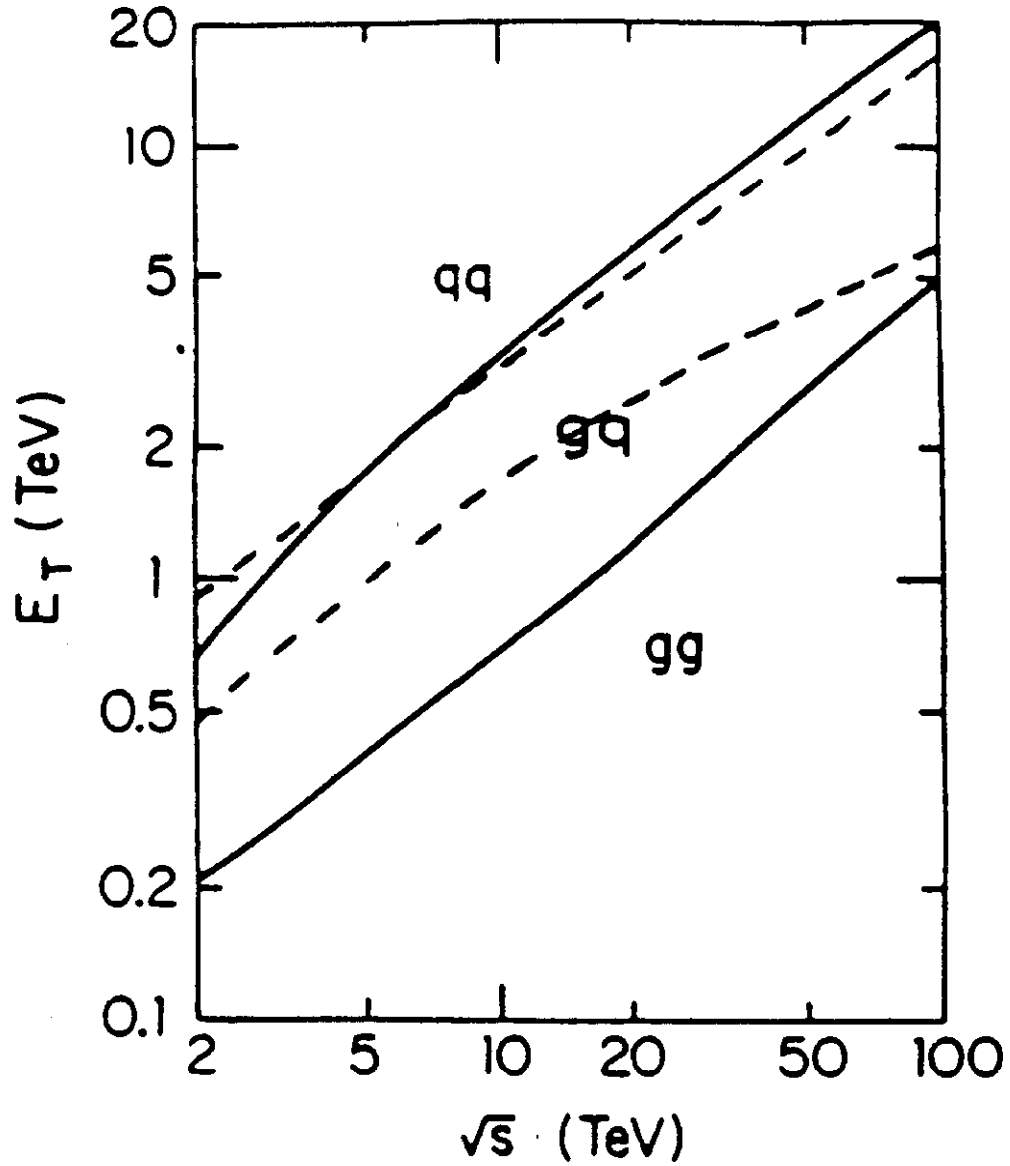In the subprocess CM frame $\vec{p_1} + \vec{p_2} + \vec{p_3} = 0$.

Figure 23: Parton composition of the two jet final states produced in pp collisions at 90° in the CM frame. The solid curves separate the regions in which gg, qg, and qq final states are dominant. The upper (lower) dashed line give maximum E_T for integrated luminosity of 10^{40} (10^{38}) cm^2.

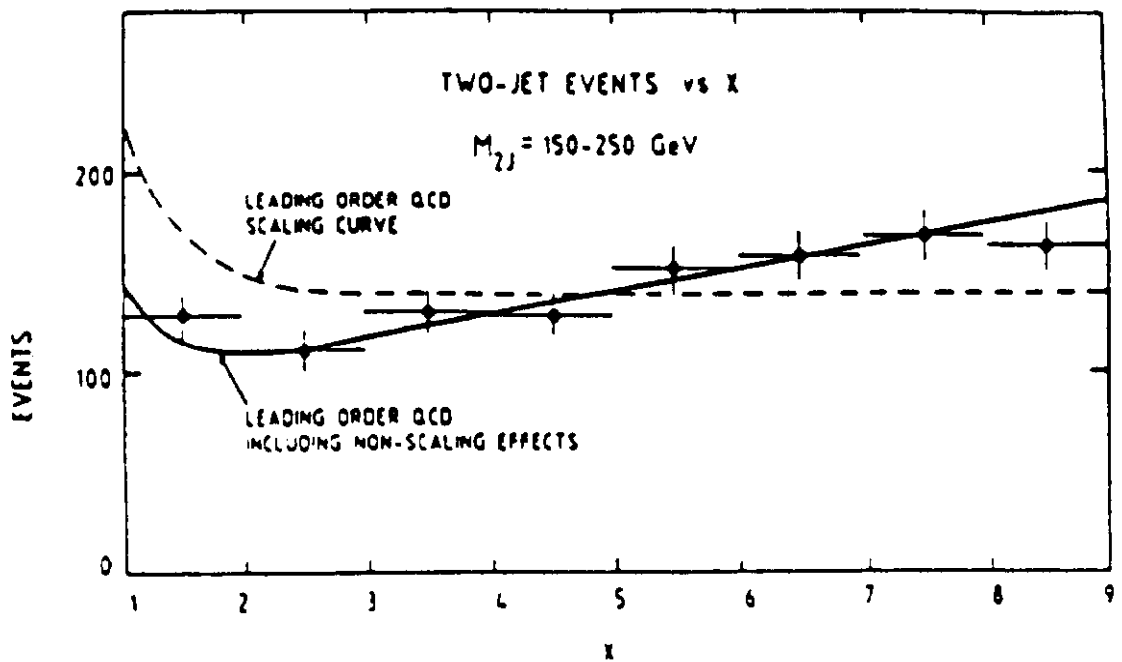Figure 24: The two jet angular distribution plotted versus $\chi = (1+\cos\theta)/(1-\cos\theta)$. The broken curve shows the leading order QCD prediction, and the solid curve includes scale breaking corrections. (From Ref. 41)
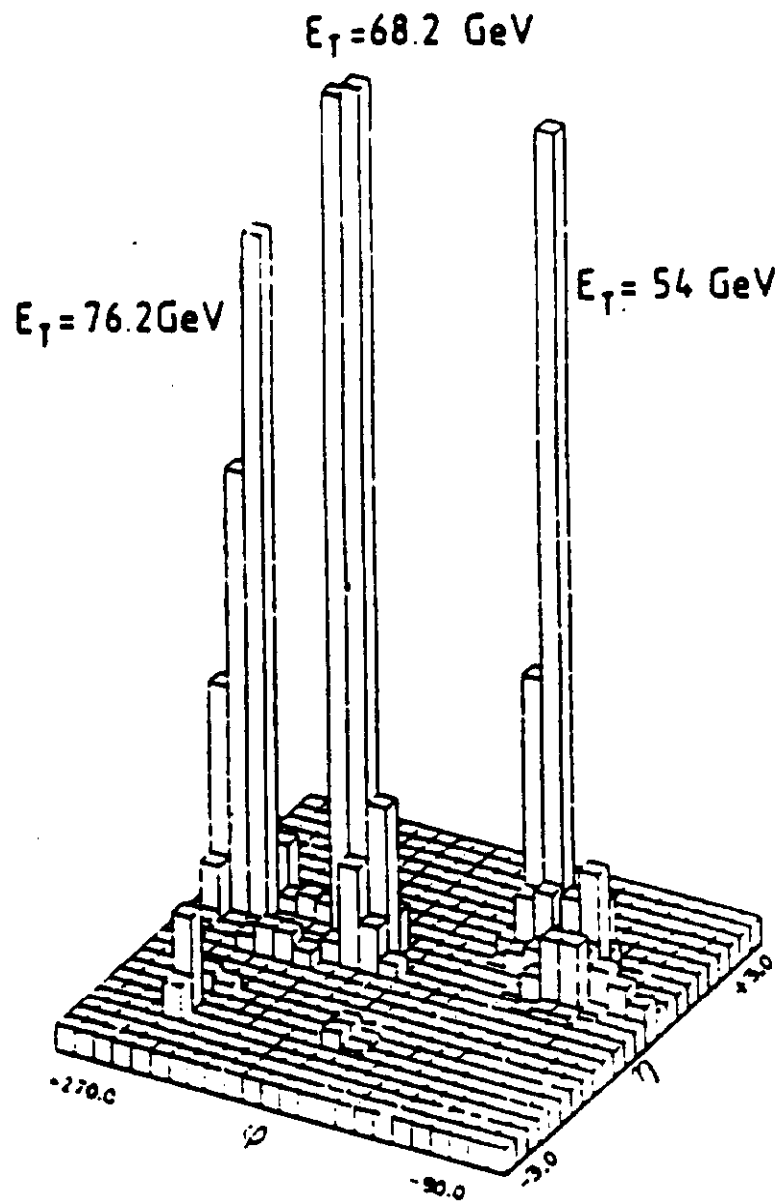
Figure 25: A typical LEGO plot for a three jet event from the UA1 data. (From Ref. 41)
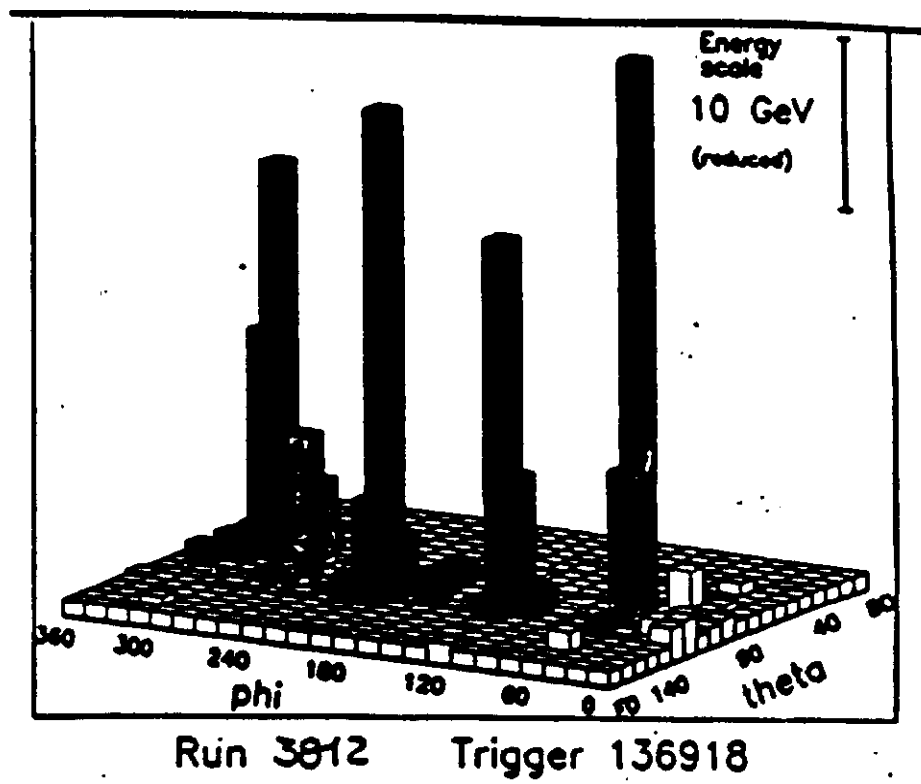
Figure 26: A LEGO plot for a four jet event observed in the UA2 data. (From Ref. 42)
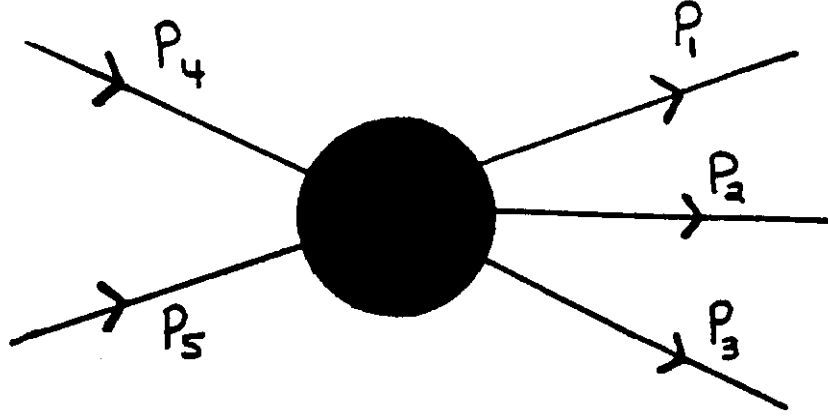
Figure 27: Two to three scattering process

The kinematics is determined in terms of five variables in addition to the total energy of the subprocess $\sqrt{\hat{s}}$. Three of these variables, $\hat{x}_i$ i=1,2,3, are the fraction of one half the CM energy taken by parton i in the final state; that is, $E_i = \hat{x}_i\sqrt{\hat{s}}/2$. Transverse momentum conservation ensures that $0 \leq \hat{x}_i \leq 1$, and overall energy conservation requires $\sum \hat{x}_i = 2$. The other variables are chosen to be θ, the angle of the plane formed by the final state partons with the beam direction; and ϕ, the azimuthal orientation of this plane with respect to the beam axis. Let

$$y_{boost} = (y_1 + y_2 + y_3)/3 \tag{2.9}$$

then the differential cross-section for this process can be written as

$$\frac{d\sigma}{d\hat{x}_1 d\hat{x}_2 dy_{boost} d\sqrt{\hat{s}} d\Omega} = \frac{\alpha_s^3(Q^2)\tau}{8\pi\sqrt{\hat{s}}} \sum_{ij} \frac{1}{1+\delta_{ij}} [f_i^{(a)}(x_a, Q^2) f_j^{(b)}(x_b, Q^2) |A_{ij}(2 \to 3)|^2$$

$$+ (i \leftrightarrow j)] \tag{2.10}$$

where

$$\tau = \frac{\hat{s}}{s} \tag{2.11}$$

$$x_a = \sqrt{\tau} e^{y_{boost}} \tag{2.12}$$

$$x_b = \sqrt{\tau}e^{-y_{boost}} \tag{2.13}$$

$$Q^2 = \hat{s}/4 . \tag{2.14}$$

and $|A_{ij}(2 \to 3)|^2$ is the absolute square of the invariant amplitudes computed by Berends, et. al.[44].

For the symmetric configuration, $\hat{x}_i = 2/3$ for $i = 1, 2, 3$, $y_{boost} = 0$ and $\theta = 0$, the expected cross section is given in Figure 28 for $\sqrt{s} = 540$ GeV. Even at the highest $p_\perp$ shown the three quark jet final state does not dominate.

Instead of a detailed analysis of the kinematics for multi-jet processes it is more useful and instructive to do a simple theoretical calculation for a particular process. One of the most straightforward is the $gg \to ggg$ which has been computed by Berends et al.[44]. Defining a symmetric set of k_i for $i = 1, ..., 5$ from the momenta of Figure 27 by:

$$k_3 = -p_1 \quad k_4 = -p_2 \quad k_5 = -p_3 \tag{2.15}$$

$$k_1 = p_5 \quad k_2 = p_4 \tag{2.16}$$

the invariant amplitude squared for the two to three process is:

$$|A|^2_{2-3} = \frac{27}{640} \frac{\sum_{m<n} k_{mn}^4}{\prod_{m<n} k_{mn}} \sum_{perms} (12345) \tag{2.17}$$

where:

$$k_{mn} = (k_m + k_n)^2/2 = k_m \cdot k_n \tag{2.18}$$

for gluons on the mass shell, and

$$(12345) = k_{12}k_{23}k_{34}k_{45}k_{51} \tag{2.19}$$

In the limit in which two of the final gluons become collinear (for example, 4 and 5), the amplitude simplifies considerably. In this case, k_4 and k_5 become parallel and may be written as

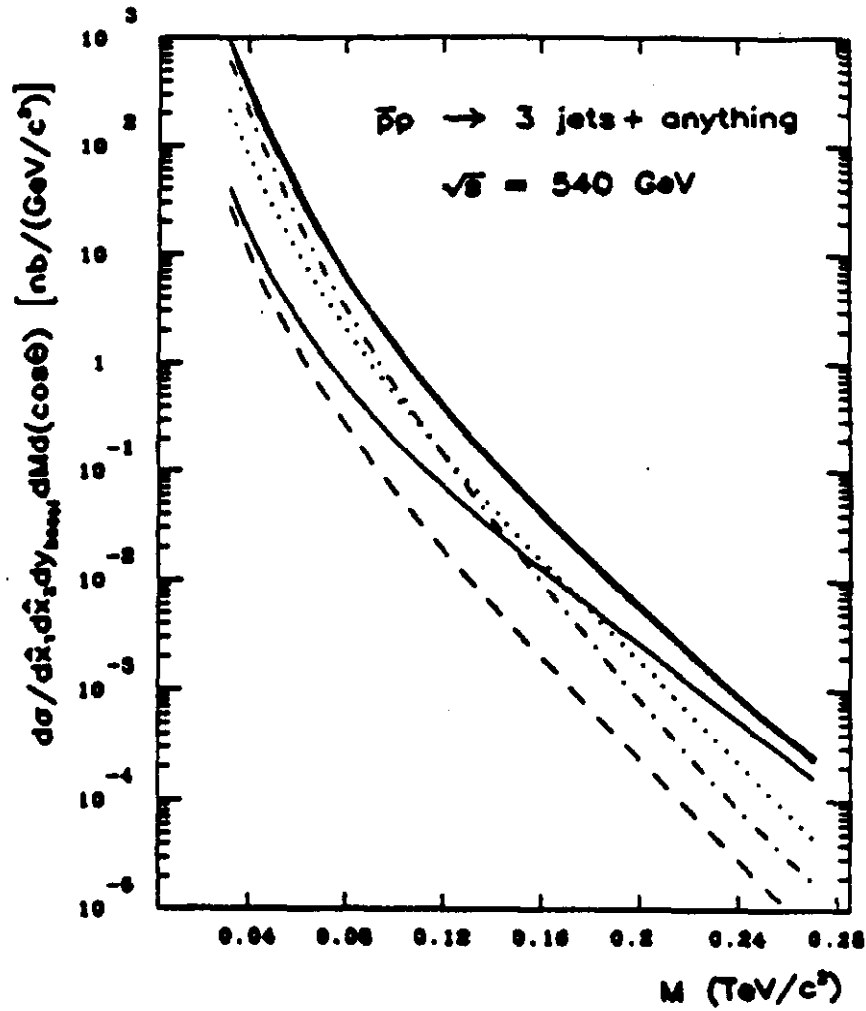$$k_4 = (1 - z)k \quad and \quad k_5 = zk \tag{2.20}$$

Figure 28: Differential cross section (thick line) for symmetric three jet production in $\bar{p}p$ collisions at 540 GeV, according to the distributions of Set 2. The ggg (dot-dashed line), ggq (dotted line), gqq (thin line), and qqq (dashed line) components are shown serarately.

where k is the total momentum of these two gluons and x is the fraction of this momentum which is carried by gluon 5. Then the leading behaviour of k_{45} is

$$k_{45} = x(1-x)k^2 \to 0. \tag{2.21}$$

The dominant contribution to the squared amplitude (Eq. 2.15) may now be calculated as follows. First the denominator is expanded to give the leading pole behaviour of $|A|^2_{2\to3}$

$$\Pi_{m<n}k_{mn} \to k_{12}k_{13}k_{23}[x(1-x)]^4 k^2 (k\cdot k_1 k\cdot k_2 k\cdot k_3)^2 \tag{2.22}$$

and the leading terms in the numerator are retained

$$\begin{aligned}
\sum_{\text{perms}} (12345) &\to \sum_{\text{perms}1,2,3} 10x^2(1-x)^2[(k\cdot k_1)(k\cdot k_3)^2(k\cdot k_2)(k_1\cdot k_2)] \\
&= 20x^2(1-x)^2(k\cdot k_1)(k\cdot k_2)(k\cdot k_3)[k_{12}(k\cdot k_3) \\
&\quad + k_{23}(k\cdot k_1) + k_{31}(k\cdot k_2)]
\end{aligned} \tag{2.23}$$

and

$$\sum_{m<n} k^4_{mn} \to k^4_{12} + k^4_{23} + k^4_{31} + (x^4 + (1-x)^4)[(k\cdot k_1)^4 + (k\cdot k_2)^4 + (k\cdot k_3)^4] \tag{2.24}$$

where the expressions in Eqs. 2.18 and 2.19 have been used for k_4, k_5, and k_{45}. Equation 2.22 may be simplified to give:

$$(k^4_{12} + k^4_{23} + k^4_{31})[1 + x^4 + (1-x)^4] \tag{2.25}$$

where $k\cdot k_i = k_m \cdot k_n$ (i,m,n are cyclic permutations of 1,2,3) since $\sum^3_{i=1} k_i + k = 0$. Now the $2 \to 3$ gluon process is rewritten to give

$$|A|^2_{2\to3} \to \frac{27}{32} \frac{[1 + x^4 + (1-x)^4]}{x^2(1-x)^2 k^2} \frac{(k^4_{12} + k^4_{23} + k^4_{31})}{k^2_{12}k^2_{23}k^2_{31}}[k^2_{12} + k^2_{23} + k^2_{31}] \tag{2.26}$$

The above squared amplitude may be compared with the $2 \to 2$ gluon process (whose squared amplitude is given in Table 1) by reexpressing the momenta k_1, k_2, k_3, and k of Eq. 2.24 in terms of the invariants of the $2 \to 2$ process:

$s = 2k_1 \cdot k_2$, $t = 2k_2 \cdot k_3$, and $u = 2k_1 \cdot k_3$. We have:

$$16(k_{12}^4 + k_{23}^4 + k_{31}^4) = s^4 + t^4 + u^4 = 2(s^2 t^2 + t^2 u^2 + u^2 s^2) \tag{2.27}$$

and

$$4(k_{12}^2 + k_{23}^2 + k_{31}^2) = s^2 + t^2 + u^2 = -2(st + tu + us) \tag{2.28}$$

Thus the factors containing the momenta k_{ij} in Eq. 2.24 become:

$$4\left[3 - \frac{tu}{s} - \frac{us}{t} - \frac{st}{u}\right] = \frac{8}{9}|A|_{2\to 2}^2 \tag{2.29}$$

Therefore, the leading pole behaviour of the $2 \to 3$ squared amplitude as two gluons (4 and 5 here) become collinear is given in terms of the $2 \to 2$ process by:

$$|A|_{2\to 3}^2 \to |A|_{2\to 2}^2 \frac{1}{s_{45}}\left(3\left[\frac{x}{1-x} + \frac{(1-x)(1+x^2)}{x}\right]\right) \tag{2.30}$$

where $s_{45} = 2x(1-x)k^2$. This equation is represented symbolically in Figure 29.

Thus the final result is that the leading behaviour of the two to three gluon scattering process as any two gluons become collinear is given by the product of: (1) The associated two to two process with the two collinear gluons being replaced by one on shell (massless) gluon with momentum, k , equal to the sum of their momenta, $k_4 + k_5$; (2) The propagator pole $1/s_{45}$, and (3) The Altarelli-Parisi (A-P) splitting function (see eq. 1.32) for $g \to gg$, i.e. the probability for a gluon to splitting into two carrying fractions x and 1-x respectively of the initial gluon momentum.

This result is a general feature of all the higher order processes in QCD, the leading behaviour of the N parton process as two parton momentum become collinear is given in terms of the associated N-1 parton process, a pole containing the singularity, and the relevant A-P splitting function. Since the amplitudes of QCD parton processes have only been calculated for $N < 4$ (even in tree approximation), Monte Carlo calculations of multijet processes in hadron collisions have taken advantage of the relation Eq. 2.28 to express the leading pole approximation to the N parton process in terms of the $2 \to 2$ process and the quark and gluon splitting functions. In fact, this approximation is then used everywhere even used outside of its range of validity; for example, for three jet events in which no two of the jets are collinear.
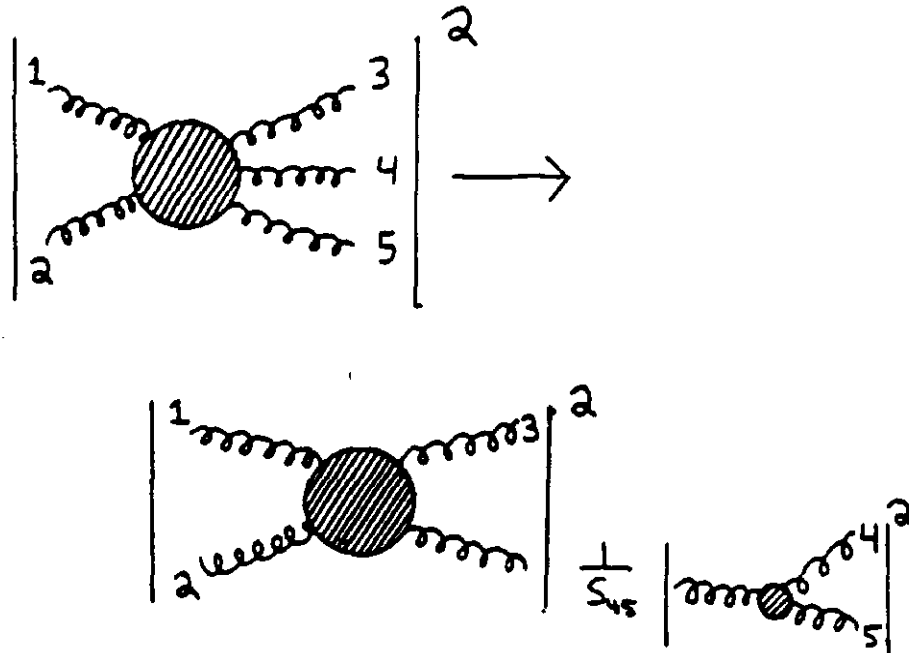
Figure 29: The leading pole behaviour of the 2 → 3 gluon process as two gluons become collinear. s_{45} is the propagator denominator for a gluon of momentum $k = k_4 + k_5$ and the squared vertex factor is exactly the Altarelli-Parisi splitting function for the gluon.

The error made in this approximation varies with the values of the invariants (i.e. $\hat{s}$, $\hat{t}$, $\hat{u}$ etc.) but is generally less that a factor of two[45].

It is an easy exercise to show that if one starts with the $gg \rightarrow ggg$ amplitude squared and then lets one of the momenta of the final gluons approach zero, that the result is again proportional to the $gg \rightarrow gg$. The remaining factor is just the infrared correction to the $gg \rightarrow gg$ process and is again given by the gluon propagator in this limit times the appropriate splitting function.

C.   Heavy Quark Production - The Top Quark

In addition to the jet structure of the strong interactions, there is another aspect of hadron physics of great current interest-- heavy quark production and, in particular, top quark production. The top quark is the only missing constituent of the three generations of the standard model. Heavy quarks can be produced in lowest order QCD perturbation theory through both the gg subprocesses and the $q\bar{q}$ subprocesses shown in Figure 30. The differential cross section for the gg production mechanism is given by:

$$\frac{d\hat{\sigma}}{d\hat{t}}(gg \rightarrow Q\overline{Q}) = \frac{\pi\alpha_s^2}{8\hat{s}^2}(\frac{6}{\hat{s}^2}(\hat{t} - m^2)(\hat{u} - m^2) + [(\frac{4}{3}\frac{(\hat{u} - m^2)}{(\hat{t} - m^2)}$$
$$-\frac{8}{3}\frac{m^2(\hat{t} + m^2)}{(\hat{t} - m^2)^2} + 3\frac{(\hat{t} - m^2)(\hat{u} - m^2) + m^2(\hat{u} - \hat{t})}{\hat{s}(\hat{t} - m^2)})$$
$$+(\hat{t} \leftrightarrow \hat{u})] - \frac{m^2(\hat{s} - 4m^2)}{3(\hat{t} - m^2)(\hat{u} - m^2)}) \tag{2.31}$$

where m is the heavy quark mass. The $q\bar{q}$ mechanism is less important since the quark-quark luminosities don't dominate at subenergies which give reasonable event rates (see Fig. 23) and because the color factors in the cross section are smaller than for gluon production. The differential cross section for $q\bar{q}$ production is given by:

$$\frac{d\hat{\sigma}}{d\hat{t}}(q\bar{q} \rightarrow Q\overline{Q}) = \frac{4\pi\alpha_s^2}{9\hat{s}^2}[\frac{(\hat{t} - m^2)^2 + (\hat{u} - m^2)^2 + 2m^2\hat{s}}{\hat{s}^2}] \tag{2.32}$$

Another mechanism for producing heavy quarks, one which is especially important at the $S\bar{p}pS$ and the Tevatron, is decay of the weak vector bosons $W^\pm$ and Z^0. A full discussion of electroweak processes will be given in the next lecture.
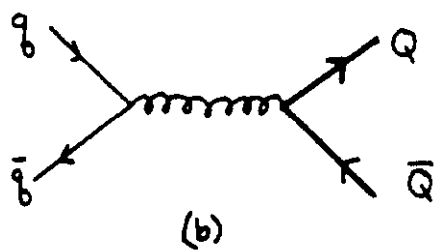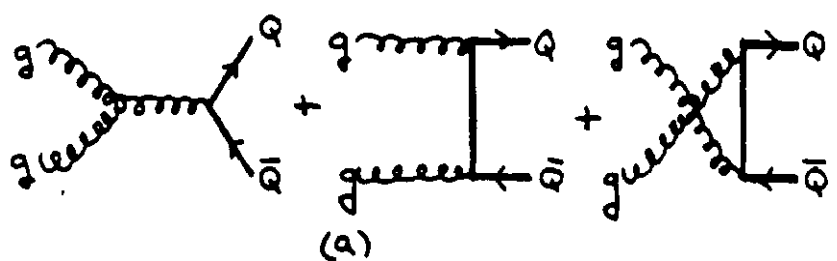
Figure 30: Lowest order Feynman diagrams for the process (a) $gg \rightarrow Q\overline{Q}$ and (b) $q\overline{q} \rightarrow Q\overline{Q}$

The relevant lowest order diagrams are shown in Figure 31. The charged W's are produced by $u\bar{d}$ and $d\bar{u}$ initial states whereas the neutral boson Z is produced by $u\bar{u}$ and $d\bar{d}$ initial states.

For the top quark production at the $S\bar{p}pS$ or even the Tevatron, only real production of the weak bosons and subsequent decay to top quarks is significant. Away from the W or Z pole the addition power of α_{EM} makes the production rates negligible. To calculate the rate of top quark production associated with real weak boson production we must multiply the weak boson production rate by the branching ratio into a final state containing a top quark. The phase space factor for the final state containing a top quark, is given by

$$\frac{2p_W}{m_W} = \sqrt{[1 - \frac{(m_t + m_b)^2}{m_W^2}][1 - \frac{(m_t - m_b)^2}{m_W^2}]} \qquad (2.33)$$

for the $W^\pm$ and

$$\frac{2p_Z}{m_Z} = \sqrt{[1 - \frac{4m_t^2}{m_Z^2}]} \qquad (2.34)$$

for the Z^0.

The various contributions to the total cross section for heavy quark (top) production as a function of quark mass is shown in Figure 32 for $\sqrt{s} = 630$ GeV in $\bar{p}p$ collisions. The gluon production contribution drops rapidly as the top quark mass increases, while the W^+ contribution is nearly flat up to the phase space factor above (Eq. 2.31) for top quark masses low enough to be associated with the decays of real $W^\pm$ and it drops precipitously as the W^+ mass is reached and only virtual W^+ production is possible. The Z boson contribution is always small compared to the W contribution. Gluon production dominates for $m_t < 40$ GeV; while at higher (observable) m_t, W^+ production dominates.

D.   A Higher Order QCD Process

As a final example of multijet processes, it is instructive to consider the next order QCD contribution to heavy quark production. For example, a typical reaction would be $gg \to g\bar{Q}Q$, which is suppressed by an additional factor of α_s relative to the lowest order process (α_s^2). For $\alpha_s = .1$, we would naively expect the higher order
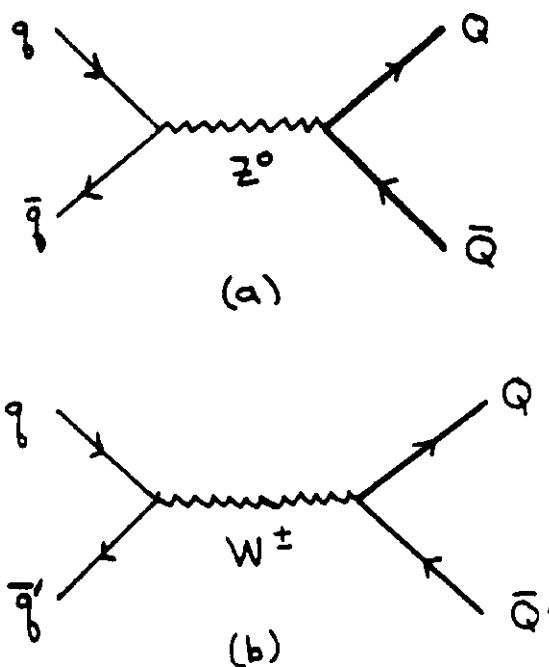
Figure 31: Lowest order Feynman diagrams for the production of (a) heavy quark pairs via a real or virtual Z^0 intermediate state, and (b) a heavy quark and a light quark via a real or virtual $W^\pm$ intermediate state.
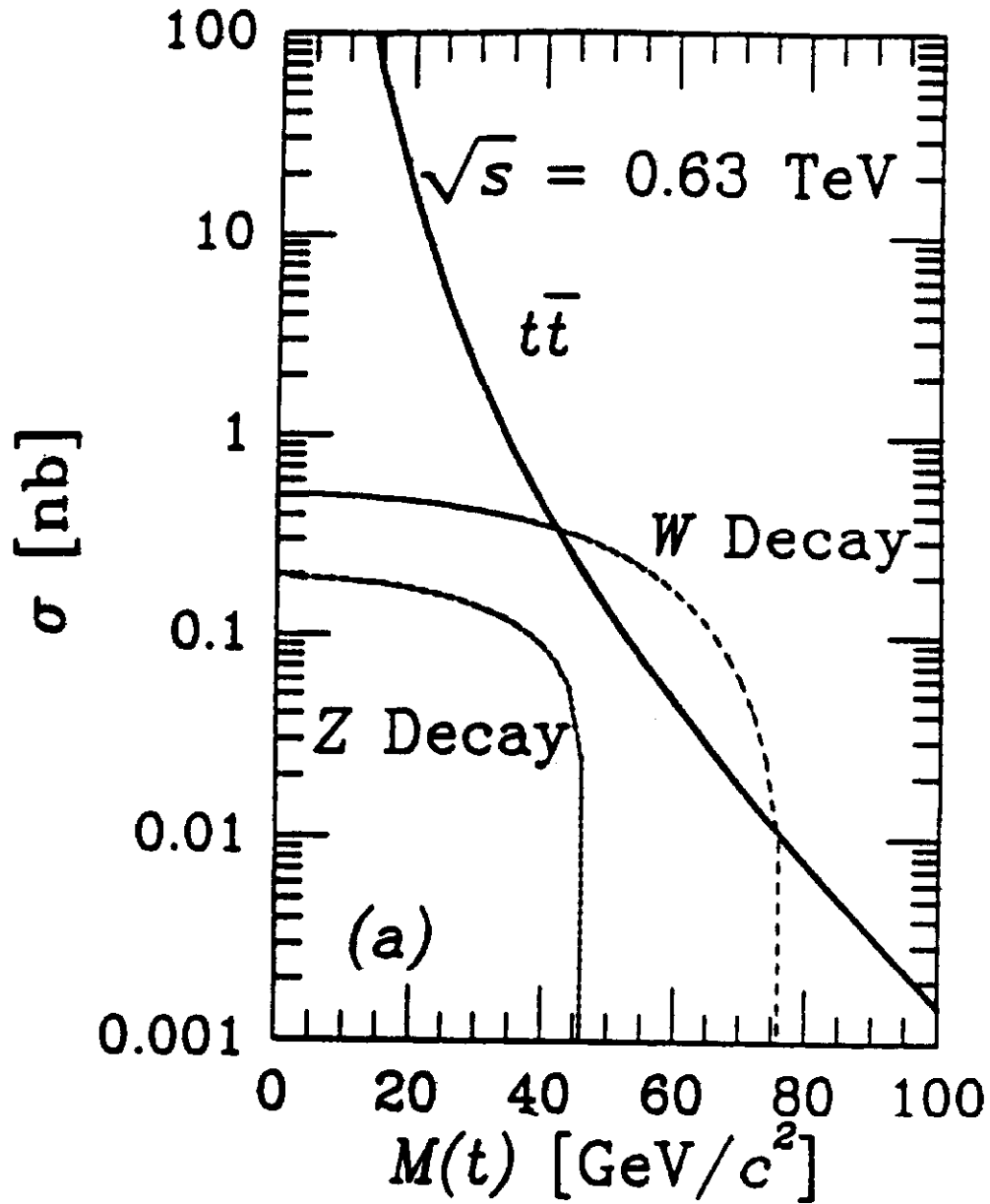
Figure 32: Cross sections for production of t or $\bar{t}$ quarks in $\bar{p}p$ collisions at $\sqrt{s} = 630$ GeV as a function of the mass of the heavy quark. The gluon production, W decay, and Z decay contributions are shown by solid, dashed, and dotted lines respectively.

terms to be down by a factor of ten from the lowest order processes. Although this process has a different topology than the simple process $gg \to \overline{Q}Q$, it will contribute to inclusive top production. This process can be analyzed in the leading pole approximation as in the $gg \to ggg$ process discussed in Section 2.2. When the $\overline{Q}Q$ invariant mass, $\sqrt{s_{\overline{Q}Q}}$, although large, is assumed to be small compared with the total energy of the subprocess, $\sqrt{s}$; then, we obtain the following expression for the subprocess cross section:

$$\sigma(a + b \to Q + \overline{Q} + c) \approx \sigma(a + b \to g + c) \int \frac{ds_{\overline{Q}Q}}{s_{\overline{Q}Q}} dx \frac{\alpha_s}{2\pi} P_{g \to Q\overline{Q}}(x) \qquad (2.35)$$

which is shown schematically in Figure 33. Here the splitting function for a gluon into quark-antiquark is given by:

$$P_{g \to Q\overline{Q}}(x) = \frac{1}{2}[x^2 + (1 - x)^2] \qquad (2.36)$$

In most of the relevant kinematic range, this approximation to the exact $gg \to g\overline{Q}Q$ process is good to within 20 percent.

To see the relative contribution to heavy quark production one can simple calculate the ratio of this $2 \to 3$ cross section to that for the $gg \to \overline{Q}Q$ process. Roughly for production at 90° in the CM frame one obtains:

$$\frac{\sigma(gg \to gQ\overline{Q})}{\sigma(gg \to Q\overline{Q})} = \frac{\sigma(gg \to gg)}{\sigma(gg \to Q\overline{Q})} \frac{\alpha_s}{3\pi} \ln\left(\frac{\hat{s}}{4m_Q^2}\right) \qquad (2.37)$$

Estimating each the terms we find that, even though there is the $\frac{\alpha_s}{3\pi} \approx .03$ suppression, the $gg \to gQ\overline{Q}$ cross section is considerably larger than the lower order $gg \to Q\overline{Q}$ process because the basic $gg \to gg$ cross section is larger than the $gg \to q\overline{q}$ cross section by a factor of 104. Aside from a larger QCD color factor for two gluon final state, there some dynamic cancellations between terms for the quark-antiquark final state. The logarithmic term in Eq. 2.35 adds a factor of 2-4, leading to a total factor of 5-10 for the ratio of cross sections for production of heavy quark-antiquark plus energetic gluon to heavy quark-antiquark alone. The first to point out this fact was Z. Kunszt, et.al.[46]. It is important to point out that this is not a breakdown of QCD perturbation theory at high energy. These are two physically distinct processes. This exercise does however illustrate that naive α_s power counting is not
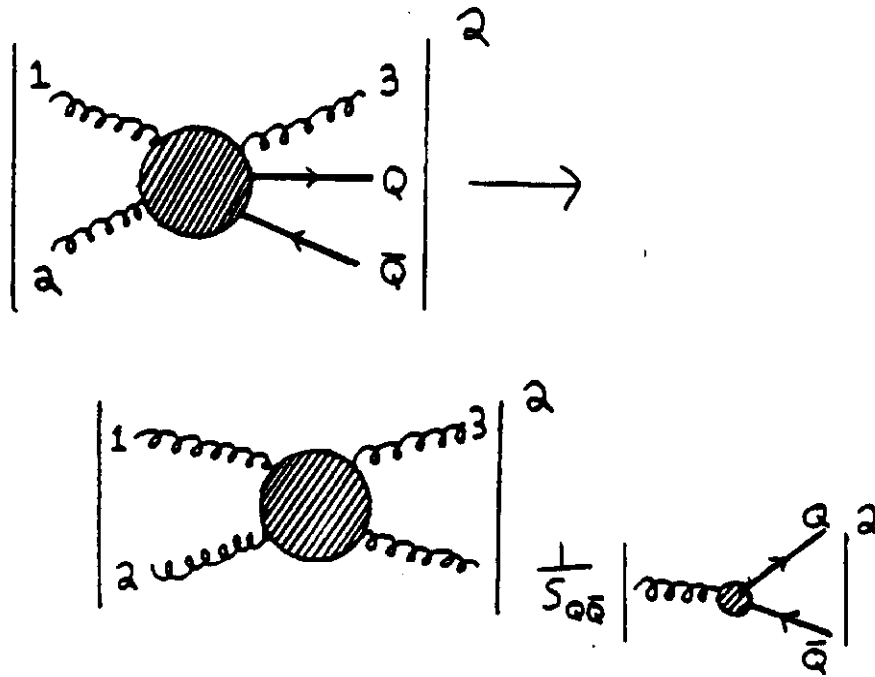
Figure 33: The $gg \to g\bar{Q}Q$ process in leading logarithmic approximation. As Q and $\bar{Q}$ become collinear we can express the process in terms of the on shell $gg \to gg$ process times the A-P splitting function for $g \to \bar{Q}Q$ and a singular propagator $1/s_{\bar{Q}Q}$.

always sufficient to determine the relative importance of various subprocesses in a given experimental situation.

The relative strengths of these two contributions to inclusive production of charm and bottom quarks at the $S\bar{p}pS$ collider has been analysed by Halzen and Hoyer[47]. The results are shown in Figure 34. Experimentally, these two process have very different topological structure and therefore can be differentiated. The $2 \rightarrow 2$ contribution produces relatively large heavy quark pair mass, $\hat{s}_{\bar{Q}Q}/\hat{s}$ near 1, and the Q and $\bar{Q}$ move in approximately opposite directions to each other; whereas, the $2 \rightarrow 3$ contribution tends to produce relatively small pair mass and both the Q and $\bar{Q}$ will tend to move in roughly the same direction. In Fig. 34 a cut on the minimum $p_\perp$ of 7 GeV/c has been imposed on the jet opposite the heavy quark to avoid a divergence in the $2 \rightarrow 3$ amplitude as the gluon momentum becomes soft. Moreover, folding in the experimental jet cuts will enhance the $2 \rightarrow 2$ contribution to the point that it dominates the observed events.

E.   Jets - Present and Future

To summarize, jets have emerged at $S\bar{p}pS$ collider energies as clear and distinct tags of the underlying quarks and gluons. The predictions of QCD have been verified within the accuracy of present experimental data. Futhermore, the one to one association of jets with the underlying quarks and gluons will provide an important tool for studying QCD at all higher energy hadron colliders.

Future tests of QCD in hadron-hadron colliders will depend on detailed analysis of rare events and on precision measurements of basic jet physics. Jets will be used to identify the specific parent quark or gluon. But to do this methods are needed:

- To distinguish reliably light quark from gluon jets. We know that at the lowest $p_\perp$'s gluon jets dominate and as the $p_\perp$ increases the fraction of quark jets also increase. This should be of some aid in finding the distinguishing characteristics of light quark vis-a-vis gluon jets.

- To find a signature of heavy quark jets, t and b, which distinguishes them from ordinary quark jets. Heavy quark are produced copiously at very high energies (eg. at the SSC) and if the jets associated with heavy quarks could
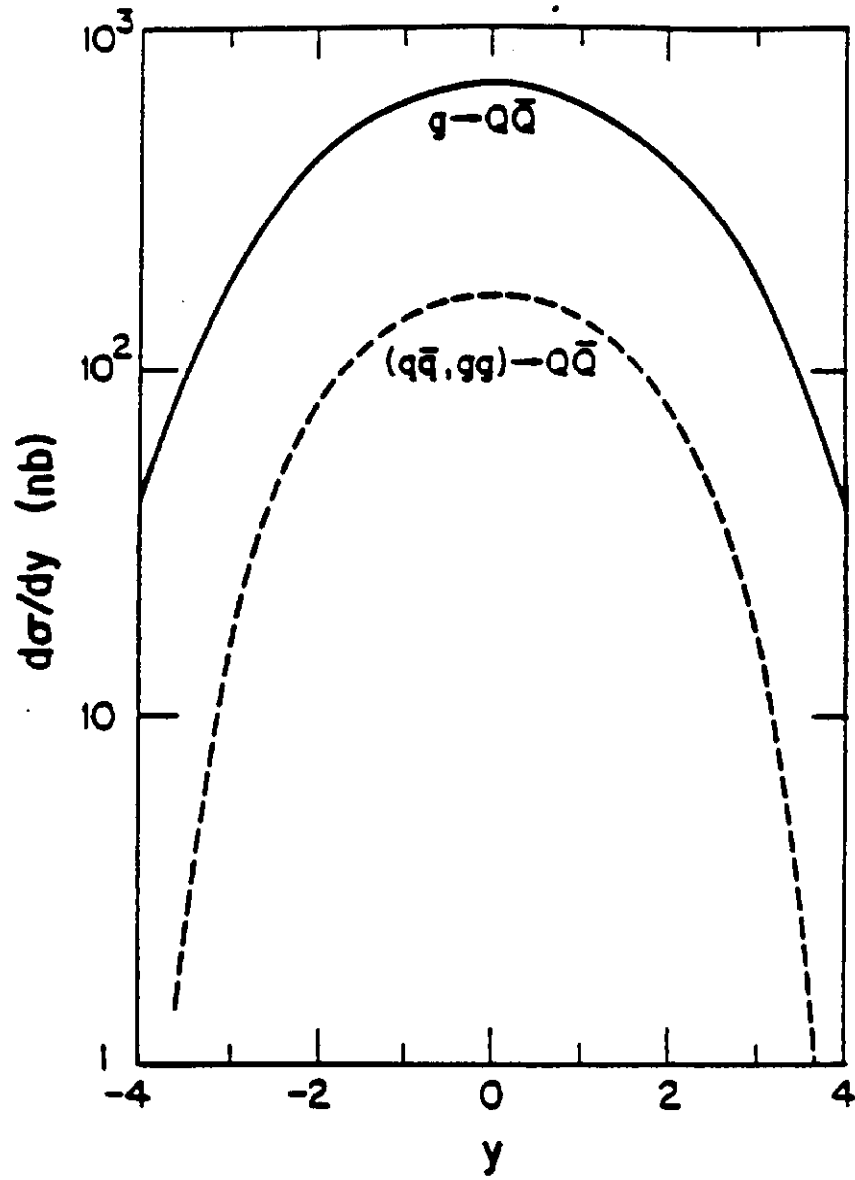
Figure 34: Rapidity distribution for heavy quark production(charm and bottom) by the 2 → 2 (dashed line) and 2 → 3 (solid line) processes. (From Ref. 47)

be tagged many properties of the quarks could be studied. Also heavy quark jets are important signatures of many of the new physics possibilities to be discussed in the last three lectures.

Both of these problems are presently being vigorously investigated by both theorists and experimentalists[48,49].

III. ELECTROWEAK PHYSICS

The electroweak interactions, which provide the remaining gauge structure in the standard model, is the topic of this lecture. Since both leptons and quarks participate in these interactions, the electroweak force is probed both in lepton and in hadron colliders.

The Lagrangian for the electroweak interactions has the gauge structure $SU(2)_L \otimes U(1)_Y$ with massless gauge bosons $W^\pm, W^3$ and B respectively. The charged $SU(2)_L$ bosons acquire mass from symmetry breakdown as well as one combination of the neutral W and B bosons, the Z^0 boson, while the other neutral boson, the photon, remains massless. The fermions are grouped into three generations (k), each generation having the same $SU(2)_L$ and $U(1)_Y$ classification. For the first generation the representations for the quarks and leptons are

$$
\begin{array}{ccccc}
SU(2)_L & & U(1)_Y & & \\
 & & Y_L & Y_{Ru} & Y_{Rd} \\
\begin{pmatrix} u \\ d \end{pmatrix}_L & u_R \quad d_R & 1/3 & 4/3 & -2/3 \\
\begin{pmatrix} \nu_e \\ e \end{pmatrix}_L & e_R & -1 & & -2
\end{array}
$$

The full Lagrangian for the Weinberg-Salam standard model is given by:

$$
\begin{aligned}
\mathcal{L} =\ & \sum_k \sum_{f=u,d,\nu,e} [i\overline{f}_k \gamma^\mu (\partial_\mu - ig\frac{\tau^a}{2}(\frac{1-\gamma_5}{2})W_{\mu a} - i\frac{g'}{2}(\frac{1-\gamma_5}{2})Y_L B_\mu \\
& - i\frac{g'}{2}(\frac{1+\gamma_5}{2})Y_R B_\mu)f_k] - \frac{1}{4}\sum_a (\partial_\mu W_{\nu a} - \partial_\nu W_{\mu a} + g\epsilon_{abc}W_{\mu b}W_{\nu c})^2 \\
& - \frac{1}{4}(\partial_\mu B_\nu - \partial_\nu B_\mu)^2 + (D_\mu \phi)^\dagger (D^\mu \phi) - [-\mu^2 \phi^\dagger \phi + \lambda(\phi^\dagger \phi)^2] \\
& - \sum_k \sum_{f=u,d,\nu,e} \Gamma_{kf}\overline{f}_L^{(k)} f_R^{(k)}\overline{\phi} + h.c. \qquad\qquad (3.1)
\end{aligned}
$$

In addition to the gauge bosons and their self interactions and the fermions with minimal couplings to the gauge fields, there are elementary scalar fields, sometimes called Higgs fields for the role they play in electroweak symmetry breaking. Here

the Higgs particles are a complex doublet under $SU(2)_L$ with $Q_Y = 1$, so their gauge interactions are through the covariant derivative:

$$D_\mu = \partial_\mu - ig\frac{\tau^a}{2}W_{\mu a} - ig'\frac{B_\mu}{2} \qquad (3.2)$$

and their self interactions (the Higgs potential) are responsible for the electroweak symmetry breakdown. Finally, the Yukawa couplings of the Higgs particles to the fermions are responsible for fermion mass generation.

A. Electroweak Symmetry Breaking

It is worthwhile examining in some detail the structure of the symmetry breakdown mechanism. The Higgs scalars are written in terms of a complex doublet field:

$$\phi \equiv \frac{1}{\sqrt{2}}\begin{pmatrix} \phi_2 + i\phi_1 \\ \phi_0 - i\phi_3 \end{pmatrix} \quad \text{and} \quad \overline{\phi} = i\sigma_2\phi^* \qquad (3.3)$$

The Higgs potential consists of a mass term of the wrong sign with coefficient μ^2, and a quartic term of strength $\lambda > 0$:

$$V = -\mu^2(\phi^\dagger\phi) + \lambda(\phi^\dagger\phi)^2 \qquad (3.4)$$

This potential is shown in Figure 35.

The symmetry of the Higgs potential is $SU(2)_L \otimes SU(2)_R \otimes U(1)$, a larger symmetry than the gauged $SU(2)_L \otimes U(1)_Y$ symmetry. To exposed this additional symmetry the Higgs potential can be rewritten in terms of

$$\Phi \equiv \frac{1}{2}(\tau_0\phi_0 + i\tau_a\phi^a) \qquad (3.5)$$

where τ_a are the Pauli matrices and τ_0 is the 2x2 unit matrix. In terms of Φ, the scalar self interactions are given by:

$$\mathcal{L}_S = Tr(\partial_\mu\Phi^\dagger\partial^\mu\Phi) - \lambda[Tr(\Phi^\dagger\Phi) - \frac{\mu^2}{2\lambda}]^2 + \frac{\mu^4}{4\lambda} . \qquad (3.6)$$

Now there is a manifest symmetry of this part of the Lagrangian under the transformations:

$$\Phi \rightarrow U_L\Phi U_R^\dagger \quad \text{where} \quad \begin{aligned} U_L &= e^{-i\Lambda_L^a\tau_a} \\ U_R &= e^{-i\Lambda_R^a\tau_a} \end{aligned} \qquad (3.7)$$

$$V(|\phi|)$$
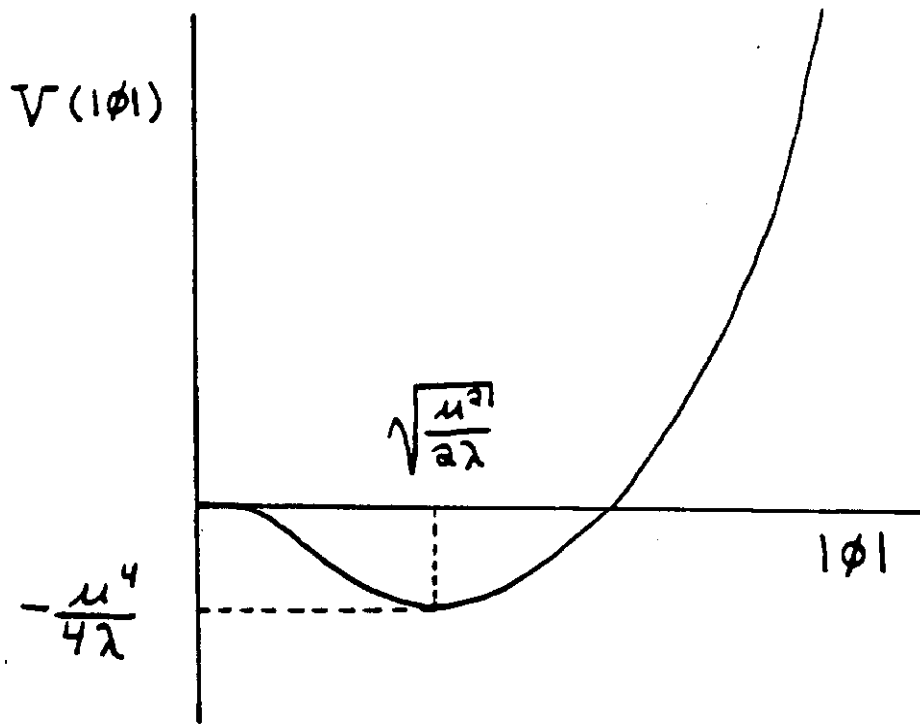
Figure 35: Higgs potential for a complex scalar field, ϕ .

This symmetry is not valid for the full Lagrangian since:

- The Yukawa couplings distinguish members of the $SU(2)_R$ doublets. That is, $\Gamma_u \neq \Gamma_d$ in Eq. 3.1.

- The electroweak gauge interactions of the scalar fields also break the $SU(2)_R$ global symmetry of the Higgs potential.

Nonetheless, this extra invariance will be important to our discussions in lectures 4 and 5.

Now minimizing the Higgs potential in terms of Φ gives

$$< \Phi >= (v/\sqrt{2})r_0 \quad \text{where} \quad v = \sqrt{\frac{\mu^2}{2\lambda}} \tag{3.8}$$

Shifting the Higgs fields by this vacuum expectation value

$$\tilde{\Phi} \equiv \Phi - < \Phi >= \Phi - (v/\sqrt{2})r_0 \tag{3.9}$$

replaces $Tr(\Phi^\dagger \Phi)$ by

$$Tr(\tilde{\Phi}^\dagger \tilde{\Phi}) + \frac{v}{\sqrt{2}} Tr[(\tilde{\Phi}^\dagger + \tilde{\Phi}) \cdot \tau_0] + v^2 \tag{3.10}$$

The new expressions (Eqs. 3.9 and 3.10) are invariant under the vector subgroup of transformations $U_R = U_L$ so there is a residual $SU(2)_V \otimes U(1)_V$ symmetry. Rewriting the scalar potential in terms of a physical Higgs scalar $H = \frac{1}{2}Tr(\tau_0(\tilde{\Phi} + \tilde{\Phi}^\dagger))$ and $\tilde{\Phi}$:

$$V = -\frac{\mu^4}{4\lambda} + \frac{1}{2}m_H^2 H^2 + \sqrt{2\lambda}m_H Tr(\tilde{\Phi}^\dagger \tilde{\Phi})H + \lambda[Tr(\tilde{\Phi}^\dagger \tilde{\Phi})]^2 \tag{3.11}$$

where the Higgs scalar mass is $m_H^2 = 2\mu^2$ and the remaining three scalar fields are massless Goldstone bosons, $\phi^\pm = \frac{1}{\sqrt{2}}(\phi_1 \mp i\phi_2)$ and ϕ_3, corresponding to the three broken symmetries. These Goldstone bosons then provide masses for the $W^\pm$ and Z^0 bosons by the usual Higgs mechanism[50].

The mass terms for the gauge bosons can be seen explicitly by considering the interactions between the scalar fields and the gauge fields. Since the $SU(2)_L \otimes SU(2)_R$ symmetry of the scalar potential is not respected by these gauge interactions we will use the complex doublet notation of Eq. 3.3 for the scalar particles. The covariant coupling of the scalar particles to the electroweak gauge fields can be reexpressed in terms of the shifted scalar field $\tilde{\phi} \equiv \phi - <\phi>$:

$$(D_\mu \phi)^\dagger (D^\mu \phi) = (D_\mu \tilde{\phi})^\dagger (D^\mu \tilde{\phi}) + g^2 v^2/2 \, W_\mu^+ W^{-\mu} + v^2/2 \, (gW_3^\mu - g'B^\mu)^2$$

$$[(0,v)(ig\frac{\tau_a}{2}W_{a\mu} + ig'\frac{B_\mu}{2})\partial_\mu \tilde{\phi} + h.c.] \tag{3.12}$$

One linear combination of the two neutral gauge bosons, the Z^0, has acquired a mass while the other linear combination, the photon, remains massless. The mass eigenstates can be seen directly in Eq. 3.12 are:

$$Z^0 = \frac{gW_3 - g'B}{\sqrt{g^2 + g'^2}} \qquad m_Z = \sqrt{g^2 + g'^2}v/\sqrt{2} \tag{3.13}$$

$$A = \frac{g'W_3 + gB}{\sqrt{g^2 + g'^2}} \qquad m_A = 0 \tag{3.14}$$

$$W^\pm \qquad m_W = gv/\sqrt{2} \tag{3.15}$$

The Weinberg angle, θ_w is defined by:

$$x_w \equiv \sin^2 \theta_w = \frac{g'^2}{g^2 + g'^2} \tag{3.16}$$

Furthermore, we can define a parameter ρ, by:

$$\rho = \frac{m_W^2}{m_Z^2 \cos^2 \theta_w} \tag{3.17}$$

Because of the custodial $SU(2)_V$ symmetry of the Higgs sector after symmetry breaking

$$\rho = 1 \tag{3.18}$$

if quantum loop corrections are ignored.

Rewriting the interaction of the longitudinal degrees of freedom for the electroweak bosons in terms of mass eigenstates gives:

$$[(0, v)(ig\frac{\tau_a}{2}W_{\mu a} + ig'\frac{B_\mu}{2})\partial^\mu \bar{\phi} + h.c.] \rightarrow gv(W_{1\mu}\partial^\mu\phi_1 + W_{2\mu}\partial^\mu\phi_2 + Z_\mu\partial^\mu\phi_3) . \tag{3.19}$$

We see explicitly that the Goldstone bosons, ϕ_1, ϕ_2, ϕ_3, mix with the $W^\pm$ and Z^0 to become the longitudinal degrees of freedom for the corresponding gauge boson.

The charged weak currents have been described by the Fermi constant, G_F, long before the W-S model was proposed. The $W^\pm$ mass may be expressed in terms of this constant by:

$$m_W^2 = g^2 v^2/2 = g^2/(4\sqrt{2}G_F) \tag{3.20}$$

so that the vacuum expectation value v is determined in terms of the Fermi constant as

$$tr < \Phi > = \sqrt{2}v = (2\sqrt{2}G_F)^{-\frac{1}{2}} = 246 GeV \tag{3.21}$$

This sets the scale of the weak interactions.

B.   The $W^\pm$ and Z^0 Gauge Bosons

The gauge structure of the Weinberg-Salam model has been confirmed experimentally by the observation of W and Z bosons at the $S\bar{p}pS$ collider[51,52]. The Z^0 was observed in its decays into high energy e^+e^- and $\mu^+\mu^-$ pairs. These events have

essentially no backgrounds. Identifying the Z^0 is purely a matter of event rate. The $W^\pm$ decays are more numerous but their study is more complicated since only the charged lepton is observed directly. The neutrino escapes the detector, hence its signature is large missing transverse energy E_T in the event. There is no actual resonance peak at the $W^\pm$ mass, although there is a Jacobian (phase space) peak in the charged lepton spectrum at a somewhat lower energy[53]. The measured masses are:

Experiment	m_W (GeV)	m_Z (GeV)
UA1 Ref. 51	83.5 $^{+1.1}_{-1.0}$ ± 2.7	93.0 $\pm 1.4 \pm 3.0$
UA2 Ref. 52	81.2 $\pm 1.1 \pm 1.3$	92.5 $\pm 1.3 \pm 1.5$

The first error quoted is the statistical error and the second is the systematic error. The width of the Z^0 measured by UA2[52] is

$$\Gamma_{\rm exp}(Z^0) = 2.19 \ ^{+\ 0.7}_{-\ 0.5} \pm 0.22 {\rm GeV} \qquad (3.22)$$

The theoretical values[54] for the masses and other properties of the $W^\pm$ and Z^0 are collected in Table 2.

The value of x_w of .217 $\pm$ .014 determined from other experiments[54] is used in this comparison. The theoretical calculations include one-loop corrections to the masses and widths. The calculations of their widths which assume a top quark mass of 40GeV. Theory and experiment agree within the present accuracy.

The background of ordinary two jet events with invariant pair mass equal to the W mass (within the experimental mass resolution) is of the same order of magnitude as the signal of hadronic W decays. Experimentalist are seeking addition cuts on such events which would establish a clear signal for hadronic decays of the W and Z, but as yet none have been identified. Experimental determination of the total cross sections for $W^\pm$ and Z^0 production times the leptonic branching ratio for $\bar{p}p$ collisions give:

Table 2: Selected properties of the $W^{\pm}$ and Z^0 electroweak gauge bosons. Here $sin^2\theta_w \equiv x_w$ is assumed to be $.217 \pm .014$. Primes on down quarks denote electroweak eigenstates. The factor $f_s = 1 + \alpha_s/\pi$ includes the leading order QCD correction for decays.

Process	$W^{\pm}$	Z^0
Mass (GeV/c^2)	83.0 ± 2.8	93.8 ± 2.3
Branching Fractions Leptons ($l^+ = e^+, \mu^+, or\ \tau^+$)	$(l^+\nu) = 1$	$(\overline{\nu}\nu) = 2$ $(\bar{l}l) = 1 + (1 - 4x_w)^2$
Light Quarks	$\begin{pmatrix} \overline{d}'u \\ \overline{s}'c \end{pmatrix} = 3f_s$	$\begin{pmatrix} \overline{u}u \\ \overline{c}c \end{pmatrix} = 3f_s(1 + (1 - \tfrac{8}{3}x_w)^2)$ $\begin{pmatrix} \overline{d}d \\ \overline{s}s \\ \overline{b}b \end{pmatrix} = 3f_s(1 + (1 - \tfrac{4}{3}x_w)^2)$
Top Quarks (mass $= m_t$)	$(\overline{b}'t) = 3f_s\left(1 - \frac{m_t^2}{M_W^2}\right)^2$ $\left(1 + \frac{m_t^2}{2M_W^2}\right)$	$(\bar{t}t) = 3f_s\sqrt{1 - 4\frac{m_t^2}{M_z^2}}$ $[1 + 2m_t^2/M_z^2 + (1 - \frac{4m_t^2}{M_z^2})(1 - \tfrac{8}{3}x_w)^2]$
Total Width (GeV) ($m_t = 40 GeV/c^2$)	2.8	2.9

| $\sqrt{s}$ (GeV) | Experiment | $\sigma \cdot \mathrm{BR}(e^+ e^-)$ (in picobarns) | |
		$W^+ + W^-$	Z^0
546	UA1 Ref. 51	$550 \pm 80 \pm 90$	$42 \; {}^{+\,25}_{-\,18} \pm 6$
	UA2 Ref. 52	$500 \pm 90 \pm 50$	$110 \pm 39 \pm 9$
630	UA1 Ref. 51	$630 \pm 50 \pm 90$	$79 \; {}^{+\,23}_{-\,20} \pm 11$
	UA2 Ref. 52	$530 \pm 60 \pm 50$	$52 \pm 19 \pm 4$

The experimental errors (statistical plus systematic) are sufficiently large that the growth of the cross sections with energy is not apparent. The theoretical predictions for the total cross sections at 630GeV, based on the analysis of Altarelli et. al.[55,56] are:

$$\sigma(\bar{p}p \rightarrow W^+ \text{ or } W^-) = 5.3 \; {}^{+\,1.6}_{-\,0.9}$$

$$\sigma(\bar{p}p \rightarrow Z^0) = 1.6 \; {}^{+\,0.5}_{-\,0.3} \tag{3.23}$$

There are a number of sources for the theoretical uncertainties given above. The lower theoretical error takes into account the uncertainty in the determination of the parton distribution functions and the QCD Λ parameter. Altarelli et al.[55,56] considered a variety of different parametrizations for the parton distributions. The upper theoretical error also includes the uncertainty in what value to choose for the momentum scale which determines the scale violations in the distribution functions. This scale is determined in higher order in QCD perturbation theory, but these calculations have not yet been done. Ambiguity in this scale factor leads to an uncertainty in the total cross section. However, since the cross sections are being evaluated at high Q^2, a factor of two change in this momentum scale only results in small corrections to the cross section. The usual estimates are obtained by using the intermediate boson mass to set this momentum scale. The upper error uses the transverse momentum of the final lepton to set the momentum scale.

The ratio of the cross sections should be less sensitive to these theoretical ambiguities, and in fact theory and experiment are in good agreement for the ratio of W to Z total cross sections.

The relative branching ratios for various decays of the $W^\pm$ and Z^0 are also shown in Table 2 normalized to $W^+ \rightarrow l + \nu = 1$. Now using the theoretical branching

Table 3: Total cross sections for production of single electroweak gauge bosons. All cross sections are in nanobarns.

Collider	$\sqrt{s}$	Gauge Boson		
	(TeV/c^2)	W^+	W^-	Z^0
$\bar{p}p$	.63	3.4	3.4	1.2
$\bar{p}p$	1.8	10.2	10.2	3.9
$\bar{p}p$	2.0	11.2	11.2	4.9
pp	10	41	28	22
pp	20	73	54	41
pp	40	122	95	72

ratio (assuming $m_t = 40\ GeV/c^2$) one predicts for the cross section, σ, times leptonic branching ratio, B, at $\sqrt{s} = 630$ GeV:

$$\sigma \cdot B(W^+ + W^-) = 460 \ {}^{+\ 140}_{-\ 80}\text{pb}$$

$$\sigma \cdot B(Z^0) = 51 \ {}^{+\ 16}_{-\ 9}\text{pb} \qquad (3.24)$$

The theoretical and experimental cross sections agree within the rather large errors although they do not coincide.

Table 3 shows the theoretical predictions for the total cross sections for single $W^\pm$ and Z^0 production at present and future hadron colliders. The structure functions of Set 2 (Eq. 1.24) are used for these cross sections.

A cross section of 10 (nb) corresponds to an expectation of 10^6 W^+ events/year for a luminosity of $10^{30}cm^{-2}sec^{-1}$. Hadron colliders provide a copious source of $W^\pm$ and Z^0 bosons. With such statistics:

- It is possible to study rare decays such as those expected in supersymmetry models (lecture 7), in extensions of the standard model with additional doublets of Higgs scalars, or in technicolor models (lecture 5).

- Precision (one loop) tests of the electroweak interactions will be possible. However most of these tests are better suited to e^+e^- colliders such as the SLC or LEPI, which provide a clean and copious source of Z^0 bosons.

- The total width of the Z^0 is sensitive to the number of generations, since there is a contribution of 186 MeV to the width of the Z^0 for every neutrino type. Hence the measurement of the Z^0 width to an accuracy of 100 MeV will determine the number of standard generations.

At SSC energies and luminosities the rates for production of $W^\pm$ and Z^0 bosons are even more impressive. However since much of the production will be at sizable rapidities the events will not be as clean as at $S\bar{p}pS$ collider energies where the electroweak bosons are produced essentially at rest. Some ingenuity will be required to take advantage of these rates[57].

Next we will consider some of the details of $W^\pm$ production. For example the cross section for $p\bar{p} \rightarrow W^\pm + X$ is shown in Figure 36. This cross-section rises steeply near threshold because of both the threshold kinematics of the elementary process and the steep decrease in the the parton-parton luminosities as x approaches one. The production cross section in pp collisions (also shown in Fig. 36) is smaller than $\bar{p}p$ at the same $\sqrt{s}$ because of the lack of valence antiquarks in pp collisions. There are small differences between the W^+ and W^- production in pp collisions because the valence quarks contribute more to W^+ than to W^- production.

The rapidity distribution of W^+ production is relatively flat at SSC energies. The net helicity of W^+ inclusive production in pp and $\bar{p}p$ interactions can be calculated straightforwardly and is shown as a function of the rapidity for $\sqrt{s} = 40$ TeV in Figure 37. To understand qualitatively the behaviour of these helicities consider the two production modes:

- A W^+ can be produced from a u_L quark from the "beam" p or $\bar{p}$ carrying fraction x_1 of the beam momentum (defined to be in the $+z$ direction) and a $\bar{d}_R$ antiquark carrying fraction x_2 of the "target" proton. The resulting W^+ will have momentum along the beam direction

$$p_\parallel = (\frac{x_1 - x_2}{2})\sqrt{s} \qquad (3.25)$$
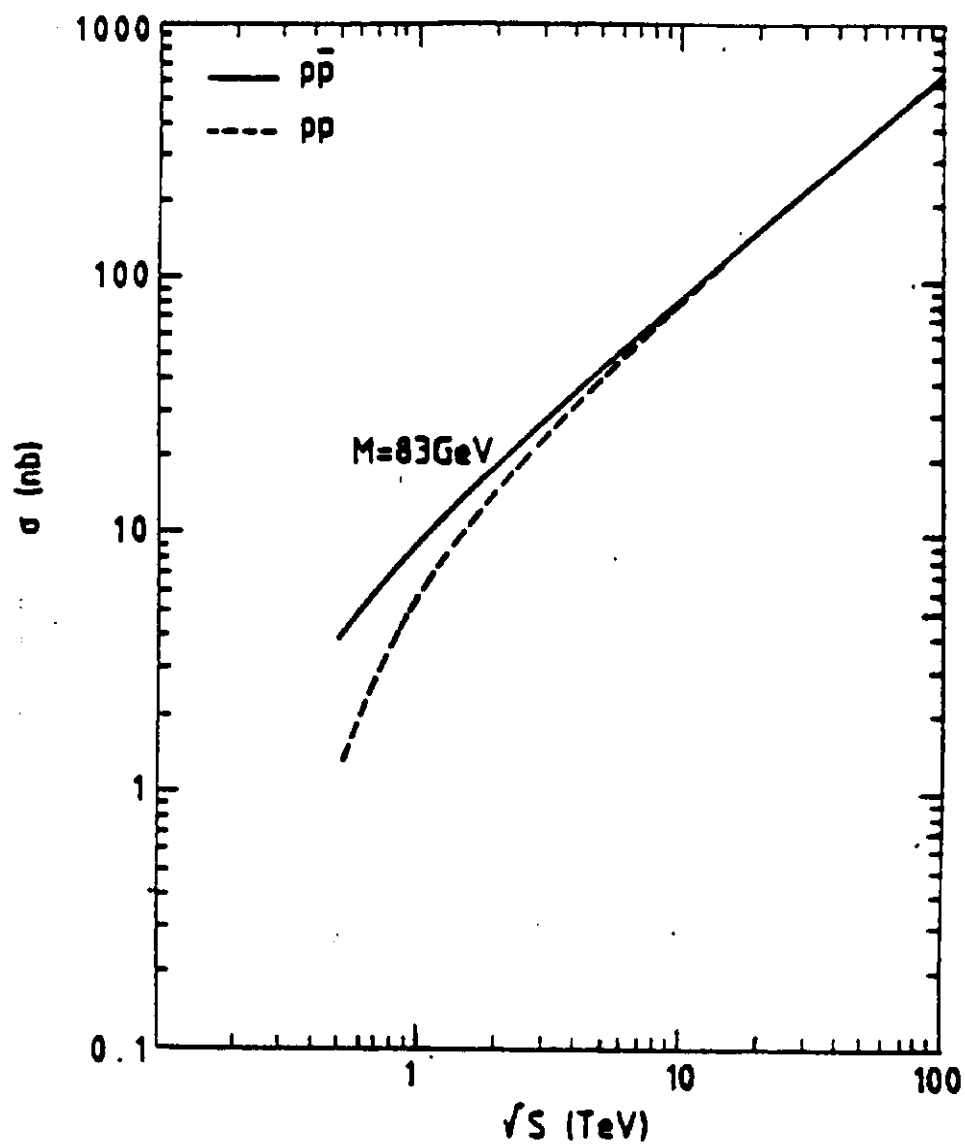
Figure 36: Total cross section for the production of W^+ and W^- (for $M_W = 83$ GeV/c^2) versus center of mass energy. The solid line is for $\bar{p}p$ collisions and the dashed line is for pp collisions. Adapted from Ref. 56
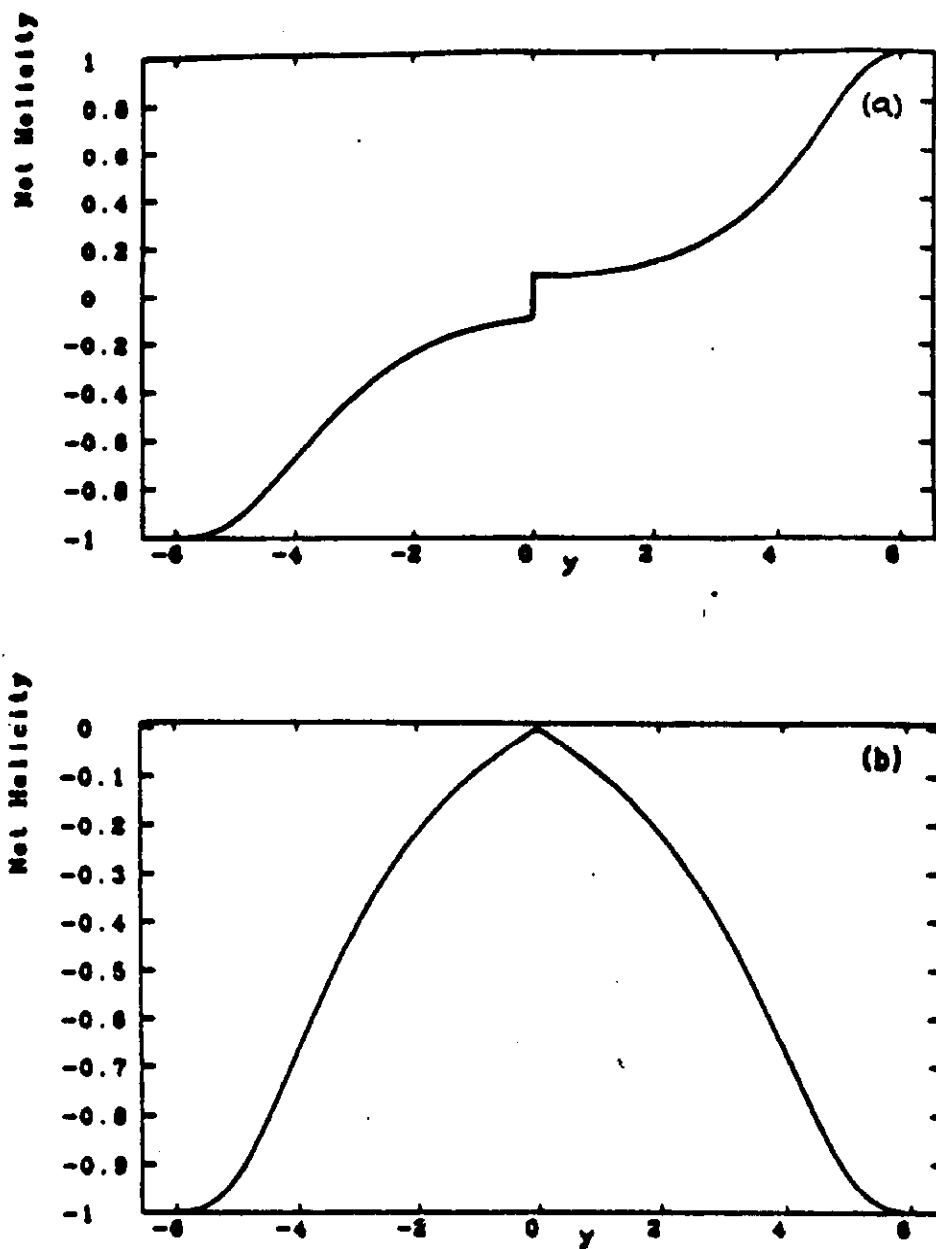
Figure 37: The net helicity of the W^+ as a function of the rapidity y. The W^+ production is shown both for $\bar{p}p$ (a) and for pp (b) collisions at $\sqrt{s} = 40$ TeV. Parton distributions of Set 2. (From EHLQ)

and spin $J_z = -1$, since the u_L has spin $J_z = -1/2$ and the $\bar{d}_R$ also has spin $J_z = -1/2$. Hence the helicity of the resulting W^+ is opposite to the sign of the longitudinal momentum $p_{||}$.

- A W^+ can also be produced from a $\bar{d}_R$ antiquark from the beam p or $\bar{p}$ carrying fraction x_1 of the beam momentum and a u_L quark carrying fraction x_2 of the target proton. In this case, the resulting W^+ will now have spin $J_z = +1$, since the $\bar{d}_R$ has spin $J_z = 1/2$ and the u_L also has spin $J_z = 1/2$. Hence the helicity of the resulting W^+ is the same as the sign of the longitudinal momentum $p_{||}$.

The net helicity of the W^+ results from the sum of these two production processes. For pp collisions the quark distributions are of course identical for the "beam" and "target" particles. The contribution to W^+ production of the first process above for W^+ rapidity y equals the contribution of the second process for rapidity $-y$. Thus the net helicity $h_w(y)$ is symmetric about $x_1 = x_2$, (i.e. $y = 0$); thus $h_w(-y) = h_w(y)$. For $x_1 > x_2$, the valence quarks dominates so that for $y > 0$ the helicity is negative. For $\bar{p}p$ collisions the second process dominates since there both the quark and antiquark are valence quarks. Therefore the helicity is antisymmetric $h_w(-y) = -h_w(y)$; positive for $y > 0$; and is discontinuous at $y = 0$ since the net helicity does not vanish there.

The net helicity of the produced W^+ is a result of the W^+'s chiral coupling and leads to a measurable front-back asymmetry in the decay lepton spectrum. Measuring this helicity as a function of rapidity will distinguish chiral couplings (L,R) from nonchiral couplings (V,A) for the W or any new gauge boson of the electroweak type (i.e. coupling to both leptons and quarks).

C.   Associated Production

In addition to the production of W's and Z's in the lowest order of QCD perturbation theory, there are the next order processes in which the W or Z are produced in association with a quark or a gluon jet. These processes are shown in Figure 38.

Since the transverse momenta of the incoming partons is negligible at high energy, the gauge bosons produced by the lowest order subprocess have small trans-
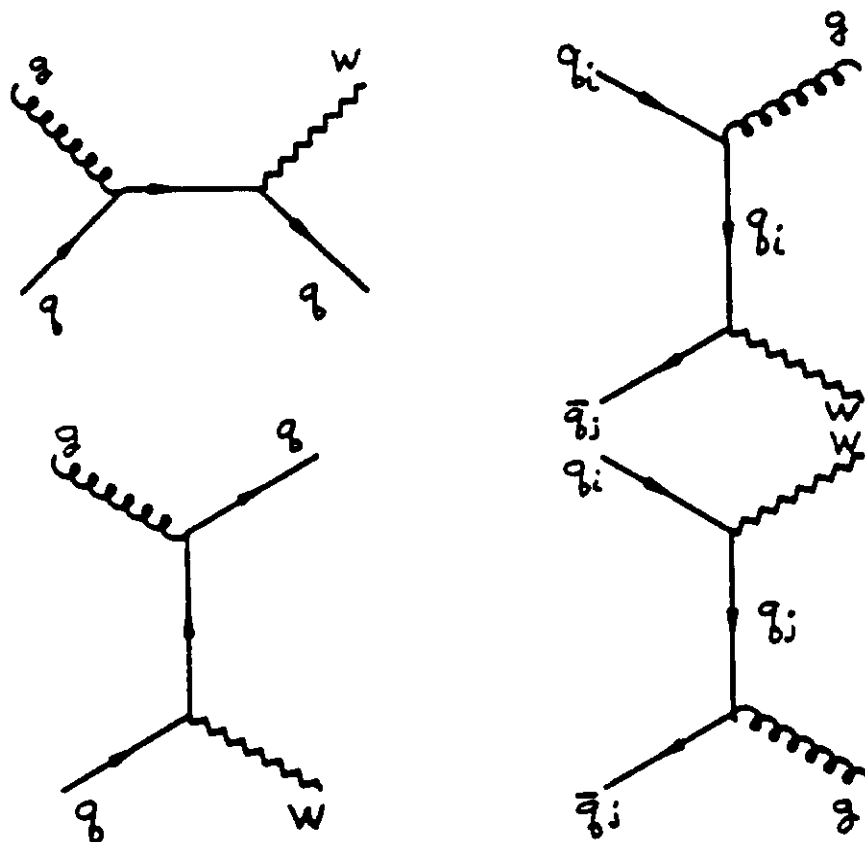
Figure 38: Lowest-order Feynman diagrams for the reactions $g + q \rightarrow W + q$ and $\bar{q} + q \rightarrow W + g$.

verse momentum whereas in associated production the gauge bosons may have large transverse momentum. One consequence of this associated production is the production of monojet events; which occur when the associated gluon or quark produces a jet with transverse momentum and the Z decays into an undetected $\nu\bar{\nu}$ pair. A few such events have been seen at UA1[58].

Calculations of the transverse momentum distribution of W's and Z's has been carried out by Altarelli et al.[55,56] for $\sqrt{s} = 630$ GeV. In these calculations the leading log terms terms have been summed to all orders of perturbation theory. Their result is shown in Figure 39 for $y = 0$, i.e. at 90°. For example, at 630 GeV 1% of all W's associatively produced have transverse momentum greater than 45 GeV. At higher energies the resummation becomes less important at least at high p_T. The lowest order associated production of W's is shown in Figure 40. To get a feeling for event rates remember that a cross section of 10^{-5} (nb/GeV) corresponds to 100 events/yr/GeV for a luminosity of $10^{33} cm^{-2} sec^{-1}$. Therefore, very high transverse momentum W's are produced at SSC energies.

D. Electroweak Pair Production

The present experimental data show that the gauge bosons of the electroweak interactions exist and have approximately the properties required of them in the Weinberg-Salam model. However, the crucial property of the electroweak gauge theory, the non-Abelian self-couplings of the W's, Z's, and γ's has not yet been tested. These couplings can be tested in hadron colliders by electroweak boson pair production processes.

An elementary calculation will illustrate the importance of the non-Abelian gauge boson couplings. The tree approximation to W^+W^- production from the $\bar{u}u$ initial state is given by the three Feynman diagrams shown in Figure 41. In an Abelian theory only the t-channel graph would exist. The kinematic variables are given in Figure 41 along with the appropriate polarization tensors $(\epsilon_\pm)$. Evaluating the t-channel graph gives:

$$M_1 = -i\frac{g^2}{2}\bar{v}(p_2)\not{\epsilon}_-\frac{\not{Q}}{Q^2}\not{\epsilon}_+(\frac{1-\gamma_5}{2})u(p_1)$$

(3.26)
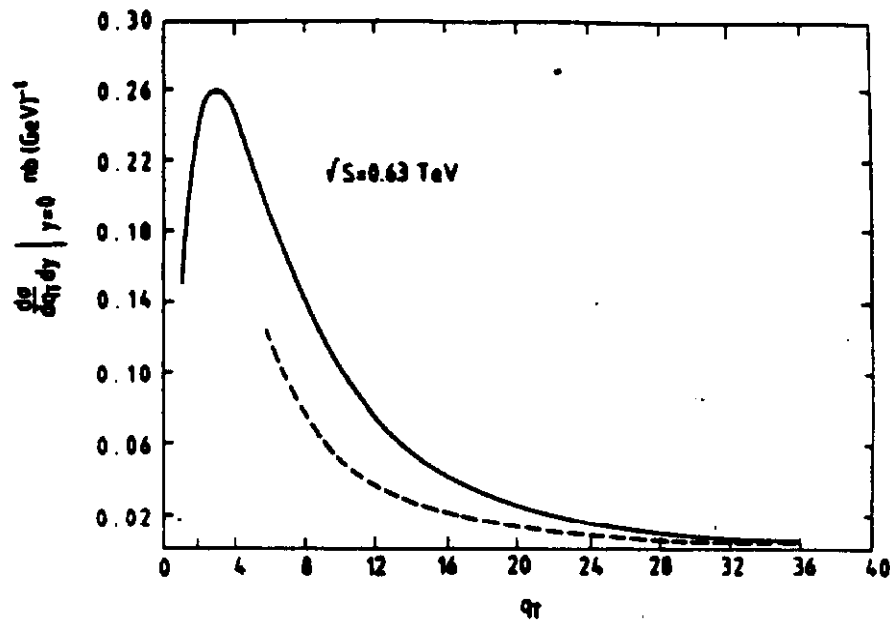
Figure 39: Comparison of the resummed expression for $d\sigma/dp_\perp dy|_{y=0}$ (solid line) with the first order perturbative expression (dashed line) at $\sqrt{s} = 630$ GeV. (From Ref. 56)
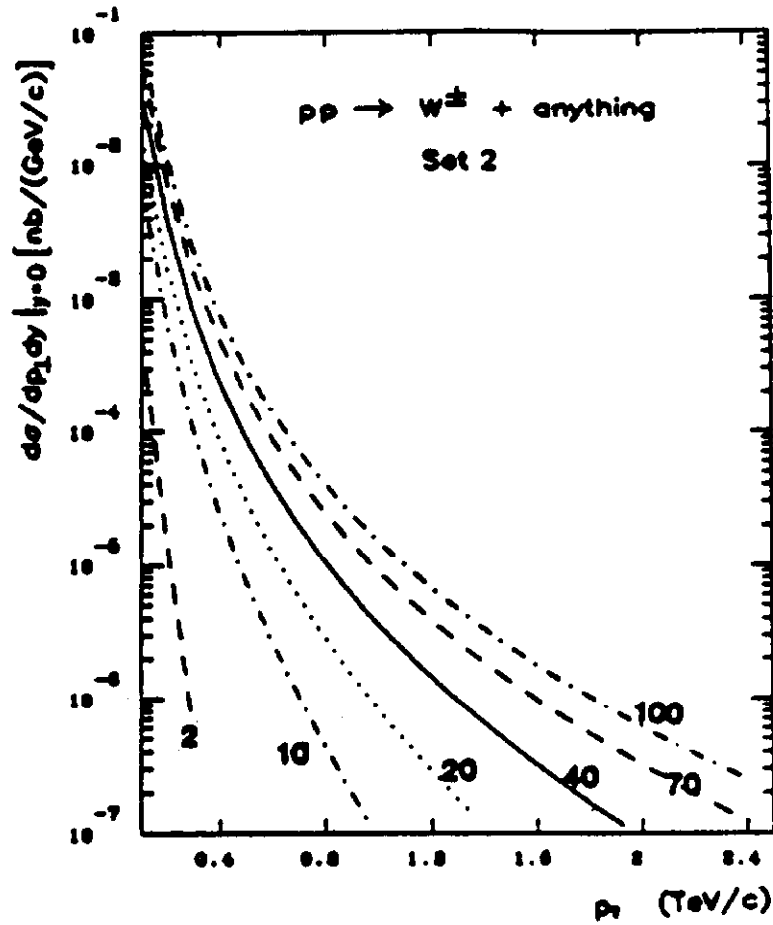
Figure 40: Differential cross section $d\sigma/dp_\perp dy|_{y=0}$ for the production of a W^+ as a function of the W^+ transverse momentum $p_\perp$ at $\sqrt{s} = 2$, 10, 20, 40, 70, and 100 TeV (from bottom to top curve). Parton distributions of Set 2 were used. (From EHLQ)
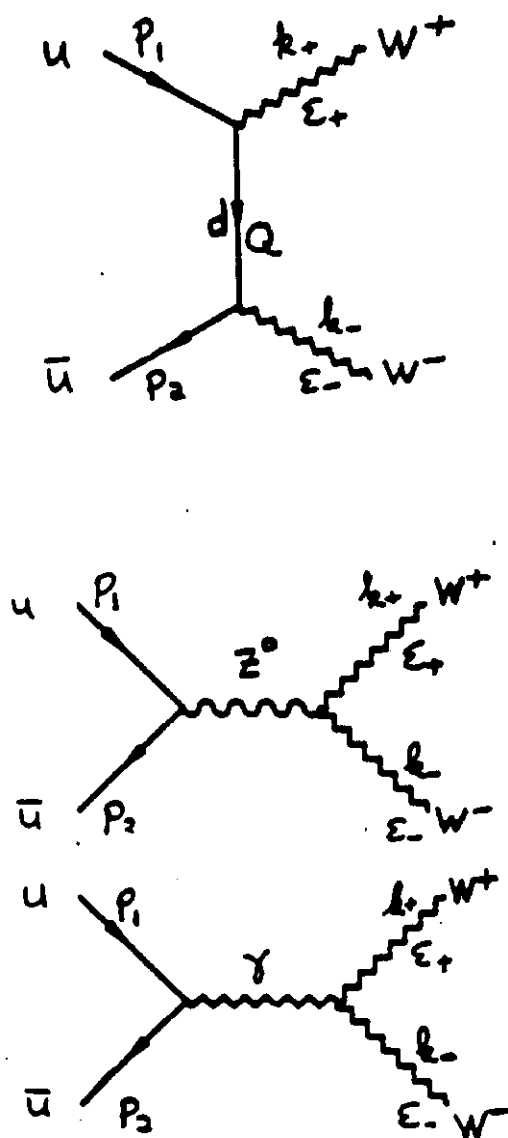
Figure 41: Lowest-order Feynman diagrams for the reaction $u + \bar{u} \rightarrow W^+ + W^-$. A direct channel Higgs boson diagram vanishes because the quarks are idealized as massless.

where $Q = p_1 - k_+$ and in the CM frame the momenta can be chosen:

$$p_1 = (P, 0, 0, P)$$

$$p_2 = (P, 0, 0, -P)$$

$$k_+ = (P, K\sin\theta, 0, K\cos\theta)$$

$$k_- = (P, -K\sin\theta, 0, -K\cos\theta) \tag{3.27}$$

with $P^2 - K^2 = m_W^2$ and quark masses ignored. The polarization tensors are

$$\epsilon_\pm = (\vec{k}_\pm \cdot \hat{\epsilon}_\pm / m_W, \quad \hat{\epsilon}_\pm + \vec{k}_\pm(\vec{k}_\pm \cdot \hat{\epsilon}_\pm)/[m_W(P + m_W)]) \tag{3.28}$$

in terms of the polarization states in the $W^\pm$ rest frame:

$$\hat{\epsilon}_\pm = (0, \vec{\hat{\epsilon}}_\pm) . \tag{3.29}$$

At high energies $(K \to \infty)$ the longitudinal polarizations dominate and simplify to:

$$\epsilon_\pm \to k_\pm / m_W \tag{3.30}$$

Now inserting the above formulas into the expression for $\mathcal{M}_1$ in Eq. 3.26 and using the equation of motions for the $W^\pm$ fields give

$$\mathcal{M}_1 = \frac{ig^2}{2m_W^2}\bar{v}(p_2)\frac{\not{Q}\not{Q}\not{Q}}{Q^2}(\frac{1 - \gamma_5}{2})u(p_1)$$

$$= iG_F 2\sqrt{2}\bar{v}(p_2)\not{Q}(\frac{1 - \gamma_5}{2})u(p_1) \tag{3.31}$$

for the amplitude. If this were the only contribution, then the invariant matrix element squared for this production process would be

$$|\mathcal{M}|^2 = 2G_F^2 s(s - 4m_W^2)\sin^2\theta \tag{3.32}$$

so that the total cross-section would be
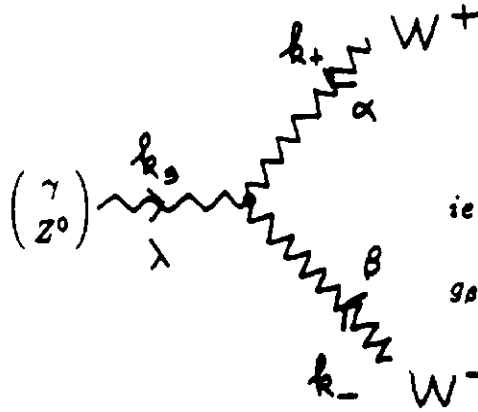
$$\sigma(W^+W^-) \sim \frac{G_F^2 s}{3\pi} \tag{3.33}$$

which grows linearly with s and violates unitarity at high energies (see lecture 4). Of course, including the gauge self interactions in the remaining Feynman diagrams of

Fig. 41 restore unitarity. In the present case both the photon and Z^0 contributions must be included to recover unitarity.
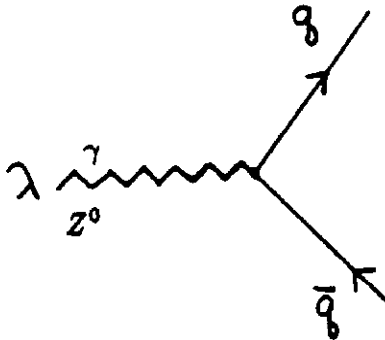
We will explicitly show the cancellation between the t-channel and the s-channel exchange diagrams for left-handed initial quarks. The contributions for right-handed initial quarks must satisfy unitarity including only the s-channel photon and Z^0 exchanges, since the t-channel graph only exists for left-handed initial quarks . This behaviour for right-handed initial quarks can also be easily checked.

The three gauge boson vertices are:

$$ie \begin{pmatrix} 1 \\ cot\theta_w \end{pmatrix} [g_{\alpha\beta}(k_+ - k_-)_\lambda]$$

$$g_{\beta\lambda}(k_- - k_3)_\alpha + g_{\lambda\alpha}(k_3 - k_+)_\beta \qquad (3.34)$$

and the quark-antiquark-gauge boson vertices are:

$$-ieQ_q\gamma_\lambda \qquad (3.35)$$

$$-i\frac{e}{sin2\theta_w}\gamma_\lambda[L_q(\frac{1-\gamma_5}{2}) + R_q(\frac{1+\gamma_5}{2})] \qquad (3.36)$$

where

$$L_q = \tau_3 - 2Q_q sin^2\theta_w \qquad (3.37)$$

$$R_q = -2Q_q sin^2\theta_w \qquad (3.38)$$

and

$$(\sqrt{2}G_F m_Z^2)^{\frac{1}{2}} = \frac{e}{sin2\theta_w} = \frac{g'}{2sin\theta_w} = \frac{g}{2cos\theta_w} \qquad (3.39)$$

The amplitude for the two s-channel graphs for the initial state of a left handed up quark-antiquark is

$$M_2 = i\frac{g}{2}\bar{v}(p_2)\gamma_\mu(\frac{1-\gamma_5}{2})u(p_1)[\frac{2Q_q sin^2\theta_w}{s} + \frac{1-2Q_q sin^2\theta_w}{s-m_W^2}]$$

$$[\epsilon_+ \cdot \epsilon_-(k_+ - k_-)^\mu + k_- \cdot \epsilon_+\epsilon_-^\mu - k_+ \cdot \epsilon_-\epsilon_+^\mu] \qquad (3.40)$$

As $s \to \infty$ the amplitude simplifies as for M_2 and in addition one has the relation $k_+ \cdot k_3 = k_- \cdot k_3 = s/2$ so that for large s the amplitude becomes:

$$M_2 \to \frac{ig^2}{16m_W^2}\bar{v}(p_2)(k_+ - k_-)(\frac{1-\gamma_5}{2})u(p_1)$$

$$= -iG_F 2\sqrt{2}\bar{v}(p_2)\not{Q}(\frac{1-\gamma_5}{2})u(p_1) \qquad (3.41)$$

where again the equation of motion has been used. To leading order in s the sum of M_1 and M_2 (Eqs. 3.31 and 3.41) cancel so that the elementary cross section goes as:

$$\sigma \to constant/s \qquad (3.42)$$

as $s \to \infty$. Hence unitarity is explicitly maintained.

The cross section for $pp \to W^+W^-$ pair production is shown in Figure 42. The slow rise with collision energy of the total cross section is the result of the combined effects of the $1/\hat{s}$ behaviour of the elementary cross section and growth (at fixed $\hat{s}$) of the $\bar{q}q$ luminosities with s. The top curve gives the total production cross section without any rapidity cuts. However large rapidities are associated with production of W's near the beam direction (see Fig. 20) where measurements are very difficult; hence more realistic rates are obtained when rapidity cuts are included.

Similar gauge cancellations occur in the $W^\pm\gamma$ and $W^\pm Z^0$ total cross sections. The $Z^0 Z^0$ and $Z^0\gamma$ cross sections are uninteresting in the present context, since the only graphs which appear are present in the Abelian theory and therefore the non-Abelian gauge couplings are not probed. The rates of electroweak pair production are shown in Table 4. These processes are large enough to be interesting only at
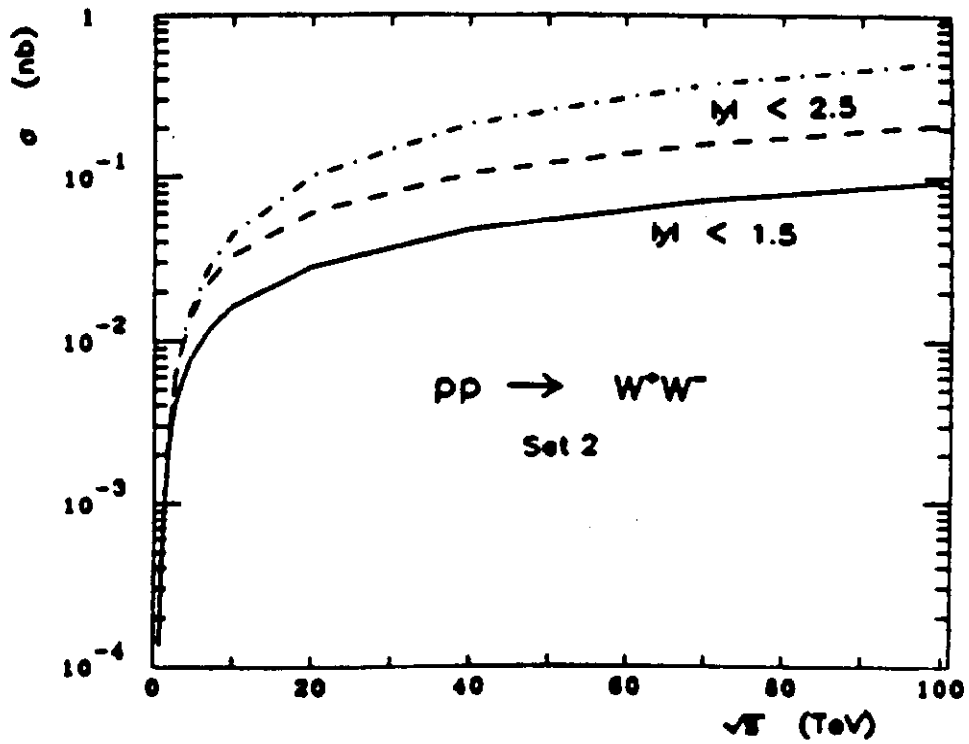
Figure 42: Yield of W^+W^- pairs in pp collisions, according to the parton distributions of Set 2. Both W's must satisfy the rapidity cuts indicated. (From EHLQ)

Table 4: Total cross sections for pair production of electroweak gauge bosons. No rapidity cuts were imposed. The invariant mass of the $W^{\pm}\gamma$ (or $Z^0\gamma$) pair was required to be more than 200 GeV/c^2 . All cross sections are in *picobarns* .

Collider	$\sqrt{s}$	Process				
	(TeV/c^2)	W^+W^-	$W^{\pm}Z^0$	Z^0Z^0	$W^+\gamma$	$Z^0\gamma$
$\bar{p}p$	.63	.037	.006	.003	.001	.003
$\bar{p}p$	1.8	2.4	.69	.28	.16	.41
$\bar{p}p$	2.0	3.1	.90	.37	.21	.55
pp	10	45	16.5	6.5	3.6	10
pp	20	102	38	15.3	8.2	23
pp	40	214	73	33	18	50

supercollider energies. For an integrated luminosity of 10^{40} cm^{-2} at $\sqrt{s}$ = 40 TeV there are $\approx$ 2 $\times$ 10^8 W^+W^- pairs produced.

Some other tests of the non-Abelian gauge couplings are the following:

- If the $W^{\pm}$ were just a massive spin one boson, then the W kinetic interaction

$$-\frac{1}{2}(\partial_\mu W_\nu^+ - \partial_\nu W_\mu^+)(\partial_\mu W_\nu^- - \partial_\nu W_\mu^-) \qquad (3.43)$$

would generate the minimal QED coupling with the photon given by

$$(D_\mu^{EM}W_\nu^+ - D_\nu^{EM}W_\mu^+)(D^{\mu EM}W^{\nu-}D^{\nu EM}W^{\mu-}) = -\frac{1}{2}(F_{\mu\nu}^+ F^{-\mu\nu})_{EMpart} \qquad (3.44)$$

Therefore the non-Abelian term

$$-ieF_{\mu\nu}^{EM}W^{+\mu}W^{-\nu} \qquad (3.45)$$

of the W-S model is a nonminimal coupling from the point of view of QED - a Pauli term which generates an anomolous magnetic moment for the W. However, without this additional term the high energy behaviour of the $W^{\pm}\gamma$ production cross section will violate unitarity at sufficiently high energy[59].

- The lowest order production cross-section for $W^\pm \gamma$ has a zero in the Born amplitude at

$$\hat{t} = 2\hat{u} \tag{3.46}$$

or equivalently at CM angle

$$\cos \theta_{\text{CM}} = -\frac{1}{3} \tag{3.47}$$

due to specific form of the non-Abelian couplings[60]. There is a dip in the elementary cross section which is still visible when the parton distributions have been folded in to give the hadron-hadron production cross section. (See EHLQ Fig. 137)

E.   Minimal Extensions

The simplest and most natural generalization of the standard model is the possibility of a fourth generation of fermions. This possibility requires no modification of our basic ideas; in fact, we have no explanation why there are three generations in the first place. So it is natural to consider new quarks and/or leptons within the context of our discussion of the standard model.

In general, consistency of the $SU(2)_L \otimes U(1)_Y$ gauge interactions requires that any additional quarks and leptons satisfy the anomaly cancellation conditions[61]:

$$\sum_f Q_Y^3(f) = 0 \tag{3.48}$$

and

$$\sum_f Q_Y(f) = 0 \tag{3.49}$$

where $Q_Y(f)$ is the weak hypercharge of the new fermion f. Hence a new quark doublet with standard weak charge assignments would require new leptons as well to avoid gauge anomalies. Of course a fourth generation satisfies these conditions in exactly the same way as each of the three ordinary generations.

1. New Fermions

The production of new heavy quarks in hadron colliders occurs via the same mechanisms as already discussed for top quark production (Section 2.3): gluonic production and production via the decays of real (or virtual) $W^\pm$ and Z^0 bosons. For new quark masses above $\approx m_W$ the main mechanism is gluonic production. Figure 43 shows the cross section for heavy quark production as a function of m_Q for $\bar{p}p$ collisions at $S\bar{p}pS$ and Tevatron energies. The corresponding cross sections at SSC energies are given in EHLQ (p. 646)

New sequential leptons will be pair produced via real and virtual electroweak gauge bosons in the generalized Drell-Yan mechanism[62]. For the $S\bar{p}pS$ and Tevatron collider energies, only decays of real $W^\pm$ and Z^0 can be significant. Hence the discovery limit for a new charged lepton, $L^\pm$, is ≈ 45 GeV in Z^0 decays: while if the associated neutral lepton, N^0, is massless (neutrino-like), the discovery limit for the $L^\pm$ is extended to ≈ 75 GeV in $W^\pm$ decays.

At Supercollider energies, higher mass charged leptons can be produced through virtual electroweak gauge bosons. The pair production of charged heavy leptons proceeds via virtual γ and Z^0 states. The cross section at various energies is shown in Figure 44 for pp collisions.

Neutral lepton pairs, $N^0\overline{N^0}$, can be produced by virtual Z^0 states however in the most conventional case in which N^0 is effectively stable these events are undetectable. Also, heavy leptons can be be produced by the mechanism:

$$pp \rightarrow W^\pm_{\text{virtual}} \rightarrow L^\pm N^0 . \tag{3.50}$$

If the neutral lepton is essentially massless as in the most conventional cases, then significantly higher charged lepton masses are accessible at a given luminosity and $\sqrt{s}$. The cross section for this process at Supercollider energies is shown in Figure 45. The principal decays of very heavy fermions will involve the emission of a real W. If, for example, $Q_u > Q_d$ then Q_u will decay into a real W^+ and a light charge $-1/3$ quark or Q_d (if kinematically allowed). Q_d will decay into a W^- and a charge $2/3$ quark. While for a new lepton, $L^\pm$, the decay will give a real $W^\pm$ and its neutral partner, N^0. These signals should be relatively easy to identify experimentally, so it is likely that 100 produced events will be enough to discover a new quark or lepton.
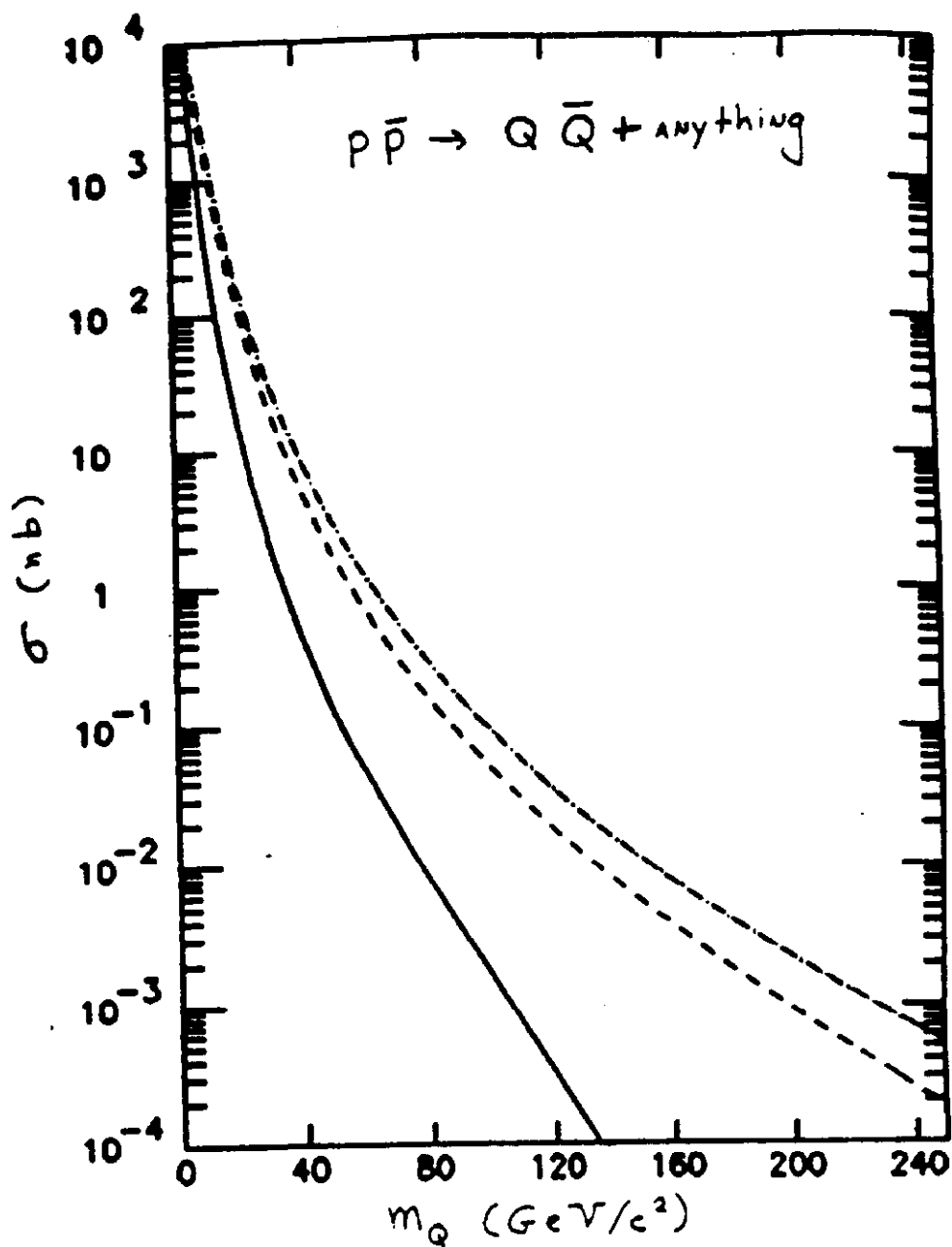
Figure 43: The total cross section for heavy quark pair production via gluon fusion as a function of heavy quark mass, m_Q, for $\bar{p}p$ collisions at $\sqrt{s} = 630$ GeV (solid line), 1.8 TeV (dashed line), and 2.0 TeV (dot-dashed line). The parton distributions of Set 2 used.
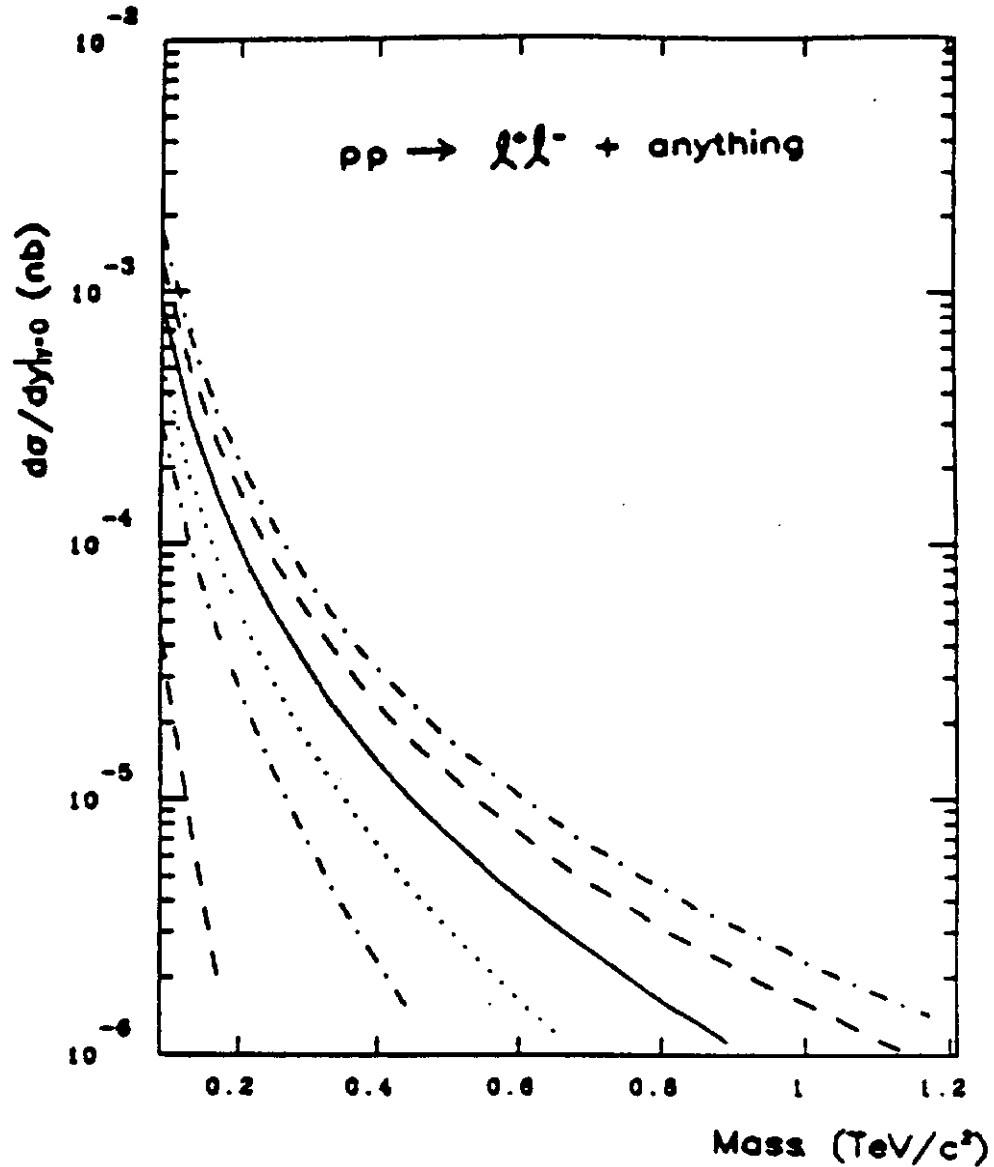
Figure 44: Cross section $d\sigma/dy|_{y=0}$ for the production of L^+L^- pairs in pp collisions by the generalized Drell-Yan mechanism. The contributions of both γ and Z^0 intermediate states are included. The calculation is carried out using distribution Set 2. The energies are $\sqrt{s} = 2, 10, 20, 40, 70, 100$ TeV for the bottom to top curve. (From EHLQ)
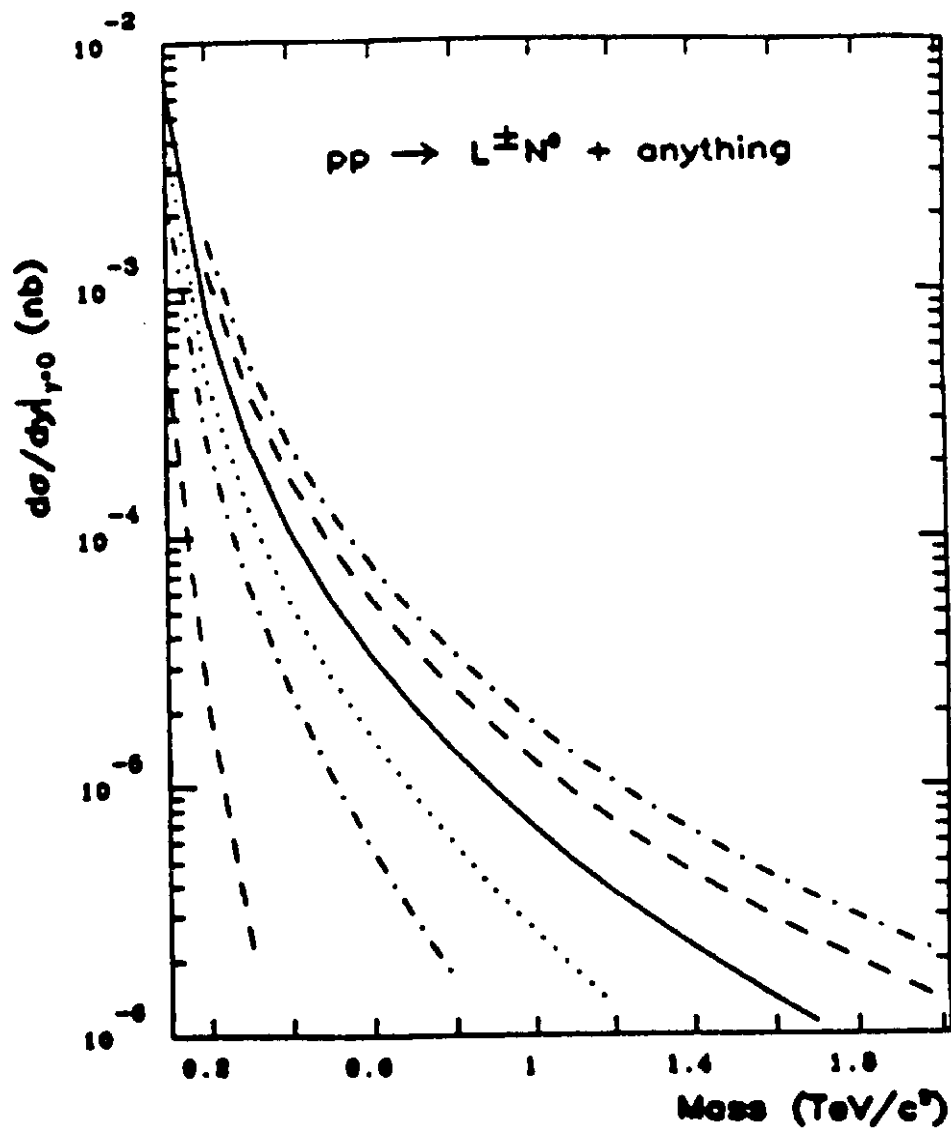
Figure 45: Cross section $d\sigma/dy|_{y=0}$ for the production of $L^{\pm}N^0$ pairs in pp collisions. The N^0 is assumed to be massless, and the parton distributions are those of Set 2. The energies are the same as in Fig. 44. (From EHLQ)

Table 5: Expected discovery limits for new generation of quarks and leptons at present and planned hadron colliders. Basic discovery condition assumed here is 100 produced events. A more detailed analysis of the discovery conditions and detection issues can be found in EHLQ.

| Collider	$\sqrt{s}$ (TeV)	$\int dt \mathcal{L}$ (cm)$^{-2}$	Mass limit (Gev/c^2)		
			New Quark Q	New Lepton	
				L$^\pm$ or L^0 $m(L^\pm) = m(L^0)$	L$^\pm$ $m(L^0) = 0$
$S\bar{p}pS$ $\bar{p}p$	.63	3×10^{36}	65	40	60
upgrade		3×10^{37}	90	45	70
$TEVI$ $\bar{p}p$	1.8	10^{37}	135	48	75
upgrade	2	10^{38}	220	55	95
SSC pp	40	10^{38}	1,250	130	280
		10^{39}	1,900	300	610
		10^{40}	2,700	620	1,250

The discovery limits using this criterion is given in Table 5 for both present and future colliders.

There are interesting constraints on the masses of new fermions which arise from the requirement that partial wave unitarity be respected perturbatively in the standard model. I will leave the discussion of these limits until the next lecture.

2. New Electroweak Bosons

A number of proposals have been advanced for enlarging the electroweak gauge group beyond the $SU(2)_L \otimes U(1)_Y$ of the standard model. One class contains the "left-right symmetric" models[63] based on gauge groups containing

$$SU(2)_L \otimes SU(2)_R \otimes U(1)_Y \qquad (3.51)$$

which restores parity invariance at high energies. Other models, notably the electroweak sector derived from $SO(10)$ or E_6 unified theories, exhibit additional $U(1)$ invariances[64]. These will contain an extra neutral gauge boson. All these models have new gauge coupling constants which are of the order of the $SU(2)_L$ coupling of the standard model. This implies that the mass of any new gauge boson be at least a few hundred GeV/c^2 to be consistent with existing limits from deep inelastic leptoproduction experiments.

Assuming a new charged gauge boson, W', with the same coupling strengths as the ordinary W, we obtain the cross section for production in $\bar{p}p$ collisions cross section shown in Figure 46 for present collider energies, and in EHLQ (p.648) for supercollider energies.

For a new neutral gauge boson, Z', with the same coupling strengths as the ordinary Z we obtain the production cross sections shown in Figure 47 for present collider energies, and in EHLQ (p.649) for supercollider energies.

Requiring 300 produced events for discovery, the mass limits for discovering a new W' or Z' in present and future hadron colliders is given in Table 6.

It is interesting to notice that at SSC energies the ratio of production for W'^+ to W'^- becomes significantly greater than one for very heavy $W'^\pm$'s. This is because for large $\tau = M_{W'}^2/s$ the production rate is sensitive to the valence quark distributions in the proton. In fact, at the discovery limit, the ratio even exceeds the naive ratio of $u_v/d_v = 2$ of the proton - This is precisely the way the actual valence distribution functions behave at large x. (Compare Eq. 1.22).

Figure 46: Total cross section, σ (nb), for production of a new charged gauge boson, $W'^{\pm}$ in $\bar{p}p$ collisions at $\sqrt{s} = 630$ GeV (lower solid line), 1.8 TeV (upper solid line), and 2.0 TeV (dashed line). The parton distributions of Set 2 used. The same couplings as the standard $W^{\pm}$ assumed.
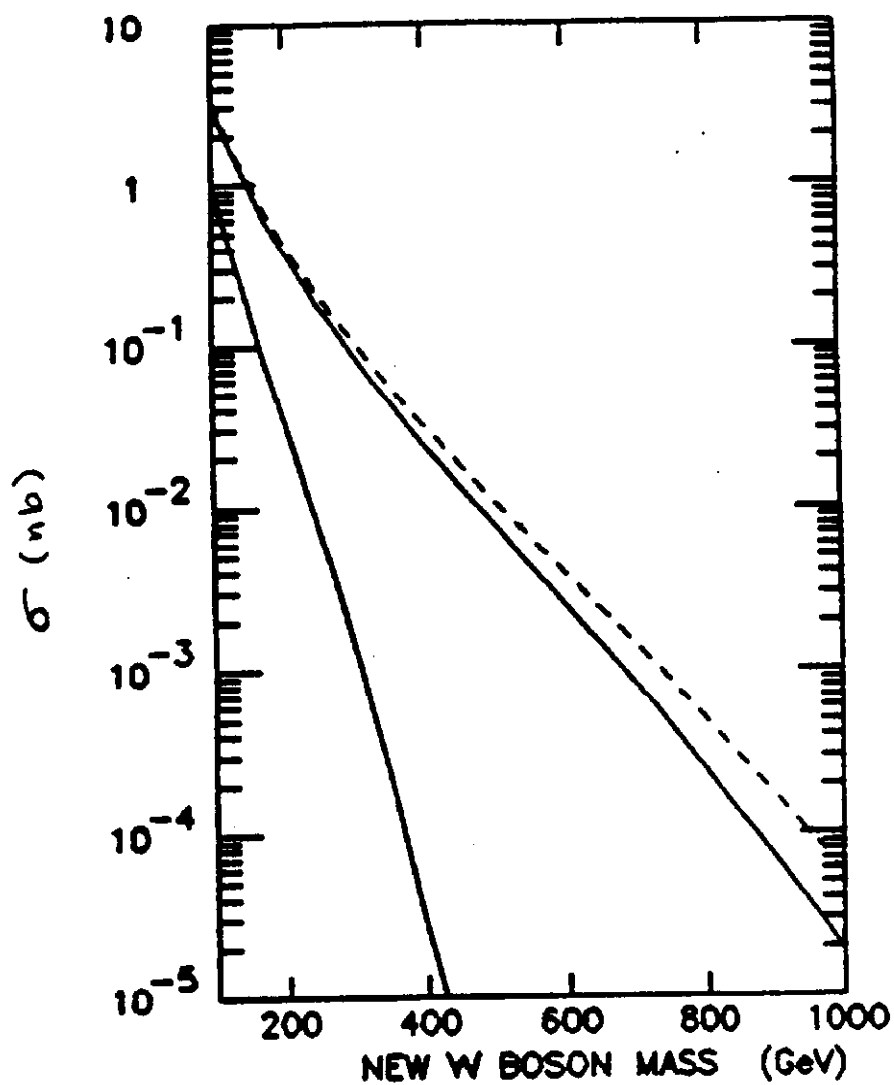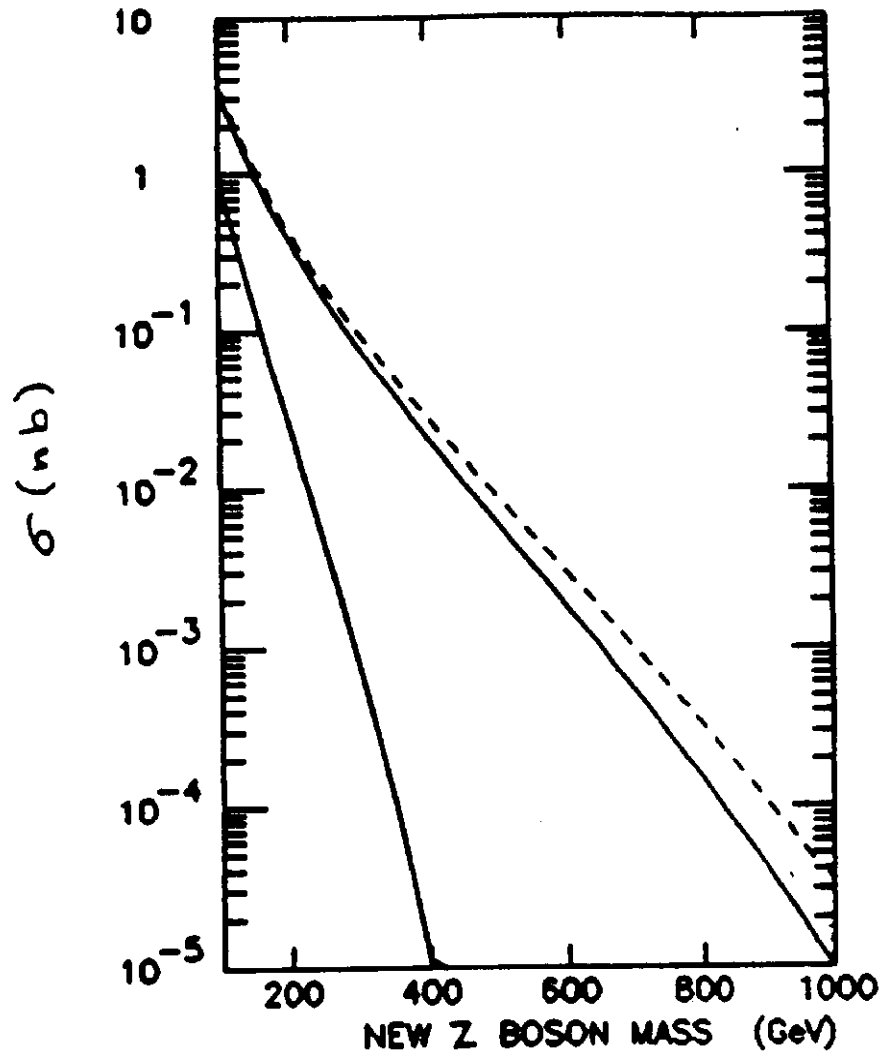
Figure 47: Total cross section, σ (nb), for production of a new neutral gauge boson, Z'^0 in $\bar{p}p$ collisions at $\sqrt{s}$ = 630 GeV (lower solid line), 1.8 TeV (upper solid line), and 2.0 TeV (dashed line). The parton distributions of Set 2 used. The same couplings as the standard Z^0 assumed.

Table 6: Expected discovery limits for new intermediate gauge bosons $W'^{\pm}$ and Z'^0 at present and planned hadron colliders. For a Z' 300 produced events are required; while for $W'^+ + W'^-$ a total of 600 produced events are required. Standard model couplings are assumed. For pp collisions the ratio of W'^+ to W'^- production $R(+/-)$ need not be one. This ratio R for $W'^{\pm}$ mass at the discovery limit is also shown.

Collider		$\sqrt{s}$ (TeV)	$\int dt \mathcal{L}$ (cm)$^{-2}$	Mass limit (Gev/c^2) Intermediate Boson		
				$W'^{\pm}$	$R(+/-)$	Z'^0
$S\bar{p}pS$	$\bar{p}p$	.63	3×10^{36}	155	1	160
upgrade			3×10^{37}	225	1	230
$TEVI$	$\bar{p}p$	1.8	10^{37}	370	1	375
upgrade		2	10^{38}	560	1	610
SSC	pp	40	10^{38}	2,700	2.0	2,400
			10^{39}	4,600	2.4	4,200
			10^{40}	6,900	2.8	6,700

IV. THE SCALAR SECTOR

A. The Higgs Scalar

1. Lower Bound on the Higgs Mass

A lower bound of the Higgs mass (m_H) arises from requiring that the symmetry breaking minimum of the potential $V(\phi)$ be stable with respect to quantum corrections[65]. If m_H is too small there could be tunneling to a symmetry preserving vacuum.

To illustrate this, we do a simple one loop calculation using the standard symmetry breaking potential for a Higgs doublet[66]:

$$V(\phi^\dagger \phi) = -\mu_0^2 \phi^\dagger \phi + |\lambda|(\phi^\dagger \phi)^2 \ . \tag{4.1}$$

It is sufficient to consider an external scalar field with its only non-zero component along the direction of symmetry breaking. This amounts to taking only the real neutral component so that $< \phi^\dagger \phi > = < \phi >^2$. This field couples to those particles that acquire mass as a result of the symmetry breaking: $W^\pm$ and Z^0, and the fermions ψ.

$$< \phi^\dagger \phi > [\frac{g^2}{2}W_\mu^+ W^{-\mu} + \frac{(g^2 + g'^2)}{4}Z_\mu^0 Z^{0\mu}] + \sum_{i=1}^{3} \phi[\Gamma_{u_i}\overline{\psi}_{u_i}\psi_{u_i} + \Gamma_{d_i}\overline{\psi}_{d_i}\psi_{d_i}] \quad (4.2)$$

Because the Yukawa couplings are small we shall ignore the fermions and only consider the contribution to the effective potential from vector particle loops, with ϕ insertions:
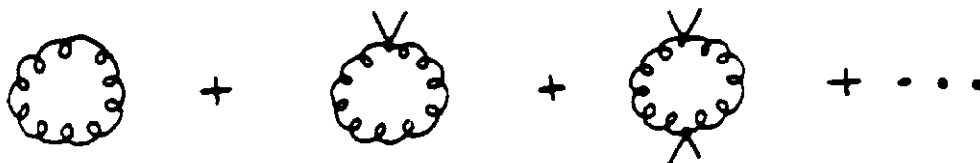
The form of the integral for these processes is:

$$-i \int \frac{d^4k}{(2\pi)^4} \frac{k^2}{k^2 - g^2 < \phi >^2/4} \tag{4.3}$$

which may be regulated to give :

$$A_0 + A_1 <\phi>^2 + \frac{g^4}{128\pi^2} <\phi>^4 \ln(\frac{<\phi>^2}{A_2}) \qquad (4.4)$$

That is, a sum of a quartically, quadratically and logarithmically divergent term.

When the effective potential is renormalized we can ignore A_0 , and absorb A_1 into the scalar mass renormalization. The term A_2 is absorbed into the scalar coupling renormalization, while the finite part appears with a renormalization scheme dependent scale parameter M in the resulting one-loop effective potential.

$$V_{1loop}(<\phi>^2) = -\mu^2 <\phi>^2 + C <\phi>^4 \ln(\frac{<\phi>^2}{M^2}) \qquad (4.5)$$

This is the form of the general answer. A careful calculation taking into account fermions and scalars as well was performed by E. Gildner and S. Weinberg[67]. They obtained

$$C = \frac{1}{64\pi^2} \frac{1}{<\phi>_0^4} (3(2M_W^4 + M_Z^4) - 4\sum_F m_F^4 + m_H^4) \qquad (4.6)$$

where $<\phi>_0^2 = 1/(2\sqrt{2}G_F)$ and the Yukawa and gauge couplings are reexpressed in terms of particle masses.

In models with a non minimal Higgs sector, m_H^4 would be replaced with $\sum m_H^4$. Note that $C > 0$ as is required for overall stability at large values of $<\phi>^2$.

This potential has a local minimum at $<\phi>^2 = <\phi>_0^2$ where $\frac{\partial V}{\partial <\phi>^2}|_{<\phi>_0^2} = 0$ so

$$<\phi>_0^2 (\ln(\frac{<\phi>_0^2}{M^2}) + \frac{1}{2}) = \frac{\mu^2}{2C} . \qquad (4.7)$$

Because in general there is another local minimum at $<\phi>^2 = 0$, we must check that $V(<\phi>_0^2) < V(0)$ to insure that $<\phi>^2 = <\phi>_0^2$ is an absolute minimum. This requires

$$\ln(\frac{<\phi>_0^2}{M^2}) > -1 . \qquad (4.8)$$

This condition that the symmetry breaking minimum is more stable that the symmetry preserving one can be expressed as a limit on m_H by using the definition $m_H^2 = \frac{\partial^2 V}{\partial \phi^2}|_{<\phi>_0}$. This implies

$$m_H^2 > 2C <\phi>_0^2 \simeq \frac{3G_F\sqrt{2}}{16\pi^2} (2M_W^4 + M_Z^4) = 7.1 GeV/c^2 . \qquad (4.9)$$

In the context of the minimal Higgs model, this represents a strict lower bound for m_H consistent with symmetry breaking. A slightly simpler calculation[68] can be done for the case $\mu = 0$, leading to $m_H > 10 GeV/c^2$, however the assumption that $\mu = 0$ has no theoretical justification.

2. Unitarity Bounds

The simplest upper bound on m_H arises from the requirement of preturbative unitarity. That is, on the assumption that the couplings are sufficiently weak to make perturbation theory valid, we require that all processes obey the constraint of unitarity order by order in perturbation theory. Of course, it is possible that perturbation theory is not valid , in that case there is likely to be new physics associated with the interactions becoming strong. We postpone that discussion until the next lecture.

Unitarity in general requires:

$$S^\dagger S = (1 + iT^\dagger)(1 - iT) = 1 \tag{4.10}$$

or

$$i(T - T^\dagger) = -ImT = T^\dagger T \tag{4.11}$$

To set up the unitarity argument in its simplest form we only consider two particle quasi-elastic scattering for equal mass scalar particles (i.e. internal quantum numbers but not masses can change from the initial to final state). The scattering process in the center of mass frame is shown in Fig. 48 In this simple case, the T matrix is:

$$T_{fi} = (2\pi)^4 \delta^4(p_1 + p_3 - p_2 - p_4) \frac{1}{(2\pi)^6} \frac{1}{s} M_{fi}(s,t) \tag{4.12}$$

where $s = (p_1 + p_3)^2 = (p_2 + p_4)^2$ and $t = (p_1 - p_2)^2$ and the scattering angle in the CM Frame, θ, is given by

$$t = -\frac{(s - 4m^2)}{2}(1 - \cos\theta) . \tag{4.13}$$

The invariant amplitude can be expanded into partial waves:

$$M = 16\pi \sum_{J=0}^{\infty} (2J + 1) A_J(s) P_J(\cos\theta) . \tag{4.14}$$

$$S = (p_1 + p_3)^2$$
$$t = (p_1 - p_2)^2$$
$$u = (p_1 - p_4)^2$$
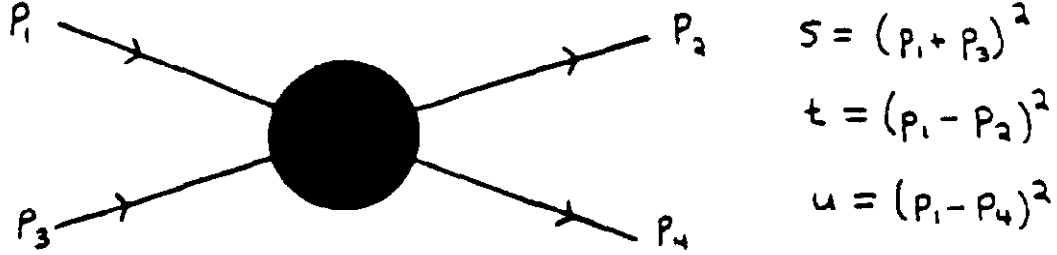
Figure 48: Kinematics of the 2 → 2 scattering amplitude for equal mass scalar particles.

For s below the inelastic threshold, so that there are only two particle intermediate states, the unitarity condition may be written entirely in terms of the two particle amplitude $\mathcal{M}$ as:

$$- Im\,\mathcal{M}(s, \cos\theta_{fi}) = \frac{1}{64\pi^2}\sqrt{\frac{s - 4m^2}{s}} \int d\Omega_k \mathcal{M}^*(s, \cos\theta_{fk}) \mathcal{M}(s.\cos\theta_{ki}) \qquad (4.15)$$

where the momentum integration has been done to obtain the phase space factor $\sqrt{(s - 4m^2)/s}$.

Now, using the partial wave expansion for $\mathcal{M}$ and performing the angular integration we find that each partial wave satisfies:

$$|A_J(s)| \geq \sum_{n=1}^{\infty} A_J^{(n)} = \sum_{n=1}^{\infty} c_{Jn} g^{2n} . \qquad (4.16)$$

The Born contribution (first order) corresponds to $A_J^{(1)} = c_{J1}g^2$. The criterion for validity of perturbation theory is that successive terms in the expansion are smaller, i.e. $|c_1 g^2| \gg |c_2 g^4| \gg \ldots$ etc.. Thus we will consider only the lowest order terms in the following.

The $J = 0$, s-wave scattering condition is

$$- Im A_0 \geq |A_0|^2 \qquad (4.17)$$

so

$$- Im(c_1 g^2 + c_2 g^4 + \ldots) \geq |c_1 g^2 + c_2 g^4 + \ldots|^2 . \qquad (4.18)$$

It is a property of the Born amplitude that at high energy $(s \to \infty)$ it is essentially real. Thus the imaginary term of c_1 can be dropped to obtain:

$$|c_1 g^2| > -Im(c_2 g^4) \geq |c_1 g^2|^2 \; . \tag{4.19}$$

Thus the perturbative unitarity constraint on the Born amplitude is[69]

$$1 > |c_1 g^2| = |A_0^{(1)}| \; . \tag{4.20}$$

We proceed to apply this constraint to the scalar sector of the standard (W-S) electroweak theory.

3. Upper Bound on the Higgs Mass[70]

Now we apply the general unitarity arguments specifically to the W-S Model. We start by showing that at high energy we need only consider an effective scalar theory, so that the simple bound (Eq. 4.20) just derived can be applied even in this more complicated theory[71].

As discussed in Section 3, massive vector particle (V_μ) scattering has potentially bad behaviour at high energy. This is apparent from the form of the polarization sum:

$$-\sum_\lambda \xi^\mu(k,\lambda)\xi^\nu(k,\lambda) = g^{\mu\nu} - k^\mu k^\nu/M_V^2 \; . \tag{4.21}$$

The dominant term here is the $k^\mu k^\nu / M_V^2$ piece which comes from the longitudinal polarization (λ_L)

$$\xi^\mu(k,\lambda_L) = \frac{1}{M_V}(|\bar{k}|, k^0 \frac{\bar{k}}{|\bar{k}|}) \tag{4.22}$$

and has the potential to violate the unitarity bounds.

It has been shown that the only renormalizable theories with massive non-Abelian vector bosons are those in which the masses arise from a spontaneously broken gauge symmetry[72]. In such cases one can replace the longitudinal components of the vector fields by scalar fields and get an effective Lagrangian that is valid at high energy. The most appropriate gauge for showing this is the t'Hooft-Feynman gauge[73],

$$\partial_\mu V^\mu + M_V \phi = 0 \tag{4.23}$$

where ϕ is the Goldstone Boson associated with giving mass to the vector boson. In momentum space, the longitudinal component of the vector field is

$$\bar{V}_L(k) = \xi_L^\mu V_\mu(k) = \frac{1}{M_V}(|\vec{k}|\bar{V}_0 - k^0 \frac{\vec{k}}{|\vec{k}|} \cdot \vec{V}) \; ; \tag{4.24}$$

which, using the gauge condition (Eq. 4.23), just becomes the scalar field in the high energy limit:

$$\bar{V}_L(k) \rightarrow -i\bar{\phi} + \bigcirc(\frac{M_V}{|\vec{k}|}) \quad for \; |\vec{k}| \gg M_V \; . \tag{4.25}$$

In discussing the high energy unitarity constraints we may therefore ignore the transverse degrees of freedom of the vector fields and only consider an effective Lagrangian describing scalars interacting with fermions. The scalars include both the Higgs (h) and the 'eaten' Goldstone Bosons (w^+, w^-, z) that describe the longitudinal degrees of freedom of the gauge bosons. The notation is

$$\phi = \frac{1}{\sqrt{2}} \begin{pmatrix} \sqrt{2} \, iw^+ \\ v + h - iz \end{pmatrix} \tag{4.26}$$

with $m_H^2 = 2\mu^2$, $v^2 = 1/(\sqrt{2}G_F)$, and $\lambda = G_F m_H^2/\sqrt{2}$.

The full effective Lagrangian is given by:

$$\begin{aligned}
\mathcal{L}_{eff} = \;& (\partial_\mu w^+)(\partial^\mu w^-) - m_W^2 w^+ w^- + \frac{1}{2}(\partial_\mu z)(\partial^\mu z) - \frac{1}{2}m_z^2 z^2 \\
& + \frac{1}{2}(\partial_\mu h)(\partial^\mu h) - \frac{1}{2}m_H^2 h^2 \\
& - \lambda v h(2w^+ w^- + z^2 + h^2) - \frac{1}{4}\lambda(2w^+ w^- + z^2 + h^2)^2 \\
& + \bar{u}\gamma^\mu D_\mu^G u - m_u \bar{u}u + \bar{d}\gamma^\mu D_\mu^G d - m_d \bar{d}d \\
& + \bar{\nu}\gamma^\mu D_\mu^G \nu + \bar{e}\gamma^\mu D_\mu^G e - m_e \bar{e}e \\
& - \Big(\Gamma_u[i \, \bar{d}\frac{(1+\gamma_5)}{2}u \; w^- + \bar{u}\frac{(1+\gamma_5)}{2}u \, \frac{(h \; + \; iz)}{\sqrt{2}}] \\
& + \Gamma_d[i \, \bar{u}\frac{(1+\gamma_5)}{2}d \; w^+ + \bar{d}\frac{(1+\gamma_5)}{2}d \, \frac{(h \; - \; iz)}{\sqrt{2}}] \\
& + \Gamma_e[i \, \bar{\nu}\frac{(1+\gamma_5)}{2}e \; w^+ + \bar{e}\frac{(1+\gamma_5)}{2}e \, \frac{(h \; - \; iz)}{\sqrt{2}}] + h.c.\Big) \tag{4.27}
\end{aligned}$$

Using this Lagrangian, all Born amplitudes for neutral channels can be easily calculated. The results are summarized in Fig. 49.

The limiting behaviour of these processes at high energy ($s \gg m_H^2 > m_W^2$, m_Z^2) is collected in matrix form

$$M = -2\sqrt{2}G_F m_H^2 \begin{pmatrix} 1 & \frac{1}{\sqrt{8}} & \frac{1}{\sqrt{8}} & 0 \\ \frac{1}{\sqrt{8}} & \frac{3}{4} & \frac{1}{4} & 0 \\ \frac{1}{\sqrt{8}} & \frac{1}{4} & \frac{3}{4} & 0 \\ 0 & 0 & 0 & \frac{1}{2} \end{pmatrix} \begin{array}{l} w^+ w^- \\ z^2/\sqrt{2} \\ h^2/\sqrt{2} \\ hz \end{array} \tag{4.28}$$

As in the previous section we expand in partial waves and identify the s-wave Born term as

$$A_0^{(1)} = \frac{M}{16\pi} \equiv \frac{G_F m_H^2}{4\pi\sqrt{2}} t_0 . \tag{4.29}$$

To obtain the best bound we diagonalize the matrix t_0 (defined above). The largest eigenvalue is 3/2, for the combination of channels above which correspond to the isoscalar channel $(2w^+w^- + zz + hh)$.

Substituting this into the perturbative unitarity condition $|A_0^{(1)}| \leq 1$ we find an upper bound on m_H:

$$m_H \leq \sqrt{\frac{8\pi\sqrt{2}}{3G_F}} = .98 TeV/c^2 . \tag{4.30}$$

We close this section with a comment on the nature a perturbative unitarity bound. If such a bound is violated then perturbative expansion must be invalid since the Lagrangian is unitary. That is, the interactions are strong and perturbation theory is therefore unreliable. An up to date analysis of the physics of a strongly interacting scalar sector has been given by Chanowitz and Gaillard[74].

Whether the scalar sector of the W-S Model is, in fact, strongly interacting is presently unknown. Because the scalar sector is protected by an order of α_{em} from showing up in low energy electroweak measurements (e.g. in the ρ parameter[75]) no experiment to date rules out the possibility of a strongly interacting Higgs sector. Only direct observation of the Higgs scalar or strong interactions at (or below) the TeV scale will settle this question experimentally.

$$w^+ w^- \rightarrow w^+ w^- :$$

$$-2i\lambda[2 + \frac{m_H^2}{s - m_H^2} + \frac{m_H^2}{t - m_H^2}]$$

$$z z \rightarrow z z :$$

$$-2i\lambda[3 + \frac{m_H^2}{s - m_H^2} + \frac{m_H^2}{t - m_H^2} + \frac{m_H^2}{u - m_H^2}]$$

$$h h \rightarrow h h :$$

$$-6i\lambda[1 + 3\frac{m_H^2}{s - m_H^2} + 3\frac{m_H^2}{t - m_H^2} + 3\frac{m_H^2}{u - m_H^2}]$$

$$h z \rightarrow h z :$$

$$-2i\lambda[1 + \frac{m_H^2}{s - m_H^2} + 3\frac{m_H^2}{t - m_H^2} + \frac{m_H^2}{u - m_H^2}]$$

$$w^+ w^- \rightarrow z z :$$

$$-i\lambda[1 + \frac{m_H^2}{s - m_H^2}]$$

$$w^+ w^- \rightarrow h h :$$

$$-2i\lambda[1 + 3\frac{m_H^2}{s - m_H^2} + \frac{m_H^2}{t - m_H^2} + \frac{m_H^2}{u - m_H^2}]$$

$$z z \rightarrow h h :$$

$$-2i\lambda[1 + 3\frac{m_H^2}{s - m_H^2} + \frac{m_H^2}{t - m_H^2} + \frac{m_H^2}{u - m_H^2}]$$

Figure 49: Born amplitudes for neutral channels.

B. Constraints on Fermion Masses

1. Perturbative Unitarity Bounds

We can use the same W-S effective Lagrangian (Eq. 4.27) and perturbative unitarity for the Yukawa couplings to put upper bounds on fermion masses. In general because of spin the perturbative unitarity condition will be more complicated than the one we derived (Eq. 4.20), futhermore the neutral fermion-antifermion channels $(\overline{F}F)$ will couple to the channels $w^+ w^-$, zz, hh, and zh already discussed.

The general case is discussed fully by M. Chanowitz, M. Furman, and I. Hinchliffe[76]. However in the $J = 0$ partial wave things are simpler and if we further assume that m_H is small relative to the fermion masses to be bounded we can avoid having a coupled problem. In this case the helicity amplitudes in the CM Frame for the $\overline{F}F$ channels are defined by:

$$\frac{\vec{\Sigma} \cdot \vec{p}}{|\vec{p}|} u^{(\lambda)}(p) = \lambda u^{(\lambda)}(p)$$

$$\frac{\vec{\Sigma} \cdot \vec{p}}{|\vec{p}|} v^{(\lambda)}(p) = -\lambda v^{(\lambda)}(p) \tag{4.31}$$

If $F = \begin{pmatrix} F_1 \\ F_2 \end{pmatrix}$ is a quark (or lepton) doublet then the relevant Born amplitudes are shown in Figure 50.

For the amplitudes in Fig. 50 we can construct a matrix of the $J = 0$ partial wave amplitudes for the various channels just as in the scalar case (Eq. 4.28). The only complication is that we must consider each helicity channel as well. The non zero helicity amplitudes are:

$$\begin{pmatrix} + & + & \rightarrow & + & + \\ - & - & \rightarrow & - & - \\ + & - & \rightarrow & - & + \\ - & + & \rightarrow & + & - \end{pmatrix} . \tag{4.32}$$

The unitarity condition is simply $|M_0^{(1)}| \leq 1$ as before. Applying this condition to the largest eigenvalue of $|M|$ in the fermion case leads to the following upper

$J = 0$ (uncoupled)

$$\xrightarrow[S\to\infty]{}\mathcal{M} = \sqrt{2}\,G_F m_i m_j \delta_{\lambda\bar\lambda}\delta_{\lambda'\bar\lambda'}$$

$$[(1 - \lambda\lambda') - 2\delta_{ij}]$$

$$\xrightarrow[S\to\infty]{}\mathcal{M} = -\sqrt{2}\,G_F m_i^2 \delta_{\lambda-\lambda'}\delta_{\bar\lambda-\bar\lambda'}$$

$$[1 - \lambda\bar\lambda]$$

$$\xrightarrow[S\to\infty]{}\mathcal{M} = -2\sqrt{2}\,G_F\{\delta_{\lambda\bar\lambda}\delta_{\lambda'\bar\lambda'}\, m_1 m_2[(1 + \lambda\lambda')]/2$$

$$+\delta_{\lambda-\lambda'}\delta_{\bar\lambda-\bar\lambda'}[m_1^2\delta_{\lambda,+1} + m_2^2\delta_{\lambda,-1}]$$

$$[1 - \lambda\bar\lambda]/2\}$$
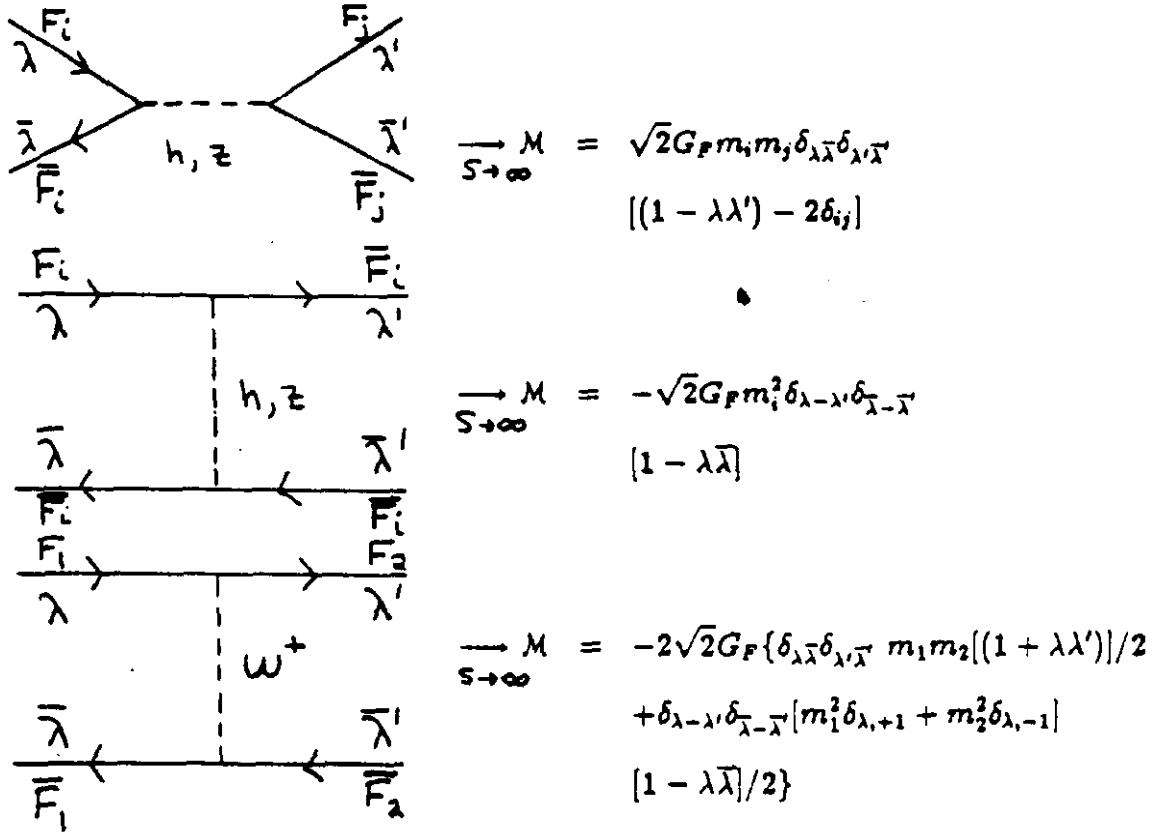
Figure 50: Born graphs for the $\bar F F$ amplitudes in the uncoupled limit ($m_H \ll m_i$). $\mathcal{M}$ is the amplitude for the $J = 0$ partial wave in the high energy limit.

bounds for a quark doublet[76]:

$$\frac{G_F}{8\sqrt{2}\pi}[3(m_1^2 + m_2^2) + \sqrt{9(m_1^2 - m_2^2)^2 + 8m_1^2 m_2^2}] \leq 1 \qquad (4.33)$$

which for equal mass quarks $(m = m_1 = m_2)$ becomes:

$$m \leq (\frac{4\sqrt{2}\pi}{5G_F})^{1/2} = 530 GeV/c^2 . \qquad (4.34)$$

For a lepton doublet, the bound is:

$$\frac{G_F}{8\sqrt{2}\pi}[m_1^2 + m_2^2 + |m_1^2 - m_2^2|] \leq 1 . \qquad (4.35)$$

and for the case $m_1 = 0$, $m_2 = m$ the limit becomes:

$$m \leq (\frac{4\sqrt{2}\pi}{G_F})^{1/2} = 1.2 TeV/c^2 . \qquad (4.36)$$

A slightly better bound for leptons of $\approx 1TeV/c^2$ comes from considering the more complicated case of the $J = 1$ partial wave[76].

Although only one generation of quarks and/or leptons has been considered it is possible to interpret the bounds as being on the sum over generations of masses with the other quantum numbers the same. Of course in practice this sum is dominated by the heaviest fermion in any case.

It is interesting to compare these unitarity bounds on fermion masses within the standard model with the discovery limits of the various hadron colliders present and planned. These limits are shown in Table 5. We see that the SSC will be able to discover any new fermion with mass satisfying the bounds given above.

2. Experimental Bounds

In addition to the lower bounds on the masses of new quark or leptons arising from discovery limits summarized in Table 5 there is also the possibility of upper bounds on fermion masses arising from experimental measurements. This was first was realized by M. Veltman[77]. The basic point is that the Higgs sector of the W-S theory has an $SU(2)_L \otimes SU(2)_R$ symmetry (as we discussed in Section 3.2). This

symmetry is spontaneously broken down to an $SU(2)_V$ symmetry when the scalar field acquires a vacuum expectation value. It is the residual $SU(2)_V$ symmetry that ensures:

$$\frac{M_W^2}{M_Z^2 \cos^2 \theta_w} \equiv \rho = 1 .$$ (4.37)

The Yukawa couplings and electroweak gauge interactions break the $SU(2)_V$ symmetry explicitly. In particular, for $\Gamma_u \neq \Gamma_d$, the fermion one loop corrections to the $W^\pm$ and Z^0 masses will change the value of the ρ parameter.

For a heavy fermion doublet the correction is[77]

$$\rho = 1 + \xi \frac{G_F}{8\sqrt{2}\pi^2} [\frac{2m_1^2 m_2^2}{m_1^2 - m_2^2} \ln(\frac{m_2^2}{m_1^2}) + m_1^2 + m_2^2]$$ (4.38)

where ξ is 1 for leptons and 3 for quarks. For example, in the case of the leptons, with $m_1 = 0$, $m_2 = m$:

$$\rho = 1 + \frac{G_F}{8\sqrt{2}\pi^2} m^2 .$$ (4.39)

A compilation of the present data yields a measured value for ρ [78]

$$\rho = 1.02 \pm 0.02$$ (4.40)

which leads to the bounds on new lepton and new quark masses:

$$m_L \leq 620 GeV/c^2$$ (4.41)

and

$$|m_u^2 + m_d^2 + \frac{2m_u^2 m_d^2}{m_u^2 - m_d^2} \ln(\frac{m_d^2}{m_u^2})|^{1/2} \leq 350 GeV/c^2$$ (4.42)

respectively.

C. Finding the Higgs

1. Higgs Mass Below $2M_W$

Finding a Higgs boson with a low mass $m_H \leq M_Z$ is possible through real or slightly virtual Z^0 production by the mechanism shown in Figure 51
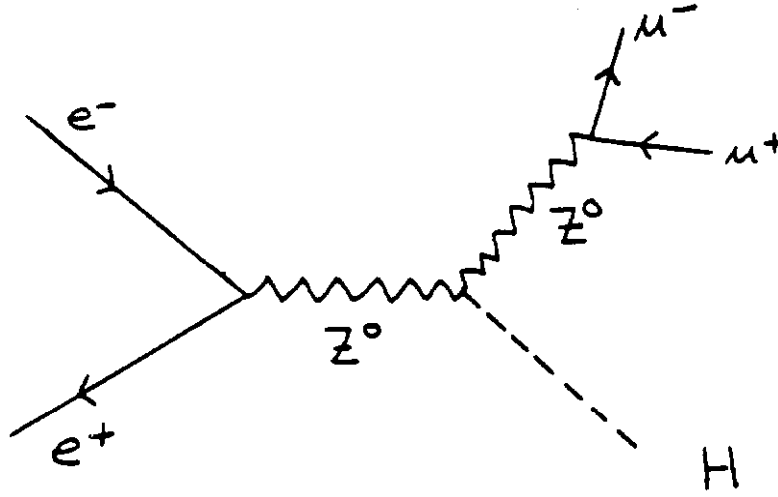
Figure 51: Associated Production Mechanism for a Low Mass Higgs Boson.

Although hadron colliders will produce 10^4 to 10^5 Z^0's a year, the best place to find the Higgs boson in this mass range is an e^+e^- collider where the energy can be tuned to the region of the Z^0 pole to yield a clean, high statistics sample of Z^0 decays. In particular LEP should have approximately 10^7 Z^0 decays per year.

For the intermediate mass range ($M_Z \leq m_H \leq 2M_W$) no convincing signal for detecting a Higgs boson is presently known. The production rate (by the mechanism in Fig. 51) is small even in a e^+e^- collider with $\sqrt{s} = 200$ GeV. On the other hand, in hadron colliders additional production mechanisms exist and the total rate of Higgs boson production in the mass range can be substantial. Thus hadron colliders provide the best hope for finding a Higgs boson with a mass in this intermediate range.

The first and most obvious additional Higgs production mechanism in a hadron collider is direct production by a quark pair (shown in Figure 52a). Because the Higgs coupling is proportional the mass of the fermion, we might expect the heaviest pair, namely the top quarks, be the dominant subprocess. Indeed,

$$\sigma(\bar{p}p \to H_0 + X) \;=\; \frac{G_F \pi}{3\sqrt{3}} \sum_i \frac{m_i^2}{m_H^2} \tau \frac{d\mathcal{L}_{ii}}{d\tau}$$

$$=\; 3.36nb \sum_i \frac{m_i^2}{m_H^2} \tau \frac{d\mathcal{L}_{ii}}{d\tau} \tag{4.43}$$

where m_i is the mass of the ith quark flavor. However, referring back to Fig. 17 we see that the $\bar{t}t$ luminosity is small even at supercollider energies. For example at $\sqrt{s} = 40$ TeV assuming a 30 GeV/c^2 top quark the Higgs production cross section

$$\sigma(\bar{t}t \to H^0) = 9 \ pb \ . \tag{4.44}$$

. For lighter quarks, where the luminosity is greater, the mass proportional coupling suppresses production.

There is however a second production mechanism which gives large production cross sections. This is the gluon fusion process shown in Figure 52b. This one loop coupling of gluons to the Higgs through a quark loop takes advantage of both the large number of gluons in a proton at these subenergies and the large coupling of the Higgs to heavy quarks in the loop. The cross section is[79]:

$$\sigma(\bar{p}p \to H^0 + X) = \frac{G_F \pi}{32\sqrt{2}} (\frac{\alpha_s}{\pi})^2 |\eta| \tau \frac{d\mathcal{L}_{gg}}{d\tau} \tag{4.45}$$

where $\eta = \sum_i \eta_i$ and

$$\eta_i = \frac{\epsilon_i}{2} [1 + (\epsilon_i - 1)\phi(\epsilon_i)] \tag{4.46}$$

and $\epsilon_i = \frac{m_i^2}{m_H^2}$ and

$$\phi(\epsilon) = \left\{ \begin{array}{ll} -[\sin^{-1}(1/\sqrt{\epsilon})]^2 & \epsilon > 1 \\ \frac{1}{4}[\ln(\frac{1+\sqrt{1-\epsilon}}{1-\sqrt{1-\epsilon}}) + i\pi]^2 & \epsilon < 1 \end{array} \right\} \ . \tag{4.47}$$

For small ϵ_i, η can be approximated by $0.7 m_i^2/m_H^2$.

This gluon fusion mechanism leads to large cross sections for Higgs production:

m_H	$\sigma(\bar{p}p \to H^0 + X)$ via gluon fusion	
(GeV/c^2)	$\sqrt{s} = 2$ TeV	$\sqrt{s} = 40$ TeV
100	3 pb	300 pb
200	.1 pb	25 pb

In this mass range the principal decay mode of the Higgs is the heaviest fermion pair available, presumably top. Hence a top jet pair with the invariant mass m_H is the signal of the Higgs. However, this signal is buried in the background of QCD
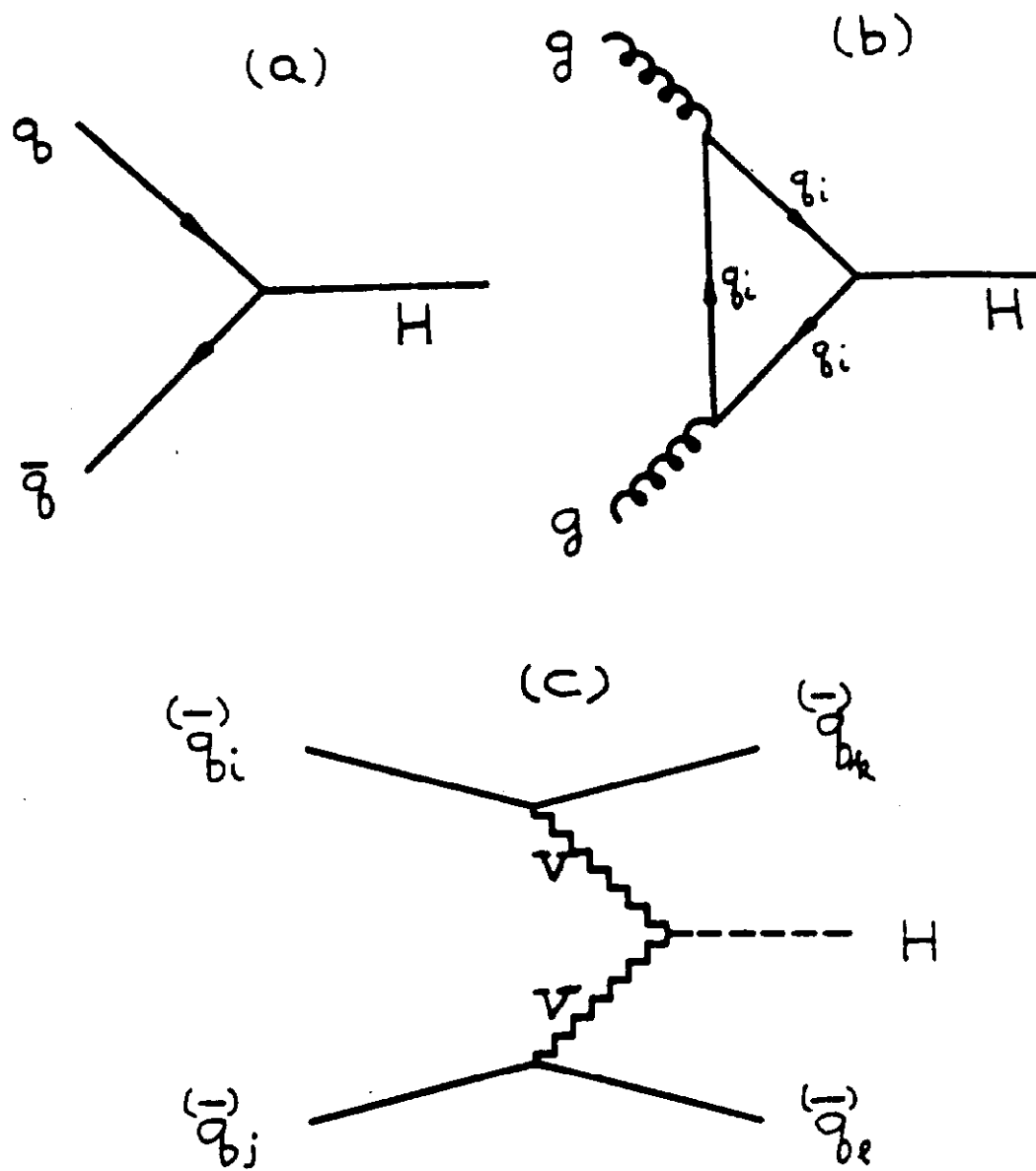
Figure 52: Higgs production mechanisms in hadron colliders: (a) direct production from quark-antiquark annihilation, (b) gluon fusion, and (c) intermediate vector boson fusion.

jet pairs. Even if a perfectly efficient means of tagging top quark jets existed, the signal/background ratio is hopeless small. For example, at $\sqrt{s} = 40$ TeV with a 30 GeV/c^2 top quark

M_{pair}	$\frac{d\sigma}{dM_{pair}}(\bar{p}p \to t + \bar{t} - X)$
100 GeV	7 nb
200 GeV	.7 nb

which swamps the gluon fusion cross sections given above.

At SSC energies it may be possible the find a Higgs in this intermediate mass range by associated production with $W^{\pm}$ or Z from a $q\bar{q}$ initial state. This is basically the same mechanism used for seeing a low mass Higgs in e^+e^- shown in Fig. 51. Although the production rate is low even for SSC energies, the signal/background ratio is much better than in the gluon fusion mechanism because the associated $W^{\pm}$ or Z^0 can be identified through its leptonic decays. The rate is marginal and the success of the method depends on the efficiency of detecting top jets. For a detailed discussion of these issues see Ref. 80.

2. Higgs Mass Above 2 M_W

For high mass Higgs, there is a new production mechanism, in addition to direct production (Fig. 52a) and gluon fusion (Fig 52b), intermediate vector boson (IVB) fusion[81] shown in Figure 52c. This mechanism becomes significant because (as we saw in Fig. 18) the proton contains a substantial number of electroweak gauge bosons constituents at high energies.

The total width (along with the principal partial widths) is shown in Figure 53 for a Higgs boson with mass above the threshold for decay in W^+W^- and Z^0Z^0 pairs. The decays into W^+W^- and Z^0Z^0 pairs dominate for Higgs masses above 250 GeV/c^2; hence the detection signal for a Higgs in the high mass range is a resonance in electroweak gauge boson pair production. The width of this resonance grows rapidly with the Higgs mass. For a Higgs as massive as the unitarity bound (1 TeV/c^2) the width is approximately 500 GeV/c^2, making the resonance difficult to observe.
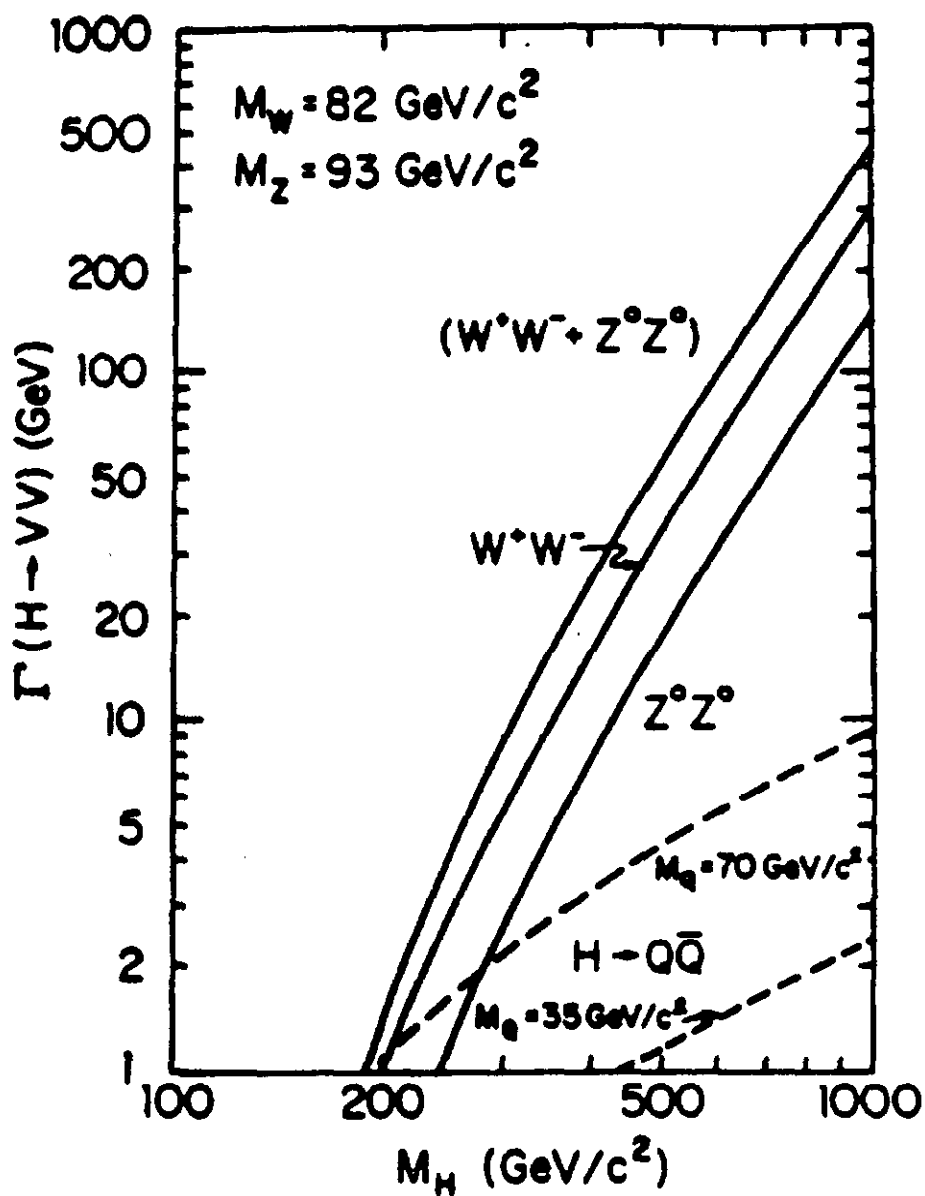
Figure 53: Partial decay widths of the Higgs boson into intermediate boson pairs as a function of the Higgs mass. For this illustration $M_W = 82$ GeV/c^2 and $M_Z = 93$ GeV/c^2. (From EHLQ)

The cross section for the production and decay

$$
\begin{aligned}
pp \ \rightarrow\ & H^0 + \text{anything} \\
& \llcorner\rightarrow Z^0 Z^0
\end{aligned}
\tag{4.48}
$$

at $\sqrt{s} = 40$ TeV is shown in Figure 54. The rapidity of each Z^0 is restricted so that $|y_Z| < 2.5$ and m_t is assumed to be 30 GeV/c^2. The cut ensures that the decay products of the Z^0 will not be confused with the forward-going beam fragments. The contributions from gluon fusion and IVB fusion are shown separately.

The background from ordinary $Z^0 Z^0$ pairs is given by

$$
\Gamma \frac{d\sigma(pp \rightarrow ZZ + X)}{dM}
\tag{4.49}
$$

where $M = m_H$ and $\Gamma = \max(\Gamma_H, 10 \text{ GeV})$. As can be seen from Fig. 54, the background of standard $Z^0 Z^0$ pairs is small.

To compare the reach of various machines the following criterion to establish the existence of a Higgs boson have been adopted in EHLQ. There must be at least 5000 events , and the signal must stand above background by five standard deviations. The 5000 events should be adequate even if we are restricted to observing the leptonic decay modes of the Z^0 (or $W^{\pm}$). In particular, 18 detected events would remain from a sample of 5000 $Z^0 Z^0$ pairs where both Z's decay into $e^+ e^-$ or $\mu^+ \mu^-$. Figure 55 shows the maximum detectable Higgs mass in the $Z^0 Z^0$ final state, with $|y_Z| < 2.5$, and $m_t = 30$ GeV/c^2 as a function of $\sqrt{s}$ for various integrated luminosities. Similar limits apply for the $W^+ W^-$ final state. More details of this analysis can be found in EHLQ.

The assumptions made in the analysis resulting in the discovery limits of Fig. 55 are conservative. It was assumed that $m_t = 30$ Gev/c^2 and that there are no additional generations of quarks. If m_t is heavier or there are additional generations then the Higgs production rate will increase considerably. Hence we can safely conclude that at the SSC with $\sqrt{s} = 40$ TeV and $\mathcal{L} = 10^{33} cm^{-2} sec^{-1}$ the existence of a Higgs with mass $m_H > 2M_W$ can be established. If at least one Z^0 can be detected in a hadronic mode then $\mathcal{L} = 10^{32} cm^{-2} sec^{-1}$ would be sufficient.
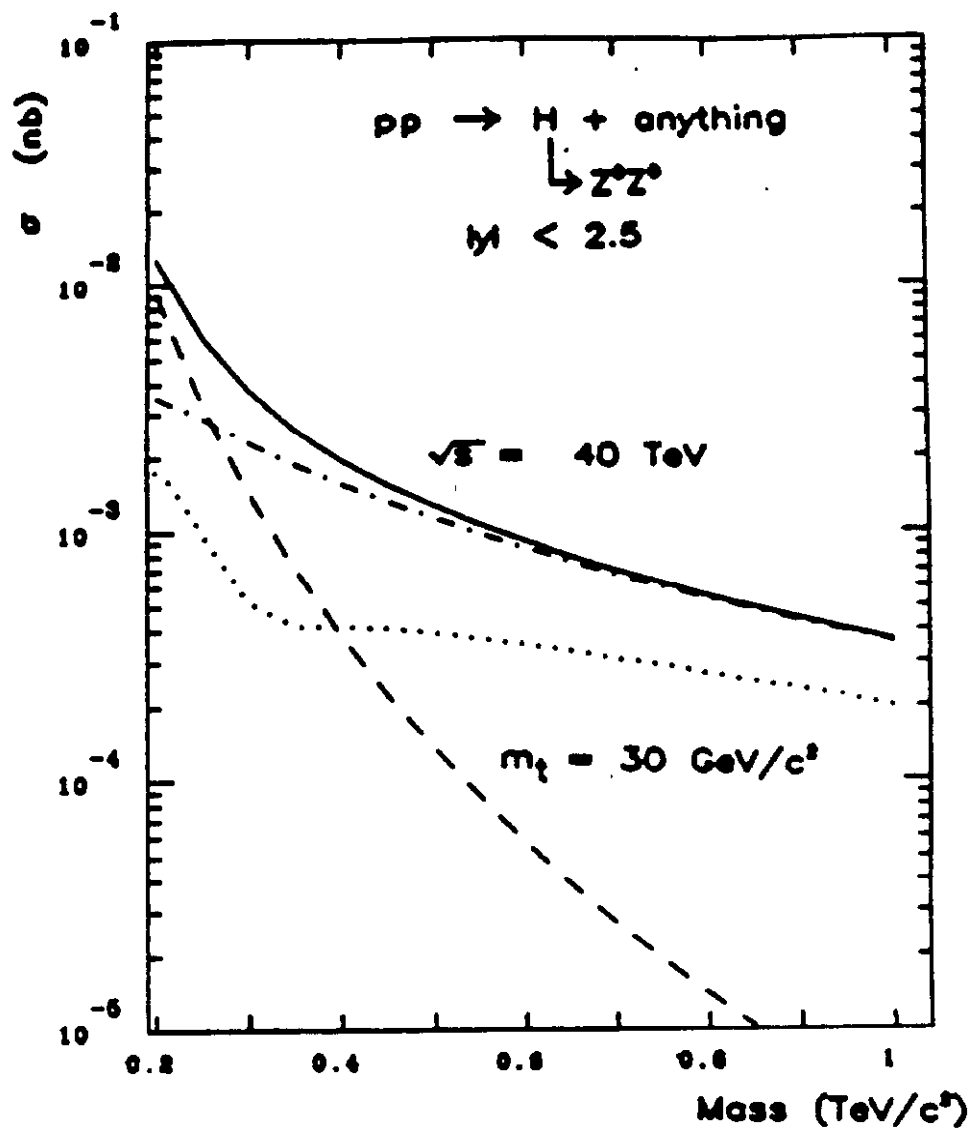
Figure 54: Cross section for the reaction $pp \rightarrow (H \rightarrow ZZ)+$ anything according to EHLQ parton distribution with $\Lambda = .29$GeV. The contribution of gluon fusion (dashed line) and IVB fusion (dotted-dashed line) are shown separately. Also shown (dotted line)is ZZ pair background.
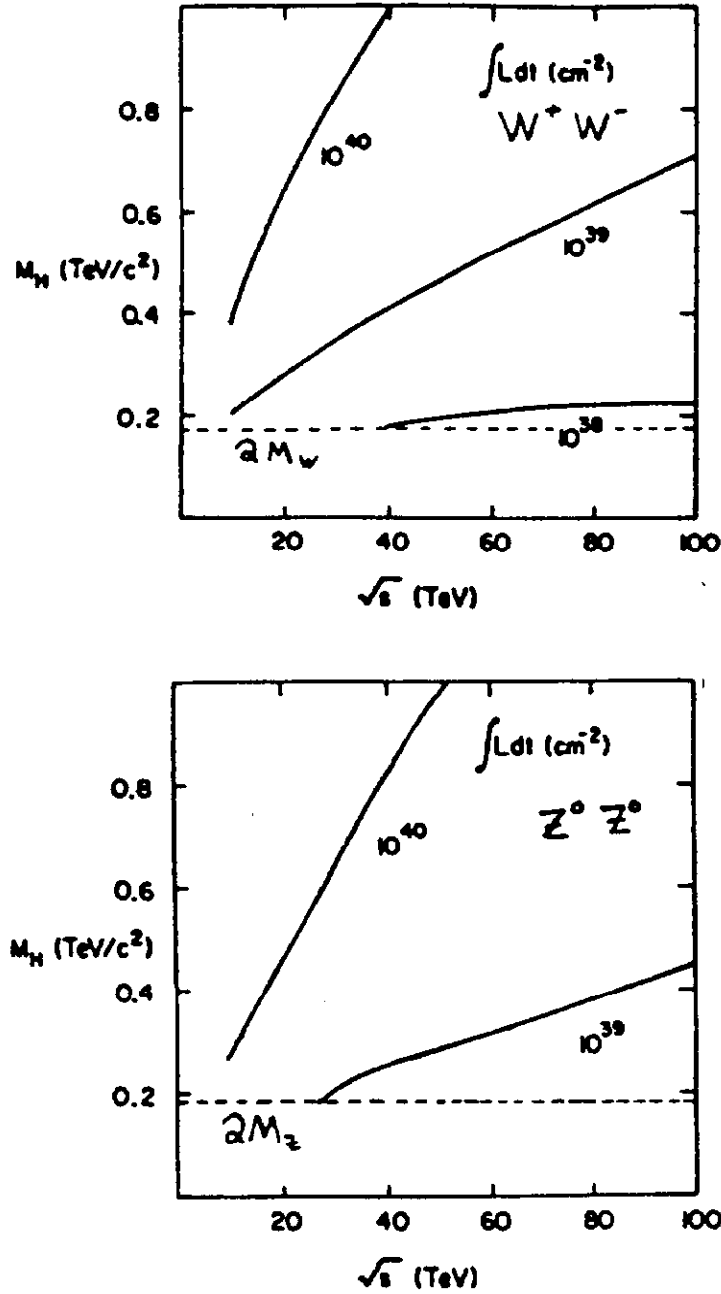
Figure 55: Discovery limit of m_H as a function of $\sqrt{s}$ in $pp \to H \to W^+W^-$ and $pp \to Z^0Z^0$ for integrated luminosities of 10^{40}, 10^{39}, and (for the W^+W^- final state) $10^{38} cm^{-2}$, according to the criteria explained in the text. The dashed line is the kinematic threshold for the appropriate Higgs decay.

D.   Unnaturalness of the Scalar Sector

Presently there is no experimental evidence that requires the modification or extension of the standard model. The motivations for doing so are based upon aesthetic principles of theoretical simplicity and elegance. Perhaps the most compelling argument that the standard model is incomplete is due to 't Hooft[82] .

In general the Lagrangian $\mathcal{L}(\Lambda)$ provides a description of the physics at energy scales at and below Λ in terms of fields (degrees of freedom) appropriate to the scale Λ. In this sense any Lagrangian should be considered as an effective Lagrangian describing physics in terms of the fields appropriate to the highest energy scale probed experimentally. One can never be sure that at some higher energy Λ' $\mathcal{L}(\Lambda')$ may not involve different degrees of freedom. This in fact has happened many times before in the history of physics; the most recent time being the replacement of hadrons with quarks at energy scales above a GeV.

It is a sensible to ask which type of effective Lagrangian can consistently represent the low energy effective interactions of some unknown dynamics at some higher energy scale. This type of question is in a sense metaphysical since it concerns the theory of theories, however much can be learned from studying the classes of possible theories. In this respect one very important property of a Lagrangian is whether it is "natural" or not. There are many different properties of a theory which have been called naturalness[83] . Here I am discussing only the specific definition of 't Hooft[82] :

> A Lagrangian $\mathcal{L}(\Lambda)$ is natural at the energy scale Λ if and only if each small parameter ξ(in units of the appropriate power of Λ) of the Lagrangian is associated with an approximate symmetry of $\mathcal{L}(\Lambda)$ which in the limit $\xi \to 0$ becomes an exact symmetry.

Within the context of an effective Lagrangian this definition of naturalness is simply a statement that it would require a dynamical accident to obtain small ξ except as defined above. This definition of naturalness has two important properties: First to determine whether a theory is nature at some energy scale Λ does not require any knowledge of physics above Λ; and second, if a Lagrangian becomes unnatural at some energy scale Λ_0 then it will be unnatural at all higher scales Λ. Hence if naturalness is to be a property of the ultimate theory of interactions at very high

energy scales, then the effective Lagrangian at all lower energy scales must have the property of naturalness. The W-S theory will elementary scalars becomes unnatural at or below the electroweak scale as we shall see below; therefore if we demand that the final theory of everything is natural, the standard model must be modified at or below the electroweak scale!

The problem with naturalness in the W-S Model comes from the scalar sector. To see the essential difficulty, we consider a simple ϕ^4 theory:

$$\mathcal{L} = \frac{1}{2}(\partial_\mu \phi)^2 - \frac{1}{2}m^2\phi^2 - \frac{\lambda}{4!}\phi^4 \tag{4.50}$$

Consider the naturalness of the parameters in this Lagrangian. λ can be a small parameter naturally because in the limit $\lambda = 0$ the theory becomes free and hence there is an additional symmetry, ϕ number conservation. For the parameter, m^2, the limit $m^2 = 0$ apparently enhances the symmetry by giving a conformally invariant Lagrangian; however this symmetry is broken by quantum corrections[84] and thus can not be used to argue that a small m^2 is natural. Finally, if both λ and m^2 are taken to zero simultaneously, we obtain a symmetry $\phi(x) \rightarrow \phi(x) + c$. Hence we can have an approximate symmetry at energy Λ_0 where:

$$\lambda \sim \bigcirc(\epsilon) \quad \text{and} \quad m^2 \sim \bigcirc(\epsilon\Lambda_0^2) \tag{4.51}$$

Therefore

$$\Lambda_0 = \bigcirc(\frac{m}{\sqrt{\lambda}}) \tag{4.52}$$

ignoring factors of order one. Thus naturalness breaks down for $\Lambda \geq \Lambda_0$.

Returning to the W-S Lagrangian of Eq. 3.1, we can ask if there is any approximate symmetry which can allow for a small scalar mass consistent with naturalness? We have seen that the only possibility is the symmetry $\phi \rightarrow \phi + c$. But this symmetry is broken by both the gauge interactions and the scalar self interactions; hence

$$\frac{m_H^2}{\Lambda^2} \geq \bigcirc(2\lambda) \geq \bigcirc(\alpha_{em}) \tag{4.53}$$

and remembering that $m_H^2 = 4\lambda v^2$ Eq 4.53 implies

$$\Lambda \leq \bigcirc(\sqrt{2}v) = 246 GeV \tag{4.54}$$

the electroweak scale. The W-S model becomes unnatural at approximately the electroweak scale. Also

$$m_H = \frac{2\sqrt{2\lambda}}{g} M_W \geq \bigcirc(M_W) \tag{4.55}$$

Hence values of m_H much below M_W are unnatural.

To summarize, the W-S model is unnatural at energy scales $\Lambda > G_F^{-\frac{1}{2}}$ because m_H^2/Λ^2 is a small parameter which does not has any associated approximate symmetry of the Lagrangian. This unnaturalness is not cured in GUTS models (e.g. SU(5)). The theory must be modified at the electroweak scale in order to remain natural.

Two solutions have been proposed to retain naturalness of the Lagrangian above the electroweak scale:

- Eliminate the scalars as fundamental degrees of freedom in the Lagrangian for $\Lambda \gg G_F^{-\frac{1}{2}}$. We will consider this possibility in the next two lectures on Technicolor and Compositeness.

- Associate an approximate symmetry with the scalars being light. The only possible symmetry known is Supersymmetry, which we will discuss in the last lecture. Since supersymmetry relates boson and fermion masses, and chiral symmetry protects zero values for fermion masses; by combining these two symmetries we can associate a symmetry with masses of scalar fields being zero. However to be effective in protecting scalar masses at the electroweak scale the scale of supersymmetry breaking must be of the order of a TeV or less.

Hence both alternatives for removing the unnaturalness of the standard model require new physics at or below the TeV scale. We will consider the possible physics in detail in the remaining lectures.

V.   A NEW STRONG INTERACTION ?

As we discussed in the last section, the Weinberg-Salam Lagrangian is unnatural for $\Lambda \gg G_F^{-\frac{1}{2}}$. One remedy is to make the scalar doublet of the standard model composite. Then the usual Lagrangian is only the appropriate effective Lagrangian for energies below the scale Λ_T of the new strong interaction which binds the constituents of the electroweak scalar doublet. Clearly this new scale Λ_T cannot be much above the electroweak scale if it is to provide a solution to the naturalness problem.

It should be noted that the standard model itself will be strongly interacting for m_H near the unitarity bound of Eq 4.30 since $m_H^2 = 4\lambda v^2$. So many results presented here will be applicable to that case as well. See M.K. Gaillard's lecture at the 1985 Yale Summer School for a detailed discussion of this possibility[85].

A.   Minimal Technicolor

1.   The Model

The simplest model for a new strong interaction is called technicolor and was first proposed by S. Weinberg[86] and L. Susskind[87]. This model is build upon our knowledge of the ordinary strong interactions (QCD).

The minimal technicolor model introduces a new set of fermions (technifermions) interacting via a new non-Abelian gauge interaction (technicolor). Specifically the technicolor gauge group is assumed to be $SU(N)$ and the technifermions are assumed to be massless fermions transforming as the $N + \overline{N}$ representation. None of the ordinary fermions carry technicolor charges.

The technifermions will be denoted by U and D. In the minimal model the technifermions have no color and transform under the $SU(2) \otimes U(1)$ as:

$$
\begin{array}{ccc}
 & SU(2)_L & U(1)_Y \\
\begin{pmatrix} U \\ D \end{pmatrix}_L & 2 & 0 \\
U_R & & 1 \\
 & 1 & \\
D_R & & -1
\end{array}
$$

The values of the weak hypercharge Y of the technifermions is consistent with the requirement of an anomaly free weak hypercharge gauge interaction. With these assignments the technifermion charges are:

$$Q = I_3 + Y/2 \quad \text{thus} \quad Q_U = +1/2 \text{ and } Q_D = -1/2 \tag{5.1}$$

The usual choice for N is $N = 4$.

Technicolor becomes strong at the scale Λ_T at which $\alpha_T(\Lambda_T) \approx 1$. As with the ordinary strong interactions, the chiral symmetries of the technifermions

$$SU(2)_L \otimes SU(2)_R \tag{5.2}$$

are spontaneously broken to the vector subgroup[88]

$$SU(2)_V \tag{5.3}$$

by the condensate $< \overline{\Psi}\Psi > \neq 0$. The $SU(2)_L \otimes SU(2)_R$ symmetry of the technifermions accounts for the $SU(2)_L \otimes SU(2)_R$ symmetry of the effective Higgs potential. Associated with each of the three broken symmetries is a Goldstone boson. These are $J^{PC} = 0^{-+}$ isovector massless states:

$$\Pi_T^+ \sim \overline{D}\gamma_5 U$$

$$\Pi_T^0 \sim \frac{1}{\sqrt{2}}(\overline{U}\gamma_5 U - \overline{D}\gamma_5 D)$$

$$\Pi_T^- \sim \overline{U}\gamma_5 D \tag{5.4}$$

Goldstone bosons associated with the spontaneous breakdown of the global chiral symmetries of the technifermions are commonly called technipions.

The couplings of the three Goldstone bosons to the EW currents are given by current algebra:

$$< 0|J_a^\mu(0)|\Pi_b(q) > = iq^\mu F_\pi \delta_{ab} g/2$$

$$< 0|J_Y^\mu(0)|\Pi_b(q) > = iq^\mu F_\pi \delta_{a3} g'/2. \tag{5.5}$$

These couplings determine the couplings of the Goldstone bosons to the $W^\pm$ and Z^0. To see how the Higgs mechanism works here, consider the contribution of the

Goldstone bosons to the polarization tensor of an electroweak boson:

$$\int d^4 z e^{ik \cdot z} < 0|T J_a^\mu(x) J_j^\nu(0)|0 >= -i\Pi_{a\beta}^{\mu\nu}(k) = -i(g^{\mu\nu}k^2 - k^\mu k^\nu)\Pi_{a\beta}(k) \quad (5.6)$$

Using the couplings of the Goldstone bosons to the currents given in Eq. 5.5, we see that the Goldstone bosons contribute to give a pole to $\Pi(k)$ as $k^2 \to 0$ so

$$\Pi_{a\beta}(k) = \frac{M_{a\beta}^2}{k^2} \quad (5.7)$$

where

$$\mathcal{M}^2 = \frac{F_\pi^2}{4} \begin{pmatrix} g^2 & 0 & 0 & 0 \\ 0 & g^2 & 0 & 0 \\ 0 & 0 & g^2 & -gg' \\ 0 & 0 & -gg' & g'^2 \end{pmatrix} \begin{matrix} + \\ - \\ 3 \\ Y \end{matrix} \quad (5.8)$$

This is simply the standard Higgs mechanism with the scalars replaced by composite bosons. The mass matrix M gives a massive $W^\pm$ and Z^0 with

$$M_W/M_Z = cos(\theta_w) = \frac{g}{\sqrt{g^2 + g'^2}} \quad (5.9)$$

and a massless photon. To obtain the proper strength of the weak interactions we require

$$F_\pi = 246 GeV \ . \quad (5.10)$$

The usual theory of the spontaneously broken symmetries of the $SU(2)_L \otimes U(1)_Y$ model is completely reproduced. The custodial $SU(2)_V$ symmetry of the technicolor interactions (Eq. 5.2) guarantee the correct W to Z mass ratio.

Technicolor provides an elegant solution to the naturalness problem of the standard model; however it has one major deficiency. The chiral symmetries of ordinary quarks and leptons remain unbroken when the technicolor interactions become strong. Hence no quark or lepton masses are generated at the electroweak scale. Another way of saying the same thing is that the interactions generated by the technicolor do not generate effective Yukawa couplings between the ordinary quarks and leptons and the composite scalars. We return to discuss attempts to remedy this problem later.

2. Technicolor Signatures

Knowing the spectrum of ordinary hadrons, and attributing its character to QCD, we may infer the spectrum of the massive technihadrons. The spectrum should mimic the QCD spectrum with two quark flavors. It will include:

- An isotopic triplet of $J^{PC} = 1^{--}$ technirhos

$$\rho_T^+ = \overline{D}\gamma^\mu U$$

$$\rho_T^0 = \frac{1}{\sqrt{2}}(\overline{U}\gamma^\mu U - \overline{D}\gamma^\mu D) \qquad (5.11)$$

$$\rho_T^- = \overline{U}\gamma^\mu D$$

The masses and widths of the technirho mesons can be estimated using the QCD analogs and large N arguments[69]. We obtain

$$m_{\rho_T} = m_\rho \frac{F_\Pi}{f_\pi}\sqrt{\frac{3}{N}} \approx 2TeV/c^2\sqrt{\frac{3}{N}} \qquad (5.12)$$

$$\Gamma(\rho_T \to \Pi_T\Pi_T) = \Gamma(\rho \to \pi\pi)(\frac{3}{N})[\frac{m_{\rho_T}}{m_\rho}][1 - \frac{4m_\pi}{m_\rho}]^{-\frac{3}{2}} \qquad (5.13)$$

For the choice $N = 4$, $M_{\rho_T} = 1.77$ TeV/c^2 and $\Gamma_{\rho_T} = 325$ GeV.

- An isoscalar $J^{PC} = 1^{--}$ techniomega

$$\omega_T^0 = \frac{1}{\sqrt{2}}(\overline{U}\gamma^\mu U + \overline{D}\gamma^\mu D) \qquad (5.14)$$

with a mass approximately degenerate with the technirho and which decays principally into three technipions.

- An isoscalar $J^{PC} = 0^{-+}$ technieta

$$\eta_T = \frac{1}{\sqrt{2}}(\overline{U}\gamma_5 U + \overline{D}\gamma_5 D) \qquad (5.15)$$

with a mass ≈ 1 TeV/c^2.

- An isoscalar $J^{PC} = 0^{++}$ technisigma,

$$H_0 = \frac{1}{\sqrt{2}}(\overline{U}U + \overline{D}D) \qquad (5.16)$$

with a mass expected to be $\approx 2\Lambda_T$ and ordinary technicolor strong decays. The technisigma is the analogy of the physical Higgs scalar in the Weinberg-Salam model. Here the dynamics determines the mass of the Higgs-like scalar; it is not a free parameter as it is in the standard model; and in particular, it cannot be light.

In addition there are other more massive scalars, axial vectors, and tensors. There will also be a rich spectrum of (T^N) technibaryons. Some of these might well be stable against decay, within technicolor.

In hadron-hadron collisions, technifermions of the minimal model will be pair produced by electroweak processes. One possible experimental signature is the creation of stable technibaryons, which for all odd values of N would carry half-integer charges. The production rate cannot exceed the overall rate of technifermion pair production, which even at the SSC will be minuscule - on the order of the Drell-Yan cross section at $\sqrt{s} \approx 2m(\text{technibaryon})$.

The signature of the minimal technicolor scheme is the expected modifications to the electroweak processes in the 1-TeV regime. Thus only a supercollider will have sufficient energy to observe these signals. The most prominent of these are the contributions of the s-channel technirho to the pair production of electroweak gauge bosons. Because of the weak hypercharge assignments of the technifermions the techniomega (unlike the omega in QCD) does not mix with the photon or Z^0 to produce a s-channel resonance.

Because of the strong coupling of the technirhos to pairs of longitudinal W's or Z's (the erstwhile technipions), the processes[90]

$$q_i \bar{q}_i \to (\gamma \text{ or } Z^0) \to W_L^+ W_L^- \tag{5.17}$$

and

$$q_i \bar{q}_j \to W^\pm \to W_L^\pm Z_L^0 \tag{5.18}$$

where the subscript L denotes longitudinal polarization, will produce significant enhancements in the pair production cross sections.

Including the s-channel technirho enhancement, the differential cross section for production of W^+W^- is given by

$$\frac{d\sigma}{dt}(u\bar{u} \to W^+W^-) = \frac{\pi\alpha^2}{12s^2}\Big\{2(1 + \frac{M_Z^2}{s - M_Z^2}L_u)(\frac{ut - M_W^4}{st} - \frac{2M_W^2}{t}) + \frac{ut - M_W^4}{t^2}$$

$$-4(\frac{M_Z^2}{s - M_Z^2})L_u + \frac{M_Z^2 s\beta_W^2}{(s - M_Z^2)^2}\frac{(L_u^2 + R_u^2)}{1 - x_w}$$

$$+\frac{(ut - M_W^4)}{s^2}[2 + X + (\frac{6M_W^2 - sX}{s - M_Z^2})(\frac{L_u}{1 - x_w})]$$

$$+(\frac{s}{s - M_Z^2})^2[\beta_W^2 - 1 + X + \frac{12M_W^4}{s^2}]\frac{(L_u^2 + R_u^2)}{4(1 - x_w)^2}\Big\} \qquad (5.19)$$

where $\beta_W \equiv \sqrt{1 - 4M_W^2/s}$, $L_u = 1 - 4x_w/3$, $R_u = 4x_w/3$, and

$$X = \frac{M_{\rho_T}^4}{(s - M_{\rho_T}^2)^2 + M_{\rho_T}^2\Gamma_{\rho_T}^2} \qquad (5.20)$$

All the effects of the technirho are contained in the factor X , setting $X = 1$ corresponds to the standard model expression. The corresponding expressions for the contribution of technirhos to $d\sigma/dt$ for $d\bar{d} \to W^+W^-$ and $u\bar{d} \to W^+Z^0$ are given in EHLQ(Eqs. 6.22-6.23 respectively). There is no ρ_T^0 enhancement in the Z^0Z^0 final state since ρ_T^0 has $I_T = 1$ and $I_{T3} = 0$ (i.e. W_3 couples only to W^+W^- not to W_3W_3 or BB; hence the ρ_T^0 will not couple to them either).

We show in Figure 56 the mass spectrum of W^+W^- pairs produced in pp collisions at 20, 40 and 100 TeV, with and without the technirho enhancement. Both intermediate bosons are required to satisfy $|y| < 1.5$. The yields are slightly higher in the neighborhood of the ρ_T in $\bar{p}p$ collisions. This is a 25 percent effect at 40 TeV.

We show in Figure 57 the mass spectrum of $W^{\pm}Z^0$ pairs produced in pp collisions at 20, 40 and 100 TeV, with and without the $\rho_T^{\pm}$ enhancement. Again both intermediate bosons are required to satisfy $|y| < 1.5$.

The technirho enhancement amounts to nearly a doubling of the cross section in the resonance region for W^+W^- pair production and an even greater signal to background (S/B) ratio in the $W^{\pm}Z^0$ case. However, because the absolute rates are small, the convincing observation of this enhancement makes nontrivial demands on both collider and detector.
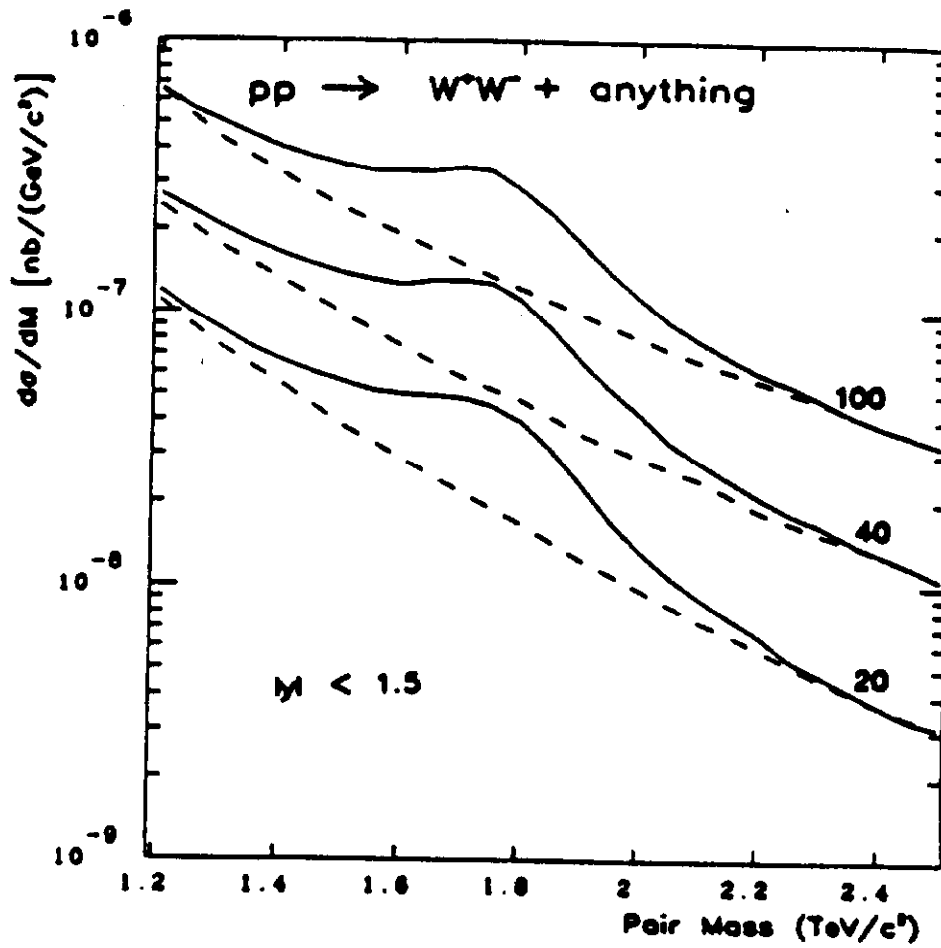
Figure 56: Mass spectrum of W^+W^- pairs produced in pp collisions, according to the parton distribution of Set 2 in EHLQ. The cross sections are shown with (solid lines) and without (dashed lines) the technirho enhancement of Eq. 5.19. $M_{\rho_T} = 1.77$ TeV/c^2 and $\Gamma_{\rho_T} = 325$ GeV.
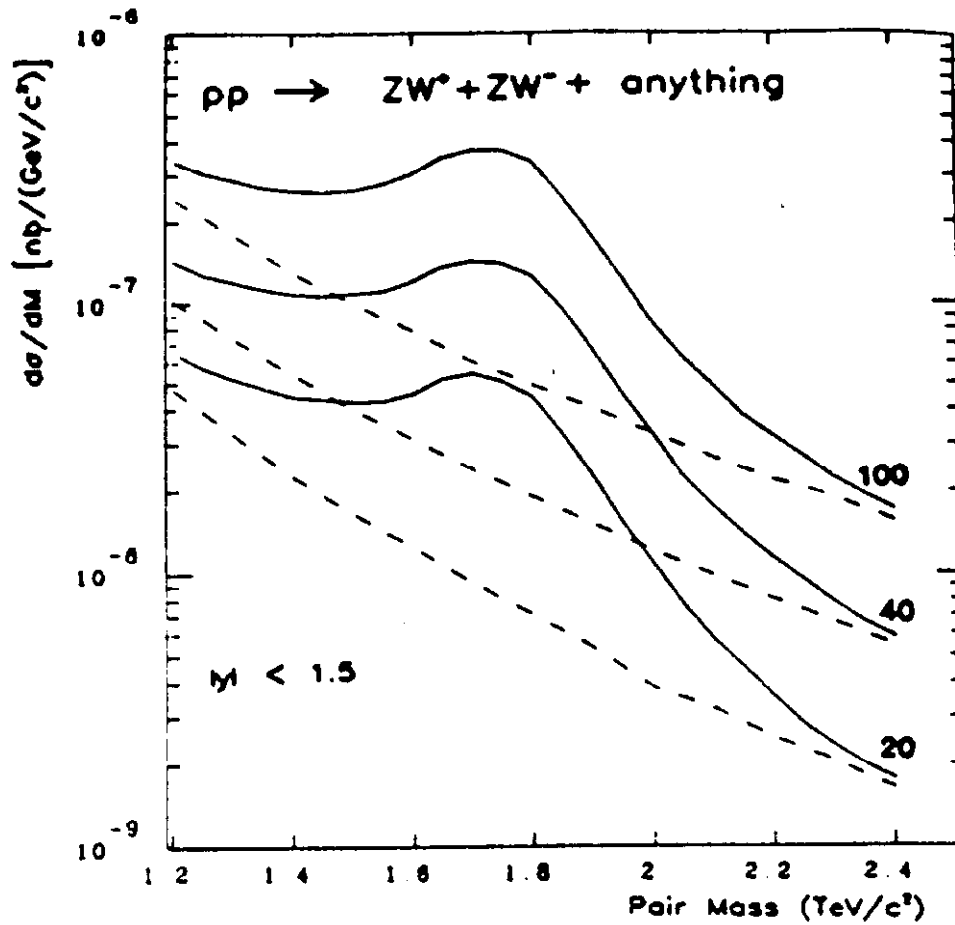
Figure 57: Mass spectrum of W^+Z^0 and W^-Z^0 pairs produced in pp collisions, according the the parton distributions of Set 2 in EHLQ. The cross sections are shown with (solid lines) and without (dashed lines) the technirho enhancement. $M_{\rho_T} = 1.77$ TeV/c^2 and $\Gamma_{\rho_T} = 325$ GeV.

Table 7: Detecting the ρ_T of the Minimal Technicolor Model at a pp Supercollider. For an assumed integrated luminosity $\int dt \mathcal{L} = 10^{40}(cm)^{-2}$, the total signal/background rates (S/B) are given for the channels $W^+ W^-$ (column 2) and $W^\pm Z^0$ (column 4). Detecting 25 excess events with a 5σ S/B requires minimum detection efficiencies ϵ_W and ϵ_Z given in column 3 and 5 respectively.

$\sqrt{s}$	$W^+ W^-$		$W^\pm Z^-$	
(TeV)	S/B	ϵ_W	S/B	$\sqrt{\epsilon_W \epsilon_Z}$
10	—	—	28/10	1
20	100/110	.52	152/50	.41
40	240/300	.36	420/130	.24

An estimate of the background of standard gauge boson pairs can be obtained be integrating that cross section over the resonance region

$$1.5 TeV/c^2 \leq \mathcal{M} \leq 2.1 TeV/c^2 \tag{5.21}$$

The resulting signal and background events for a standard run with integrated luminosity of $10^{40}cm^{-2}$ are given Table 7. We require that the enhancement consist of at least 25 detected events, and that the signal represent a five standard deviation excess over the background. This criterion translates into minimum detection efficiency for the gauge bosons also listed in Table 7.

Since the leptonic branching ratio for the Z^0 is only 3 percent per charged lepton, we can conclude (from Table 7) that detection of the technirho at $\sqrt{s} = 40$ TeV requires observation of at least the Z^0 in its hadronic decay modes. Realistically it will also be necessary to detect the $W^\pm$'s in their hadronic modes. In these cases the two jet backgrounds to the $W^\pm$ or Z^0 must be separated. The severity of the 2 jet + W and 4 jet backgrounds is still an open question, but it is under intense study[91].

Whatever the conclusions of present studies, it is safe to say that discovering the technirho signature of the minimal technicolor model is one of the hardest challenges facing experimentalist at the future SSC.

B.   Extended Technicolor

1.   Generating Fermion Masses

The minimal model just presented illustrates the general strategy and some of the consequences of a technicolor implementation of dynamical electroweak symmetry breaking.   However it does not provide a mechanism for generating masses for the ordinary quarks and leptons.   Various methods of overcoming this problem have been proposed , in this section we consider the original proposal - extended technicolor[92,93] as a prototype.

The basic idea of extended technicolor (ETC) is to embed the technicolor group G_T into a larger extended technicolor group $G_{ETC} \supseteq G_T$ which couples quarks and leptons to technifermions. This extended gauge group is assumed to break down spontaneously $G_{ETC} \to G_T$ at an energy scale

$$\Lambda_{ETC} \sim 30 \; - \; 300 TeV \tag{5.22}$$

producing masses for the ETC gauge bosons of order

$$M^2_{ETC} \approx g^2_{ETC} \Lambda^2_{ETC} \; . \tag{5.23}$$

Since the ETC bosons couple technifermions to ordinary fermions, ETC boson exchange induces an effective four fermion interaction at energy scales below Λ_{ETC}:

$$\mathcal{L}_{ETC} = \frac{g^2_{ETC}}{M^2_{ETC}} \overline{q}_L \gamma^\mu Q_L \overline{Q}_R \gamma_\mu q_R + h.c \tag{5.24}$$

where by Eq. 5.23:

$$g^2_{ETC}/M^2_{ETC} = 1/\Lambda^2_{ETC} \; . \tag{5.25}$$

Now when technicolor becomes strong and the chiral symmetries of the technifermions are spontaneously broken at scale Λ_T , forming the condensate

$$< 0|\Psi_L \overline{\Psi}_R|0 > +h.c. \approx \Lambda^3_T \; , \tag{5.26}$$

the effective Lagrangian of Eq. 5.24 becomes

$$\mathcal{L}_{ETC} = \frac{\Lambda^3_T}{\Lambda^2_{ETC}} (\overline{q}_L q_R + h.c) \; . \tag{5.27}$$

This is just a mass term for the ordinary fermion field q. Hence, by this mechanism the ETC interactions can generate a mass

$$m_q = \frac{\Lambda_T^3}{\Lambda_{ETC}^2} \tag{5.28}$$

for the ordinary fermions.

2.   The Farhi-Susskind Model[94]

In any of the more nearly realistic technicolor models produced so far, there are at least four flavors of technifermions. As a consequence, the chiral flavor group is larger than the $SU(2)_L \otimes SU(2)_R$ of the minimal technicolor model(Eq. 5.2), so more than three massless technipions result from the spontaneous breakdown of chiral symmetry. These addition technipions remain as physical spinless particles. Of course, these cannot and do not remain massless, but acquire calculable masses considerably less than 1 TeV/c^2. These particles are therefore accessible to present and planned hadron colliders.

At present there is no completely realistic model that incorporates the ideas of ETC. In particular, the lack of an obvious analog of the Glashow-Iliopoulos-Maiani(GIM) mechanism[95] is precisely the feature of all known ETC models that makes them phenomenologically problematic[92,96,97]. Recently several attempts have been made to construct a GIM-like mechanism for ETC theories[98]. However, no proposal has yet been a complete success.

Here we consider a simple toy technicolor model due to Farhi and Susskind[94], which has quite a rich spectrum of technipions and technivectormesons. This model has been developed further by Dimopoulos[99], Peskin[100], Preskill[101], and Dimopoulos, Raby, and Kane[102]. Of course this model is not correct in detail, but many of the observable consequences should not be affected by these problems.

In the Farhi-Susskind model the technicolor group is $SU(4)$. The technifermions transform under $SU(3) \otimes SU(2)_L \otimes U(1)_Y$ as:

$$\begin{pmatrix} U \\ D \end{pmatrix}_L \quad \mathbf{3} \quad \mathbf{2} \qquad Y$$

$$U_R \quad \mathbf{3} \quad \mathbf{1} \qquad Y+1$$

$$D_R \qquad\qquad\qquad Y-1$$

$$\begin{pmatrix} N \\ E \end{pmatrix}_L \quad \mathbf{1} \quad \mathbf{2} \qquad -3Y$$

$$N_R \quad \mathbf{1} \quad \mathbf{1} \qquad -3Y+1$$

$$E_R \qquad\qquad\qquad -3Y-1$$

The choice $Y = 1/3$ gives the technifermions the same charges as the corresponding ordinary fermions.

The global flavor symmetries G_f of the massless technifermions in this model are:

$$G_f = SU(8)_L \otimes SU(8)_R \otimes U(1)_V \qquad (5.29)$$

which are spontaneously broken by the strong technicolor interactions at the scale Λ_T to the nonchiral subgroup:

$$SU(8)_V \otimes U(1)_V \ . \qquad (5.30)$$

Associated with each spontaneously broken chiral symmetry is a massless Goldstone boson. There are $8^2 - 1 = 63$ such Goldstone bosons in this model. As before, there are three Goldstone bosons which are associated with the electroweak symmetries. When the electroweak gauge interactions are included these Goldstone bosons combine with the gauge fields to make the massive physical $W^\pm$ and Z^0 particles. The other Goldstone bosons will acquire masses when the ETC, $SU(3)$ color, and electroweak interactions are included. For this reason these remaining states are sometimes called Pseudo-Goldstone-Bosons (PGB's). More commonly, these additional states are called technipions in analog with corresponding states in QCD.

3. Masses for Technipions

The method of analysis used to determine the masses for technipions is a generalization of the Dashen's analysis for pion masses in QCD[103]. Let me briefly review

this idea here.

Consider a Hamiltonian H_0 invariant under a set of symmetries with charges Q_a: i.e.

$$[Q_a, H_0] = 0 . \tag{5.31}$$

Some of these symmetries may be spontaneously broken by the dynamics of the theory, as in the theory we are considering. We denote the spontaneously broken symmetries by Q_a^A; since they are axial global symmetries in the case at hand. While the remaining unbroken symmetries will be denoted by Q_a^V, as they are in fact vector symmetries here.

The vacuum state of the theory $|\Omega >$ will therefore annihilate the unbroken charges

$$Q_a^V |\Omega_0 >= 0 \tag{5.32}$$

while for spontaneously broken charges

$$e^{-iQ_a^A \Lambda_a} |\Omega_0 >= |\Omega(\Lambda) >\neq 0 . \tag{5.33}$$

That is, the spontaneously broken charges are not symmetries of the vacuum. They rotate the vacuum into other states which because the charges commute with H_0 are degenerate in energy with the vacuum. This is exactly what happened in the Higgs potential of the Weinberg-Salam model discussed in Sec.3; spontaneous symmetry breaking occurs when the Hamiltonian has a degenerate set of lowest energy states (i.e. associated with a rotational invariance under the charge Q_a^A). The physical theory must chose one vacuum (i.e. align along one direction), thus breaking the symmetry. The physical degree of freedom associated with rotation in the direction of the original degeneracy (ie. rotations generated by Q_a^A) is a Goldstone boson. The Goldstone bosons are massless because these rotations leave the energy of the system unchanged.

Now consider what happens when a small perturbation δH_I is added which explicitly breaks one of the symmetries that is spontaneously broken in the unperturbed theory described by H_0. The degeneracy of the vacuum states is broken by δH_I and there is now a unique lowest energy state. If we define an energy $E(\Lambda_a)$ by:

$$E(\Lambda_a) \equiv < \Omega_0 | e^{-iQ_a^A \Lambda_a} \delta H_I e^{iQ_a^A \Lambda_a} |\Omega_0 > \tag{5.34}$$

then if the minimum of $E(\Lambda_a)$ occurs for $\Lambda_a = \Lambda_a^P$ the physical vacuum state will be

$$|\Omega_{phy}> = e^{iQ_a^A \Lambda_a^P}|\Omega_0>$$ (5.35)

Reexpressing E in terms of the physical vacuum

$$E(\bar{\Lambda}) = <\Omega_{phy}|e^{-iQ_a^A \bar{\Lambda}_a}\delta H_I e^{iQ_a^A \bar{\Lambda}_a}|\Omega_{phy}> .$$ (5.36)

Now the minimum occurs at $\bar{\Lambda}_a = 0$ for each a. Hence at $\bar{\Lambda}_a = 0$

$$\frac{\partial E}{\partial \bar{\Lambda}_a} = 0 \quad \Rightarrow <\Omega_{phy}|[Q_a, \delta H_I]|\Omega_{phy}> = 0$$ (5.37)

and

$$\frac{\partial^2 E}{\partial \bar{\Lambda}_a \partial \bar{\Lambda}_b} = M_{ab}^2$$ (5.38)

or equivalently

$$<\Omega_{phy}|[Q_a,[\delta H_I,Q_b]]|\Omega_{phy}> = M_{ab}^2 .$$ (5.39)

The matrix M_{ab}^2 is simply related to the mass squared matrix for the pseudo Goldstone bosons associated with the the spontaneously broken symmetries of H_0. If the PGB decay constants are defined by

$$<0|j_a^{A\mu}(0)|\Pi_b> = iF_\Pi \delta_{ab}q^\mu$$ (5.40)

then

$$m_{ab}^2 = \frac{1}{F_\Pi^2}M_{ab}^2 .$$ (5.41)

4. Colored Technipion Masses

One mechanism by which technipions get masses is via the explicit symmetry breaking resulting when the color and electroweak gauge interactions of the technifermions are included. These radiative corrections have been considered in detail by Peskin and Chadha[104], Preskill[101], and Baluni[106].

The lowest order color gluon exchange leads to a explicit symmetry breaking interaction

$$\delta H_I = -g^2 \int d^4x D_{\mu\nu}(x)J_a^\mu J_b^\nu(0)$$ (5.42)

where $D_{\mu\nu}$ is the gluon propagator and

$$J_a^\mu(x) = \overline{\Psi}(x)\gamma^\mu T_a \Psi(x) \tag{5.43}$$

with T_a is a flavor matrix of the technifermions. Defining

$$Q_a^A \equiv \int d^3x \overline{\Psi}(x)\gamma^0 \gamma_5 X_a \Psi(x) \tag{5.44}$$

then the mass matrix for the technipions is given from Eq. 5.39 and Eq. 5.41 by

$$m_{ab}^2 = \frac{1}{F_\Pi^2}\frac{\partial}{\partial\Lambda_a}\frac{\partial}{\partial\Lambda_b}\int d^4x g^2 D_{\mu\nu}(x) < \Omega_{phy}|T\tilde{J}_a^\mu(x)\tilde{J}_a^\nu(0)|\Omega_{phy} > |_{\Lambda=0} \tag{5.45}$$

where

$$\tilde{J}_a^\mu(x) \equiv e^{-iQ_a^A\Lambda_a}J_a^\nu(x)e^{iQ_a^A\Lambda_a} \tag{5.46}$$

Using Eq. 5.43, Eq. 5.45, and Eq. 5.46 and fact that the technicolor interactions are flavor blind the mass matrix for the colored technipions can be written as:

$$m_{ab}^2 = \frac{g^2}{4\pi}\text{Tr}([X_a, T_a][X_b, T_a])\{M_{TC}\}^2 \tag{5.47}$$

where all the technicolor strong dynamics is contained in the factor M_{TC}

$$\{M_{TC}\}^2 = \frac{4\pi}{F_\Pi^2}\int d^4x D_{\mu\nu}(x) < \Omega|T(J_V^\mu(x)J_V^\nu(0) - J_A^\mu(x)J_A^\nu(0))|\Omega >\} . \tag{5.48}$$

The magnitude the dynamic term in Eq. 5.48 can be estimated by analog with QCD. Dashen proved that

$$m_{\pi^+}^2 - m_{\pi^0}^2 = \alpha M_{QCD}^2 \tag{5.49}$$

where

$$M_{QCD}^2 = \frac{4\pi}{f_\pi^2}\int d^4x D_{\mu\nu}(x) < 0|T(J_V^\mu(x)J_V^\nu(0) - J_A^\mu(x)J_A^\nu(0))|0 > . \tag{5.50}$$

with $D_{\mu\nu}$ the photon propagator. Experimentally the value of M_{QCD} is given by

$$M_{QCD}^2/m_\rho^2 = .3 \tag{5.51}$$

and the dependence on the gauge group $SU(N)$ can also be estimated using large N arguments[89]. The result is

$$\frac{\sqrt{N}M}{f_\pi} \approx 8 \tag{5.52}$$

Thus for $SU(4)$ Farhi-Susskind model, $F_\Pi = 126$ GeV and dynamic factor in Eq. 5.48 is

$$M_{TC} = 500 \ GeV/c^2 \ . \tag{5.53}$$

Turning explicitly to the technipions in the Farhi-Susskind model, we find 32 color octet technipions:

$$(P_8^+ \quad P_8^0 \quad P_8^-) \quad \rightarrow \quad \overline{Q}\gamma_5\frac{\tau^a}{2}\frac{\lambda^a}{2}Q \tag{5.54}$$

$$P_8^{0'} \quad \rightarrow \quad \overline{Q}\gamma_5\frac{\lambda^a}{2}Q \tag{5.55}$$

$$\tag{5.56}$$

all with mass

$$m(P_8) = (3\alpha_s)^{1/2} \ 500 \ GeV/c^2 \approx 240 \ GeV/c^2 \tag{5.57}$$

and 24 color triplet technipions:

$$(P_3^+ \quad P_3^0 \quad P_3^-) \quad \rightarrow \quad \overline{L}\gamma_5\frac{\tau^a}{2}Q_i \tag{5.58}$$

$$P_3^{0'} \quad \rightarrow \quad \overline{L}\gamma_5 Q_i \tag{5.59}$$

$$(\overline{P}_3^- \quad \overline{P}_3^0 \quad \overline{P}_3^+) \quad \rightarrow \quad \overline{Q}'\gamma_5\frac{\tau^a}{2}L \tag{5.60}$$

$$\overline{P}_3^{0'} \quad \rightarrow \quad \overline{Q}'\gamma_5 L \tag{5.61}$$

$$\tag{5.62}$$

with mass

$$m(P_3) = (\frac{4}{3}\alpha_s)^{1/2} \ 500 \ GeV/c^2 \approx 160 \ GeV/c^2 \ . \tag{5.63}$$

5.   Color Neutral Technipion Masses

The total number of technipions in the Farhi-Susskind model is 63. As we have shown in the last section, 56 of these are colored and receive masses from radiative

corrections involving color gluon exchange. The remaining 7 technipions are color neutral. Three of these are true Goldstone bosons remaining exactly massless:

$$(\Pi_T^+, \quad \Pi_T^0, \quad \Pi_T^-) \rightarrow \frac{1}{\sqrt{2}}(\overline{Q}\gamma_5 \frac{\tau^a}{2}Q + \overline{L}\gamma_5 \frac{\tau^a}{2}L) \tag{5.64}$$

and become the longitudinal components of the W^+, Z^0, and W^- by the Higgs mechanism. So finally we are left with four additional color neutral technipions:

$$(P^+, \quad P^0, \quad P^-) \rightarrow \frac{1}{\sqrt{6}}(\overline{Q}\gamma_5 \frac{\tau^a}{2}Q - 3\overline{L}\gamma_5 \frac{\tau^a}{2}L)$$

$$P'^0 \rightarrow \frac{1}{\sqrt{6}}(\overline{Q}\gamma_5 Q - 3\overline{L}\gamma_5 L). \tag{5.65}$$

$$\tag{5.66}$$

The mechanism for mass generation is more complicated for these neutral technipions. It is discussed in detail by Peskin and Chadha[104] and Baluni[105]. The main points are:

- Before symmetry breaking effects are included the electroweak gauge interaction do not induce any masses for the technipions P^+, P^0, P^-, and P'^0.

- Including the symmetry breaking effects, in particular the nonzero mass for the Z^0, the charged P's acquire a mass[92,104,105]

$$m_{\rm EW}(P^+) = m_{\rm EW}(P^-) = \sqrt{\frac{3\alpha}{4\pi}log(\frac{\Lambda^2}{M_Z^2})}M_Z \approx 6GeV/c^2 . \tag{5.67}$$

while the neutral states P^0 and P'^0 remain massless.

- The lightest neutral technipions can only acquire mass from the symmetry breaking effects of the ETC interactions.

The effects of ETC gauge boson exchanges induce masses of the order of[92,105]:

$$m_{\rm ETC}^2 \approx \frac{1}{F_\Pi^2} \frac{\Lambda_{\rm TC}^6}{\Lambda_{\rm ETC}^2} \tag{5.68}$$

where the ETC scale $\Lambda_{\rm ETC}$ is related to the quark (and lepton) mass scale m_q by Eq. 5.28

$$m_{\rm ETC}^2 \approx \frac{m_q \Lambda_{\rm TC}^3}{F_\Pi^2} \tag{5.69}$$

However the scale of quark masses range from $m_u \approx 4 MeV/c^2$ to $m_t > 25 GeV/c^2$. Which value to use for the ETC scale is very uncertain. A reasonable guess[92,106] for the total masses $m = \sqrt{m_{EW}^2 + m_{ETC}^2}$ of these lightest technipions are:

$$7 GeV/c^2 \leq m(P^\pm) \leq 45 GeV/c^2$$

$$2 GeV/c^2 \leq m(P^0) \text{ or } m(P'^0) \leq 45 GeV/c^2 \qquad (5.70)$$

$$(5.71)$$

6. Technipion Couplings

The coupling of technipions to ordinary quarks and leptons depend on the details of the ETC interactions in the particular model. However, in general, the couplings of these technipion are Higgs-like. Thus the naive expectation is that the technipion coupling to ordinary fermions pairs will be roughly proportional to the sum of the fermion masses. A discussion of various possibilities has been given by Lane[107].

In addition, there are couplings to two (or more) gauge bosons which arise from a triangle (anomaly) graph containing technifermions, analogous to the graph responsible for the decay $\pi^0 \to \gamma\gamma$ in QCD. The details of these couplings can be found elsewhere[1,107].

The major decay modes of the technipions are summarized in Table 8.

C.   Detecting Technipions

The masses of the color neutral technipions are within the range of present experiments. Some constraints already exist on the possible masses and couplings of these technipions.

The strongest constraints on the charged technipions ($P^\pm$) come from limits on their production in e^+e^- collisions at PEP and PETRA[108]. A charged technipion decaying into $\tau \bar{\nu}_\tau$ or light quarks is ruled out for

$$m(P^\pm) < 17 GeV/c^2 \qquad (5.72)$$

; however decays into $b\bar{c}$ are not constrained by these experiments.

Table 8: Principal decay modes of technipions if Pf_1f_2 couplings are proportional to fermion mass.

Technipion	Principal decay modes
P^+	$t\bar{b},\ c\bar{b},\ c\bar{s},\ \tau^+\nu_\tau$
P^0	$b\bar{b},\ c\bar{c},\ \tau^+\tau^-$
$P^{0\prime}$	$b\bar{b},\ c\bar{c},\ \tau^+\tau^-,gg$
P_3,P_3' (if unstable)	$t\tau^-,\ t\nu_\tau,\ b\tau^-,\ ...$ or $\bar{t}t,\ \bar{t}b,\ ...$
P_8^+	$(t\bar{b})_8$
P_8^0	$(t\bar{t})_8$
P_8^-	$(b\bar{t})_8$
$P_8^{\prime 0}$	$(t\bar{t})_8,\ gg$

For the neutral technipions the constraints are indirect and generally rather weak. A detailed discussion all the existing limits is contained in Eichten, Hinchliffe, Lane, and Quigg[109].

Finally consider the detection prospects in hadron colliders for technipions. My discussion will draw heavily on the detailed analysis presented by Eichten, Hinchliffe, Lane, and Quigg[109] for present collider energies and EHLQ for supercollider energies.

The principal production mechanisms for the color-singlet technipions in $\bar{p}p$ collisions are:

- The production of $P^\pm$ in semiweak decays of heavy quarks.

- The production of the weak-isospin-singlet states $P^{\prime 0}$ by the gluon fusion mechanism.

- pair production of $P^\pm P^0$ through the production of real or virtual $W^\pm$ bosons.

- Pair production of P^+P^- by the Drell-Yan mechanism , especially near the Z^0 pole.

each of these mechanisms will be discussed in turn.

If the the top quark is heavy enough for the decay:

$$t \rightarrow P^+ + (b \text{ or } s \text{ or } d) \tag{5.73}$$

to be kinematically allowed, then this decay will proceed at the semiweak rate[109]:

$$\Gamma(t \rightarrow P^+ q) \approx \frac{G_F \sqrt{2}}{\pi} |\mathcal{M}|^2 (m_t^2 + m_q^2 - M_P^2) p \tag{5.74}$$

where

$$p = \frac{[m_t^2 - (m_q + M_{P_+})^2]^{\frac{1}{2}} [m_t^2 - (m_q - M_{P_+})^2]^{\frac{1}{2}}}{2m_t} . \tag{5.75}$$

With more or less conventional couplings of the $P^\pm$ to quarks and leptons, the coupling matrix $|\mathcal{M}| \approx 1$ and thus this decay mode of the top quark will swamp the normal weak decays. Hence the production of top quarks in hadron colliders will be a copious source of charged technipions if the decay is kinematically allowed. On the other hand, seeing the top quark though the normal weak decays will put strong constraints of the mass and couplings of any charged color neutral technipion.

The single production of the neutral isospin singlet technipion, P'^0, proceeds by the gluon fusion mechanism as for the usual Higgs scalar. The production rate is given by:

$$\frac{d\sigma}{dy}(ab \rightarrow P'^0 + \text{anything}) = \frac{\alpha_s^2}{48\pi F_\pi^2} \tau f_g^{(a)}(x_a, M_P^2) f_g^{(b)}(x_b, M_P^2) \tag{5.76}$$

where $\tau = M_P^2 / s$. This differential cross section for P'^0 production at $y = 0$ is shown in Figure 58 as a function of technipion mass, M_P, for the $S\bar{p}pS$ and Tevatron colliders. The corresponding rates for Supercollider energies are shown in EHLQ (Fig. 181).

The principal decays of the P'^0 are: gg, $\bar{b}b$, and $\tau^+\tau^-$. The relative branching fractions are shown in Figure 59. Comparing the rates of P'^0 production with the background of QCD $\bar{b}b$ jet events (see for example Fig. 16), it becomes clear that detecting P'^0 in its hadronic decays is not possible. The background is more that two orders of magnitude larger than the signal. The only hope for detection is the leptonic final states - principally $\tau^+\tau^-$. For this channel the signal to background
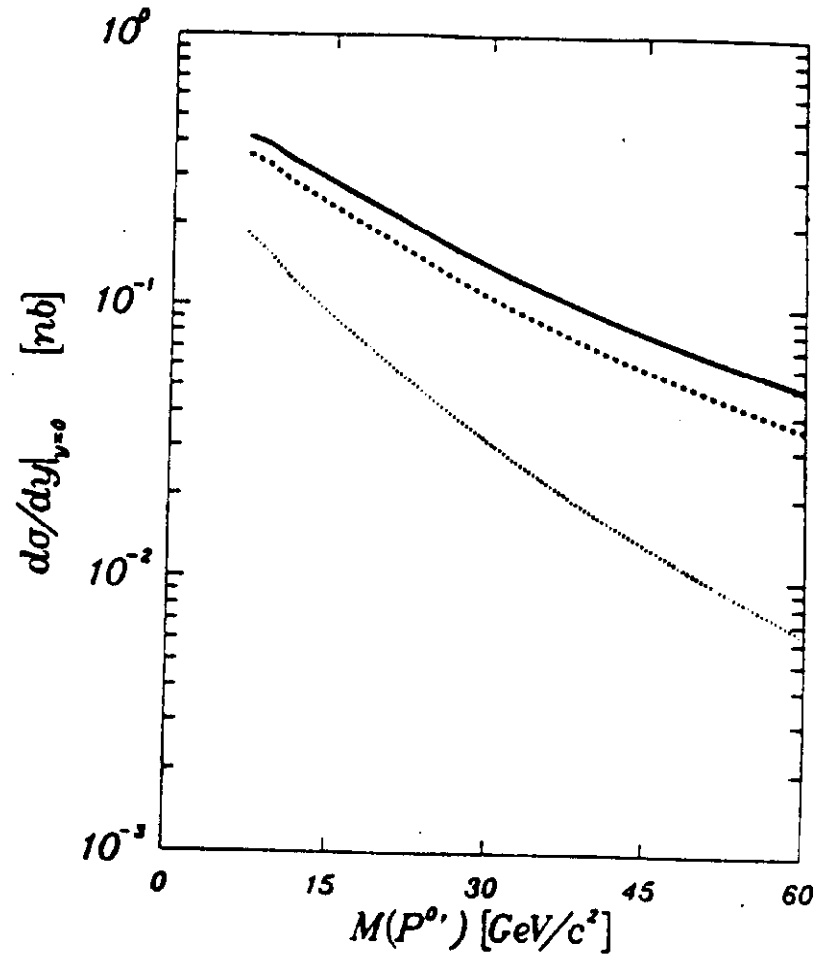
Figure 58: Differential cross section for the production of color singlet technipion $P^{\prime 0}$ at $y = 0$ in $\bar{p}p$ collisions, for $\sqrt{s} = 2$ TeV (solid curve) , 1.6 TeV (dashed curve), and 630 GeV (dotted curve). (From Ref. 109)
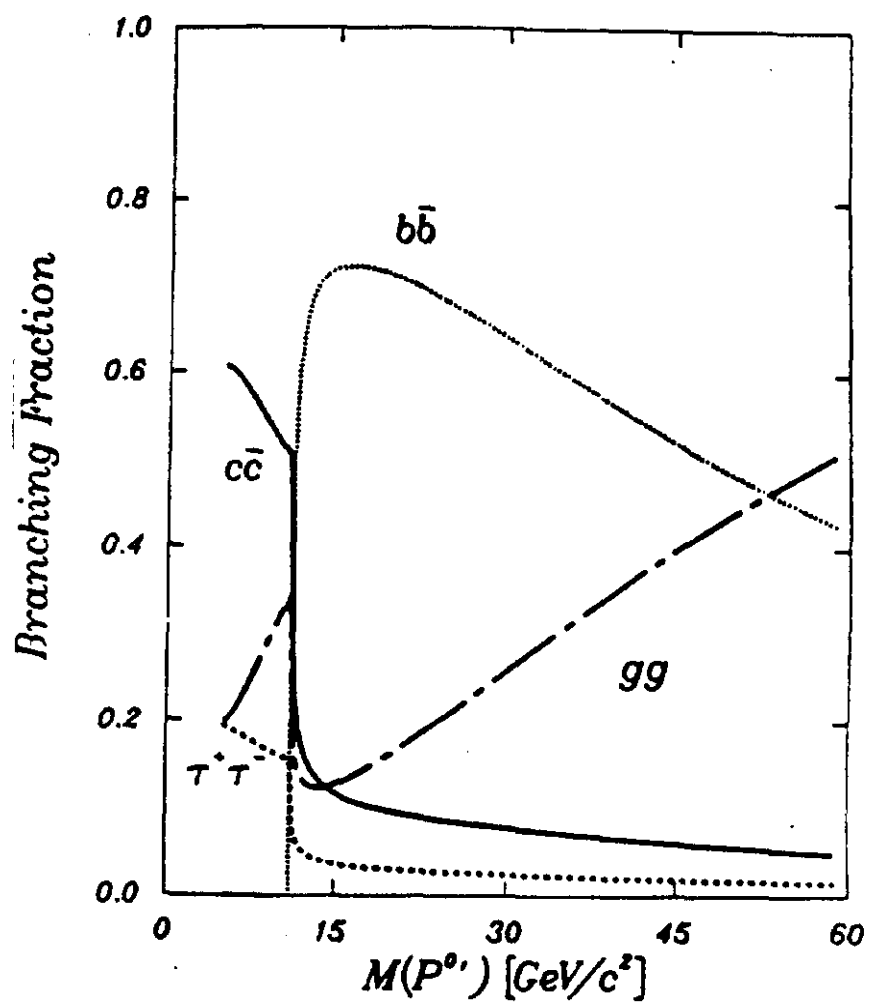
Figure 59: Approximate branching ratios for P'^0 decay. (From EHLQ)

ratio is good; but this crucially depends on the reconstruction of the P'^0 invariant mass which is difficult since each of the r decays contains a undetectable neutrino.

Finally there is the pair production of color singlet technipions through the chains:

$$\bar{p}p \;\rightarrow\; W^\pm + \text{anything}$$
$$\qquad\hookrightarrow P^\pm + P^0 \tag{5.77}$$

and

$$\bar{p}p \;\rightarrow\; Z^0 + \text{anything}$$
$$\qquad\hookrightarrow P^+ + P^- \tag{5.78}$$

where the intermediate bosons may be real or virtual. The couplings of these technipion pairs to the $W^\pm$ and Z^0 are typically $1 - 2\%$. For more details see Ref. 109.

The cross section for $P^\pm P^0$ pairs produced in $\bar{p}p$ collisions at present collider energies is shown in Figure 60. Both $P^\pm$ and P^0 are required to have rapidities $|y_i| < 1.5$. The cross sections are appreciable only if $(M_{P^+} = M_{P_-}) < m_W/2$, for which the rate is determined by real $W^\pm$ decays.

Under the usual assumption that these lightest technipions couple to fermion pairs proportional to the fermion masses, the signal for these events would be four heavy quark jets, eg. $t\bar{b}b\bar{b}$. If heavy quark jets can be tagged with reasonable efficiency this signal should be observable. However, the couplings of $P^\pm$ and P^0 to fermion pairs are the result of the ETC model-dependent mixings and in general are more complicated than the simple mass proportional form usually assumed. Thus the search for scalar particles from $W^\pm$ decays should be as broad and thorough as practical.

Similarly, the cross section for production of P^+P^- pairs is only of experimental interest in present collider energies if $M_{P^\pm} < m_Z/2$. These cross sections are shown in Figure 61. The rate of production of P^+P^- is low. It is not likely that this channel could be detected at a hadron collider in the near future. However this signal should be observable at the e^+e^- "Z^0 factories" at SLC and LEP.
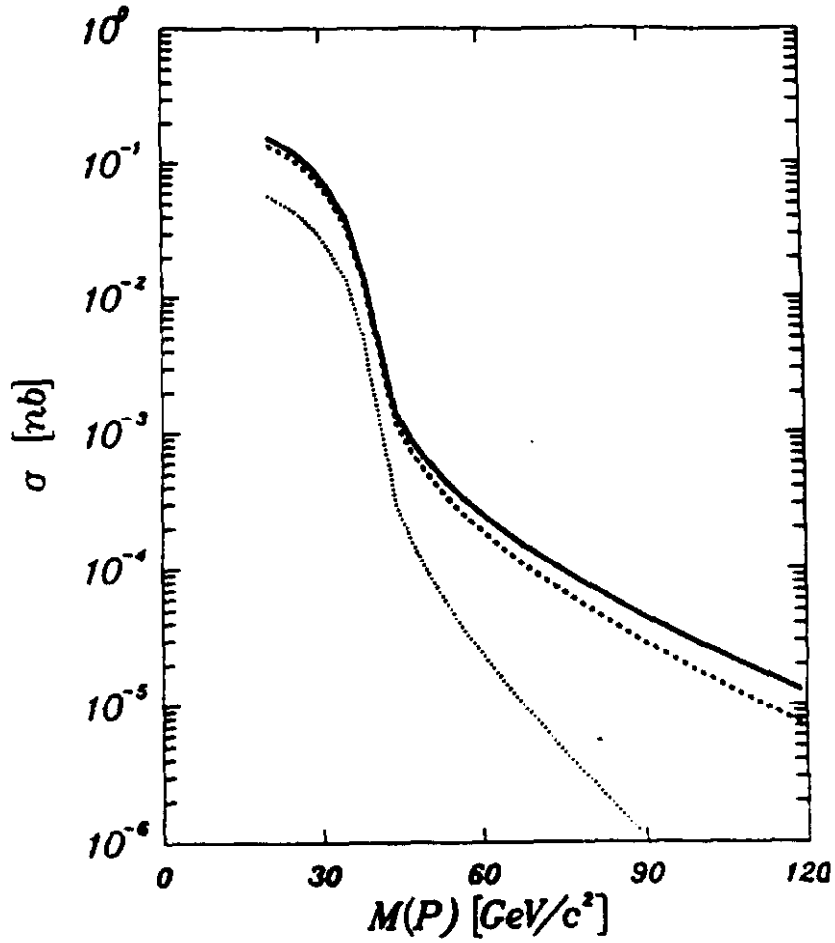
Figure 60: Cross section of the production of P^+P^0 and P^-P^0 (summed) in $\bar{p}p$ collisions as a function of the common (by assumption) mass of the technipions, for $\sqrt{s} = 2$ TeV (solid curve), 1.6 TeV (dashed curve), and 630 GeV (dotted curve). (From Ref. 109)

Figure 61: Cross section of the production of P^+P^- pairs in $\bar{p}p$ collisions as a function of the P^+ mass, for $\sqrt{s} = 2$ TeV (solid curve), 1.6 TeV (dashed curve), and 630 GeV (dotted curve). (From Ref. 109)

1. Colored Technipions

The principal production mechanisms for the colored technipions in $\bar{p}p$ collisions are:

- Production of the weak isospin singlet state $P_8'^0$ by gluon fusion.

- Production of $(P_3\bar{P}_3)$ or $(P_8\bar{P}_8)$ pairs in gg and $\bar{q}q$ fusion.

The gluon fusion mechanism for the single production of $P_8'^0$ is the same as just discussed for P'^0 production. The differential cross section is 10 times the cross section for P'^0 production given in Eq. 5.76. The differential cross section (summed over the eight color indices) at $y = 0$ is shown as a function of the technipion mass in Figure 62 for present collider energies. The expected mass (Eq. 5.57) is approximately 240 GeV/c^2. The production for Supercollider energies is shown in EHLQ (see Fig. 184).

The principal decay modes are expected to be gg and $\bar{t}t$. The rates for the expected mass $M(P'^0) = 240$ GeV/c^2 are too small for detection for $\sqrt{s}$ below 2 TeV. The best signals for detection are decays into top quark pairs.

Pairs of colored technipions are produced by the elementary subprocesses shown in Figure 63. The main contribution comes from the two gluon initial states (just as in the case of heavy quark pair production discussed in Lecture 2). Details about the production cross sections may be found in Ref. 109.

The total cross sections for the process $\bar{p}p \rightarrow P_3\bar{P}_3$ are shown in Figure 64; and the total cross sections for the process $\bar{p}p \rightarrow P_8\bar{P}_8$ are shown in Figure 65. In both cases rapidity cuts $|y| < 1.5$ have been imposed. The expected mass for the P_3 technipion is approximately 160 GeV/c^2 (Eq. 5.63) and for the P_8 approximately 240 GeV/c^2 (Eq. 5.57). The corresponding cross sections for Supercollider energies are given in EHLQ (Figs. 187-190). The implications of these production rates for discovery of colored technipions are presented in next section.

2. Discovery Limits

If the technicolor scenario correctly describes the breakdown of the electroweak gauge symmetry, there will be a number of spinless technipions, all with masses less
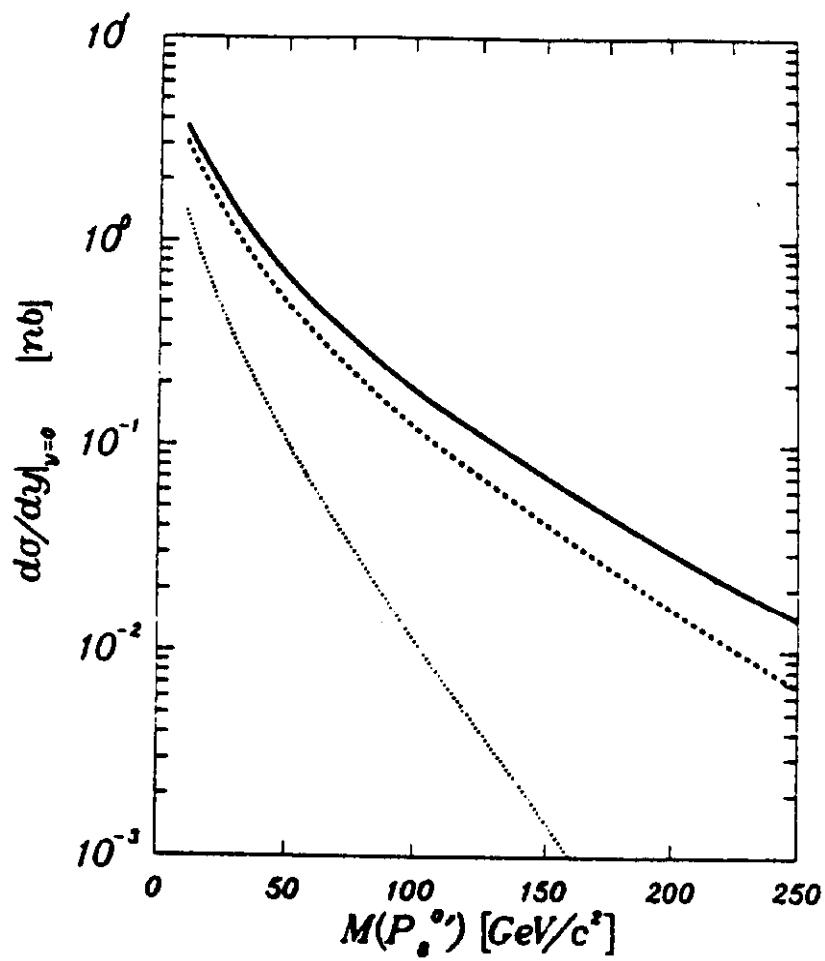
Figure 62: Differential cross section for the production of the color-octet technipion P_8^0 at $y = 0$ in $\bar{p}p$ collisions, for $\sqrt{s} = 2$ TeV (solid curve) , 1.6 TeV (dashed curve), and 630 GeV (dotted curve). (From Ref. 109)
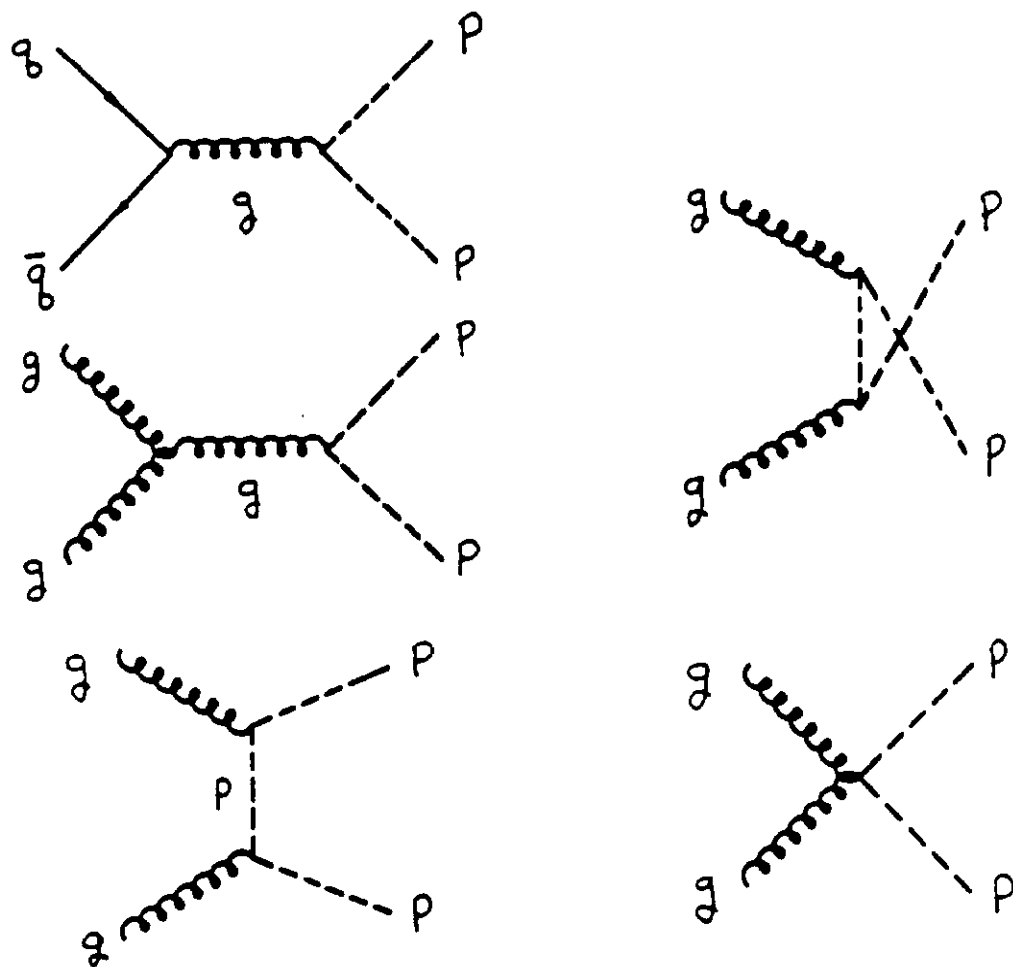
Figure 63: Feynman diagrams for the production of pairs of technipions. The curly lines are gluons, solid lines are quarks, and dashed lines are technipions. The graphs with s-channel gluons include the $\rho_8'^0$ enhancement.
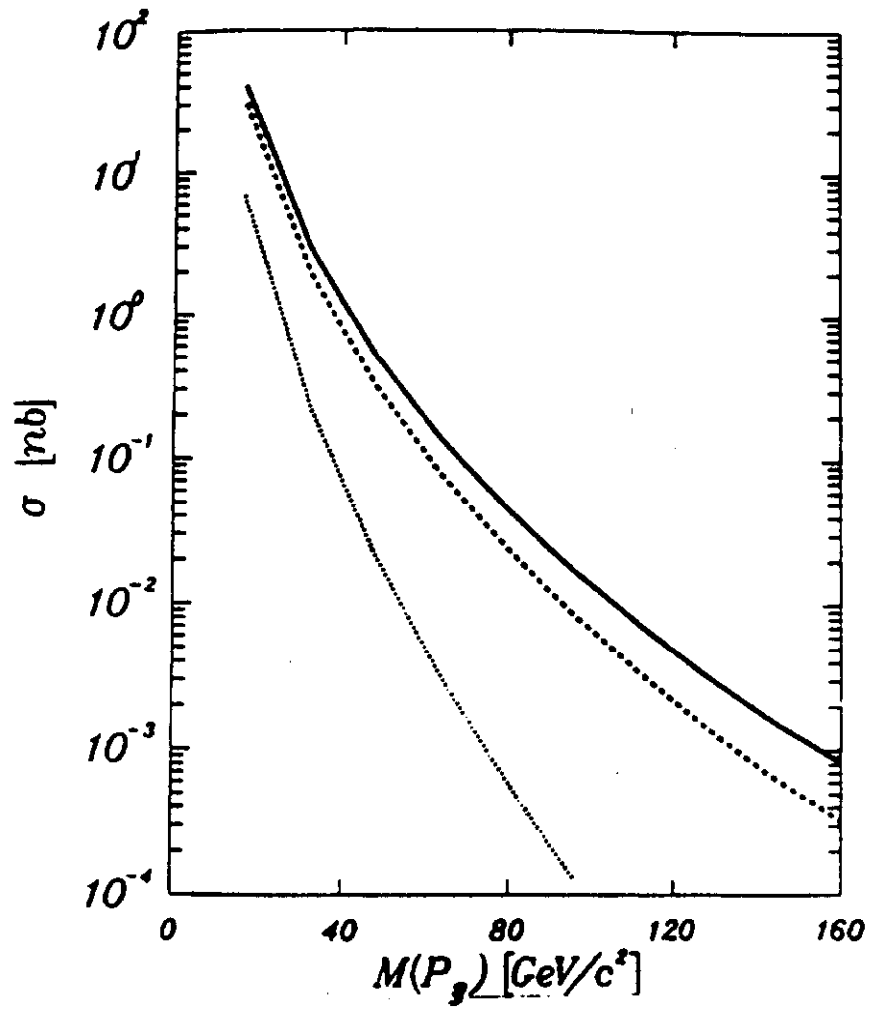
Figure 64: Cross sections for the production of $P_3\overline{P}_3$ pairs in $\overline{p}p$ collisions, for $\sqrt{s} = 2$ TeV (solid curve) , 1.6 TeV (dashed curve), and 630 GeV (dotted curve). (From Ref. 109)
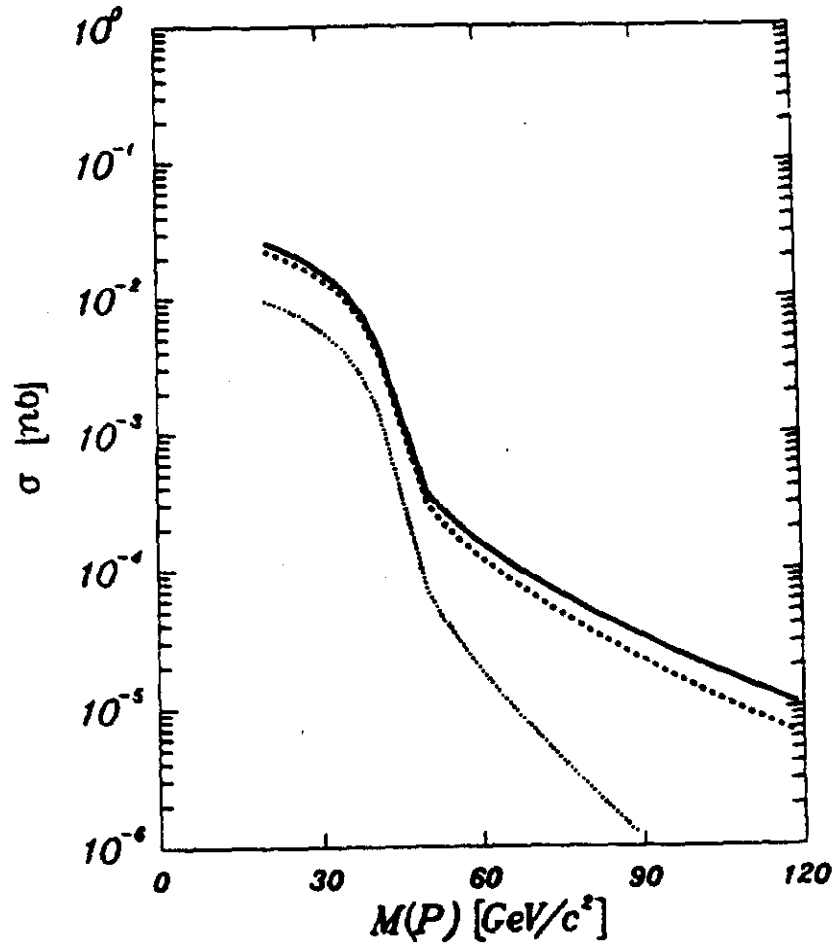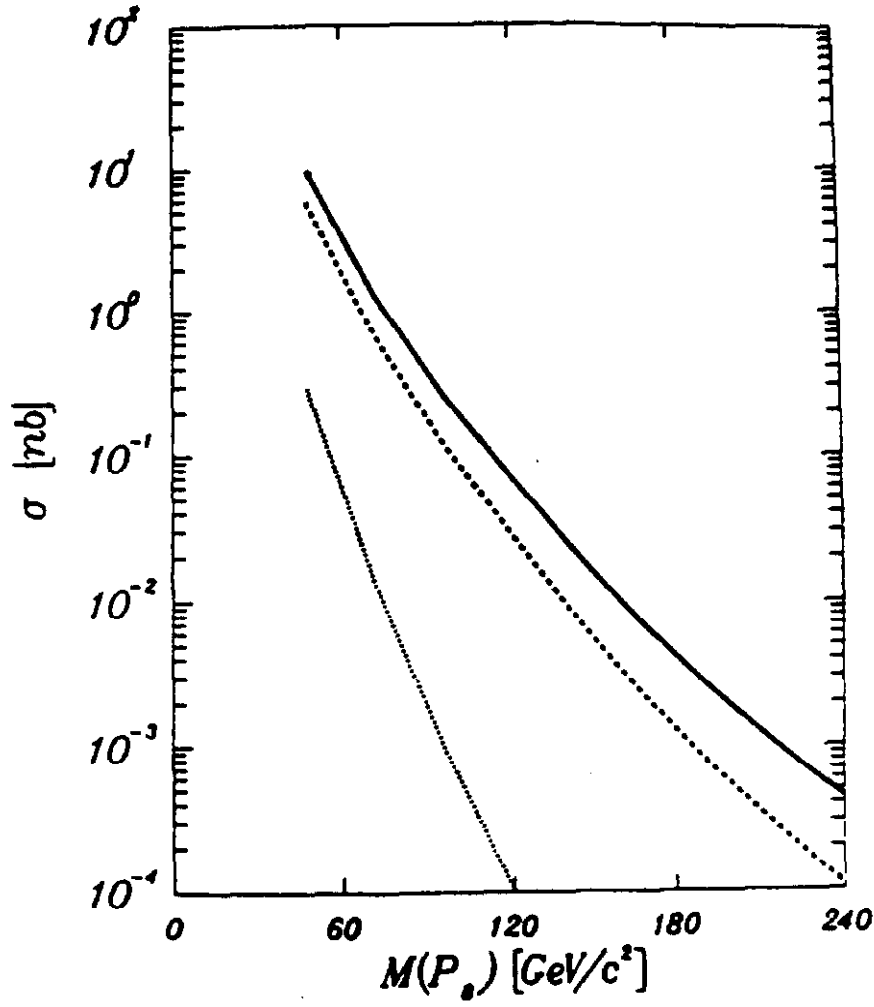
Figure 65: Cross sections for the production of $P_8\overline{P}_8$ pairs in $\bar{p}p$ collisions, for $\sqrt{s} = 2$ TeV (solid curve) , 1.6 TeV (dashed curve), and 630 GeV (dotted curve). (From Ref. 109)

Table 9: Minimum *effective* integrated luminosities in cm^{-2} required to establish signs of extended technicolor (Farhi-Susskind Model) in various hadron colliders. To arrive at the required integrated luminosities, divide by the efficiencies ϵ_i to identify and adequately measure the products.

| | Collider Energy | | | |
| | 2 TeV | 10 TeV | 20 TeV | 40 TeV |
Channel	$\bar{p}p$	pp	pp	pp
$P^{0'} \rightarrow \tau^+\tau^-$	5×10^{36}	8×10^{35}	3×10^{35}	2×10^{35}
$P_8^{0'} \rightarrow t\bar{t}$ $(m(P_8^{0'}) = 240 GeV/c^2)$	2×10^{36}	7×10^{34}	3×10^{34}	10^{34}
$P_3\bar{P}_3$ $(m(P_3) = 160 GeV/c^2)$	2×10^{38}	2×10^{36}	4×10^{35}	2×10^{35}
$(m(P_3) = 400 GeV/c^2)$	—	10^{38}	2×10^{37}	4×10^{36}
$P_8\bar{P}_8$ $(m(P_8) = 240 GeV/c^2)$	10^{38}	2×10^{35}	5×10^{34}	2×10^{34}
$(m(P_8) = 400 GeV/c^2)$	—	2×10^{36}	4×10^{35}	10^{35}
$\rho_T^{\pm} \rightarrow W^{\pm}Z^0$	—	2×10^{39}	7×10^{38}	3×10^{38}

than the technicolor scale of about 1 TeV. The simple but representative model of Farhi and Susskind[94] was considered here.

A rough appraisal of the minimum effective luminosities required for the observation of technipions of this model is given in Table 9 for present and future hadron colliders. The discovery criteria require that for a given charged state, the enhancement consists of at least 25 events, and that the signal represent a five standard deviation excess over background in the rapidity interval $|y| < 1.5$. The top quark mass was assumed to be 30 GeV.

We can conclude that a 40 TeV $p^{\pm}p$ collider with a luminosity of at least $10^{39} cm^{-2}$ will be able to confirm or rule out technicolor.

VI. COMPOSITENESS ?

In the previous lectures, it was assumed that the quarks, leptons, and gauge bosons all are elementary particles. One extension of this standard picture, to which a considerable amount of attention has been given, is the possibility that the quarks and leptons are composite particles of more fundamental fields. However, the gauge bosons will still be assumed to be elementary excitations; so any masses for these gauge bosons are generated by spontaneous symmetry breakdown through the Higgs mechanism.

There is no experimental data to indicate any substructure for the quarks and leptons. Therefore all speculation about compositeness is theoretically motivated. Consequently a good fraction of this lecture is devoted to the theoretical aspects of composite model building. So far no obviously superior model has been proposed. Since the idea of quark and lepton compositeness is still in the early stages of development, the emphasis here is on the motivation for composite models and on the general theoretical constraints on composite models. After a general discussion we turn to the expected experimental consequences of compositeness. First the present limits on quark and lepton substructure will be reviewed. Then the signals for compositeness in the present generation of colliders as well as in supercolliders will be explained. Finally, the signals of crossing a compositeness threshold will be mentioned.

A.   Theoretical Issues

1. Motivation

Several factors have contributed to speculation that the quarks and leptons are not elementary particles.

- The most obvious suggestion of compositeness is the proliferation of the number of quarks and leptons in a repeated pattern of left-handed doublets and right-handed singlets. This three generation spectra is suggestive of an excitation spectrum of more fundamental objects. Finding a repeated pattern has been a precursor to the discovery of substructure before; for example, the periodic table of elements in atomic physics.

- The complex pattern of the quark and lepton masses together with the mixing angles needed to describe the difference between the strong and electroweak flavor eigenstates suggests that these parameters are not fundamental.

- It is, moreover, very likely that at least the Higgs sector of the Weinberg-Salam model is not correct at energies above the electroweak scale. Therefore the scalar particles which implement the symmetry breakdown may be composites formed by a new strong interaction, such as technicolor. Although there is no compelling reason to associate a composite quark-lepton scale with these composite scalars, certainly it is an option which introduces a minimal amount of new physics.

For these reasons the idea of compositeness presently enjoys wide theoretical interest.

2. Consistency Conditions for Composite Models

To begin the theoretical discussion of composite models we will, following 't Hooft[110], consider a prototype composite theory of quarks and leptons consisting of a non-Abelian gauge interaction called metacolor which is described by a simple gauge group $\mathcal{G}$ with coupling constant g_M. Assuming that the gauge interaction is asymptotically free there will be some scale Λ_M at which the coupling becomes strong

$$\alpha_M \equiv \frac{g_M^2}{4\pi} = 1 \tag{6.1}$$

This is the characteristic scale for the dynamics and hence for the masses of the physical states.

In addition this prototype theory has a set of massless fundamental spin 1/2 fermions, sometimes called preons, which carry metacolor. The massless fermions will be represented here by Weyl spinors. (The ordinary Dirac representation can be constructed whenever both a Weyl spinor and its complex conjugate representation appear.)

Metacolor dynamics is similar to QCD except that the gauge interaction will not in general be vectorlike. A theory is termed vectorlike if the fermion represen-

tation under the gauge group R is real; that is, every irreducible representation is accompanied by its complex conjugate representation hence $R^* = R$.

The fermions will exhibit global symmetries described by a global chiral flavor symmetry group G_f. No global symmetry whose current conservation is spoiled by the presence of the metacolor gauge interactions will be included in G_f. Therefore the symmetry structure of the fermions consists of two relevant groups:

- the gauge group - $\mathcal{G}$, and

- the global flavor group - G_f.

The physical masses of the quarks and leptons are very small relative to the compositeness scale; this is one essential feature that any prototype model of composite quarks and leptons must explain. Therefore, with the assumption that the gauge interaction $\mathcal{G}$ is confining, there must exist a sensible limit of the theory in which the quarks and leptons are massless composite states. Thus the most relevant feature of any prototype composite model is its spectrum of massless excitations, of which the spin 1/2 particles are the candidates for quarks and leptons.

The spectrum of massless composites is directly related to the pattern global chiral symmetry breaking which occurs as metacolor becomes strong. In QCD the $SU_L(n) \otimes SU_R(n) \otimes U(1)$ flavor symmetry breaks down to the vector subgroup. In a metacolor theory one expects that the global symmetry group breaks down to a subgroup:

$$G_f \to S_f \qquad (6.2)$$

at energy scale Λ_M. Associated with each spontaneously broken symmetry is a composite spin zero Goldstone bosons. Any massless composite fermions will form representations under the remaining unbroken subgroup S_f of the global symmetry group G_f.

A few simple examples of asymptotically free metacolor gauge groups $\mathcal{G}$, and fermion representations R; and the associated flavor groups G_f are presented below:

Gauge Group	Fermion Representation	Global Group
$SU(N)$	$m(\ \otimes\ )$	$SU(m) \otimes SU(m) \otimes U(1)$
$O(10)$	m(spinor)	$SU(m)$
$SU(N)$	$\otimes(N-4)$	$SU(N-4) \otimes U(1)$
$SU(3)$	$\otimes 2$	$SU(2) \otimes U(1)$
$SU(8)$	$\otimes 5$	$SU(5) \otimes U(1)$

The first example shows how the standard $SU(N)$ vectorlike theory is denoted for m flavors of Dirac fermions in the fundamental representation. The flavor symmetries are just the usual $SU_L(m) \otimes SU_R(m) \otimes U(1)$. All the other examples are non-vector theories (i.e. the fermion representation is not real) and thus are prototypes for metacolor theories. The first such example is O(10) with fermions in the lowest dimensional spinor representation, a **16**. The number m of spinor representations is limited by the requirement that the theory be asymptotically free. In order to have a sensible theory, the fermion representation must be such that any gauge anomalies must cancelled. $O(10)$ is anomaly safe; however, in the remaining examples, the anomalies are cancelled by judiciously choice of the fermion representations. The next example is a generalization of the Georgi-Glashow $SU(5)$ model[111] with fermions in the fundamental and antisymmetric tensor representations. If one wants to consider fermion representations of rank greater than two, then only an $SU(N)$ gauge group with a low N will maintain the asymptotic freedom of the gauge interactions.

Several general characteristics of the global symmetry breaking are relevant here:

- For real fermion representations, when the gauge interaction becomes strong the axial symmetries are broken and only the vector symmetries remain unbroken[88]. This case is uninteresting because the only massless particles are the Goldstone bosons associated with the broken axial symmetries. There are no massless composite fermions. Vectorlike gauge theories are not good candidates for a prototype theory of composite quarks and/or leptons.

- General arguments guarantee that only spin 0 and spin 1/2 particles can couple to global conserved currents[112]. Hence only spin 0 and 1/2 massless states are relevant to the realization of the global symmetries in a metacolor theory.

The most powerful consistency condition on the massless spectrum of any proposed composite model is provided by 't Hooft[110]. These constraints provide a framework for studying the possible massless spectra of a metacolor model even though they do not imply a unique solution. To understand these constraints consider any global current $j^\mu(x)$ which is conserved at the Lagrangian level:

$$\partial_\mu j^\mu(x) = 0 \qquad (6.3)$$

This current involves preon fields and is associated with a conserved charge

$$Q = \int d^3 x j^0(x) \qquad (6.4)$$

When this current is coupled to a weak external gauge field, via a $j^\mu A_\mu$ interaction, the conservation may be destroyed by an anomaly, such as occurs for the axial $U(1)$ current in QCD. The divergence of the current in the presence of the external gauge field is proportional to $\mathcal{F}\tilde{\mathcal{F}}$

$$\partial_\mu j^\mu = \frac{T_f}{4\pi^2} \mathcal{F}^{\mu\nu} \tilde{\mathcal{F}}_{\mu\nu} \qquad (6.5)$$

where $T_f = Tr(Q_f^3)$ and $\mathcal{F}^{\mu\nu} = \partial^\mu A^\nu - \partial^\nu A^\mu$. Q_f is the charge matrix for the massless preon fields. Any current for which $T_f \neq 0$ is called anomalous. It is important to remember that this anomaly is in a global current and not in the metacolor interactions which are required to be anomaly free for the consistency of the theory. This global anomaly may also be seen in one fermion loop contribution to the three point correlation function.
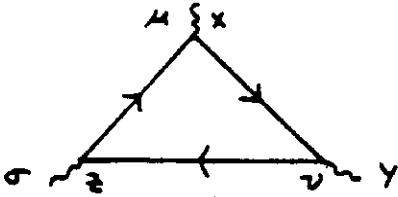
$$< 0| T j^\mu(x) j^\nu(y) j^\sigma(z) |0 > \qquad (6.6)$$

At the preon level the anomalous contribution to this three point function is simple. The structure of the anomaly is given by Bose symmetry in the three currents and current conservation while the coefficient is proportional to $T_f = Tr(Q_f^3)$. It is only necessary to consider a general diagonal charge of the global symmetry group to determine the complete anomaly structure. All the off diagonal anomalies can be reconstructed from the coefficients of a general diagonal current.

We are now ready to state 't Hooft's condition explicitly. He states that the value of the anomaly calculated with the massless physical states of the theory

must be the same as the value calculated using the fundamental preon fields of the underlying Lagrangian[110]. In the absence of the gauge interactions, these massless states are just the preons and therefore 't Hooft's condition can be restated that the gauge interactions do not modify the anomalies. It has been shown[113] that this constraint follows from general axioms of field theory. One important consequence of this condition is that if $T_f \neq 0$, then there must be massless physical states associated with the charge Q_f. This condition is the strongest constraint we have at present on composite model building.

To further elucidate 't Hooft's consistency condition consider adding some metacolor singlet fermions to the theory to cancel the anomalies in the global currents. Then including these spectator fermions the global symmetries are anomaly free and may themselves be weakly gauged. Thus, at distances large relative to the metacolor interaction scale, there must still be no anomaly when all the massless physical states are included.

We will assume that the metacolor gauge interaction is confining. It should be remembered, however, that this is an ad hoc assumption. It is not presently possible to calculate (even by lattice methods) the behaviour of nonvectorlike theories.

The fundamental dynamical question for composite models is how 't Hooft's constraint is satisfied. There are two possibilities:

- If the global symmetry which has the anomaly is spontaneously broken when the metacolor interaction becomes strong, i.e. $Q_f \notin S_f$, then the massless physical state required by the anomaly consistency condition is just the Goldstone boson associated with the spontaneously broken symmetry. The strength of the anomaly T_f determines the coupling of the Goldstone boson to the other matter fields.

- If the anomalous symmetry remains unbroken when the metacolor interaction becomes strong, $Q_f \in S_f$, then there must be massless spin 1/2 fermions in the physical spectrum which couple to the charge Q_f and produce the anomaly with the correct strength, T_f. Therefore, for unbroken symmetries, there must be a set of massless composite physical states for which the trace $Tr(Q^3_{\text{physical}})$ over the charges of the massless physical fermions equals the trace $Tr(Q^3_f)$ over the charges of the elementary preon fields.

Thus 't Hooft's consistency condition implies a relation between the symmetry breaking pattern $G_f \rightarrow S_f$ and the massless spectrum of fermions. However, it does not completely determine the massless fermion spectrum for a given Lagrangian. In his original paper[110] 't Hooft added two additional conditions. The first condition requires that if a mass term for a preon $(m\bar{\psi}\psi)$ is added to the Lagrangian, then, at least in the limit that the mass of this preon field becomes large, all composite fermions containing this preon acquire a mass and therefore no longer contribute to the anomaly. It is reasonable to expect this decoupling. The other condition is that the metacolor gauge interactions are independent of flavor except for mass terms. So that the solution to the anomaly constraints depend only trivially on the number of flavors in any given representation.

For vectorlike theories these two additional constraints allow definite conclusions about the massless spectrum of the theory. However in nonvector theories these additional conditions are generally not meaningful. For example, in our examples, a mass term cannot be introduced for any of the preon fields without explicitly breaking the metacolor gauge invariance. We will not consider these additional constraints further.

3. A Simple Example

It is instructive to give one explicit example which implements t'Hooft's condition and constrains the massless the physical spectrum. Unfortunately, this simple model (and in fact all other known models) is too naive to be phenomenologically relevant. Consider the model with metacolor gauge group $\mathcal{G} = SU(N)$ and preons in the antisymmetric tensor representation A_{ij} and $N-4$ fundamental representations ψ^i. The number of fundamental representations is fixed by the requirement that the gauge interaction has no anomalies.

The global symmetry group of this model is $G_f = SU(N-4) \otimes U(1)$. The origin of the U(1) symmetry can be seen as follows. For each type of representation a $U(1)$ symmetry can be defined; however only one combination of these two $U(1)$ symmetries is free of an anomaly associated with coupling of the current to two metacolor gauged currents (the generalization of the axial $U(1)$ anomaly in QCD). The coefficient of this coupling for each of the global $U(1)$ currents is:

Representation	$U(1)$ Anomaly Coefficient
A_{ij}	$(N - 2)$
ψ^i	1

Hence the combination of global $U(1)$ charges which remains conserved in the presence of gauge interactions is:

$$Q = \int d^3x[(N - 4)\overline{A}^{ij}\gamma^0 A_{ij} - (N - 2) \sum_{\text{flavors}} \overline{\psi}_i\gamma^0\psi^i] . \tag{6.7}$$

Assuming confinement, any spin 1/2 massless physical state must be a singlet under the gauge group $\mathcal{G}$. One possible candidate for such a composite field is

$$F_{nm} = (A_{ij}\sigma_2\psi^i_n)(\sigma_2\psi^j_m) \tag{6.8}$$

where n and m are flavor indices. In particular, we consider the symmetric tensor representation ($F_{nm} = F_{mn}$) under the global symmetry group $SU(N - 4) \in G_f$. The dimension of this representation is $(N - 4)(N - 3)/2$. The $U(1)$ charge of the F_{nm} fields is $-N$. Although it cannot be proven that the F_{nm} represents massless fields[114], it is consistent with 't Hooft's condition for these states to be massless. To show this we need to demonstrate that all the anomaly conditions are satisfied by these massless fields. Comparing the anomalies for the preons and these physical states gives:

Anomaly	Preons	Composites F_{nm}
$Tr[(SU(N - 4))^3]$	N	$(N - 4) + 4 = N$
$Tr[(SU(N - 4))^2Q]$	$-N(N - 2)$	$-N[(N - 4) + 2]$
		$= -N(N - 2)$
$Tr[Q^3]$	$(N - 4)^3(N - 1)N/2$	$-N^3(N - 4)(N - 3)/2$
	$-(N - 2)^3(N - 4)N$	
	$= -N^3(N - 4)(N - 3)/2$	

The anomalies match exactly between the elementary and the composite particles. Therefore this model provides a non-trivial example in which massless composite fermions can be introduced in such a way that 't Hooft's consistency condition is satisfied with the global symmetry group G_f completely unbroken. It should be remembered that the anomaly matching does not guarantee that the states F_{nm}

are in fact massless composites in this theory or that the maximal flavor group remains unbroken. We can only show that it is a consistent possibility. It could also happen that only a subgroup of G_f is remains unbroken; then there will be massless Goldstone bosons and some of these states F_{nm} may acquire masses. In any case, the existence of the solution above for the case G_f is completely unbroken ensures that for any subgroup $S_f \in G_f$ the subset of the fermions which remain massless together with the Goldstone bosons associated with the broken symmetries satisfy 't Hooft's consistency condition.

The consistency condition of 't Hooft provides some guideline to which massless composite fermions could be produced by an strong metacolor dynamics. It is also possible to envision mechanisms which would provide the small explicit symmetry breaking required to generated small masses for initially massless composite quarks and leptons. However, it is very difficult to understand the generation structure of quarks and leptons as an excitation spectra of the metacolor interactions. Excited states would be expected to have a mass scale determined by the strong gauge interactions; but all of the generations of observed quarks and leptons have very small masses on the energy scale Λ_M of the composite binding forces. Hence all masses and mixings would be required to originate from explicit symmetry breaking not directly associated with the metacolor strong interactions.

In this brief introduction to the theoretical issues of composite model building it is clear that many of the original advantages of composite models remain unattained.

B. Phenomenological Implications of Compositeness

If the quarks and leptons are in fact composite, what are the phenomenological consequences of this substructure? At energies low compared to the compositeness scale the interactions between bound states is characterized by the finite size of the bound states, indicated by a radius R. Since the interactions between the composite states are strong only within this confinement radius, the cross section for scattering of such particles at low energies should be essentially geometric, that is, approximately $4\pi R^2$. The compositeness scale can also be characterized by a energy scale $\Lambda^* \sim 1/R$.

Another naive view of the scattering process would replace constituent exchange
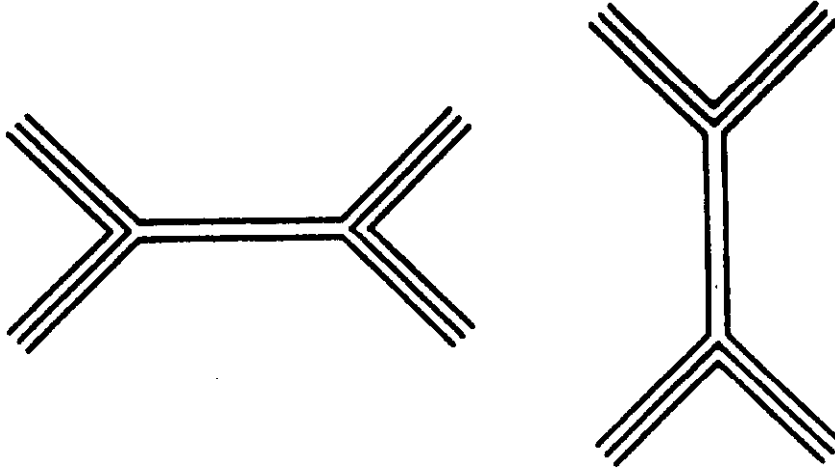
Figure 66: Elastic scattering between composite states at energies much below the compositeness scale. The dominant term is simply the exchange of the lowest-lying massive composite boson.

by an exchange of a composite massive boson as shown in Figure 66. This approximation is analogous to the one particle exchange approximation for the usual strong interactions at low energies; for example, ρ exchange in $\overline{N}N$ collisions. The strength of the coupling $g_M^2/4\pi$ may be estimated by taking this analog one step further. The coupling $g_{\rho\overline{N}N}/4\pi \approx 2$ suggests that the coupling $g_M^2/4\pi \approx 1$ is not unreasonable.

The interaction at low energies is given by an effective four fermion interaction, or contact term, of the general form:

$$\frac{g_M^2}{M_V^2}(\overline{f}_1\gamma^\mu f_2)(\overline{f}_3\gamma_\mu f_4) \tag{6.9}$$

Using $g_M^2/4\pi = 1$ and identifying M_V with Λ^* the effective interaction is of the expected geometric form.

1.   Limits From Rare Processes

The possible contact terms in the effective low energy Lagrangian are of the general form:

$$\frac{4\pi}{\Lambda^{*d}}\, O \tag{6.10}$$

where O is a local operator of dimension $4 + d$ constructed of the usual quark, lepton, and gauge fields. Ignoring quark and lepton masses, the contribution of these contact terms of the effective Lagrangian to the amplitude of some physical process involving quarks, leptons, or gauge fields must be proportional to the energy scale $\sqrt{s}$ of the process considered raised to a power determined by the dimension of the operator. High dimension operators are suppressed by high powers of $\sqrt{s}/\Lambda^*$; and hence are highly suppressed at ordinary energies. Some possible operators which would contribute to rare processes at low energies are given in Table 10. The present limits on rare processes involving ordinary quarks and leptons provide severe restrictions on the scale Λ^* for the associated operator as shown in Table 10. For example, if the $K_L^0 - K_S^0$ mass difference has a contribution from a contact term as shown in Table 10, then the scale of that interaction $\Lambda^* > 6,100$ TeV. Therefore these flavor changing contact terms can not be present in any composite model intended to describe dynamics at the TeV energy scale. Thus, in addition to the theoretical constraints imposed by 't Hooft, rare processes such as those listed in Table 10 provide strong phenomenological constraints on composite model building.

2. Limits On Lepton Compositeness

The correct strategy for composite model building has not yet emerged. All that is known is that the mass scale Λ^* which characterizes the preon binding interactions and the mass scale of the composite states is ≥ 1 TeV. Very little is known in a model-independent way about the composite models except for the experimental and theoretical restrictions discussed above. For example, it is also entirely possible that some of the quarks and leptons are elementary while others are composite. Therefore a conservative approach is to consider only those four fermion interactions which in addition to conserving $SU(3) \otimes SU(2) \otimes U(1)$ gauge symmetries are also completely diagonal in flavor. These interactions must be present in any composite model. For example, if the electron is a bound state; then, in addition to the usual Bhabha scattering, there must be electron-positron scattering in which there is constituent interchange between the electron's and positron's preonic components. These diagonal contact terms test the compositeness hypothesis in a direct and model independent way. The effective Lagrangian for electron weak doublet

Table 10: Limits of contact terms from rare processes. The interaction type assumed for each rare process is shown along with the resulting limit on the compositeness scale Λ^*.

Process	Contact Interaction	Limit on Λ^* (TeV)
$(g-2)_e$	$\dfrac{m_e}{\Lambda_*^2}\, \bar{e}\sigma^{\alpha\beta}e\; F_{\alpha\beta}$	.03
$(g-2)_\mu$	$\dfrac{m_\mu}{\Lambda_*^2}\, \bar{\mu}\sigma^{\alpha\beta}\mu\; F_{\alpha\beta}$	.86
$\mu \to e\,\gamma$	$\dfrac{4\pi}{\Lambda_*^2}\, \bar{\mu}\gamma^\alpha \dfrac{1}{2}(1-\gamma_5)e\; \bar{e}\gamma_\alpha \dfrac{1}{2}(1-\gamma_5)e$ $+\;(\mu \leftrightarrow e)$	60
$\mu \to 3e$	$\dfrac{4\pi}{\Lambda_*^2}\, \bar{\mu}\gamma^\alpha \dfrac{1}{2}(1-\gamma_5)e\; \bar{e}\gamma_\alpha \dfrac{1}{2}(1-\gamma_5)e$	400
$\mu\,N \to e\,N$	$\dfrac{4\pi}{\Lambda_*^2}\, \bar{\mu}\gamma^\alpha \dfrac{1}{2}(1-\gamma_5)e\; \bar{d}\gamma_\alpha \dfrac{1}{2}(1-\gamma_5)d$	460
$K_L \to e^\pm\,\mu^\mp$	$\dfrac{4\pi}{\Lambda_*^2}\, \bar{s}\gamma^\alpha \dfrac{1}{2}(1-\gamma_5)d\; \bar{e}\gamma_\alpha \dfrac{1}{2}(1-\gamma_5)\mu$	140
$K^+ \to \pi^+\,e^-\,\mu^+$	$\dfrac{4\pi}{\Lambda_*^2}\, \bar{s}\gamma^\alpha \dfrac{1}{2}(1-\gamma_5)u\; \bar{e}\gamma_\alpha \dfrac{1}{2}(1-\gamma_5)\mu$	210
$\Delta M(K_L - K_S)$	$\dfrac{4\pi}{\Lambda_*^2}\, \bar{s}\gamma^\alpha \dfrac{1}{2}(1-\gamma_5)d\; \bar{s}\gamma_\alpha \dfrac{1}{2}(1-\gamma_5)d$	6,100

compositeness is[116]

$$\mathcal{L}_{\text{eff}} = \frac{4\pi}{\Lambda^{*2}}[\frac{1}{2}\eta_{LL}(\bar{l}\gamma^\mu l)(\bar{l}\gamma_\mu l) + \eta_{RL}(\bar{l}\gamma^\mu l)(\bar{e}_R\gamma_\mu e_R)$$

$$\frac{1}{2}\eta_{RR}(\bar{e}_R\gamma^\mu e_R)(\bar{e}_R\gamma_\mu e_R)] \tag{6.11}$$

where l is the left-handed (ν, e) doublet. All of the terms in Eq. 6.11 are helicity conserving in for $m_l \ll \sqrt{s} \ll \Lambda^*$. The coefficients η are left arbitrary here since they are model dependent.

For the left-handed components, a composite electron implies a composite neutrino since they are in the same electroweak doublet, but no such relation exists for the right-handed components. The interactions in Eq. 6.11 imply that there will be new terms in addition to the Bhabha scattering and Z^0 exchange graphs in the cross section for electron-positron scattering which in lowest order is given by:

$$\frac{d\sigma}{d\Omega}(e^+e^- \rightarrow e^+e^-) = \frac{\pi\alpha^2}{4s^2}[4A_0 + A_+(1 + \cos\theta)^2 + A_-(1 - \cos\theta)^2] \tag{6.12}$$

where

$$A_0 = (\frac{s}{t})^2|1 + \frac{L_e R_e t}{\sin^2 2\theta_w t_s} + \frac{\eta_{RL} t}{\alpha\Lambda^{*2}}|^2$$

$$A_+ = \frac{1}{2}|1 + \frac{s}{t} + \frac{R_e^2}{\sin^2 2\theta_w}(\frac{s}{s_s} + \frac{s}{t_s}) + \frac{2\eta_{RR}}{\alpha\Lambda^{*2}}s|^2$$

$$\frac{1}{2}|1 + \frac{s}{t} + \frac{L_e^2}{\sin^2 2\theta_w}(\frac{s}{s_s} + \frac{s}{t_s}) + \frac{2\eta_{LL}}{\alpha\Lambda^{*2}}s|^2$$

$$A_- = \frac{1}{2}|1 + \frac{R_e L_e s}{s_s} + \eta_{RL}\frac{s}{\alpha\Lambda^{*2}}|^2 \tag{6.13}$$

and

$$s_s = s - m_Z^2 + im_Z\Gamma_Z \qquad t_s = t - m_Z^2 + im_Z\Gamma_Z$$

$$L_e = -\cos 2\theta_w \qquad R_e = 2\sin^2\theta_w \tag{6.14}$$

This formula is valid only for energies much below the compositeness scale Λ^*. The presence of a compositeness term can be tested by comparing the cross section of Eq. 6.12 with the experimental data to give limits on the contact terms for various interaction types η, whose explicit values depend on the particular composite model.

Table 11: Present limits on electron compositeness for e^+e^- colliders. The four Fermi couplings considered are all left-left (LL), right-right (RR), vector (VV), and axial (AA). Both constructive (-) and destructive (+) interference between the contact term and the standard terms are displayed. The experimental limits are from the MAC[116], PLUTO[117], MARK-J[118], JADE[119], TASSO[120], and HRS[121] Collaborations and are in TeV.

Type	Sign	MAC	PLUTO	MARK-J	JADE	TASSO	HRS
LL	+	1.2	1.1	0.92	0.82	0.7	0.64
LL	-		.76	0.95	1.45	1.94	0.51
RR	+	1.2	1.1	0.92	0.81	0.7	0.64
RR	-		.76	0.95	1.44	1.94	0.51
VV	+	2.5	2.2	1.71	2.38	1.86	1.42
VV	-		1.9	2.35	2.92	2.91	1.38
AA	+	1.3	2.0	2.25	2.22	1.95	0.81
AA	-		1.6	0.94	2.69	2.28	1.06

In Figure 67 the deviation:

$$\Delta_{ee} = \left(\frac{d\sigma/d\Omega|_{measured}}{d\sigma/d\Omega|_{standard\ model}} - 1 \right) \qquad (6.15)$$

is plotted for e^+e^- collisions at $\sqrt{s} = 35$ GeV. At $\sqrt{s} = 35$ GeV the maximum deviation is approximately 4% for the left-left ($\eta_{LL} = \pm 1$, all other η's= 0) or right-right ($\eta_{RR} = \pm 1$, all other η's= 0) couplings with $\Lambda^* = .75$ TeV and for the vector-vector coupling ($\eta_{LL} = \eta_{RR} = \eta_{RL} = \pm 1$) with $\Lambda^* = 1.7$ TeV or for the axial-axial coupling ($\eta_{LL} = \eta_{RR} = -\eta_{RL} = \pm 1$) with $\Lambda^* = 1.4$ TeV. The present limits obtained from various experiments at PEP and PETRA are shown in Table 11. It is clear from these experimental limits that the electron is still a structureless particle on the scale of one TeV.

At LEP energies ($\sqrt{s} = 100$ GeV) a deviation of about 6 % occurs for left-left or right-right couplings with $\Lambda^* = 2$ TeV, or vector-vector or axial-axial couplings
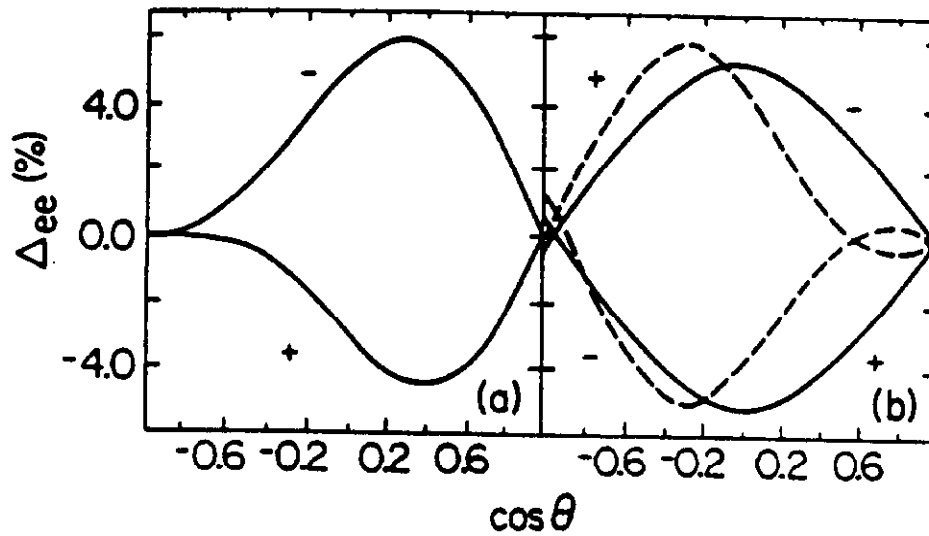
Figure 67: $\Delta_{ee}(\cos\theta)$, in percent, at $\sqrt{s} = 35\,\text{GeV}$. (a) The LL and RR models with $\Lambda^* = 750$ GeV. (b) The VV model (solid lines) with $\Lambda^* = 1700$ GeV and the AA model (dashed lines) with $\Lambda^* = 1400$ GeV. The $\pm$ signs refer to the overall sign of the contact term in each case.

with $\Delta^* = 5$ TeV.

C.   Signals for Compositeness in Hadron Collisions

Searches for compositeness in hadron collisions will naturally concentrate on looking for internal structure of the quarks. As in the case of a composite electron, if the quark is composite there will be an additional interaction between quarks which can be represented by a contact term at energy scales well below the compositeness scale. However, the reference cross section for elastic scattering of pointlike quarks, the QCD version of Bhabha scattering, has both nonperturbative and perturbative corrections and is therefore not as accurately known as Bhabha scattering in QED. Futhermore the extraction of the elementary subprocesses in the environmemt of hadron- hadron collisions involves knowledge of the quark and gluon distribution functions. Therefore larger deviations from QCD expectations will be required before a signal for compositeness can be trusted.

The most general contact interactions which:

* preserve $SU(3) \otimes SU(2) \otimes U(1)$,

* involve only the up and down quarks, and

* are helicity conserving

involve 10 independent terms.

$$
\begin{aligned}
\mathcal{L}_{\text{eff}} = {} & \frac{4\pi}{\Lambda^{*2}} [\frac{\eta_1}{2} \bar{q}_L \gamma^\mu q_L \bar{q}_L \gamma_\mu q_L + \eta_2 \bar{q}_L \gamma^\mu q_L \bar{u}_R \gamma_\mu u_R \\
& + \eta_3 \bar{q}_L \gamma^\mu q_L \bar{d}_R \gamma_\mu d_R + \eta_4 \bar{q}_L \gamma^\mu \frac{\lambda_a}{2} q_L \bar{u}_R \gamma_\mu \frac{\lambda_a}{2} u_R \\
& + \eta_5 \bar{q}_L \gamma^\mu \frac{\lambda_a}{2} q_L \bar{d}_R \gamma_\mu \frac{\lambda_a}{2} d_R + \frac{\eta_6}{2} \bar{u}_R \gamma^\mu u_R \bar{u}_R \gamma_\mu u_R \\
& + \eta_7 \bar{u}_R \gamma^\mu \frac{\lambda_a}{2} u_R \bar{d}_R \gamma_\mu \frac{\lambda_a}{2} d_R + \eta_8 \bar{u}_R \gamma^\mu u_R \bar{d}_R \gamma_\mu d_R \\
& + \frac{\eta_9}{2} \bar{d}_R \gamma^\mu d_R \bar{d}_R \gamma_\mu d_R + \frac{\eta_{10}}{2} \bar{q}_L \gamma^\mu \frac{\tau_a}{2} q_L \bar{q}_L \gamma_\mu \frac{\tau_a}{2} q_L]
\end{aligned}
\tag{6.16}
$$

This complicated form for the contact terms will not be considered in full generality here[115]. To understand the nature of the bounds on quark substructure which can

be seen in hadron collisions it is sufficient to take the simple example where only one of the 10 possible contact terms is considered. For this purpose only the left-left coupling contact terms will be considered:

$$\mathcal{L}_{eff} = \frac{\eta_{LL}}{2}\frac{4\pi}{\Lambda^{*2}}\bar{q}_L\gamma^\mu q_L \bar{q}_L \gamma_\mu q_L \qquad (6.17)$$

for both signs $\eta_{LL} = \pm 1$ of the interaction.

A typical quark-antiquark elementary subprocess including a contact term due to quark compositeness is shown in Figure 68.

Analytically the differential cross section (anti)quark-(anti)quark scattering is given by:

$$\frac{d\sigma}{d\hat{t}}(i\ j\ \to i'\ j') = \alpha_s^2 \frac{\pi}{\hat{s}^2}|A_{2\to 2}(i\ j\ \to i'\ j')|^2 \qquad (6.18)$$

where

$$
\begin{aligned}
|A(u\bar{u} \to u\bar{u})|^2 &= |A(d\bar{d} \to d\bar{d})|^2 \\
&= \frac{4}{9}[\frac{\hat{u}^2 + \hat{s}^2}{\hat{t}^2} + \frac{\hat{u}^2 + \hat{t}^2}{\hat{s}^2} - \frac{2\hat{u}^2}{\hat{t}\hat{s}}] \\
&\quad + \frac{8}{9}\frac{\eta_{LL}}{\alpha_s \Lambda^{*2}}[\frac{\hat{u}^2}{\hat{t}} + \frac{\hat{u}^2}{\hat{s}}] + \frac{8}{3}[\frac{\eta_{LL}\hat{u}}{\alpha_s \Lambda^{*2}}]^2 \\
|A(uu \to uu)|^2 &= |A(dd \to dd)|^2 = |A(\bar{u}\bar{u} \to \bar{u}\bar{u})|^2 = |A(\bar{d}\bar{d} \to \bar{d}\bar{d})|^2 \\
&= \frac{4}{9}[\frac{\hat{u}^2 + \hat{s}^2}{\hat{t}^2} + \frac{\hat{s}^2 + \hat{t}^2}{\hat{u}^2} - \frac{2\hat{s}^2}{\hat{t}\hat{u}}] \\
&\quad + \frac{8}{9}\frac{\eta_{LL}}{\alpha_s \Lambda^{*2}}[\frac{\hat{s}^2}{\hat{t}} + \frac{\hat{s}^2}{\hat{u}}] + \frac{8}{3}[\frac{\eta_{LL}}{\alpha_s \Lambda^{*2}}]^2(\hat{u}^2 + \hat{t}^2 + \frac{2}{3}\hat{s}^2) \\
|A(u\bar{u} \to d\bar{d})|^2 &= |A(d\bar{d} \to u\bar{u})|^2 \\
&= \frac{4}{9}[\frac{\hat{u}^2 + \hat{t}^2}{\hat{s}^2}] + [\frac{\eta_{LL}\hat{u}}{\alpha_s \Lambda^{*2}}]^2 \\
|A(ud \to ud)|^2 &= |A(u\bar{d} \to u\bar{d})|^2 = |A(\bar{u}d \to \bar{u}d)|^2 = |A(\bar{u}\bar{d} \to \bar{u}\bar{d})|^2 \\
&= \frac{4}{9}[\frac{\hat{u}^2 + \hat{s}^2}{\hat{t}^2}] + [\frac{\eta_{LL}\hat{u}}{\alpha_s \Lambda^{*2}}]^2 \qquad (6.19)
\end{aligned}
$$

Note that the effects of the contact term grow linearly with $\hat{s}$ relative to the QCD terms in the amplitude for elastic scattering. There is no effect in lowest order on (anti)quark-gluon or gluon-gluon scattering. The inclusive jet production in
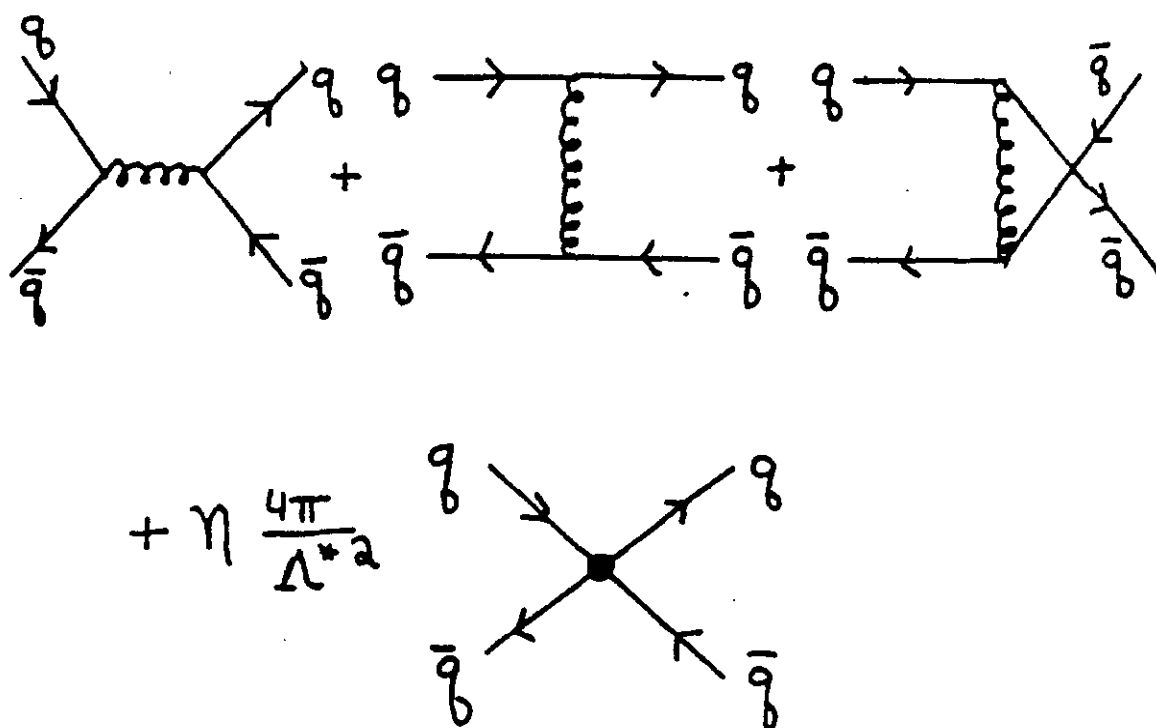
Figure 68: The Feynman diagrams contributing to the amplitude for the subprocess $\bar{q}q \rightarrow \bar{q}q$ in the presence of a contact interaction associated with quark composite-ness. The first three diagrams are simply the order α_s contribution from QCD and the last diagram represents the contribution from the contact interaction of Eq. 6.17.

$\bar{p}p$ collisions at $\sqrt{s} = 1.8$ TeV including the effect of a LL contact term in the (anti)quark-(anti)quark scattering amplitude is shown in Figure 69.

The present measurements of inclusive single jet production at the $S\bar{p}pS$ collider bounds the possible value of Λ^* associated with light quark compositeness. For the left-left coupling with $\eta_{LL} = -1$ the effects of a contact term for various values of Λ^* are shown with the UA2 data[39] in Figure 70. The analysis of the UA2 Collaboration[39] shows that $\Lambda^* \geq 370$ GeV is required to be consistent with their results. This limit is the best bound on light quark compositeness which presently exists. Hence the light quarks do not have any structure below a scale of 370 GeV. Since the contact term in the total cross section grows linearly with $\hat{s}$ while the standard terms fall off with increasing energy like $1/\hat{s}$ the contact will eventually dominate the cross section. This occurs when

$$\hat{s} \approx \alpha_s \Lambda^{*2} .\tag{6.20}$$

Therefore the contact term dominates at an energy scale well below the compositeness scale Λ^* itself.

1. Quark-Lepton Contact Term

In generalized Drell-Yan processes, a quark-antiquark initial state annihilates into a lepton pair via an intermediate virtual γ or Z^0. Therefore composite effects can contribute only if both the quark and lepton are composite and they have some constituent in common. Whether these conditions are meet is more dependent on the particular composite model.

A contact term associated with compositeness of the first generation which can contribute to Drell-Yan processes is of the general form:

$$\begin{aligned}
\mathcal{L}_{eff} = \frac{4\pi}{\Lambda^{*2}} [& \eta_{LL}\bar{q}_L\gamma^\mu q_L \bar{l}_L\gamma_\mu l_L + \eta_{LR}\bar{q}_L\gamma^\mu q_L \bar{e}_R\gamma_\mu e_R \\
& + \eta_{RU}\bar{u}_R\gamma^\mu u_R \bar{l}_L\gamma_\mu l_L + \eta_{RD}\bar{d}_R\gamma^\mu d_R \bar{l}_L\gamma_\mu l_L \\
& + \eta_{RRU}\bar{u}_R\gamma^\mu u_R \bar{e}_R\gamma_\mu e_R + \eta_{RRD}\bar{d}_R\gamma^\mu d_R \bar{e}_R\gamma_\mu e_R \\
& + \eta_V \bar{q}_L\gamma^\mu \frac{\tau_a}{2} q_L \bar{l}_L\gamma_\mu \frac{\tau_a}{2} l_L]
\end{aligned}\tag{6.21}$$
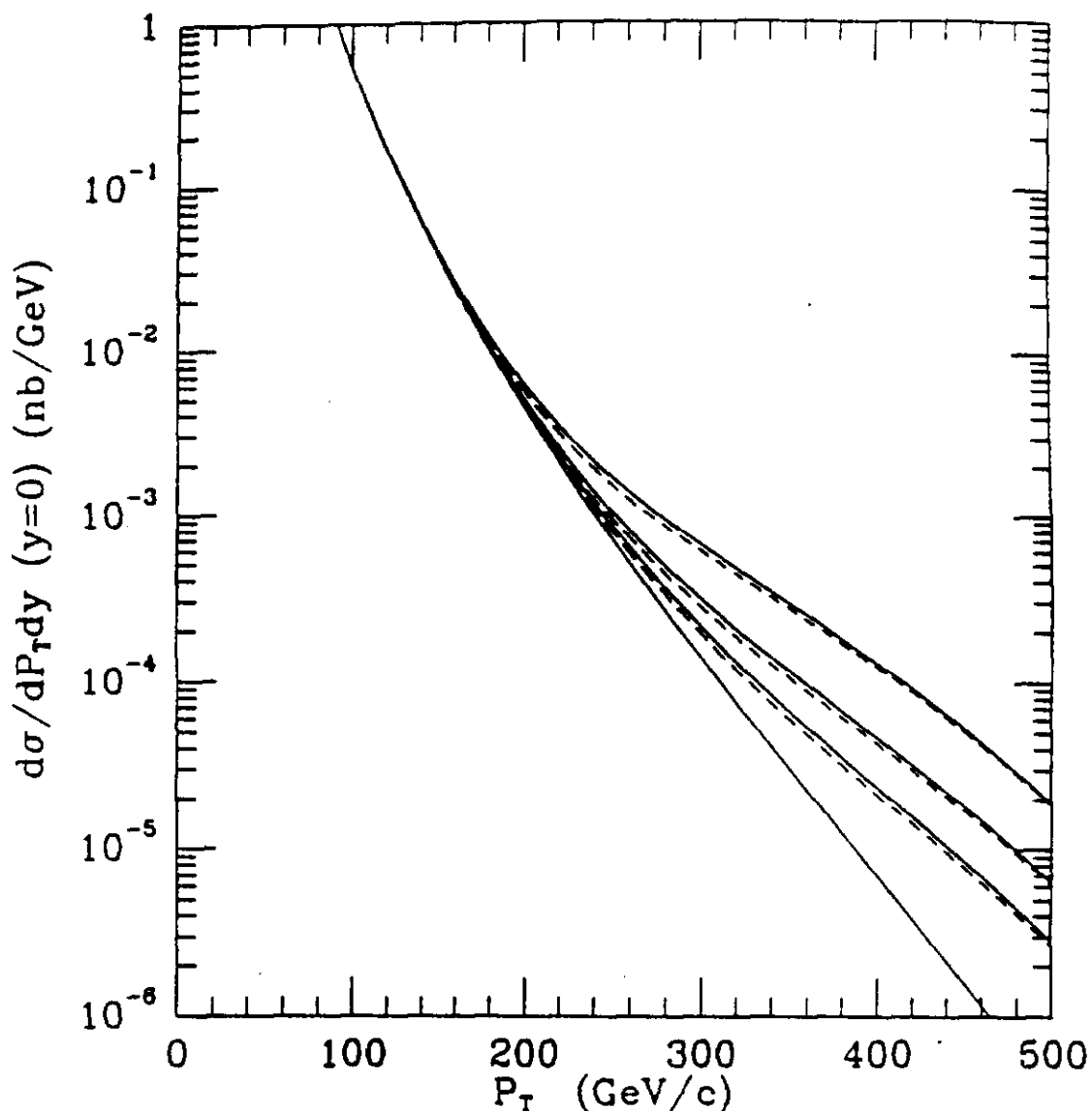
Figure 69: The inclusive jet production cross section $d^2\sigma/dp_\perp dy|_{y=0}$ in $\bar{p}p$ collisions at $\sqrt{s} = 1.8$ TeV including the effects of a contact interaction. The contact term was the LL type with $\eta_{LL} = -1$ (solid line) and $\eta_{LL} = +1$ (dashed line). The values of Λ^* are .75 (top pair of lines), 1.0 (middle pair of lines), and 1.25 (bottom pair of lines) TeV. The standard QCD prediction using the distributions of Set 2 is denoted by the single solid line at the bottom.
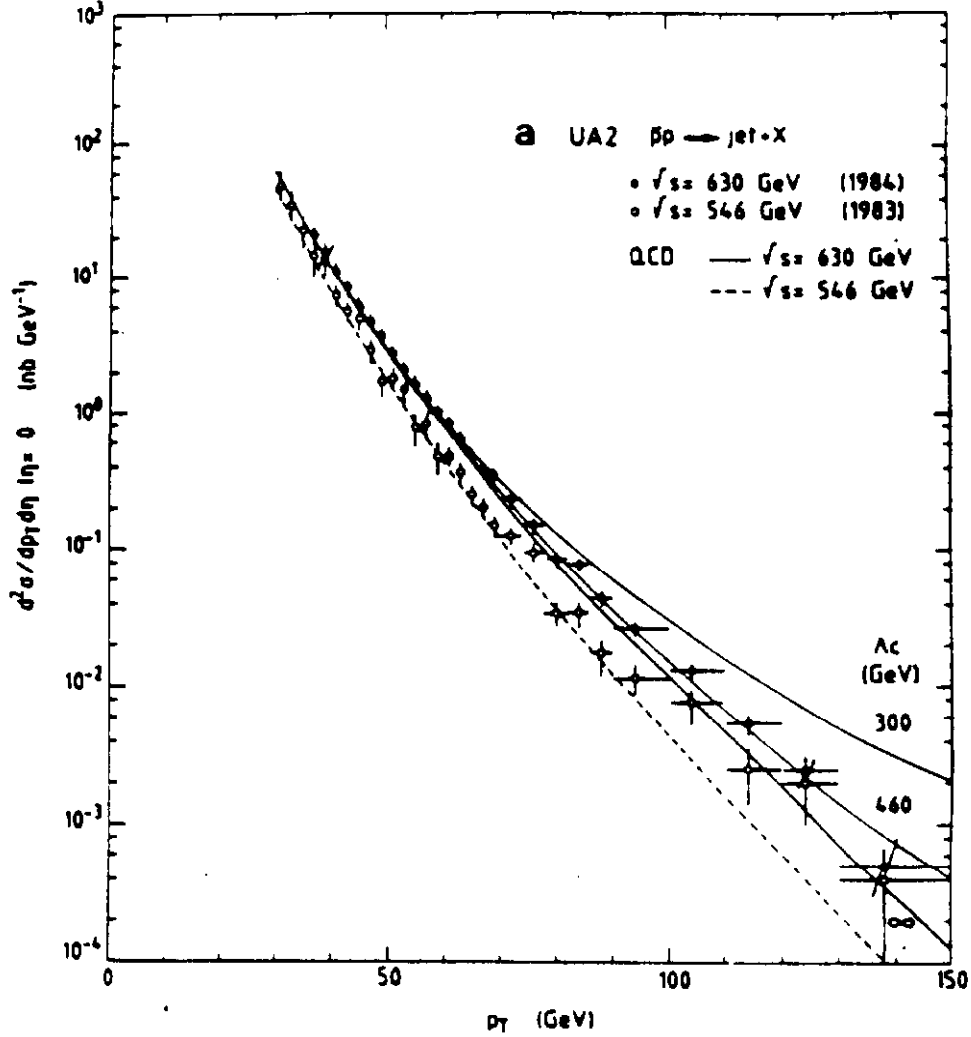
Figure 70: Inclusive jet production cross sections from the UA2 Collaboration (as shown in Fig. 22) with the effects of a composite interaction shown for $\sqrt{s} = 630$ GeV. The three solid lines (from top to bottom) represent the prediction for $d^2\sigma/dp_\perp dy|_{y=0}$ for the left-left contact term with $\Lambda^* = 300$ GeV, 460 GeV, and infinity respectively.

where $q_L = (u_L, d_L)$ and $l_L = (\nu_L, e_L)$. Again the nature of the bounds are illustrated by a simple case of a left-left coupling ($\eta_{LL} = \pm 1$ and all other η's = 0). When the contact term is added to the standard γ and Z^0 contributions to the Drell-Yan process we obtain[115]:

$$\sigma(\bar{q}q \to \bar{e}e) = \frac{\pi\alpha^2}{27\hat{s}}[A(\hat{s}) + B(\hat{s})] \tag{6.22}$$

where

$$A(\hat{s}) = 3[(\frac{1}{3} + \frac{L_q L_e}{\sin^2 2\theta_w}\frac{\hat{s}}{\hat{s}_e} + \eta_{LL}\frac{\hat{s}}{\alpha\Lambda^{*2}})^2 + (\frac{1}{3} + \frac{R_q R_e}{\sin^2 2\theta_w}\frac{\hat{s}}{\hat{s}_e})^2]$$

$$B(\hat{s}) = 3[(\frac{1}{3} - \frac{R_q L_e}{\sin^2 2\theta_w})^2 + (\frac{1}{3} - \frac{L_q R_e}{\sin^2 2\theta_w})^2] \tag{6.23}$$

and $L_e, R_e,$ and $\hat{s}_e$ are given by Eq. 6.16. Of course the cross section would be similarly modified if the μ or τ is composite and shares constituents with the light quarks.

The effect on electron pair production in $\bar{p}p$ collisions at $\sqrt{s} = 1.8$ TeV is shown in Figure 71 for various compositeness scales Λ^*. The effect of the contact term is quite dramatic. Whereas the standard Drell-Yan process drops very rapidly with increasing lepton pair mass above the Z^0 pole, the contact term causes the cross section to essentially flatten out at a rate dependent on the the value of Λ^*. This is due to the combination of the elementary cross section which grows linearly with pair mass and the rapidly dropping luminosity of quark-antiquark pairs as the subprocess energy increases. Hence the probability of observing a lepton pair with invariant mass significantly greater than the Z^0 mass becomes substantial. By this method contact scales up to approximately 1.0 TeV can be probed with an integrated hadron luminosity of $10^{37} cm^{-2}$ at this energy.

2. Compositeness at the SSC

The discover range for compositeness is greatly extended at a supercollider. For example in pp collisions at $\sqrt{s} = 40$ TeV the effects of a left-left contact term in the inclusive jet production is shown in Figure 72 for compositeness scales of $\Lambda^* = 10$, 15, and 20 TeV. In pp collisions the effects of the interference between the

Figure 71: Cross section $d\sigma/dMdy|_{y=0}$ for dilepton production in $\bar{p}p$ collisions at $\sqrt{s} = 1.8$ TeV, according to the parton distributions of Set 2. The curves are labeled by the contact interaction scale Λ^* (in TeV) for a LL interaction type with $\eta_{LL} = -1$ (solid lines). (The curves for $\eta_{LL} = +1$ are very similar to the corresponding $\eta_{LL} = -1$ curve and therefore are not separately displayed.) The standard model prediction for the Drell-Yan cross section is denoted by a dashed line.

Figure 72: Cross section $d\sigma/dp_\perp dy|_{y=0}$ for jet production in pp collisions at $\sqrt{s} = 40$ TeV, according to the parton distributions of Set 2. The curves are labeled by the compositeness scale Λ^* (in TeV) for a LL interaction type and $\eta_{LL} = -1$ (solid line) and $\eta_{LL} = +1$ (dashed line). The QCD prediction for the cross section is denoted by the bottom solid line. (From EHLQ).

Table 12: Compositeness scale Λ^* probed at various planned colliders. The left-left interaction type is assumed. The discovery limit is in TeV.

Collider			Subprocess tested		
	$\sqrt{s}$	$\int dt \mathcal{L}$	$e^+e^- \to e^+e^-$	$\bar{q}q \to \bar{q}q$	$\bar{q}q \to e^+e^-$
	(TeV)	$(cm)^{-2}$	Λ^*	Λ^*	Λ^*
HERA (ep)	.314	10^{39}	—	—	3
LEP I (or SLC) (e^+e^-)	.10	10^{39}	3.5	—	—
LEP II (e^+e^-)	.20	10^{39}	7	—	—
$S\bar{p}pS$ $(\bar{p}p)$	.63	3×10^{37}	—	.60	1.1
$TEVI$ $(\bar{p}p)$	2.0	10^{38}	—	1.5	2.5
SSC (pp)	40	10^{40}	—	17	25

usual QCD processes and the composite interaction are significantly larger than for $\bar{p}p$ collisions as can be seen by comparing Fig. 72 and Fig. 68.

The effects of a left-left contact term contributing to the Drell-Yan processes for pp collisions at $\sqrt{s} = 40$ TeV is shown in Figure 73.

D.   Summary of Discovery Limits

The discovery limits from contact terms associated with quark and/or lepton substructure is given in Table 12. The same discovery criteria were used for present hadron colliders as for the supercollider which are detailed in EHLQ. The discovery criteria LEP and HERA are found in Ref.122. Compositeness scales (for the first generation of quarks and leptons) as high as 20-25 TeV can be probed at an SSC.

E.   Crossing the Compositeness Threshold

Finally it is interesting to consider what signals will be seen in hadron colliders as the compositeness scale Λ^* is crossed. As the subprocess energy becomes comparable to the compositeness scale not only the lowest mass composite states (the usual
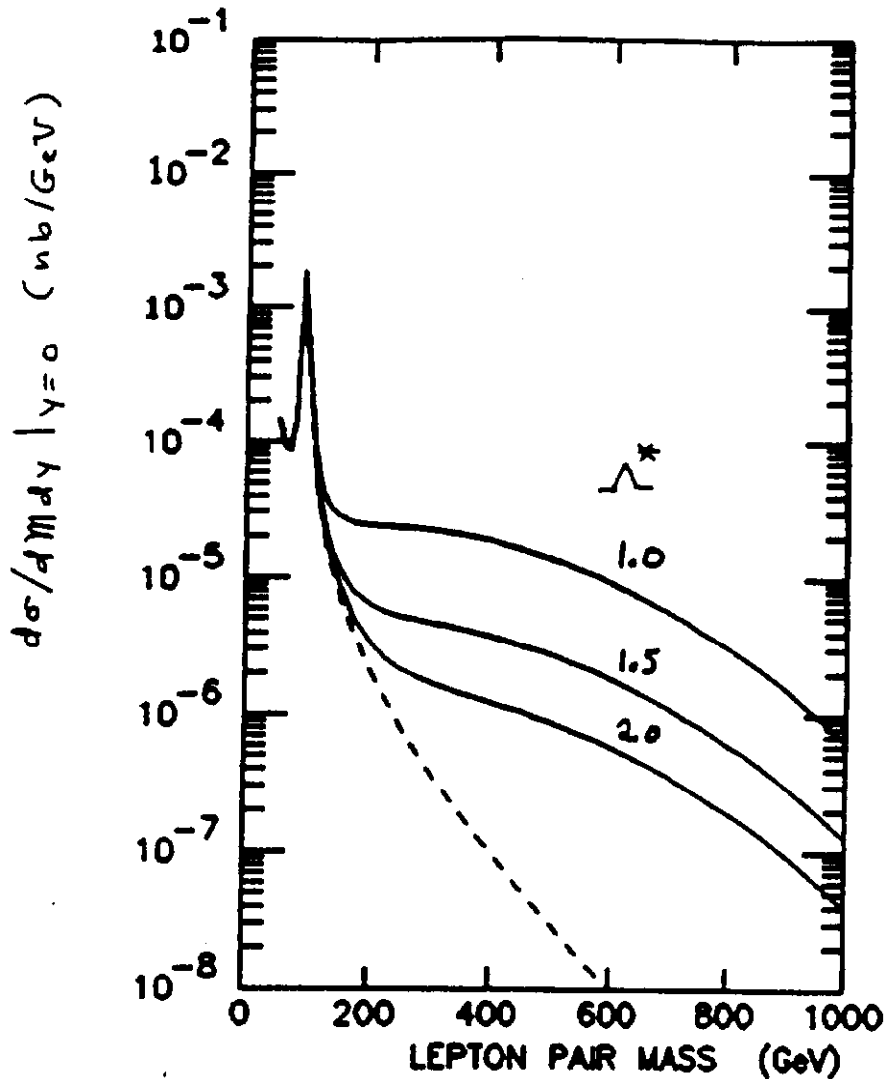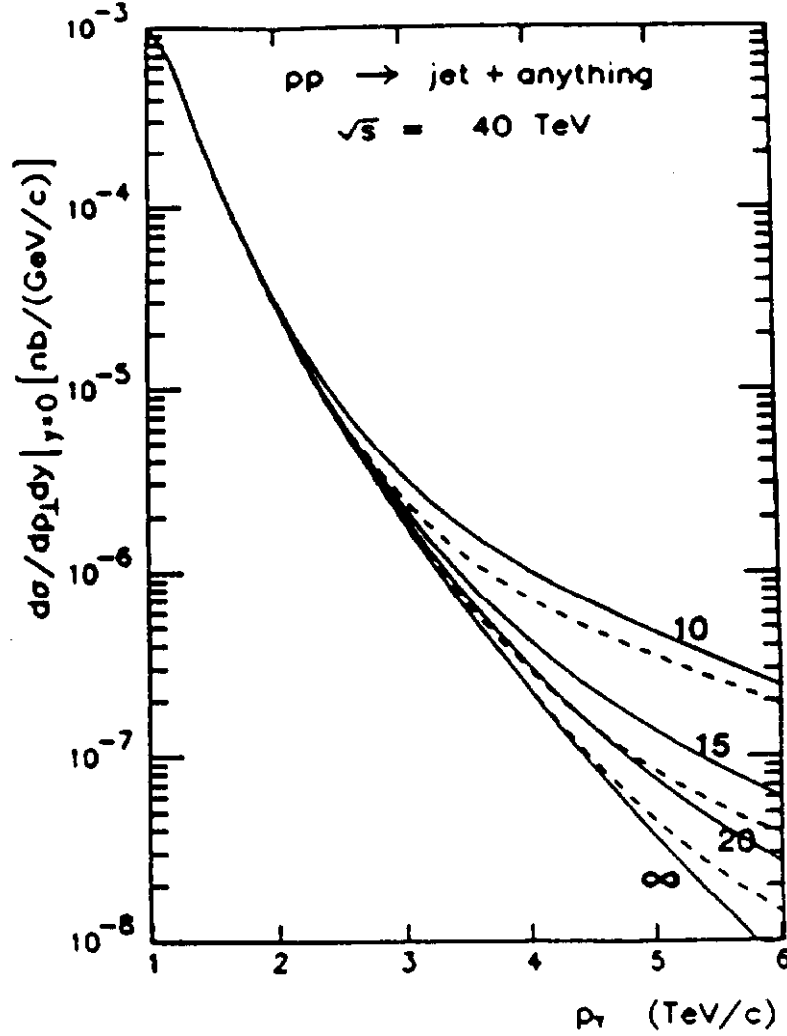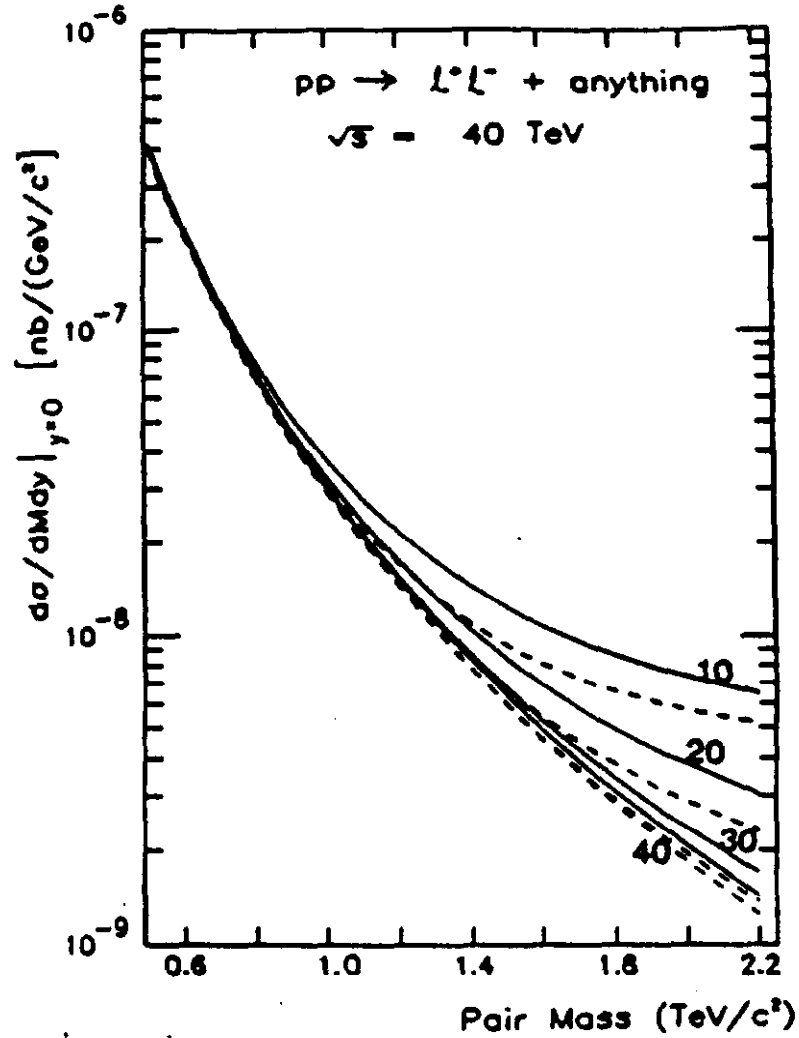
Figure 73: Cross section $d\sigma/d\mathcal{M}dy|_{y=0}$ for dilepton production in pp collisions at $\sqrt{s} = 40$ TeV, according to the parton distributions of Set 2. The curves are labeled by the contact interaction scale Λ^* (in TeV) for a LL interaction type with $\eta_{LL} = -1$ (solid lines) and $\eta_{LL} = +1$ (dashed lines). (From EHLQ)

Table 13: Expected discovery limits for fermions in exotic color representations at present and planned colliders. It is assumed that 100 produced events are sufficient for discovery.

Collider		$\sqrt{s}$ (TeV)	$\int dt \mathcal{L}$ (cm)$^{-2}$	Mass limit (Gev/c^2) Color Representation		
				3*	6	8
$S\bar{p}pS$	$\bar{p}p$	.63	3×10^{36}	65	85	88
upgrade			3×10^{37}	90	110	115
$TEVI$	$\bar{p}p$	1.8	10^{37}	135	200	205
upgrade		2	10^{38}	220	285	290
SSC	pp	40	10^{38}	1,250	2,000	2,050
			10^{39}	1,900	2,750	2,800
			10^{40}	2,700	3,700	3,750

quarks and lepton) can be produced but also excited quarks and leptons. These excited quarks could be in color representations other that the standard triplets. The masses of the lightest excited quarks would naively be expected to be of the same order as Λ^*. It is of course possible that some might be considerably lighter. In this hope the cross sections for pair production of excited quarks in $\bar{p}p$ at $\sqrt{s} = 1.8$ TeV are shown in Figure 74 for color representations 3*, 6, and 8.

The discover limits for fermions in exotic color representations at various colliders are given in Table 13.

What happens to the $\bar{q}q$ total cross section? The behaviour of this total cross section has been studied recently by Bars and Hinchliffe[123]. At energies at and above the compositeness scale this cross section would have the same general behaviour as the $\bar{p}p$ total cross section at and above 1 GeV. Using this rough analog, we would expect a resonance dominated region at energy scales a few times the compositeness scale and then at much higher energies the total cross section should rise slowly. However most of this cross section is within an angle of approximately $\arcsin(2\Lambda^*/\sqrt{s})$ to the beam directions. At energies $\sqrt{s} \gg \Lambda^*$, the large angle scat-
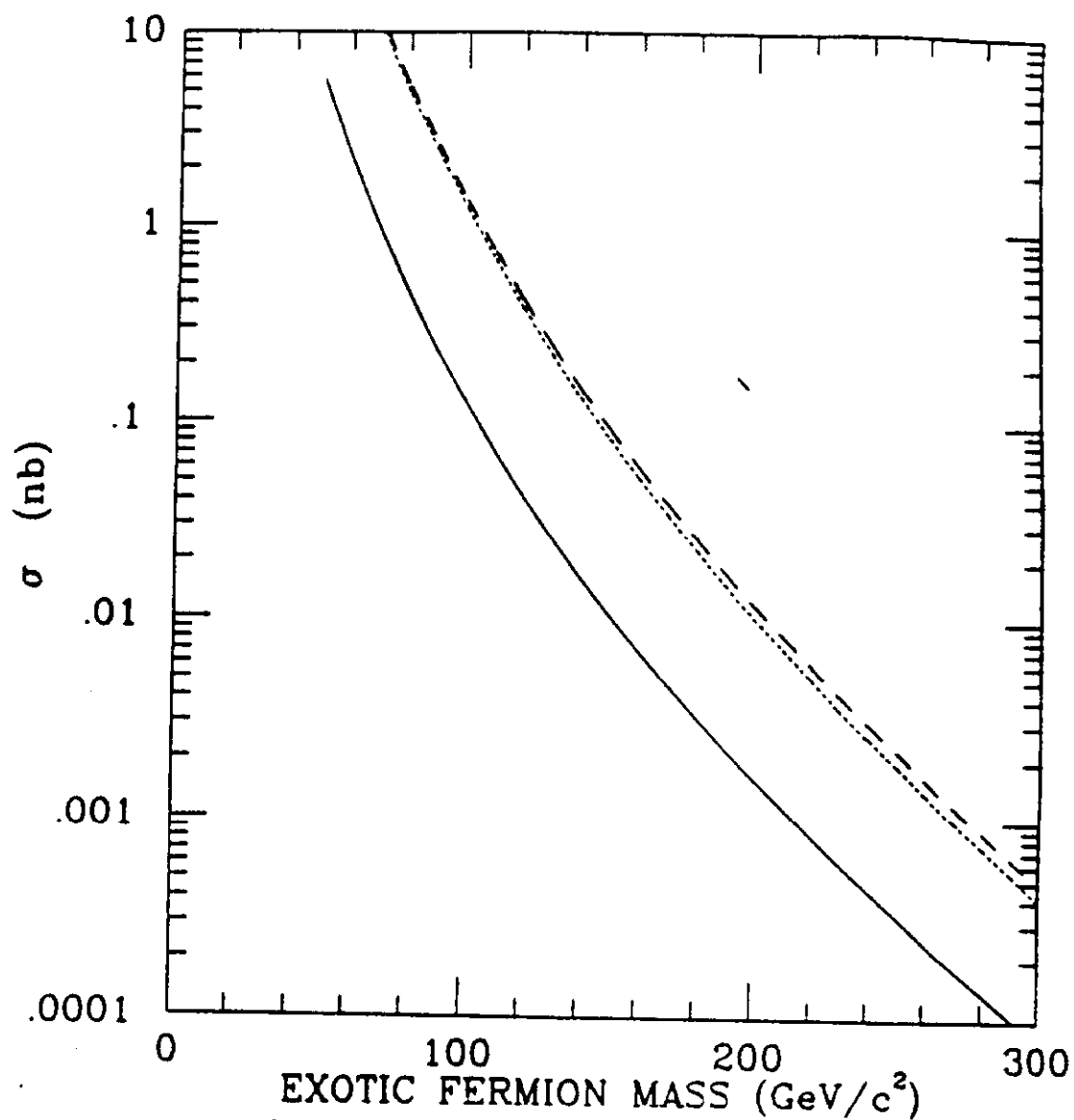
Figure 74: Total cross sections for production of excited quarks in $\bar{p}p$ collisions at $\sqrt{s} = 1.8$ TeV as a function of their mass. Color representations 3*, 8, and 6 are denoted by solid, dashed, and dotted lines respectively. The parton distributions of Set 2 was used.

tering will again exhibit the $1/\hat{s}$ behaviour expected for preon scattering via single metacolor gluon exchange.

The behaviour of the $\bar{q}q$ subprocess has to be combined with the appropriate parton distribution functions to obtain the physical cross sections in hadron-hadron collisions. The resulting inclusive jet cross section for pp collisions at $\sqrt{s} = 40$ TeV is shown in Figure 75 for a particular model of Bars and Hinchliffe[123] with various compositeness scales. These models exhibit the general behaviour discussed above. Quark-antiquark scattering is mainly inelastic at subprocess energies above the compositeness scale. Thus the two jet final state will be supplanted as the dominate final state by multijets events (possibly with accompanying lepton pairs). This will provide unmistakable evidence that the composite threshold has been crossed.
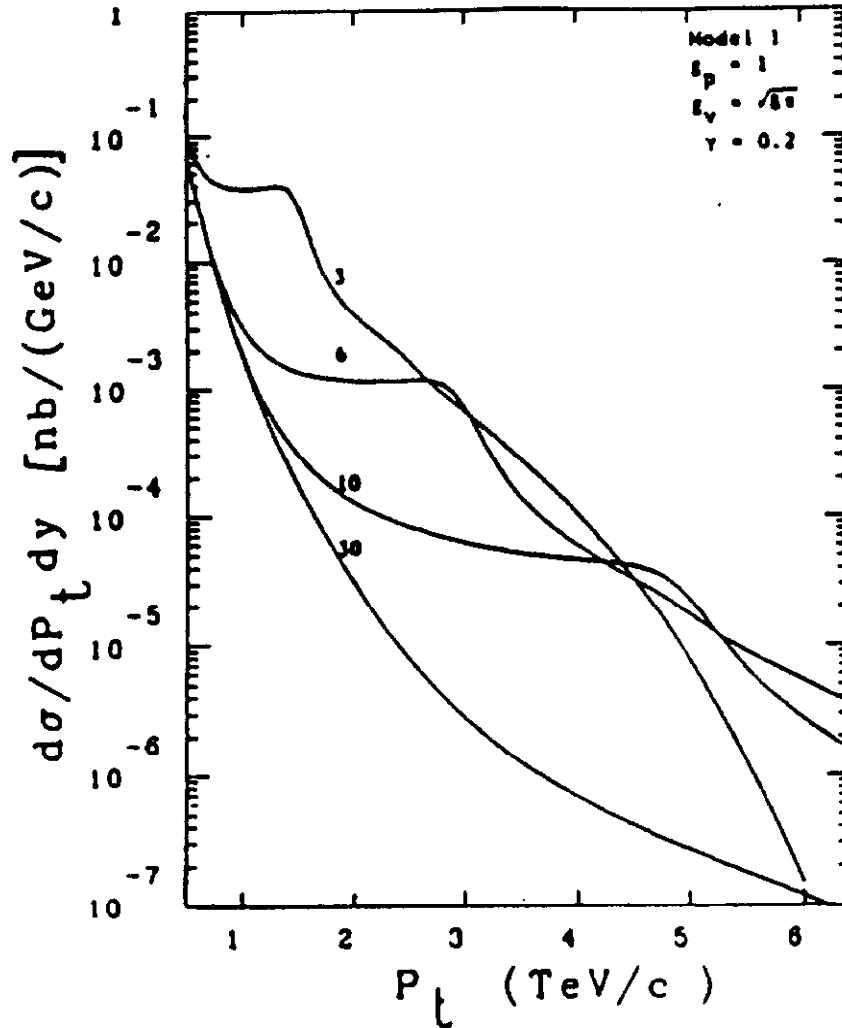
Figure 75: The differential cross section $d\sigma/dp_\perp dy|_{y=0}$ in pp collisions at $\sqrt{s} = 40$ TeV for a model of composite interactions at and above the scale of compositeness. In this model proposed by Bars and Hinchliffe[123] there is a resonance in quark-quark scattering due to the composite interactions. The expected cross section is shown for various values of the resonance mass: $M_V = 3$, 6, 10, and 30 TeV. For other details on the model and the parameter values used in these curves see Ref.123 (Fig.7)

VII. SUPERSYMMETRY ?

One set of symmetries normally encountered in elementary particle physics are the space-time symmetries of the Poincare group:

- P^μ – the momentum operator – the generator of translations.

- $M^{\mu\nu}$ – the Lorentz operators – the generators of rotations and boosts.

These symmetries classify the elementary particles by mass and spin.

The other symmetries usually encountered are internal symmetries such as color, electric charge, isospin, etc. For each non-Abelian internal symmetry there is a set of charges $\{Q_a\}$ which form a Lie Algebra:

$$-i[Q_a, Q_b] = f_{abc}Q_c \tag{7.1}$$

under which the Hamiltonian is invariant:

$$-i[Q_a, H] = 0 \tag{7.2}$$

If these symmetries are not spontaneously broken the physical states form representations under the associated Lie group, $\mathcal{G}$.

Because the charges are associated with internal symmetries they commute with the generators of space-time symmetries

$$-i[Q_a, P^\mu] = 0$$
$$-i[Q_a, M^{\mu\nu}] = 0 . \tag{7.3}$$

We have already seen that such symmetries play a central role in the physics of the standard model. The internal symmetries $SU(3) \otimes SU(2)_L \otimes U(1)_Y$ determine all the basic gauge interactions. Global symmetries such as fermion number and flavor symmetries also play an important role.

Supersymmetry is a generalization of the usual internal and space-time symmetries sharing aspects of both. Formally the concept of a Lie algebra is generalized to a structure called a graded Lie algebra[124] which is defined by both commutators

and anticommutators. A systematic development of the formal aspects of super-symmetry is outside the scope of these lectures but can be found in Wess and Bagger[125].

The simplest example of a global supersymmetry is $N = 1$ supersymmetry which has a single generator Q_α which transforms as spin $\frac{1}{2}$ under the Lorentz group:

$$-i[Q_\alpha, P^\mu] = 0$$
$$-i[Q_\alpha, M^{\mu\nu}] = (\sigma^{\mu\nu} Q)_\alpha \qquad (7.4)$$

where $\sigma^{\mu\nu}$ are the Pauli matrices. Finally the generator Q and the Hermitian conjugate generator $\overline{Q}$ must have the following anticommutation relations:

$$\{Q_\alpha, Q_\beta\} = 0$$
$$\{\overline{Q}_\alpha, \overline{Q}_\beta\} = 0$$
$$\{Q_\alpha, \overline{Q}_\beta\} = -2(\gamma_\mu)_{\alpha\beta} P^\mu \qquad (7.5)$$

These are the relations for $N = 1$ global supersymmetry. The generator Q is a spin $\frac{1}{2}$ fermionic charge. If this is a symmetry of the Hamiltonian, then

$$- i[Q_\alpha, H] = 0 \qquad (7.6)$$

and assuming this symmetry is realized algebraically the physical states of the system can be classified by these charges. Since the supercharge has spin $\frac{1}{2}$, states differing by one-half unit of spin will belong to the same multiplet. This fermion-boson connection will allow a solution to the naturalness problem of the standard model (discussed in Section 4).

A. Minimal $N = 1$ Supersymmetric Model

The minimal supersymmetric generalization of the standard model is to extend the standard model to include a $N = 1$ supersymmetry. The supercharge Q acts on an ordinary particle state to generate its superpartner. For a massless particle with helicity h (i.e. transforming as the $(0, h)$ representation of the Lorentz group) the action of the charge Q produces a superpartner degenerate in mass with helicity

$h - \frac{1}{2}$ (i.e. transforming as $(0, h - \frac{1}{2})$. Applying the supercharge again vanishes since the anticommutator of the supercharge with itself is zero (Eq. 7.5). Hence the supermultiplets are doublets with the two particles differing by one-half unit of spin. The number of fermion states (counted as degrees of freedom) is identical with the number of boson states. For massless spin 1 gauge bosons these superpartners are massless spin $\frac{1}{2}$ particles called gauginos (gluino, wino, zino, and photino for the gluon, W, Z, and photon respectively). For spin $\frac{1}{2}$ fermions these superpartners are spin 0. If the fermion is massive the superpartner will be a scalar particle with the same mass as the associated fermion. The superpartners of quarks and leptons are denoted scalar quarks (squarks) and scalar leptons (sleptons). The superpartners of the Higgs scalars of the standard model are spin $\frac{1}{2}$ fermions called Higgsinos.

Since the supercharge commutes with every ordinary internal symmetry Q_a

$$- i[Q_a, Q_a] = 0 \; . \tag{7.7}$$

all the usual internal quantum numbers of the superparticle will be identical to those of its ordinary particle partner. In nearly all supersymmetric theories, the superpartners carry a new fermionic quantum number R which is exactly conserved[126]. All the ordinary particles and their superpartners are shown in Table 14.

No superpartner of the ordinary particles has yet been observed, thus supersymmetry must be broken. This scale of supersymmetry breaking is denoted:

$$\Lambda_{ss} \; . \tag{7.8}$$

Even in the presence of supersymmetry breaking it is normally possible to retain a R quantum number for superpartners which is absolutely conserved[127]. This means that the lightest superpartner will be absolutely stable. If the supersymmetry is spontaneously broken there is an additional massless fermion the Goldstino $\mathcal{G}$, which is the analogy of the Goldstone boson in the case of spontaneous breaking of an internal symmetry. In more complete models with local supersymmetry, such as supergravity, there is a superHiggs mechanism in which the Goldstino becomes the longitudinal component of a massive spin $\frac{3}{2}$ particle - the gravitino[128]. Hence the existence of the Goldstino as a massless physical is dependent of the way global $N = 1$ supersymmetry is incorporated into a more complete theory and the mechanism of supersymmetry breaking.

Table 14: Fundamental Fields of the Minimal Supersymmetric Extension of the Standard Model

Particle		Spin	Color	Charge
gluon	g	1	8	0
gluino	$\tilde{g}$	1/2	8	0
photon	γ	1	0	0
photino	$\tilde{\gamma}$	1/2	0	0
intermediate bosons	$W^{\pm}, Z^0$	1	0	$\pm 1, 0$
wino, zino	$\tilde{W}^{\pm}, \tilde{Z}^0$	1/2	0	$\pm 1, 0$
quark	q	1/2	3	2/3, -1/3
squark	$\tilde{q}$	0	3	2/3, -1/3
electron	e	1/2	0	-1
selectron	$\tilde{e}$	0	0	-1
neutrino	ν	1/2	0	0
sneutrino	$\tilde{\nu}$	0	0	0
Higgs bosons	$H^+ \quad H'^0$ $H^0 \quad H'^-$	0	0	$\pm 1, 0$
Higgsinos ·	$\tilde{H}^+ \quad \tilde{H}'^0$ $\tilde{H}^0 \quad \tilde{H}'^-$	1/2	0	$\pm 1, 0$

The gauge interactions of the ordinary particles and the invariance of the action under supersymmetric transformations completely determine the interactions of fermions, gauge bosons, squarks, sleptons, and gauginos among themselves. The details of the Lagrangian can be found in, for example, Dawson, Eichten, and Quigg[129] (hereafter denoted DEQ).

On the other hand, the masses of the superpartners associated with supersymmetry breaking and the interactions of the Higgs scalars and Higgsinos are not similarly specified.

The Higgs sector of the minimum supersymmetric extension of the standard model requires two scalar doublets:

$$\begin{pmatrix} H^+ \\ H^0 \end{pmatrix} \qquad \begin{pmatrix} H'^0 \\ H^- \end{pmatrix} \tag{7.9}$$

and their Higgsino superpartners:

$$\begin{pmatrix} \tilde{H}^+ \\ \tilde{H}^0 \end{pmatrix} \qquad \begin{pmatrix} \tilde{H}'^0 \\ \tilde{H}^- \end{pmatrix} \tag{7.10}$$

Two Higgs doublets are required because the Higgsinos associated with the usual Higgs doublet have nonzero weak hypercharge Q_Y and therefore contribute to the $U(1)_Y$ and $(U(1)_Y)^3$ anomalies; to recover a consistent gauge theory another fermion doublet must be introduced with the opposite Q_Y charge.

One complication introduced when supersymmetry breaking is included is that color neutral gauginos and Higgsinos can be mix. So in general the true mass eigenstates will be linear combinations of the original states. For the charged sector the wino ($\tilde{w}^\pm$) and charged Higgsino ($\tilde{H}^\pm$) can mix. For the neutral sector the zino ($\tilde{z}^0$), photino ($\tilde{\gamma}$), and the two neutral Higgsinos ($\tilde{H}^0, \tilde{H}'^0$) can mix. The effects of these mixings will not be discussed further here[130].

The usual Yukawa couplings between Higgs scalars and quarks or leptons generalize in the supersymmetric theory to include Higgs-squark and Higgs-slepton couplings, as well as Higgsino-quark-squark and Higgsino- lepton-slepton transitions. Just as there is a Kobayshi-Maskawa matrix which mixes quark flavors and introduces a CP-violating phase, so too, will there be mixing matrices in the quark-squark and squark-squark interactions. There may also be mixing in the lepton-slepton and slepton-slepton interactions. These mixings have some constraints which arise

from the experimental restrictions on flavor-changing neutral currents. For a possible Super-GIM mechanism to avoid these constraints see Baulieu, Kaplan, and Fayet[131].

The actual masses and mixings are extremely model dependent. Again for simplicity it will be assumed in the phenomenological analysis presented here that:

- There is no mixing outside the quark-quark sector

- The masses of the superpartners will be treated as free parameters.

It is straightforward to see that the supersymmetric extension of the standard model can satisfy 't Hooft's naturalness condition. The mass of each Higgs scalar is equal by supersymmetry to the mass of the associated Higgsino for which a small mass can be associated with an approximate chiral symmetry. Defining the parameter ξ to be the mass of the Higgs scalar over the energy scale of the effective Lagrangian, the limit $\xi \to 0$ is associated with a chiral symmetry if supersymmetry is unbroken. Hence the scale of supersymmetry breaking Λ_{ss} must be not be much greater than the electroweak scale if supersymmetry is to solve the naturalness problem of the standard model. Therefore the masses of superpartners should be accessible to the present or planned hadron collider.

Since the masses of superpartners are not tightly constrained by theory we begin by investigating the experimental constraints on their masses.

B.   Present Bounds on Superpartners

The present bounds on superpartners are discussed in DEQ and in the review by Haber and Kane[132]. I will give a short summary of the situation. Limits on superpartner masses arise from a large variety of sources including:

- Searches for direct production in hadron and lepton colliders as well as in fixed target experiments.

- Limits are rare processes such as flavor changing neutral currents induced by the effects of virtual superpartners.

- Effects of virtual superpartners on the parameters of the standard model.

- Cosmological bounds on the abundance of superpartners.

Before beginning to discuss some of these limits one point must be stressed. In the absence of a specific model all the superpartner masses and even the scale of supersymmetry breaking must be taking as free parameters. This greatly complicates the analysis of limits and weakens the results. In general each limit depends not only on the mass of the superpartner in question but also on:

- The rate for the reaction involved; and therefore the masses of other superpartners (which are enter as virtual states in the process) and the scale of supersymmetry breaking.

- The decay chain of the superpartner. Which decays are kinematically allowed again depends on the masses of other superpartners.

This interdependence of the mass limits makes it difficult to reduce the results to a single mass limit for each superpartner.

1.   Photino Limits

The simplest models of supersymmetry breaking have a color and charge neutral fermion (the photino) as the lightest superpartner. Three cases can be distinguished:

- The photino is the lightest superpartner and $m_{\tilde{\gamma}} < 1$ MeV/c^2.

- The photino is the lightest superpartner and $m_{\tilde{\gamma}} > 1$ MeV/c^2.

- The photino decays into a photon and a Goldstino.

In the first case the photinos are stable spin $\frac{1}{2}$ fermions. An upper bound on the photino mass arises by demanding the the density of photinos in the present universe is less than the closure density[133]:

$$\rho_{\tilde{\gamma}} = 109 cm^{-3} m_{\tilde{\gamma}} < \rho_{\text{critical}} = (3.2 - 10.3) \times 10^3 eV/c^2 cm^{-3} \qquad (7.11)$$

which implies that

$$m_{\tilde{\gamma}} < 100 (eV/c^2) \qquad (7.12)$$

If the photino is the lightest superpartner and heavier than 1 MeV/c^2 Goldberg has pointed out that photino pairs can decay into ordinary fermion pairs by the virtual exchange of the associated sfermion. The annihilation rate is dependent on the photino and sfermion masses. By integrating the rate equation numerically over the history of the universe, the present photino number density can be estimated[134]. This leads to a sfermion mass dependent upper bound on the photino mass.

The resulting limits on a the mass of a stable photino are summarized in Figure76.

The photino may decay by:

$$\tilde{\gamma} \to \gamma + \tilde{\mathcal{G}} \tag{7.13}$$

if a massless Goldstino $\tilde{\mathcal{G}}$ exists. One constraint in this case is that the photons produced in photino decays must have thermalized with the cosmic microwave background[135]. This requires that the photino lifetime ($\tau_{\tilde{\gamma}}$) is less than 1000 seconds. Since

$$\tau_{\tilde{\gamma}} = 8\pi \frac{\lambda^4}{m_{\tilde{\gamma}}^5} \tag{7.14}$$

the limit on photino mass becomes

$$m_{\tilde{\gamma}} > 1.75 MeV/c^2 \left(\frac{\Lambda_{ss}}{1 Tev/c^2}\right)^{4/5} \tag{7.15}$$

The constraints from laboratory experiments on the photino mass are obtained from:

- The axion searches[136]:

$$\Psi \to \gamma + \text{unobserved neutrals} \tag{7.16}$$

  can be reinterpreted as photino searches.

- Limits on $\Psi \to$ unobserved neutrals imply that the scale of supersymmetry breaking $\Lambda_{ss} \geq 10$ GeV[137]. A stronger limit[138], $\Lambda_{ss} \geq 50$ GeV, can be inferred from constraints on emission of photinos from white dwarf or red giant stars if the Goldstino or gravitino mass is less than 10 keV/c^2.
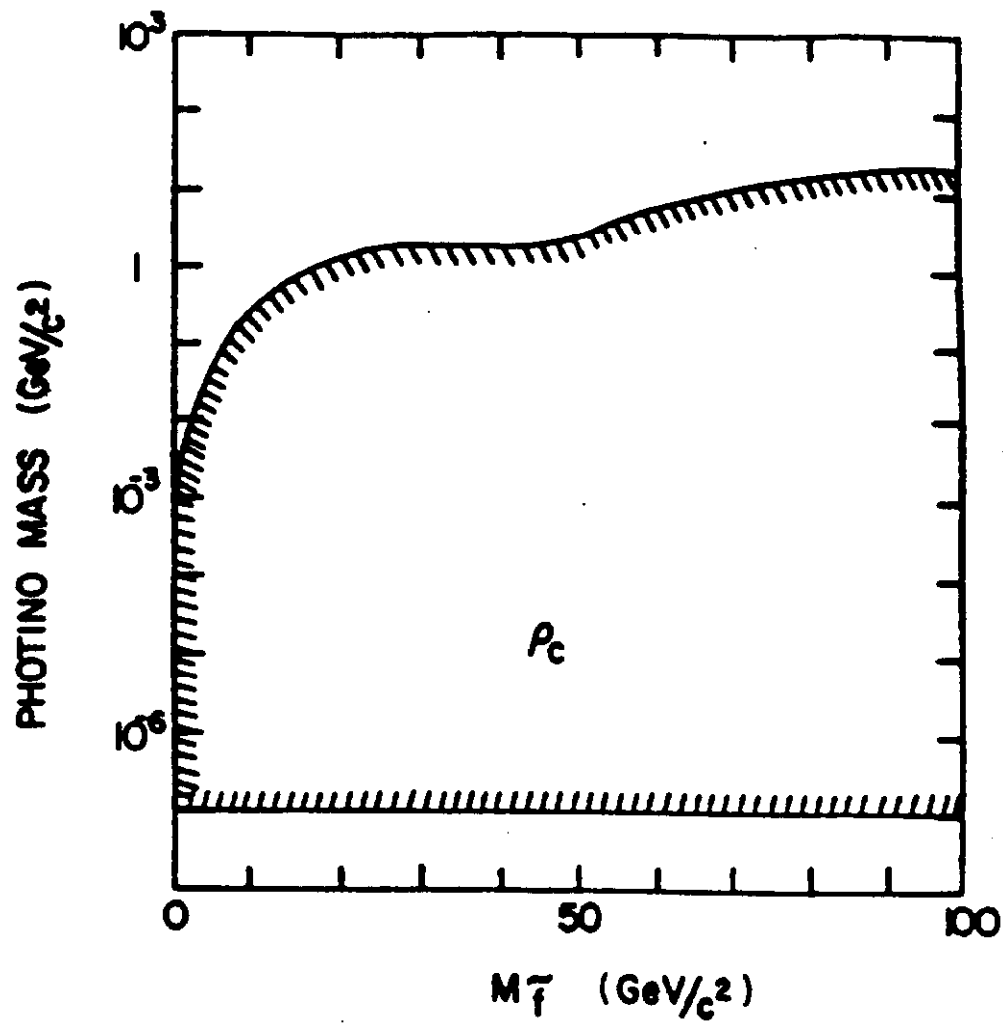
STABLE PHOTINO (GOLDBERG)

Figure 76: Cosmological limits of the allowed photino mass as a function of the mass of the lightest scalar partner of a fermion. This result assumes that the photino is stable and is the lightest supersymmetric particle. (From DEQ)

- Limits on e^+e^- production of photons plus missing energy from CELLO[139] imply limits on the processes:

$$e^+e^- \rightarrow \tilde{\gamma} + \tilde{\gamma} \rightarrow \gamma + \gamma + \tilde{g} + \tilde{g}$$

$$e^+e^- \rightarrow \gamma\tilde{\gamma}\tilde{\gamma} \tag{7.17}$$

The resulting limits on the mass of an unstable photino are given in Figure 77.

2. Gluino Limits

The gluino is the spin $\frac{1}{2}$ partner of the gluon. It is a color octet and charge zero particle. Again for the gluino there are three decay alternatives:

- The gluino is stable or long-lived.

- The gluino decays into photino and a quark-antiquark pair.

- The gluino decays into a gluon and a Goldstino.

If the gluino is long-lived ($\tau_{\tilde{g}} \geq 10^{-3}$ sec) then it would be bound into a long-lived R-hadron (so called because of the R quantum number of gluinos). Thus stable particle searches can be used to put limits on the mass of such R-hadrons. For charged hadrons these limits are[140]:

$$1.5 GeV/c^2 \leq m_R \leq 9 GeV/c^2 \tag{7.18}$$

if $\tau_{\tilde{g}} \geq 10^{-8}$ sec. While for neutral hadrons the limits are[141]:

$$2 GeV/c^2 \leq m_R \leq 9 GeV/c^2 \tag{7.19}$$

if $\tau_{\tilde{g}} \geq 10^{-7}$ sec. It seems that gluinos with $m_{\tilde{g}} \leq 1.5 GeV/c^2$ and $\tau_{\tilde{g}} \geq 10^{-8}$ sec could have escaped detection.

In the second decay scenario the decay chain is:

$$\tilde{g} \rightarrow \bar{q}\tilde{q}$$
$$\qquad \hookrightarrow q + \tilde{\gamma} \tag{7.20}$$
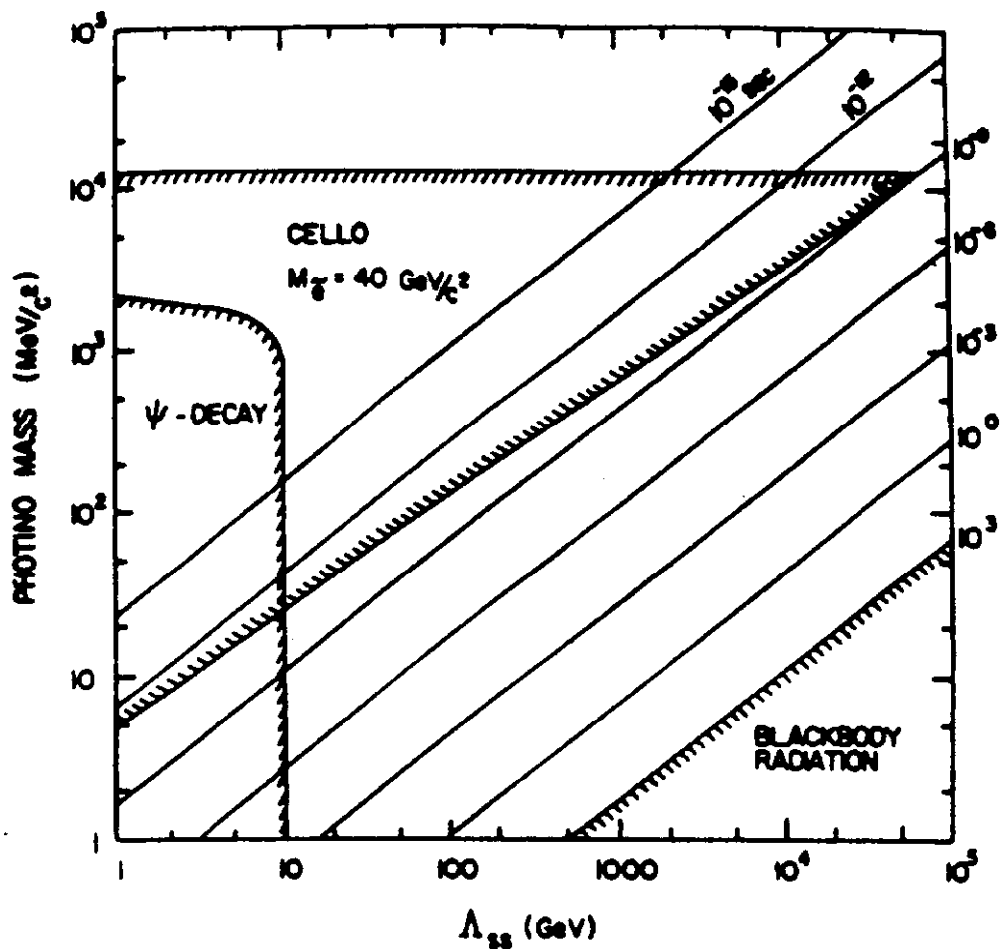
Figure 77: Limits on the allowed photino mass as a function of the supersymmetry breaking scale Λ_{ss}. This figure assumes that the photino decays to a photon and a massless Goldstino. The various limits from Ψ decay, the search for the process $e^+e^- \rightarrow \tilde{\gamma}\tilde{\gamma} \rightarrow \gamma\gamma\tilde{\tilde{g}}\tilde{\tilde{g}}$ by the CELLO Collaboration, and blackbody radiation are discussed in the text. (From DEQ)

; and therefore the decay rate is sensitive to the squark mass. For $m_{\tilde{q}} = 0$ the lifetime is:

$$\tau(\tilde{g} \to \bar{q}q\tilde{\gamma}) = \frac{48\pi m_{\tilde{q}}^4}{\alpha_s \alpha_{EM} e_q^2 m_{\tilde{g}}^5} . \qquad (7.21)$$

There are stringent bounds on the mass and lifetime of the gluino from beam dump experiments both the E-613 experiment at Fermilab[142] and the CHARM Collaboration at CERN[143]. The limits on gluino mass as a function of lifetime (or alternatively squark mass) are summarized in Figure 78 for the assumption that the resulting photino is stable. Note that for squark masses in the range 200-1,000 GeV/c^2 there is no limit on gluino mass for this decay scenario. The possibility that the photino is unstable to decay into photon and Goldstino requires a somewhat more complicated analysis. In that case the limit from E-613 beam dump experiments constrain the relation between the gluino mass, the supersymmetry breaking scale, and the photino mass. Details of these constraints can be found in DEQ.

The final possibility is that the gluino can decay into a gluon and a Goldstino. The lifetime of the gluino is given by

$$\tau(\tilde{g} \to g + \tilde{G}) = \frac{8\pi\Lambda_{ss}^4}{m_{\tilde{g}}^5} = 1.65 \times 10^{-23} sec (\frac{\Lambda_{ss}}{1GeV/c^2})^4 (\frac{1GeV/c^2}{m_{\tilde{g}}})^5 \qquad (7.22)$$

Again beam dump experiments constrain the relationship between $m_{\tilde{g}}$ and Λ_{ss}. The resulting limits are shown in Figure 79.

In *all* scenarios for gluino decay it is possible to find ranges of parameters for which light (a few GeV/c^2) gluinos are allowed by experiment. This corresponds to a gap in experimental technique for lifetimes between 10^{-10} and 10^{-12} sec in hadron initiated experiments.

3. Squark Limits

A squark is a spin zero color triplet particle with the flavor and charge of the associated quark. There are four sources of limits on squark masses.

- Free quark searches. The MAC Collaboration at PEP[144] find a limit for e^+e^- production of fractionally charged long-lived ($\tau \gg 10^{-8}$ sec) particles which corresponds to a lower bound on the mass of any squark of 14 GeV/c^2.
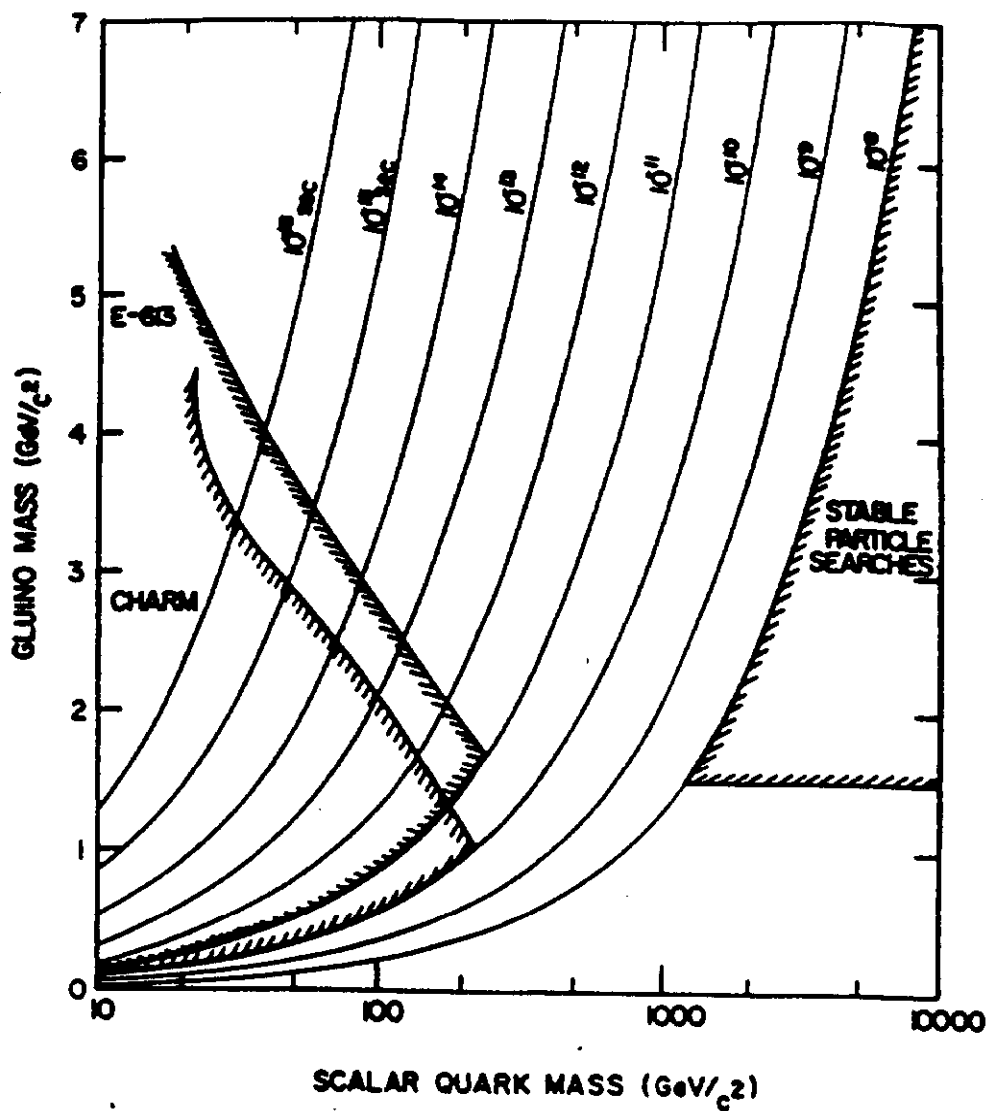
Figure 78: Limits on the gluino mass as a function of the lightest squark mass. The gluino is assumed to decay to a $\bar{q}q$ pair and a massless photino. The limits are from beam-dump experiments and stable particle searches as discussed in the text. The corresponding gluino lifetimes are also shown. (From DEQ)

Figure 79: Limits on the gluino mass as a function of the supersymmetry breaking scale Λ_{ss}. The limits are from the Fermilab beam-dump experiment[142] and the stable particle searches[140,141] and assume that the gluino decays to a gluon and a massless Goldstino. The corresponding gluino lifetimes are also shown. (From DEQ)

- Stable hadron searches. Stable hadron searches in hadron initiated reactions exclude a charged squark bearing hadron with mass in the range:

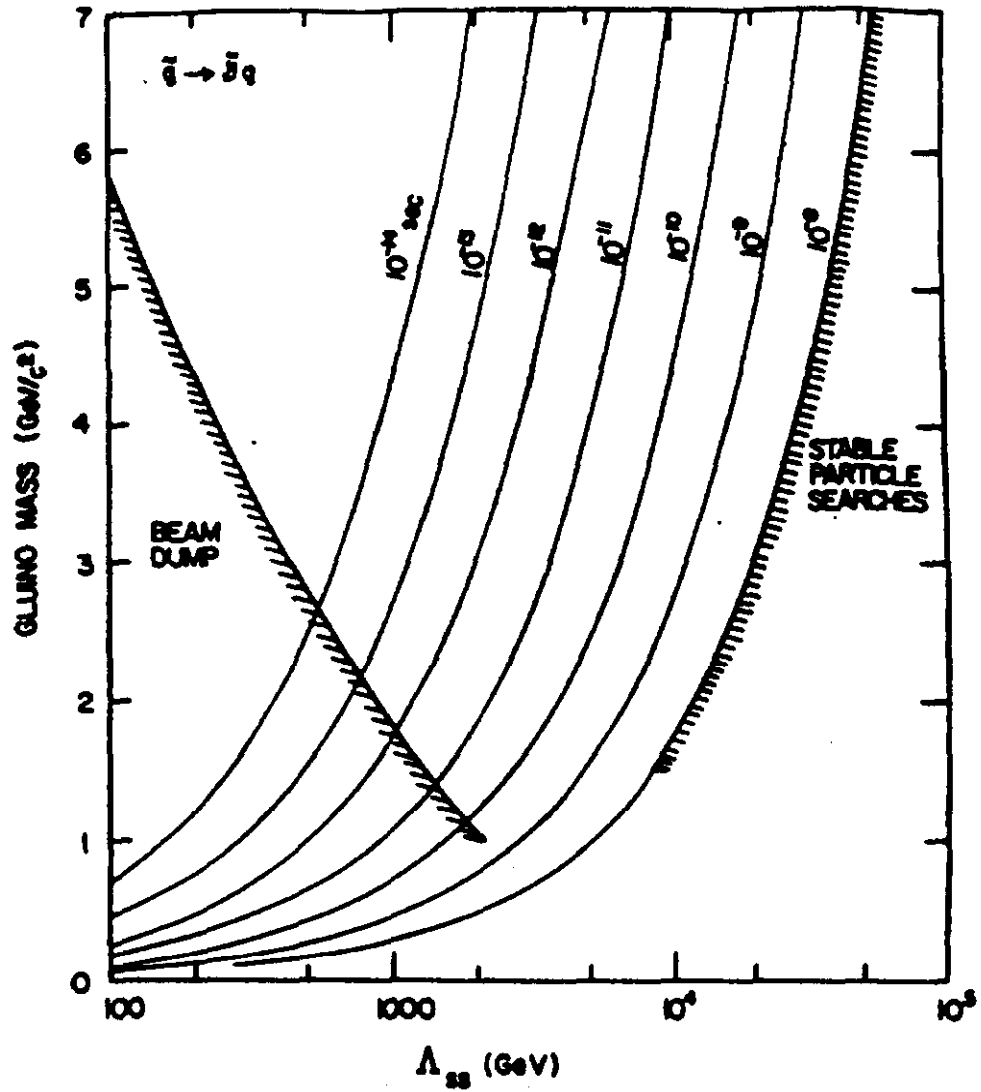$$1.5 GeV/c^2 \leq m_{\tilde{q}} \leq 7 GeV/c^2 \qquad (7.23)$$

for lifetimes $\tau \geq 5 \times 10^{-8}$ seconds[140]. The JADE Collaboration at PETRA looked for

$$e^+ e^- \rightarrow \tilde{q}\tilde{q}^* \qquad (7.24)$$

in both charged and neutral final state hadrons. Their exclude long-lived squarks in the range[141]:

$$2.5 GeV/c^2 \leq m_{\tilde{q}} \leq 15.0 GeV/c^2 \quad \text{for} \quad |e_{\tilde{q}}| = 2/3$$

$$2.5 GeV/c^2 \leq m_{\tilde{q}} \leq 13.5 GeV/c^2 \quad \text{for} \quad |e_{\tilde{q}}| = 1/3 \qquad (7.25)$$

- Narrow resonance searches in $e^+ e^-$ collisions. Squark-antisquark bound states could be produced as narrow resonances in $e^+ e^-$ collisions. The production rates have been estimated by Nappi[146] who concludes that $|e_{\tilde{q}}| = 2/3$ squarks with masses below 3 GeV/c^2 can be ruled out. No limits exist from this process for $|e_{\tilde{q}}| = 1/3$ squarks.

- Heavy Lepton searches. If a squark decays to a quark and a (assumed massless) photino the decay signature in $e^+ e^-$ collisions is similar to that for a heavy lepton decay - two acoplanar jets and missing energy. The JADE Collaboration[147] has excluded squarks with this decay pattern for:

$$3.1 GeV/c^2 \leq m_{\tilde{q}} \leq 17.8 GeV/c^2 \quad \text{for} \quad |e_{\tilde{q}}| = 2/3$$

$$7.4 GeV/c^2 \leq m_{\tilde{q}} \leq 16.0 GeV/c^2 \quad \text{for} \quad |e_{\tilde{q}}| = 1/3$$

Summarizing these limits:

1 Stable squarks must have masses exceeding ≈ 14 GeV/c^2.

2 If the photino is nearly massless, unstable $|e_{\tilde{q}}| = 2/3$ squarks are ruled out for masses ≤ 17.8 GeV/c^2; while for $|e_{\tilde{q}}| = 1/3$ squarks a window exists for masses below 7.4GeV/c^2, otherwise their mass must exceed 16 GeV/c^2.

3 If the photino is massive all that can be said is that $m_{\tilde{q}} \geq 3$ GeV/c^2 if the lifetime is less than 5×10^{-8} sec and $|e_{\tilde{q}}| = 2/3$.

4. Limits on Other Superpartners

The limits on the wino, zino, and sleptons come from limits on production in $e^+ e^-$-collisions. The wino is a spin 1/2 color singlet particle with unit charge. If the photino is light the wino can decay via:

$$\tilde{w} \;\rightarrow\; \tilde{\gamma} W$$
$$\phantom{\tilde{w} \;\rightarrow\; \tilde{\gamma} W} \hookrightarrow \bar{q} q \tag{7.26}$$

and hence the heavy lepton searches will be sensitive to a wino as well. The Mark J Collaboration at PETRA have set the limit[148]:

$$m_{\tilde{w}} \geq 25 GeV/c^2 \tag{7.27}$$

. For the zino, the JADE collaboration obtains the bound[149]

$$m_{\tilde{z}} \geq 41 GeV/c^2 \tag{7.28}$$

assuming a massless photino and $m_{\tilde{z}} = 22$ GeV/c^2.

For the charged sleptons the limits are[150]:

$$m_{\tilde{e}} \geq 51 GeV/c^2 \tag{7.29}$$

assuming $m_{\tilde{\gamma}} = 0$; and[151]:

$$m_{\tilde{\mu}} \geq 16.9 GeV/c^2$$

$$m_{\tilde{\tau}} \geq 15.3 GeV/c^2 \;. \tag{7.30}$$

C. Discovering Supersymmetry In Hadron Colliders

All the lowest order (Born diagrams) cross sections $d\bar{\sigma}/dt$ and $\bar{\sigma}$ have been calculated in DEQ for

$$(\; \tilde{q} \quad \tilde{l} \quad \tilde{\nu} \quad \tilde{g} \quad \tilde{\gamma} \quad \tilde{z}^0 \quad \tilde{H}^0 \quad \tilde{H}'^0 \quad \tilde{w}^\pm \quad \tilde{H}^\pm \;)^2 \tag{7.31}$$

final states in parton-parton collisions; including the mixing in the neutral $(\tilde{\gamma}, \tilde{z}^0, \tilde{H}^0, \tilde{H}'^0)$ and charged $(\tilde{w}^\pm, \tilde{H}^\pm)$ fermion sectors. Many of these processes have also been studied by others as well: see DEQ for complete references.

The overall production rate for pair production of superpartners is determined by the strength of the basic process. These relative rates for the various final states are:

Final State	Production Mechanism	Strength
$(\tilde{q}, \tilde{g})^2$	QCD	α_s^2
$(\tilde{q}, \tilde{g}) \times (\tilde{\gamma}, \tilde{z}, \tilde{H}^0, \tilde{H}'^0)$	QCD-Electroweak	$\alpha_s \alpha_{EW}$
$\tilde{l}\tilde{\nu}, \tilde{l}\tilde{l}^*, \tilde{\nu}\tilde{\nu}^*$	decays of real (or virtual) $W^\pm$ and Z^0	α_{EW} (α_{EW}^2)
$(\tilde{\gamma}, \tilde{z}^0, \tilde{H}^0, \tilde{H}'^0, \tilde{w}^\pm, \tilde{H}^\pm)^2$	Electroweak	α_{EW}^2

We will consider each of these processes in turn beginning with the largest rates: squark and gluino production.

The lowest order processes for gluino and squark production are shown in Figure 80. The underlined graphs in Figure 80 depend only on the masses of the produced superpartner and are therefore independent of all other supersymmetry breaking parameters. Hence hadron colliders allow clean limits (or discovery) on the masses of gluinos and squarks. The cross sections for gluino production are large, since gluinos are produced by the strong interactions. The total cross section for gluino pairs in $\bar{p}p$ collisions is shown in Figure 81 as a function of gluino mass at $\sqrt{s} = 630$, 1.8, and 2 TeV. The squark masses were all taken to be 1 TeV/c^2 so there would be not significant contribution from diagrams involving squark intermediate states. The typical effects of the diagrams with squark intermediate states is also illustrated in Fig. 81 by including the cross section for gluino pair production for $\sqrt{s} = 630$ GeV with $m_{\tilde{q}} = m_{\tilde{g}}$. Because of the dominance of gluon initial states, the dependence of the gluino pair production cross section on the squark mass is small except at the highest $\sqrt{\hat{s}/s}$. In any case, the cross section excluding the contribution from intermediate squarks gives lower bound on the gluino production for a given mass gluino ($m_{\tilde{g}}$).

Typically the supersymmetry breaking leads to gluinos not much heavier than the lightest squark. In the case that the up squark mass (assuming $m_{\tilde{u}} = m_{\tilde{d}}$) equals
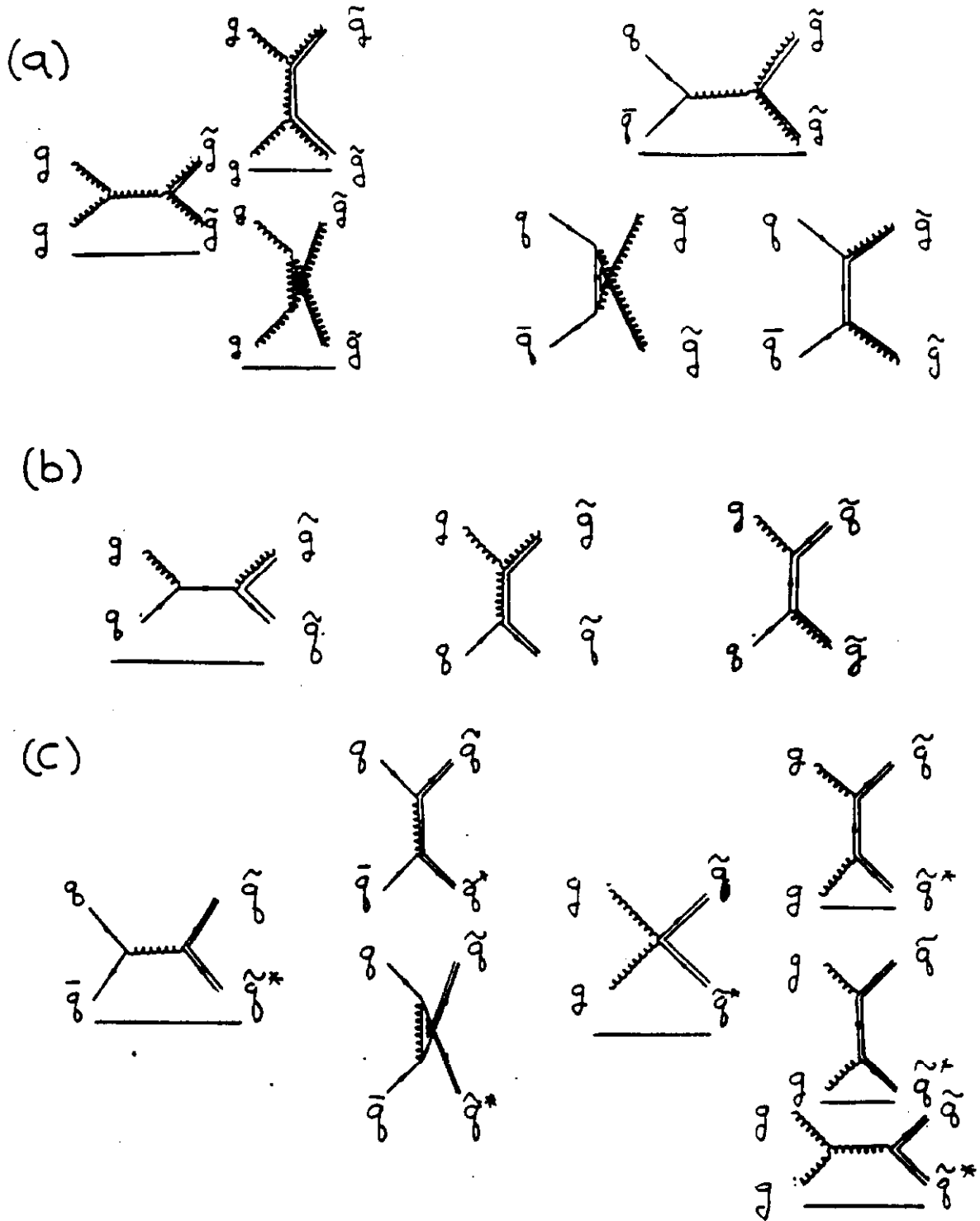
Figure 80: Feynman diagrams for the lowest order production of (a) gluino pairs, (b) gluino in association with a up squark, and (c) up squark-antisquark pair.
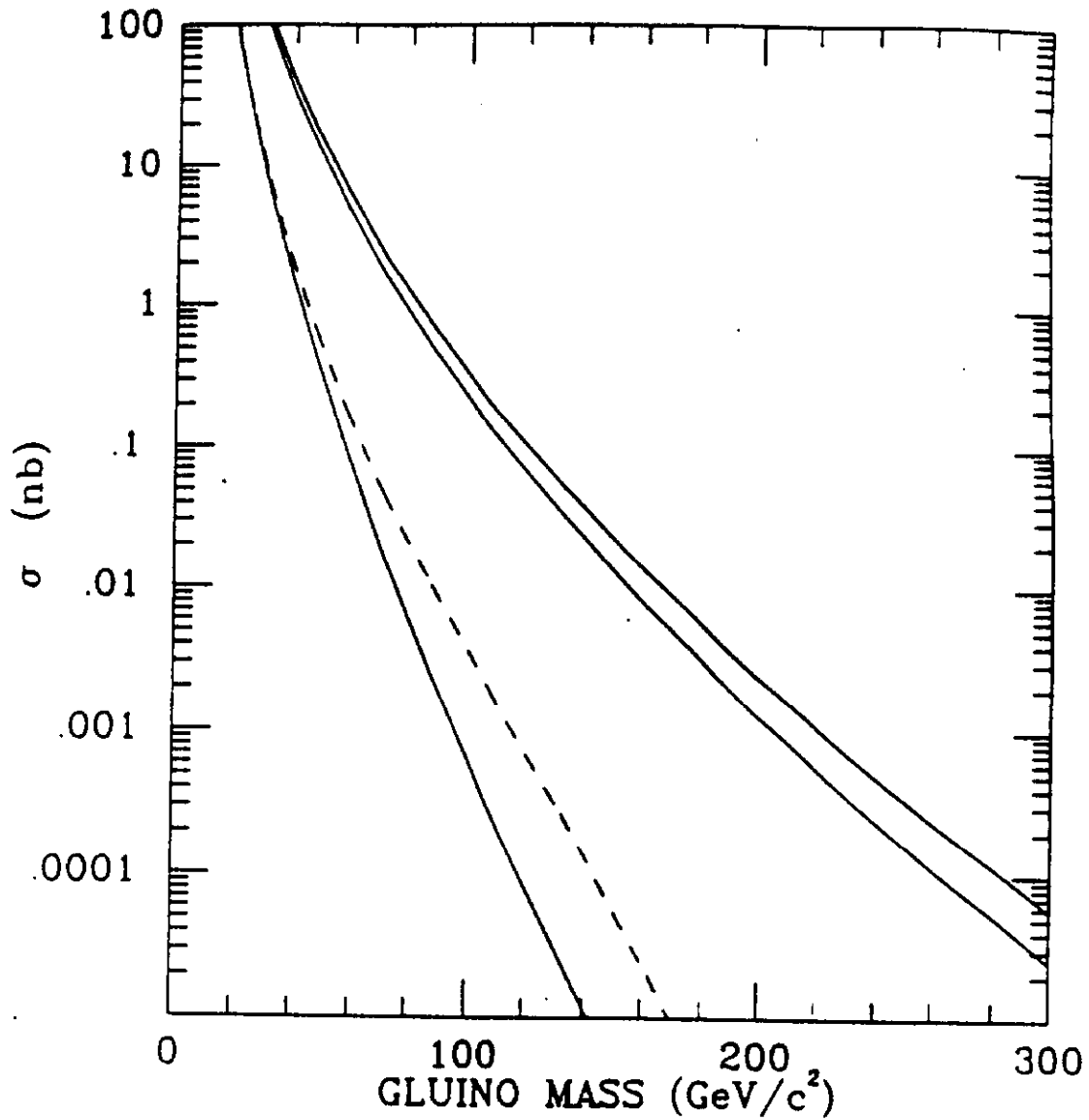
Figure 81: Total cross section for gluino pair production in $\bar{p}p$ collisions as a function of gluino mass. The rates for squark mass $m_{\tilde{q}} = 1$ TeV/c^2 are shown for $\sqrt{s} = 630$ GeV (lower solid line), 1.8 TeV (middle solid line), and 2.0 TeV (upper solid line); as well as for $m_{\tilde{q}} = m_{\tilde{g}}$ at $\sqrt{s} = 630$ GeV (dashed line). The rapidity of each of the gluinos is restricted to $|y_i| \leq 1.5$.

the gluino mass the total cross section for the reaction

$$pp \rightarrow \tilde{u} + \tilde{q}^* + \text{anything} \qquad (7.32)$$

where $\tilde{q}^* = \tilde{u}, \tilde{d}, \tilde{u}^*$, or $\tilde{d}^*$ is shown in Figure 82 as a function of the up squark mass for $\sqrt{s}$= 630, 1.8, and 2.0 TeV. This can be compared for $\sqrt{s} = 630$ GeV to the cross section for up squark production with $m_{\tilde{g}} = 1$ TeV as shown in Fig. 82. Clearly for squark production the total cross sections depend more strongly on other superpartner's (specifically the gluino's) mass.

For gluino and squark masses approximately equal there is also a comparable contribution from squark-gluino associated production. For example, for $m_{\tilde{u}} = m_{\tilde{g}} = 50$ GeV/c^2 the cross section for associated production is approximate 7 nanobarns at $\sqrt{s} = 2$ TeV.

The detection signatures for gluino and squarks are similar but model and mass dependent. Here I will consider only the usual scenario in which the lightest superparticle is the photino. Other possibilities exist, for example if the Goldstino is massless then the photino can decay:

$$\tilde{\gamma} \rightarrow \tilde{\mathcal{G}} + \gamma. \qquad (7.33)$$

In another possible model the lightest superpartner is the the sneutrino. For a discussion of these alternatives see for example Haber and Kane[132] and Dawson[152]. The basic signature of squark or gluino production is some number of jets accompanied by sizable missing energy. The decay chains for the squark and gluino are:

$$\tilde{q} \rightarrow \tilde{g} + q$$
$$\tilde{g} \rightarrow q + \bar{q} + \tilde{\gamma} \qquad (7.34)$$

if $m_{\tilde{g}} < m_{\tilde{q}}$ and :

$$\tilde{g} \rightarrow \tilde{q} + \bar{q}$$
$$\tilde{q} \rightarrow q + \tilde{\gamma} \qquad (7.35)$$

if $m_{\tilde{q}} < m_{\tilde{g}}$. The number of jets which are experimentally distinguishable depends on the masses of the superpartners and the energy of the hadron collisions in a
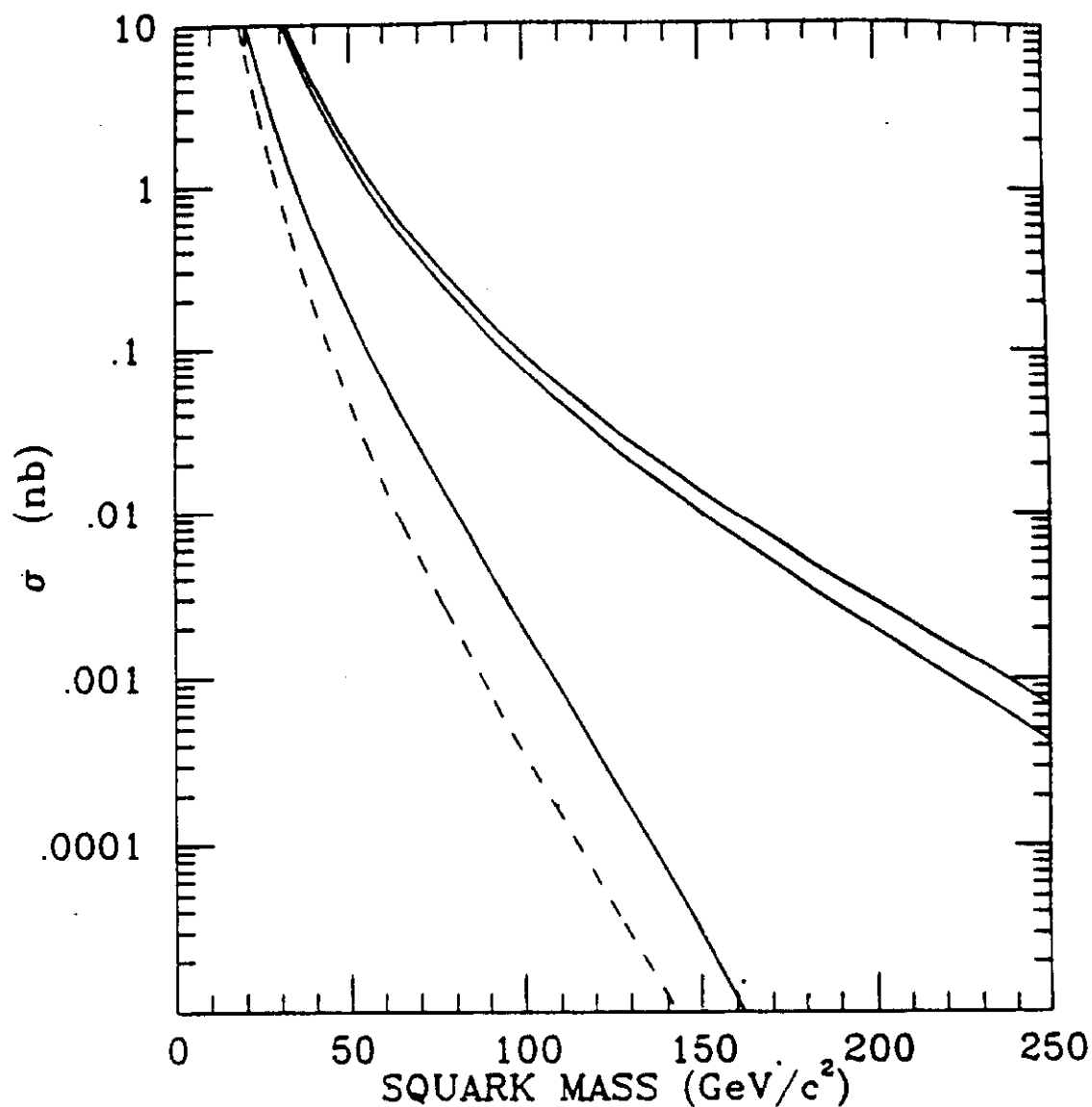
Figure 82: Total cross section for up squark production in $\bar{p}p$ collisions as a function of up squark mass. The rates for gluino mass equal up squark mass $m_{\tilde{g}} = m_{\tilde{u}}$ are shown for $\sqrt{s} = 630$ GeV (bottom solid line), 1.8 TeV (middle solid line), and 2.0 TeV (top solid line); as well as for $m_{\tilde{g}} = 1$ TeV/c^2 at $\sqrt{s} = 630$ GeV (dashed line). The rapidity of the up squark (and the associated squark) is restricted to $|y_{\tilde{u}}| \leq 1.5$

complicated experiment dependent way[153,154,155]. Clearly there are backgrounds from ordinary QCD jets which can have missing transverse energy for a variety of reasons (weak decays of a heavy quark in the jet, energy measurement inefficiencies, dead spots in the detector, etc.). Even though each decay chain above leads to an event with at least two final state quarks or gluons, the experimental requirements for a jet imply that a number of these events will appear to have only one jet - a monojet event[153].

The backgrounds for detection of squarks and gluinos in the present colliders are:

- One monojet background is the production of $W^{\pm}$ which then decays by the chain:

$$W^{\pm} \rightarrow \bar{\nu}\tau$$
$$\llcorner \rightarrow \text{hadrons} + \nu$$

(7.36)

There are of course distinguishing features of these background events. The missing transverse energy E_T of the background events will be ≤ 30 GeV since the primary $W^{\pm}$ is produced nearly at rest while for squark or gluino production the missing energy is not bounded in the same way. Also the multiplicity of charged tracks from the τ decay will be low (usually only 1 or 3) while from squark or gluino production the multiplicity should be comparable to a ordinary QCD jet of similar energy. These differences are helpful in the analysis of the monojet events.

- Another monojet background is the associated production:

$$\bar{p}p \rightarrow g(\text{ or } q)Z^0$$
$$\llcorner \rightarrow \nu\bar{\nu}$$

(7.37)

. The rate of these background events are reasonably low when minimum missing E_T cuts are imposed[153]. Also because the final state in squark or gluino production has more than one quark or gluon, monojet events arising from supersymmetric particle production typically will not be as "clean" (no significant addition energy deposition) as the monojet events from associated Z^0 production events. If the charged lepton is undetected or misidentified, associated $W^{\pm}$ production and leptonic decay can also mimic monojet events.

- The main background to multijet events with missing E_T is heavy quark weak decays inside jets. For example the decay of a b quark in one jet:

$$b \to c + \bar{\nu} + l \tag{7.38}$$

can produce large missing E_T in a two jet event. This background can be reduced if methods are found to identify charged leptons in a jet[155].

There has been a great deal of recent work on reducing these backgrounds to the detection of superpartners[153,154,155]. My best guess is that 1000 produced events will be required to obtain a clear signal for either a gluino or squark in the collider environment.

It also seems likely that experiments at the $S\bar{p}pS$ and TeV I Colliders can be designed to close any gaps in present limits for light gluinos ($m_{\tilde{g}} = 1 - 3$ GeV/c^2) and charge $-1/3$ squarks ($m_{\tilde{q}} \leq 7.4$ GeV/c^2), but careful study of this possibility will be required.

The other superpartners can be produced in hadron collisions in the following ways:

- The photino, wino, and zino can be produced in association with a squark or gluino.

- The photino, wino, zino, slepton, and sneutrino can be produced in the decays of $W^{\pm}$ or Z^0 bosons if kinematically allowed.

For present collider energies no other production mechanisms are significant.

The photino is generally assumed to be the lightest superpartner. The major mechanism for producing photinos in hadron-hadron collisions is the associated production processes:

$$p\bar{p} \to \tilde{g} + \tilde{\gamma} + \text{anything} \tag{7.39}$$

and

$$p\bar{p} \to \tilde{q} + \tilde{\gamma} + \text{anything} \tag{7.40}$$
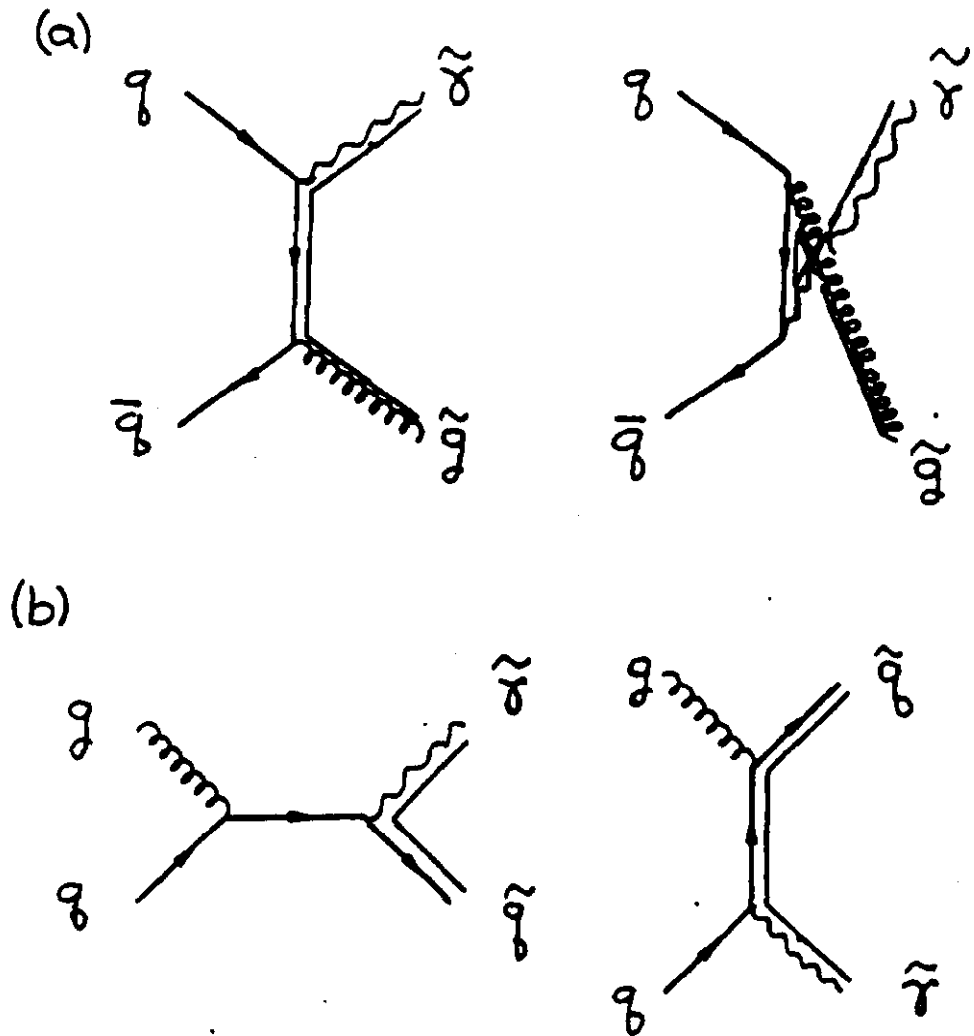
These production mechanisms are shown in Figure 83.

Figure 83: Lowest order diagrams for associated production of photino and (a) gluino or (b) squark.

The total cross section for production of $\tilde{q} + \tilde{\gamma}$ in $\bar{p}p$ collisions as a function of the squark mass where the photino mass is assumed to be zero is given in Figure 84 for $\sqrt{s} = .63$, 1.8, and 2 TeV. These production cross sections are smaller than the squark pair production cross sections in Fig. 82 by roughly α_{EW}/α, but this reaction produces a clear signature: a jet (if $m_{\tilde{q}} < m_{\tilde{g}}$) or three jets (if $m_{\tilde{q}} > m_{\tilde{g}}$) on one side of the detector and no jet on the other; hence the missing transverse energy will be large. For the one jet case there is the Z^0 plus jet background discussed previously, but the rate and characteristic of these events are well understood theoretically and hence relatively small deviations from expectations would be significant. For the production of $\tilde{g} + \tilde{\gamma}$ the same comments apply. Because of the striking signature of these events 100 produced events should be sufficient for discovery of the photino (and associated gluino or squark) through this mechanism.

The bounds on the wino and zino masses are not model independent but these gauginos are likely heavier than 40 GeV/c^2. The total cross sections for associated production of a massive wino or zino with a squark or gluino are quite small. For $m_{\tilde{w}} = m_{\tilde{z}} = m_{\tilde{q}} = m_{\tilde{g}} = 50$ GeV/c^2:

Process	Total Cross Section (nb)	Total Cross Section (nb)
	$\sqrt{s} = 630$ GeV	$\sqrt{s} = 2$ TeV
$\tilde{w}^\pm + \tilde{g}$	5×10^{-3}	5×10^{-2}
$\tilde{z}^0 + \tilde{g}$	3×10^{-3}	2×10^{-2}

It should be remembered that these electroweak gauginos are in general mixed with the Higgsinos. The physical mass eigenstates are linear combinations of the gauginos and associated Higgsinos. This mixing also effects the production cross sections. For example, for some mixing parameters, the total cross section for production of $\tilde{w}^\pm + \tilde{g}$ is $\bar{p}p$ collisions at $\sqrt{s} = 2$ TeV is 1.5×10^{-1} approximately three times larger than the unmixed case above[129].

Assuming a light photino, the wino and zino decay into quark-antiquark photino or lepton pair and photino. Since the decays into quark final states have the same characteristics as gluino decay with 1/100 the signal, observation of winos or zinos in their hadronic decays is hopeless. For the leptonic decays, the leptons will be hard to detect as their energies will typically be rather low and the background rates high from heavy quark decays. Therefore it is likely that at least 1000 produced events will be required to observe either the wino or zino.
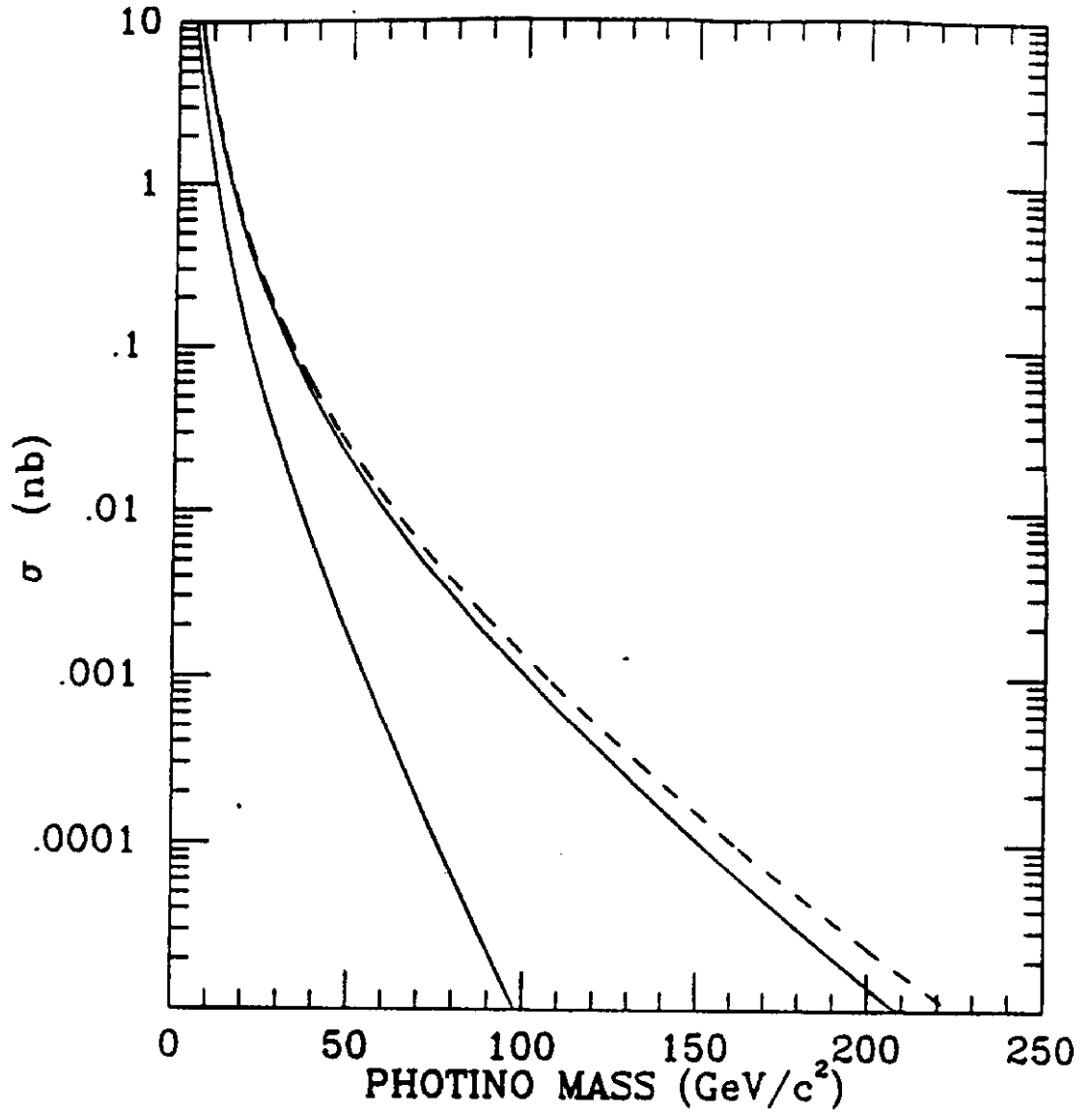
Figure 84: Total cross section for associated production in $\bar{p}p$ collisions of a photino and light squark (up or down) as a function of the photino mass (assuming $m_{\tilde{\gamma}} = m_{\tilde{u}} = m_{\tilde{d}}$). The rates are shown for $\sqrt{s} = 630$ GeV (lower solid line), 1.8 TeV (upper solid line), and 2 TeV (dashed line). The rapidity of both the photino and the squark is restricted to $|y_i| \leq 1.5$. The parton distributions of Set 2 were used.

Table 15: Expected discovery limits for superpartners at $S\bar{p}pS$ and Tevatron Colliders, based on associated production of scalar quarks and gauginos. All superpartner masses are set equal.

Superpartner	Mass limit (Gev/c^2)					
	$\sqrt{s} = 630$ GeV			$\sqrt{s} = 2$ TeV		
	$\int dt\mathcal{L}$ (cm)$^{-2}$					
	10^{36}	10^{37}	10^{38}	10^{36}	10^{37}	10^{38}
Gluino or squark (1000 events)	45	60	75	85	130	165
Photino (100 events)	35	60	90	45	90	160
Zino (1000 events)	17	30	50	22	50	95
Wino (1000 events)	20	35	55	32	60	110

The discovery limits for gauginos produced in associated production are summarized in Table 15 for present collider energies.

The other mechanism for superpartner production at present colliders is via the decay of real $W^{\pm}$ and Z^0 bosons. If $m_{\tilde{w}} + m_{\tilde{\gamma}} < m_W$ or $m_{\tilde{w}} + m_{\tilde{z}} < m_W$ or $2m_{\tilde{w}} < m_{\tilde{z}}$ winos will be a product of W or Z decays. Ignoring any phase space suppression the branching ratio for $W \to \tilde{w} + \tilde{\gamma}$ is a few percent. At $\sqrt{s} = 2$ TeV a one percent branching ratio corresponds to a total cross section of .22 (nb) or equivalently to 2×10^4 events for an integrated luminosity of $10^{38}cm^{-2}$. Comparing these rates to the discovery limits for the wino given in Table 15 for the associated production mechanism, it is clear that real decays of $W^{\pm}$ and Z^0 bosons is the main production mechanism for the masses accessible in present generation colliders. The decays of $W^{\pm}$ and Z^0 bosons are also a possible source of sleptons and sneutrinos if $m_{\tilde{l}} + m_{\tilde{\nu}} < m_W$, $2m_{\tilde{l}} < m_z$, or $2m_{\tilde{\nu}} < m_z$.

1. Supersymmetry at the SSC

At SSC energies the discovery limits for superpartners are greatly extended. For example the total cross section for gluino pair production in pp collisions as a function of the gluino mass is shown in Figure 85 for various supercollider energies. Even with the very conservative assumption that 10,000 produced events are required for detection, the discovery limit is 1.6 TeV/c^2 at $\sqrt{s}$ = 40 TeV for integrated luminosity of $10^{40} cm^{-2}$.

At supercollider energies there are additional production mechanisms for superpartners including:

- Pair production of the electroweak gauginos from quark-antiquark initial states.

- Production of electroweak gauginos, sleptons, sneutrinos, and even Higgsinos via the generalized Drell-Yan mechanism (i.e. virtual $W^{\pm}$, Z^0, and γ).

The details about the production and detection of superpartners at SSC energies may be found in EHLQ and Ref.155. The discovery limits for all the superpartners at $\sqrt{s}$ = 40 TeV are summarized in Table 16.

If supersymmetry plays a role in resolving the naturalness problem of the standard model, the scale of supersymmetry breaking can not be much higher than the electroweak scale; and therefore the masses of the superpartners should also be in this mass range. It is clear from Table 16 that in this case superpartners will be discovered at or below SSC energies.
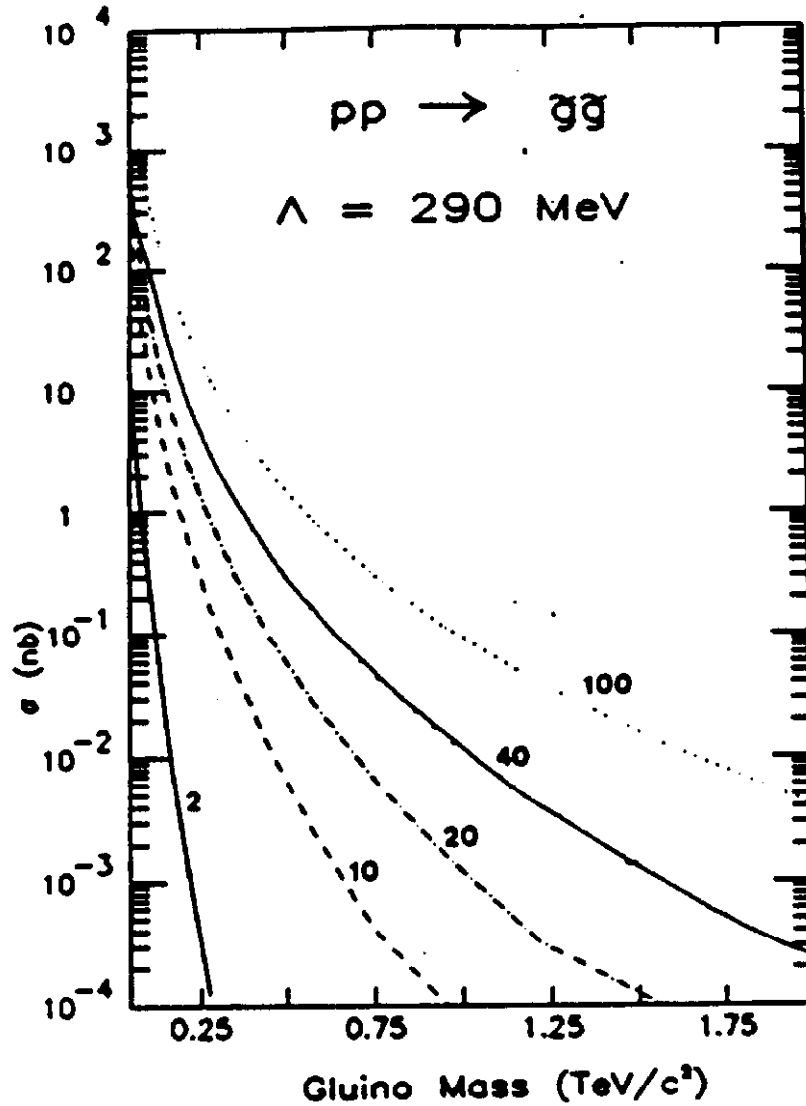
Figure 85: Cross sections for the reaction $pp \to \tilde{g}\tilde{g}$ + anything as a function of the gluino mass, according to the parton distributions of Set 2. Rates shown for collider energies $\sqrt{s} = 2$, 10, 20, 40, and 100 TeV. Both gluinos are restricted to the interval $|y_i| < 1.5$. The squark mass is set equal to the gluino mass. (From EHLQ)

Table 16: Expected discovery limits for superpartners at the SSC for various integrated luminosities. Associated production of gauginos and squarks is assumed. All superpartner masses are set equal.

p p collisions	$\sqrt{s} = 40$ TeV		
	Mass limit (Gev/c²)		
Superpartner	$\int dt \mathcal{L}$ (cm)$^{-2}$		
	10^{38}	10^{39}	10^{40}
Gluino (1000 events)	900	1,600	2,500
Squark (up and down) (1000 events)	800	1,450	2,300
Photino (100 events)	350	750	1,350
Zino (1000 events)	250	500	825
Wino (1000 events)	300	550	1,000
pair production			
Top squark (1000 events)	500	850	1,350
Slepton (100 events)	100	200	400

VIII. CONCLUDING REMARK

Hadron-hadron colliders will be one of the main testing grounds for both the standard model and possible new physics. Specific applications have been detailed in these seven lectures. However I would like to conclude these lectures with a general remark. The advances of the last decade have brought us to a deep understanding of the fundamental constituents of matter and their interactions. Progress toward a fuller synthesis will require both theoretical and experimental breakthroughs. The present generation of hadron (and also lepton) colliders are bound to provide much additional information. But the full exploration of the physics of the TeV scale will require the next generation of hadron colliders - the supercollider - as well.

REFERENCES AND FOOTNOTES

1. E. Eichten, I. Hinchliffe, K. Lane, and C. Quigg, Rev. Mod. Phys. **56**, 579 (1984); and Errata, Fermilab-Pub-86/75-T (1986).

2. See for example: L.B. Okun, *Leptons and Quarks* (North Holland, Amsterdam, 1981); D.H. Perkins, *Introduction to High Energy Physics* , 2nd ed. (Addison-Wesley, Reading, Massachusetts, 1982); or C. Quigg, *Gauge Theories of the Strong, Weak, and Electromagnetic Interactions* (Benjamin/Cummings, Reading, Massachusetts, 1983).

3. N. Minard, presented at *International Symposium on Physics of Proton - Antiproton Collisions*, University of Tsukuba, KEK, March 13-15 (1985).

4. G. 't Hooft, in *Recent Developments in Gauge Theories, Proceedings of the 1979 NATO Advanced Study Institute*, Cargese, edited by G. 't Hooft *et al.* (Plenum, New York), p.101.

5. M. Kobayashi and T. Maskawa, Prog. Theor. Phys. **49K**, 652, (1973).

6. For a general reference to the physics potential of the present and future colliders see: *Proceedings of the 1982 DPF Summer Study on Elementary Particle Physics and Future Facilities*, edited by R. Donaldson, R. Gustafson, and F. Paige (Fermilab, Batavia, Illinois, 1982).

7. For a review of the physics potential of LEP see, for example: CERN 76-16, *Physics with 100 GeV Colliding Beams*, CERN (1976); CERN 79-01, *Proceedings of the LEP Summer Study*, CERN (1979). For a review of the physics potential of the SLC at SLAC see. for example: *SLAC Linear Collider Conceptual Design Report*, SLAC Report-229, (1980).

8. For a review of the physics potential of HERA see: *Proceedings of the Discussion Meeting on HERA Experiments* , Genoa, Italy, October 1-3 1984. DESY-HERA preprint 85/01 (1985).

9. In July 1983, the New Facilities Subpanel of the High Energy Physics Advisory Panel (HEPAP) recommended to HEPAP that a 20 TeV proton-proton collider be the next high energy facility (to be completed in the 1990's). That recommendation was accepted by HEPAP and forwarded to the DOE. Many details of the proposed SSC are contained in: *Proceedings of the 1984 DPF Summer Study on the Design and Utilization of the Superconducting Super Collider*, edited by R. Donaldson, and J. Morfin (Fermilab, Batavia, Illinois, 1984), p.i.

10. Proceedings of the CERN/ICFA Workshop:*Large Hadron Collider in the LEP Tunnel*, CERN 84-10 (1984).

11. For a general discussion of QCD see any of the textbooks in Ref. 2.

12. D. J. Gross and F. Wilczek Phys. Rev. Lett. **30**, 1343 (1973) and Phys. Rev. **D8**, 3633 (1973); H. D. Politzer Phys. Rev. Lett. **30**, 1346 (1973).

13. For a sampling of the models see: F. Paige and S. Protopopescu, Brookhaven Report BNL-29777 (1980); Andersson et. al.,Phys. Rep.97, 31 (1983). ; R. D. Field and S. Wolfram, Nucl. Phys. B213, 65 (1983) ; T. Gottschalk, Nucl. Phys. B239, 349 (1984); and G. Marchesini and B. R. Webber, Nucl. Phys. B238, 1 (1984) .

14. This was first shown by : G. Sterman and S. Weinberg, Phys. Rev. Lett. 39, 1436 (19.) 77 . For a general review of the status of jets in QCD see S. Ellis lectures in the *Proceedings of the 11th SLAC Summer Institute on Particle Physics*, Edited by P. McDonough, SLAC-Report No. 267 (Stanford, California, 1984), p.1.

15. S. Orito (JADE Collaboration), *Proceedings of the 1979 International Symposium on Lepton and Photon Interactions At Very High Energies*, edited by T. B. W.Kirk and H. D. I. Abarbanel (Fermilab, Batavia, Illinois, 1979), p.52.

16. G. Hanson, et.al., Phys. Rev. Lett. 35, 1609 (1975) .

17. JADE Collaboration event published in: P. Soding and G. Wolf, Ann. Rev. Nucl. Part. Sci. 31, 231 (1981).

18. See for example: H. J. Behrend et. al., (CELLO Collaboration), DESYPreprint, DESY 82-061 (1982). Also see Ref. 19.

19. J. Dorfan, *Proceedings of the 1983 International Symposium on Lepton and Photon Interactions At High Energies*, edited by D. Cassel and D. Kreinick (Cornell University, Ithaca, New York, 1983), p.686.

20. M. Block and R. Cahn Rev. Mod. Phys. 57, 563 (1985) .

21. D. Froidevaux (UA2 Collaboration), presented at *International Symposium on Physics of Proton -Antiproton Collisions*, University of Tsukuba, KEK, March 13-15 (1985).

22. G. Altarelli and G. Parisi, Nucl. Phys. B126, 298 (1977) .

23. H. Abramowicz, et. al. (CDHS Collaboration), Z. Phys. C13, 199 (1982); and Z. Phys. C17, 283 (1983).

24. See EHLQ (Ref. 1) p.588 for details of the experimental measurements and theoretical expectations.

25. F. Eisele, *Proceedings of the 21th International Conference on High Energy Physics*, edited by P. Petiau and M. Porneuf, J. Phys. (Paris) **43**, Supp. 12, C3-337 (1982).

26. F. Bergsma, et.al. (CHARM Collaboration), Phys. Lett. **123 B**, 269 (1983).

27. D. B. MacFarlane, et. al. (CCFRR Collaboration), Z. Phys. **C26**, 1 (1984).

28. The situation is summarized by: F. Sciulli, *Proceedings of the 1985 International Symposium on Lepton and Photon Interactions At High Energies*, edited by M. Konuma and K. Takahashi (Kyoto University, Kyoto, Japan, 1986), p.8.

29. A. Mueller, Columbia University Preprint CU-TP-290 (1985).

30. M. Gluck, E. Hoffmann, and E. Reya, Z. Phys. **C13**, 119 (1982).

31. A simple derivation of these results is given, for example, in: C. Quigg, *Gauge Theories of the Strong, Weak, and Electromagnetic Interactions* (Benjamin/Cummings, Reading, Massachusetts, 1983), p.241.

32. S. Dawson, *Proceedings of the 1984 DPF Summer Study on the Design and Utilization of the Superconducting Super Collider*, edited by R. Donaldson, and J. Morfin (Fermilab, Batavia, Illinois, 1984), p.96 .

33. For a discussion of the small x behaviour see A. Mueller's discussion in Ref. 29. The $ln(1 - x)$ behaviour can actually be resummed but in any case is no problem because the distributions are negligibly small near x=1 for large Q^2 as can be seen from Figs 8, 9, 11, and 12.

34. R. K. Ellis et al., Nucl. Phys. **B173**, 397 (1980). Since these lectures were given a complete calculation of the one loop quantum corrections has been reported by: R. K. Ellis and J. C. Sexton, Fermilab - PUB-85/152-T (1985).

35. The elementary cross sections have been calculated by many authors, and collected in M. Gluck, J. F. Owens, and E. Reya, Phys. Rev. **D18**, 1501 (1978).

36. G. Arnison et.al.(UA1 Collaboration), Phys. Lett. **123 B**, 115 (1983).

37. G. Arnison et.al.(UA1 Collaboration), Phys. Lett. **132 B**, 214 (1983).

38. P. Bagnaia et.al. (UA2 Collaboration), Phys. Lett. **129 B**, 130 (1983).

39. P. Bagnaia et.al. (UA2 Collaboration), Phys. Lett. **138 B**, 430 (1984).

40. J. A. Appel et.al. (UA2 Collaboration) Phys. Lett. **160 B**, 349 (1985) .

41. W. Scott (UA1 Collaboration), presented at *International Symposium on Physics of Proton -Antiproton Collisions*, University of Tsukuba, KEK, March 13-15 (1985).

42. F. Pastore (UA2 Collaboration), presented at *Topical Conference on Proton-Antiproton Collider Physics*, Saint-Vincent, Aosta Valley, Italy Feb. 25-Mar.1 (1985).

43. These calculations have now been completed by: S. J. Parke and T. Taylor, Phys. Lett. **157 B**, 81 (1985) and Fermilab Preprint PUB-85/118-T (85); J. Gunion and Z. Kunszt, Phys. Lett. **159 B**, 167 (1985); and Z. Kunszt, CERN Preprint TH-4319 (1985).

44. F. A. Berends, et al., Phys. Lett. **103 B**, 124 (1981) .

45. R. K. Ellis and J. Owens, *Proceedings of the 1984 DPF Summer Study on the Design and Utilization of the Superconducting Super Collider*, edited by R. Donaldson, and J. Morfin (Fermilab, Batavia, Illinois, 1984), p.207.

46. Z. Kunszt et.al., Phys. Rev. **D21**, 733 (1980) .

47. F. Halzen and P. Hoyer, Phys. Lett. **154 B**, 324 (1985).

48. For methods of separating light quarks from gluons see: T. Sjostrand, *Proceedings of the 1984 DPF Summer Study on the Design and Utilization of the Superconducting Super Collider*, edited by R. Donaldson, and J. Morfin (Fermilab, Batavia, Illinois, 1984), p.84.

49. For methods of identifying heavy quarks see: K. Lane, *Proceedings of the 1984 DPF Summer Study on the Design and Utilization of the Superconducting*

Super Collider, edited by R. Donaldson, and J. Morfin (Fermilab, Batavia, Illinois, 1984), p.729 .

50. S. Coleman, "Secret Symmetry", *Laws of Hadronic Matter*, 1973 Erice School, Academic Press, New York (1975), p. 139.

51. G. Arnison et al. (UA1 Collaboration), Phys. Lett. **166 B**, 484 (1986).

52. J. A. Appel, et al. (UA2 Collaboration), Z. Phys. **C30**, 1 (1986) .

53. For a full discussion of how the W signal is extracted experimental see Ref. 52 and the references contained therein.

54. W, Marciano and A. Sirlin, Phys. Rev. **D29**, 945 (1984) .

55. G. Altarelli, R. K. Ellis, M. Greco, and G. Martinelli, Nucl. Phys. **B246**, 12 (1984) .

56. G. Altarelli, R. K. Ellis, and G. Martinelli, Z. Phys. **C27**, 617 (1985) .

57. The feasibility of studying rare $W^{\pm}$ decays at the SSC has not yet been studied in detail. Some of the issues of $W^{\pm}$ identification are presented in: I. Hinchliffe, *Proceedings of the 1984 DPF Summer Study on the Design and Utilization of the Superconducting Super Collider*, edited by R. Donaldson, and J. Morfin (Fermilab, Batavia, Illinois, 1984), p.1 and the references cited therein.

58. A few of the monojet events seen by UA1 are consistent with the Z^0 plus jet with the Z^0 decaying into $\nu\nu$. This can be determined from a measurement of the same process but where the Z^0 decays into e^+e^-. See Ref. 51. For the measurement of jet plus $Z^0 \to e^+e^-$ by the UA2 Collaboration see Ref. 52.

59. For a calculation of all the pair cross sections including a possible anomalous magnetic moment for the $W^{\pm}$ see: R. W. Brown and K. O. Mikaelian, Phys. Rev. **D19**, 922 (1979).

60. S. J. Brodsky and R. W. Brown, Phys. Rev. Lett. **49**, 966 (1982).

61. The requirement of anomaly cancellation in a renormalizable gauge theory was emphasized by: D. Gross and R. Jackiw, Phys. Rev. **D6**, 477 (1972).

62. S. Drell and T. M. Yan, Phys. Rev. Lett. **25**, 316 (1970); and Ann. Phys. **66**, 578, 1971.

63. J. C. Pati and A. Salam, Phys. Rev. **D10**, 275 (1974); R. N. Mohapatra and J. C. Pati, Phys. Rev. **D11**, 566 (1975); R. N. Mohapatra and G. Senjanovic, Phys. Rev. **D23**, 165 (1981).

64. For a general review of unified models: H. Georgi and S. Weinberg, Phys. Rev. **D17**, 275 (1978). Prospects for detecting additional Z^0's from E_6 models see, for example: J. L. Rosner, Univ. of Chicago preprint, EFI85-34, 1985.

65. A. D. Linde, Pis'ma Zh. Eksp. Teor. Fiz. **23**, 73 (1976). S. Weinberg, Phys. Rev. Lett. **36**, 294 (1973).

66. Spontaneous breaking of a continuous symmetry in the context of a scalar doublet model was first discussed by: J. Goldstone, Nuovo Cim. **19**, 154 (1961).

67. E. Gildener and S. Weinberg, Phys. Rev. **D13**, 3333 (1976). A general analysis of the effect on symmetry breaking of the one loop corrections to the effective potential was given by: S. Coleman and E. Weinberg, Phys. Rev. **D7**, 1888 (1973); also, see: S. Weinberg Phys. Rev. **D7**, 2887 (1973).

68. The case where $\mu^2 = 0$ was also considered in the first two papers in Ref. 67.

69. For a general reference on analyticity, unitarity, and perturbation theory see, for example: R. J. Eden, P. V. Landshoff, D. I. Olive, and J. C. Polkinghorne, *The Analytic S-Matrix* (Cambridge University Press, London, 1966).

70. The presentation I give here follows closely the analysis given by: B. W. Lee, C. Quigg, and H. B. Thacker, Phys. Rev. **D16**, 1519 (1977).

71. The proof is given in the Appendix of Ref. 70.

72. J. M. Cornwall, D. N. Levin, and G. Tiktopoulos, Phys. Rev. **D10**, 1145 (1974).

73. G. 't Hooft, Nucl. Phys. **B35**, 167 (1971).

74. M. Chanowitz and M. K. Gaillard, Nucl. Phys. **B261**, 379 (1985).

75. The definition of the ρ parameter is given in Eq. 3.17.

76. M. Chanowitz, M. A. Furman, and I. Hinchliffe, Nucl. Phys. **B153**, 402 (1979).

77. M. Veltman, Nucl. Phys. **B123**, 89 (1979). An upper bound on the Higgs boson mass can also be obtained by similar considerations: M. Veltman, Acta. Phys. Polon. **8**, 475 (1977).

78. W. J. Marciano and A. Sirlin, Phys. Rev. **D29**, 75 (1984).

79. H. Georgi, S. L. Glashow, M. E. Machacek, and D. V. Nanopoulos, Phys. Rev. Lett. **40**, 692 (1978).

80. J. F. Gunion, P. Kalyniak, M. Soldate, and P. Galison, SLAC-PUB-3604 (1985); J. F. Gunion, Z. Kunszt, and M. Soldate, Phys. Lett. **163 B**, 389 (1985); J. F. Gunion and M. Soldate, U. of C. Davis Preprint UCD-86-09 (1986). -PUB -3709 (1985).

81. This mechanism was proposed by: R. N. Cahn and S. Dawson, Phys. Lett. **136 B**, 196 (1984).

82. G. 't Hooft, *Recent Developments in Gauge Theories, Proceedings of the 1979 NATO Advanced Study Institute, Cargese*, edited by G. 't Hooft *et al.* (Plenum, New York), p. 135

83. One other (weaker) definition of naturalness is that the form of the Lagrangian be preserved by radiative corrections. A zero (or very small) mass parameter in the Higgs potential is not natural in this sense as was shown in the second paper of Ref. 66.

84. See, for example: S. Coleman, *1971 International School of Subnuclear Physics*, Erice, Italy, edited by A. Zichichi (Editrice Compositori, Bologna, 1973).

85. M. K. Gaillard, presented at *1985 Theoretical Advanced Study Institute*, Yale University, June 9-July 5, 1985.

86. S. Weinberg, Phys. Rev. **D19**, 1277 (1979) .

87. L. Susskind, Phys. Rev. **D20**, 2619 (1979).

88. It has been shown that the global symmetry breaking must have this pattern if the gauge interaction is vectorlike (i.e. like QCD) and confining: C. Vafa and E. Witten, Nucl. Phys. **B234**, 173 (1984).

89. For a general discussion of large N arguments see: E. Witten, Anns. Phys. **128**, 363 (1980). Also see Ref. 102.

90. This signature for technicolor was proposed in the original paper of Susskind (Ref. 87).

91. Some recent studies of these backgrounds to W pair production are contained in Ref. 80 as well as in the *Proceedings of the 1984 DPF Summer Study on the Design and Utilization of the Superconducting Super Collider*, edited by R. Donaldson, and J. Morfin (Fermilab, Batavia, Illinois, 1984) .

92. E. Eichten and K. D. Lane, Phys. Lett. **90 B**, 125 (1980).

93. S. Dimopoulos and L. Susskind, Nucl. Phys. **B155**, 237 (1979).

94. E. Farhi and L. Susskind, Phys. Rev. **D20**, 3404 (1979).

95. S. L. Glashow,J. Iliopoulos, and L. Maiani, Phys. Rev. **D2**, 1285 (1980).

96. S. Dimopoulos and J. Ellis, Nucl. Phys. **B182**, 505 (1981).

97. S. C. Chao and K. D. Lane, Phys. Lett. **159 B**, 135 (1985).

98. A. M. Hadeed and B. Holdom, Phys. Lett. **159 B**, 379 (1985); S. Dimopoulos and H. Georgi, Phys. Lett. **140 B**, 148 (1985); Also Ref.95.

99. S. Dimopoulos, Nucl. Phys. **B168**, 69 (1980).

100. M. Peskin, Nucl. Phys. **B175**, 197 (1980).

101. J. Preskill, Nucl. Phys. **B177**, 21 (1981).

102. S. Dimopoulos, S. Raby, and G. L. Kane, Nucl. Phys. **B182**, 77 (1981).

103. R. Dashen, Phys. Rev., **183**, 1245 (1969).

104. S. Chadha and M. Peskin, Nucl. Phys. **B185**, 61 (1981); **B187**, 541 (1981).

105. V. Baluni, Phys. Rev. D28, 2223 (1983).

106. This crude estimate follows from the current algebra relation $F_\pi^2 M(P^0)^2 = m_q < Q\overline{Q} >$, with the identifications $< Q\overline{Q} >= F_\pi^3 \approx (250 GeV)^3$ and $m_q = (m_u + m_d)/2 \approx 7 GeV/c^2$. For an explicit model in which this behaviour is realized, see Ref. 102.

107. K. D. Lane, *Proceedings of the 1982 DPF Summer Study on Elementary Particle Physics and Future Facilities*, edited by R. Donaldson, R. Gustafson, and F. Paige (Fermilab, Batavia, Illinois, 1982),p.222.

108. For a review of experimental constraints see: S. Komamiya, *Proceedings of the 1985 International Symposium on Lepton and Photon Interactions At High Energies*, edited by M. Konuma and K. Takahashi (Kyoto University, Kyoto, Japan, 1986), p.612.

109. E. Eichten, I. Hinchliffe, K. D. Lane, and C. Quigg, Fermilab Pub-85/145-T (1985).

110. G. 't Hooft, in Lecture 3 of Ref. 82.

111. H. Georgi and S. L. Glashow, Phys. Rev. Lett. 32, 438 (1974).

112. S. Weinberg and E. Witten, Phys. Lett. 96 B, 491 (1981).

113. S. Coleman and B. Grossman, Nucl. Phys. B203, 205 (1982).

114. The dynamics of chiral gauge theories has been studied in the large N limit by: E. Eichten, R. Peccei, J. Preskill, and D. Zeppenfeld, Nucl. Phys. B268, 161 (1986).

115. E. Eichten, K. D. Lane, and M. E. Peskin, Phys. Rev. Lett. 50, 811 (1983).

116. G. B. Chadwick, MAC Collaboration, *Proceedings of the Europhysics Study Conference on Electroweak Effects at High Energies*, Erice, Italy (1983).

117. Ch. Berger et al., PLUTO Collaboration, Z. Phys. C27, 341 (1985).

118. MARK-J Collaboration, reported in S. Komamiya, *Proceedings of the 1985 International Symposium on Lepton and Photon Interactions At High Energies*,

edited by M. Konuma and K. Takahashi (Kyoto University, Kyoto, Japan, 1986), p.612.

119. W. Bartel et al., JADE Collaboration, Z. Phys. **C19**, 197 (1983).

120. M. Althoff et al., TASSO Collaboration, Z. Phys. **C22**, 13 (1984).

121. M. Derrick, HRS Collaboration, ANL-HEP-CP-85-44 (1985).

122. M. Abolins et al., *Proceedings of the 1982 DPF Summer Study on Elementary Particle Physics and Future Facilities*, edited by R. Donaldson, R. Gustafson, and F. Paige (Fermilab, Batavia, Illinois, 1982),p.274. Also see Ref 115.

123. I. Bars and I. Hinchliffe, Phys. Rev. **D33**, 704 (1986).

124. The only graded Lie Algebras consistent with relativistic quantum field theory are the supersymmetric algebras. This was proven by: R. Haag,J. Lopuszanski, and M. Sohnius, Nucl. Phys. **B88**, 257 (1975).

125. J. Wess and J. Bagger, *Supersymmetry and Supergravity*, Princeton University Press, Princeton, New Jersey (1983).

126. P. Fayet, Nucl. Phys. **B90**, 104 (1975); A. Salam and J. Strathdee, Nucl. Phys. **B87**, 85 (1975).

127. The possibilities for a residual R symmetry are analysed by: G. Farrar and S. Weinberg, Phys. Rev. **D27**, 2732 (1983).

128. L. Hall, J. Lykken, and S. Weinberg, Phys. Rev. **D27**, 2359 (1983); L. Alvarez-Gaume, J. Polchinski, and M. Wise, Nucl. Phys. **B221**, 495 (1983).

129. S. Dawson, E. Eichten, and C. Quigg, Phys. Rev. **D31**, 1581 (1985).

130. The mixing is treated in general for the minimal supersymmetric model in Ref. 129. Also see Ref. 132.

131. L. Baulieu, J. Kaplan, and P. Fayet, Phys. Lett. **141 B**, 198 (1984).

132. H. Haber and G. Kane, Phys. Rep. **117**, 75 (1985).

133. K. Freese and D. Schramm, Nucl. Phys. **B233**, 167 (1984) .

134. H. Goldberg, Phys. Rev. Lett. **50**, 1419 (1983).

135. N. Cabibbo, G. Farrar, and L. Maiani, Phys. Lett. **105 B**, 155 (1981).

136. G. Snow (private communication).

137. P. Fayet, Phys. Lett. **84 B**, 421 (1979).

138. M. Fukugita and N. Sakai, Phys. Lett. **114 B**, 23 (1982); A. Bouquet and C. E. Vayonakis, Phys. Lett. **116 B**, 219 (1982); and J. Ellis and K. Olive, Nucl. Phys. **B223**, 252 (1983).

139. H. Behrend et al., CELLO Collaboration, Phys. Lett. **123 B**, 127 (1983).

140. B. Alper et al., Phys. Lett. **46 B**, 265 (1973); and D. Cutts et al., Phys. Rev. Lett. **41**, 363 (1978).

141. R. Gustafson et al., Phys. Rev. Lett. **37**, 474 (1976).

142. R. C. Ball et al., Phys. Rev. Lett. **53**, 1314 (1984).

143. F. Bergsma et al., CHARM Collaboration, Phys. Lett. **121 B**, 429 (1983).

144. E. Fernandez et al., MAC Collaboration, Phys. Rev. Lett. **54**, 1118 (1985).

145. W. Bartel el al., Z. Phys. **C6**, 295 (1980).

146. C. Nappi, Phys. Rev. **D25**, 84 (1982).

147. W. Bartel et al., JADE Collaboration, DESY-Preprint 84-112 (1984).

148. B. Adeva et al., Mark-J Collaboration, Phys. Rev. Lett. **53**, 1806 (1984).

149. W. Bartel et al., JADE Collaboration , Phys. Lett. **146 B**, 126 (1984).

150. G. Bartha et al., ASP Collaboration, Phys. Rev. Lett. **56**, 685 (1986).

151. See Ref. 129 for details on these limits.

152. S. Dawson, Nucl. Phys. **B261**, 297 (1985).

153. J. Ellis and H. Kowalski, Nucl. Phys. **B259**, 109 (1985).

154. R. M. Barnett, H. E. Haber, and G. Kane, Berkeley preprint, LBL-20102 (1986).

155. S. Dawson and A. Savoy-Navarro, *Proceedings of the 1984 DPF Summer Study on the Design and Utilization of the Superconducting Super Collider*, edited by R. Donaldson, and J. Morfin (Fermilab, Batavia, Illinois, 1984), p.263.